Quantum Electrodynamic and nuclear effects in Li-like ions and muonic atoms

Guojie Bian

UPMC SORBONNE UNIVERSITÉS

Laboratoire Kastler Brossel
Physique quantique et applications

THÈSE DE DOCTORAT
DE L'UNIVERSITÉ PIERRE ET MARIE CURIE

Spécialité : Physique

École doctorale n°564: Physique en Île-de-France

réalisée

au Laboratoire Kastler Brossel

sous la direction de Paul Indelicato

présentée par

BIAN GUOJIE

pour obtenir le grade de :

DOCTEUR DE L'UNIVERSITÉ PIERRE ET MARIE CURIE

Sujet de la thèse :

Effets électrodynamiques et nucléaires quantiques dans les ions de type lithium et les atomes muoniques

soutenue le 20er september 2019

devant le jury composé de :

M.	Michel Godefroid	Rapporteur
M.	Zoltan Harman	Rapporteur
Mme	Emily Lamour	Examinatrice
M.	Keh-Ning Huang	Examinatrice
M.	Paul Indelicato	Directeur de thèse

Acknowledgments

This thesis was carried out at Laboratoire Kastler Brossel of Sorbonne Université, in Paris, from 2016 to 2019. It was financed by the China Scholarship Council, a Chinese Ministry of Education's non-profit organization within the Chinese government (File No.201606240047). I give my gratitude to the financial support of the China Scholarship Council (CSC).

First, I owe the greatest thanks to my supervisor Paul Indelicato who is very patient and knowledgeable. He taught me theoretical knowledge and told me how to do physics research. No matter where he is, he will answer any of my questions at any time. From small things to scientific research, he is so caring and always provided significant help. He is also the most impressive supervisor I have ever met.

I want to thank also my tutor Philippe Jacquier and Jean-Philippe Karr in our lab, reminding us of the importance of effective communication, mutual trust and respect between the supervisor and Ph.D. student. They are responsible for supervising my doctoral research process.

Thanks to Sichuan University for giving me the opportunity to go abroad to continue research. I appreciate my master thesis supervisor, Gang Jiang who introduced me to step into the road of scientific exploration. Special thanks to Professor Kening Huang for his recommendation, whose help set me on the road to study in France.

Thanks Nancy Paul for correcting the English grammar and writing errors of my entire doctoral thesis. Thank my colleague Jorge Machado and Nancy Paul doing the experiments. Thanks to Hélène Fleurbaey and Léo Morelwho shared the same office with me in France. They are very friendly and helped me solve many small problems.

Thanks to Mingtao Cao, Ping Tang, Zhibin Yao, Jun Sun, Chenjie Ding, Tao Peng, Shuwei Qiu, Haiwa Zhang, Jialin Cai, Bin Li, and other friends for helping me. Being able to work and study with a group of friends is my most precious experience and wealth.

Parents' support and encouragement are the strong motivation that I have always insisted on. I appreciate my uncle Huaishu Xu for his all-the-time support, and you are my solid backing. I would like to take this opportunity to thank the parents of my husband wanzhi He and Xiuzhi Wang. I would also like to thank my husband doctor He Fei, for his thoughtful care. His understanding and optimism are my sources of happiness. Thank you for accompanying me for ten years.

I have had a wonderful and unforgettable three years in Paris. I would like to express my sincere gratitude to all the people that contributed to the completion of this thesis.

Contents

Introduction

Bound state quantum electrodynamics (BSQED) can describe the structure of atoms and ions very accurately, and it is one of the most important cornerstones in modern physics. Highly charged ions and muonic atoms are generally considered to be the ideal candidates for studying BSQED of the strong-field regime. Yet there are still outstanding issues that require improved accuracy in both experimental and theoretical tests. Calculations are very difficult already at second order for the one-electron system. Considering accurately enough, the electron-electron interaction in two and more electron ions is even more difficult. For 50 years, many experiments have been performed to measure the energies of few-electron ions. The experiments have used laser-generated plasmas, beam-foil spectroscopy, highly-charged ion sources such as Electron-Beam Ion traps or Electron-cyclotron resonance ion sources, and storage rings.

Our group specializes in reference-free measurements, which provide improved tests. Machado et al. [1] measured the width and transition energies in He-like $1s2p\,^1P_1 \rightarrow 1s^2\,^1S_0$ and Be-like $1s2s^22p\,^1P_1 \rightarrow 1s^22s^2\,^1S_0$ in argon ions. The experiment for measuring the transition energy of $1s2s^22p\,^1P_1 \rightarrow 1s^22s^2\,^1S_0$ is the first reference-free measurement with more than two-electrons. The group also measured $1s2s2p\,^2P_J \rightarrow 1s^22s\,^2S_{1/2}, J = 1/2, 3/2$ transitions in lithiumlike sulfur and argon, and of the $1s2s2p\,^4P_{5/2} \rightarrow 1s^22s\,^2S_{1/2}$ M2 transition in sulfur. The experiment used a double-crystal spectrometer (DCSs) connected to an Electron-Cyclotron Ion Source (ECRIS), without using any reference line. To validate the experiment and improve the theoretical model, we conducted theoretical research.

Muonic atoms are formed by a negatively charged muon that enters the orbit of an atom and decays by emitting X-rays. Detection of muonic X-rays is considered a sensitive and precise technique for determining the characteristics of the nucleus, such as charge distribution and deformation [2]. This method allows precision measurement of nuclear charge radii and has been an essential tool for more than 40 years, supplementing the knowledge of electron scattering experiments and isotope shifts by optical laser spectroscopy [3]. There will be an upcoming experiment to perform muonic atom spectroscopy aiming at a precise measurement of the absolute nuclear charge radii of radioactive ^{226}Ra with a level of 0.2% relative precision at the Paul Scherrer Institute (PSI) [4].

The experiment can map out the various level energies of muonic atoms by measuring the emitted X-ray photons. The nuclear charge radius can be extracted by comparing the measured energy level to a calculation result. Therefore, in addition to the need for experimental techniques, this experiment requires a complete theoretical method and extensive and accurate theoretical calculations.

Bergern et al. [5] measured low-lying transition energies of muonic ^{208}Pb with a

precision up to 11ppm using a Compton suppression spectrometer. They achieved the charge radius using the best-fit parameters and the fitted nuclear polarization values. We conduct a detailed analysis of muonic lead referencing many lines measured between 1s, 2s, 2p, 3p, 3d, 4f, 5f, 6f levels comparing the results with others and testing our theoretical model. Finally, we provide reliable theoretical values of ^{226}Ra and ^{248}Cm for the experiment.

We perform multi-configuration Dirac-Fock (MCDF) research on three-electrons ions and muonic atoms by improving the MCDFGME code developed by Desclaux and Indelicato. We use the newest 2018 version of the program, which improves the finite size corrected self-energy, vacuum polarization to all order and effective model operator evaluation of the one-electron self-energy screening values for electronic and muonic atoms.

The outline of this manuscript is the following:

The first chapter starts with a background of the subject. The status of Quantum Electrodynamic (QED) tests, including electronic and muonic atoms, are presented. We also briefly describe muon-electron universality and the properties of muonic atoms.

The second chapter introduces the theoretical method of atomic calculations on one and three electrons. The multiconfiguration Dirac–Fock (MCDF) method, QED corrections, and nuclear effects are discussed. We take into account all one loop and the main two-loop QED contributions. We calculate for the first time the exact one-loop self-energy for muonic atoms with finite nuclear size contribution. We also mention all corrections which affect transition energy.

Several important characteristics of muonic atoms are emphasized in the third chapter.

In the fourth chapter, the computational procedure using the relativistic atomic structure code is explained in detail.

In the last two chapters, we present the discussion and analysis of the results. For Li-like atoms, we describe the results from the Welton model and effective operator models and compare the result between calculations and experiments. The effects of each contribution are also analyzed. Finally, we give the sources of theoretical errors and uncertainty. For muonic atoms, the best fit nuclear parameters that minimize the weighted theory-experiment discrepancy are found in the muonic lead with two-parameter Fermi model and three-parameter Gauss model. We also tabulate the energy levels in muonic radium and curium with all the radiative corrections.

Chapter 1

Background

Quantum electrodynamics (QED) is a foundation for modern physics as the first relativistic quantum field theory. It can be said to be the most rigorously tested part in the standard model. In the past few years, QED and relativistic multi-body problems have been undergoing significant progress. The purpose of this part is to present the current status of experiment and theory on QED tests, with tools of one to three electronic ions and muonic atoms. Accurate tests of QED are performed by comparing experimental data with theoretical calculations. Next, we briefly introduce the muon, which can be treated as a large mass electron, and muonic atom. At last, we list several widely used methods dealing with the multi-body problem.

1.1 Basic properties of muonic atoms

1.1.1 Properties of muons

In 1936, Anderson and Neddermeyer [6] discovered the muon, a fundamental particle, when studied cosmic rays using cloud chambers and Geiger counters. Some data relevant to the basic properties of muon are summarized in Table 1.1. The muon is a lepton and does not participate in the strong interaction, and its spin is 1/2. The charge of the muon is the same as the electron within about 2 ppm. The muon has the same electromagnetic properties as the electron but with greater mass ($m_\mu \approx 207 m_e$). The muonic magnetic moment can be obtained by measuring the precession of the muon spin directly in a magnetic field or the combination of muonium transition frequencies in a strong magnetic field. The magnetic moment of the muon is smaller than that of the electron, which makes the muon less sensitive to magnetic fields and the nuclear current. Its motion is mainly governed by its electronic charge interaction with nuclear charge, so at least in terms of the nuclear interaction, there is no requirement to provide great precision information on μ.

The lifetime of the muon is known very accurately ($2.197134(77) \times 10^{-6} s$) [8]. This lifetime is determined entirely by the decay mode.

Since the mass and energy of a muon are much larger than the decay energy of common radioactive decay, a muon cannot be produced by radioactive decay. A muon can be generated by a hadron-involved nuclear reaction in a high-energy physics experiment performed on an accelerator. Besides, cosmic rays interact with the Earth's atmosphere

Table 1.1 – Properties of the Muon [7].

Mass	$206.768277(24)m_e$
Charge	$e_\mu = e_e$
Spin	1/2
Magnetic moment(μ_μ/μ_p)	$\mu = \frac{e\hbar}{2m_\mu c}(-g)$, $g = 2(1 + \frac{\alpha}{2\pi} + 0(\alpha^2) + \cdots)$
Free decay lifetime($10^{-6}s$)	2.19695(6)
	2.197078(73)
Decay mode	$e^- + \bar{\nu}_e + \nu_\mu$
Wave equation	The muon is a point particle obeying the Dirac equation and the usual quantum-electrodynamical refinements where applicable
Weak interaction	Universal Fermi ($U - A$) interaction

to produce a large number of muons, which method is the only known natural source of muons. The weak interaction of the muon is two-fold, one is the decay of $\mu^- \rightarrow e^- + \bar{\nu}_e + \nu_\mu$ and another is captured by the nucleus ($\mu^- + P \rightarrow N + \nu_\mu$). This phenomenon limits the mean lifetime of muonic atoms.

In light atoms, free decay is important. While μ^- captured by the nucleus is important, and the lifetime is around 0.08 μsec in heavy atoms. This seriously limits the possible measurements on the ground state of the muonic atom. In addition, this short lifetime seems to make the manufacture and the study of muonic atoms with two or few muons completely impractical. The validity of the QED basic theory is tested by using high-precision spectroscopy with μ-containing atoms.

1.1.2 Muonic atoms

A muonic atom is created when a negatively charged muon that enters the orbit of atom and decays a series of lower energy levels by emitting X rays. Eventually, the muon is absorbed by the nucleus.

The mass m of an orbital particle has a great influence on the atomic properties. In low-Z muonic atoms, muonic binding energies are on the order of several keV, and there is a strong overlap between the muonic wave function and that of the nucleus. This leads to a significant effect of the finite size of the nucleus on the atomic energy levels. These atoms provide an interesting opportunity to extract the properties of the nucleus with high precision.

In Table 1.2, we list the main features of muonic atoms comparing with the electronic atoms. The finite nuclear size effect plays a dominant role in muonic atoms. In heavy muonic atoms, the interaction of electric-quadrupole become of the same size as the fine-structure splitting of $2p$ or $3d$ levels. Magnetic hyperfine splitting is much smaller as it dependents on the magnetic moment of muon (in inverse proportion to mass).

There should be noticed that in addition to the mass, the other differences between the observed interactions of the electronic and muonic atom is shown in Table 1.2.

The electrons only perceive the effects of the fully unipolar field Ze/r near the nucleus. The muon can feel the shielding effect from electrons if there are residual electrons. In fact,

Table 1.2 – Some typical characteristics of muon and electron atoms [7].

	Dimensions	M,Z dependence	Approx,ratio, muon/elec.
Orbit size	$\frac{n^2\hbar^2}{e^2Zm}$	$\frac{1}{Zm}$	$\frac{m_e}{m_\mu} \simeq \frac{1}{207}$
Energy levels	$-\frac{(Z\alpha)^2c^2}{2n^2}m$	Z^2m	$\frac{m_\mu}{m_e} \simeq 207$
Finite-size effect,1s	$\frac{Ze^2(R_{nucl})^2}{\langle r^3\rangle}$	Z^4m^3	$\frac{m_\mu^3}{m_e^3} \simeq (207)^3$
Fine-structure splitting,2p	$\frac{Z\langle \boldsymbol{a}\cdot\boldsymbol{\sigma}\rangle e^2\hbar^2}{m^2c^2\langle r^3\rangle}$	Z^4m	$\frac{m_\mu}{m_e} \simeq 207$
Nuclear magnetic-dipole HFS ns,	$\frac{\mu_{nucl}\mu_{lepton}}{\langle r^3\rangle}$	Z^3m^2	$\frac{m_\mu^2}{m_e^2} \simeq (207)^2$
Nuclear electric-quadrupole HFS, $np_{3/2}$	$\frac{eQ_{nucl}}{\langle r^3\rangle}$	Z^3m^3	$\frac{m_\mu^3}{m_e^3} \simeq (207)^3$

many electrons are removed from the nucleus during the muon capture, so the screening effect of electrons is very small in muonic atoms.

Magnetic hyperfine structure (HFS) is on the size of several keV, usually two-time orders smaller than fine structures; while, this is large enough to cause internal transitions in N and O shell electrons. This, in turn, greatly enhances $M1$ transitions between magnetic hyperfine states.

The low-lying orbits of muonic atoms penetrate the nucleus deeply, so the orbit $1s_{1/2}$ is most sensitive to finite nuclear size effects. The electromagnetic interaction of the muon and the nucleus depends on the nuclear charge and current densities in these states.

1.2 Status of QED tests

A good understanding of the QED contribution is critical to physical precision testing. Determining the fundamental constants, for example, the fine structure constant, the Rydberg constant R_∞ and the mass ratio of electron and proton, also requires precise knowledge of QED contributions. The accurate testing of QED is obtained by comparing experimental results with theoretical predictions.

1.2.1 Few-electron ions

a) Theory

High precision calculations of QED effects rely on the perturbation expansion in power of the expansion parameter α, which is the fine-structure constant $\alpha = 2\pi e^2/hc$. The individual terms of the perturbation sequence can be represented by Feynman diagrams,

with the number of virtual photons indicated by the power of α. The starting point is the Dirac equation of the electrons in an external nuclear field. The interaction of the bound electrons with the electromagnetic field as a perturbation leads to radiation correction and electron-electron interactions. This interaction causes energy shifts and should be checked in the first order of m/M (m represents the electron mass and M the nuclear mass) and the first and second orders of α. Researchers have perfected the basic methods of Dirac, Pauli, Born, Fock, Wigner, Fermi, Feynman, Bethe, Schwinger, and others for calculating QED effects with more accuracy.

In light atoms, the earliest QED calculations were based on the expansion of $Z\alpha$, which characterized the Coulomb interaction between nucleus and electrons. This calculation brings accurate results for hydrogen, helium, and other low-Z atoms. But it is not suitable for high-Z systems. Therefore, there is a need for a strict theory to describe the activity of electrons in a strong nuclear field before performing a comparison between theory and experiment. So, the calculations should be performed to all orders in the parameter $Z\alpha$. This requires the development of the nonperturbative QED theory, which method is suitable for the calculations in highly charged ions.

The main difficulty is that the calculation of QED corrections on all orders in the parameter $Z\alpha$ requires a large numerical calculation. Mohr [282] reported a major achievement of the electron self-energy in H-like ions, which compiled by Mohr [9] and Johnson and Soff [10] as a standard reference for many years. Soon after, researcher calculated various corrections to the Lamb shift of H-like atoms including all orders vacuum-polarization in $Z\alpha$ [11] and two-loop self-energy in $Z\alpha$ [119, 288], the nuclear size effect to the self-energy [118], first order to all orders of nuclear recoil correction [120], even the difficult nuclear polarization correction [295]. The two-loop effects to orders $\alpha^2(Z\alpha)^5$ [12] and $\alpha^2(Z\alpha)^6$ [13, 14] are further achievements with the $Z\alpha$-expansion approach.

The first high-precision calculation in self-energy contributions was performed by Mohr [282] for the 1s level at medium and high-Z. It was extended to different n, l, j levels [117] and super-heavy elements [16]. This evaluation, in which the expansion in Z is only asymptotic, does not converge even for relatively small values of Z. Jentschura, Mohr and Soff [17] performed for $1 \leq Z \leq 5$ using highly efficient resummation techniques. This resolved the long-standing inconsistency between the $Z\alpha$-expansion approaches and numerical all-order calculations. Abnormally, large higher-order terms not included in the $Z\alpha$-expansion lead to the disagreement. It is considered that in the $1S$ and $2S$ levels, this work eliminated another theoretical uncertainty of the hydrogen Lamb shift.

In recent years, QED test has also made significant progress based on the theory of predecessors. Yerokhin and Shabaev [19] carried out a high-precision nonperturbative (in $Z\alpha$) calculation of Lamb shift, where the nuclear recoil effect is considered in $n = 1$, and $n = 2$ states in light hydrogenic atoms. This method extended the calculation of fractional Z as low as 0.3 and improved the numerical accuracy by 2–3 orders of magnitude. The result is exactly consistent with the terms of $Z\alpha$ expansion. Also, the nonperturbative high-order remainder can be accurately identified. Yerokhin and Shabaev [20] systematically summed up the latest tabulation of the $n = 1$ and $n = 2$ level energies with the nuclear Z from 1 to 110 of H-like atoms, which is considered an ideal test QED effects for stretching the theory up to the utmost precision.

The study of one-electron ions is expected to be the best way to test QED corrections, which have been plotted in Fig. 1.1 including all the QED contributions and nuclear

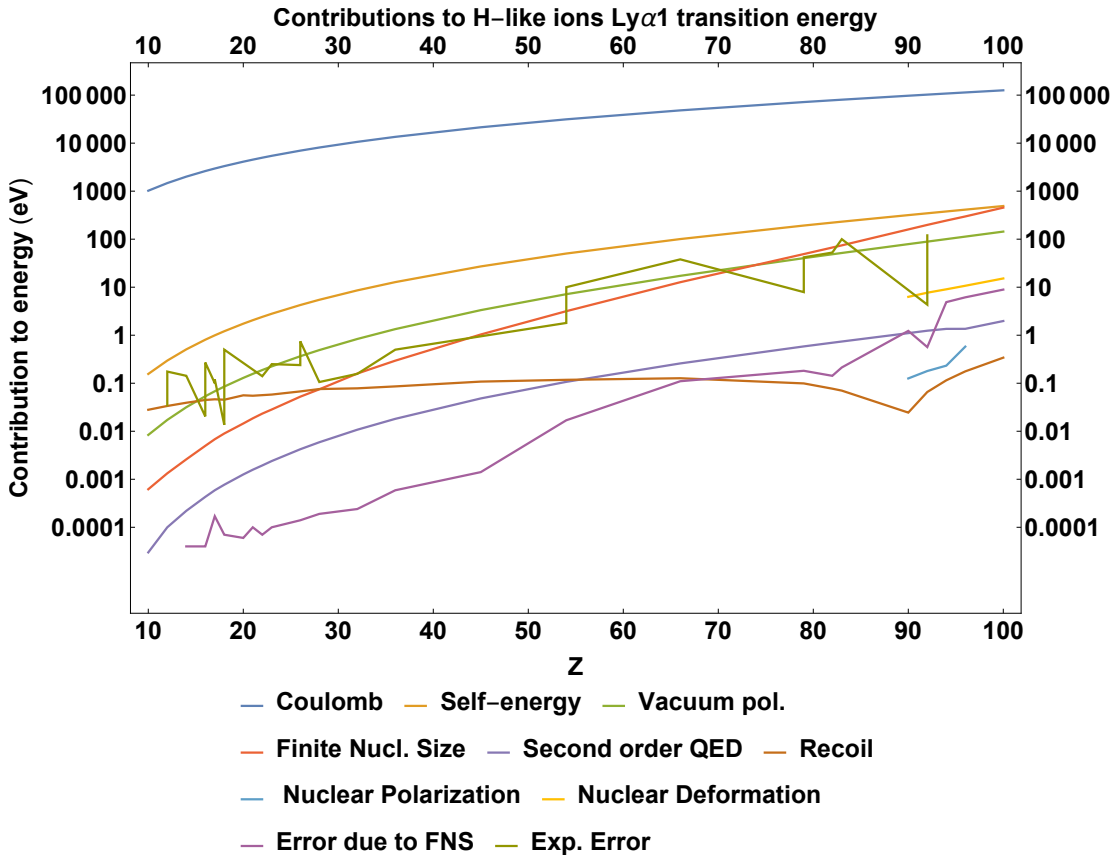

Fig. 1.1 *Size of all the one-electron QED contributions to the Lyman α_1 transition energy as a function of Z. Figure from Indelicato P [15].*

contributions as a function of Z for the Lyman α_1 transition. The calculations were performed using the 2018 version of the MDFGME program developed by Indelicato and Desclaux [105, 155, 156, 108, 177, 109, 157].

For systems with more than one electron, QED corrections are much more difficult to perform because of the nuclear potential screened, which is caused by the additional electrons. The electron-electron interactions can be considered as a perturbation. However, the expansion in $Z\alpha$ cannot be used at high Z. As a result, the electron-electron interaction results in a perturbative-expansion factor of $1/Z$. By calculating several terms of the expansion, the electron correlation and one-loop QED screening correction can be strictly described with an accuracy sufficient to deduce the two-loop Lamb shift, which has been presented in [21, 22, 23].

Yerokhin, Indelicato and Shabaev [24] carried out all order calculations of the two-loop self-energy, especially for heavy Hydrogen-like ions. This calculation eliminated the largest theoretical uncertainty of $2p - 2s$ transitions and produced the first experimental determination of the two-loop QED correction. Worth mentioning, the researchers performed systematic QED corrections to the lithium isoelectronic sequences with accurate numerical results. A strict QED evaluation was proposed for the first two terms of the expansion using zeroth-order approximation, instead of a local model potential for $n = 2$

states by Yerokin et al. [25]. The three-photon exchange correction was also included under the many-body perturbation theory (MBPT). Sapirstein and Cheng [26] conducted a similar study of S-matrix calculations with all one and two-photon diagrams, and part of three-photon diagrams in lithium isoelectronic sequence using modified Furry representation. Lithium-like uranium provided the testing of first-order QED effects with a 0.2% accuracy level and second-order with a 6% accuracy level in α by Volotka et al. [27]. The nuclear polarization correction eventually becomes the limiting uncertainty in the theoretical accuracy of QED tests with HCI.

Researchers generally believe that the significant contributions of nuclear size effects, nuclear polarization correction, and nuclear recoil correction, which are not well known, affect the extraction of higher-order QED contribution information. Shabaev et al. [28] proposed different scaling method of the QED effects and nuclear size corrections with Z and n. Nuclear deformation corrections are investigated on the level energies of Li-like U^{89+} by Kozhedub et al. [29]. Consequently, the theoretical uncertainties of the $2s-2p_{1/2}$ transition energy are obviously reduced.

For complex multi-electron ions, the mean-field approximation (like the Dirac-Fock approximation) is indispensable under the framework of relativistic quantum mechanics. The QED correction can be contained by the radiative potential [30]. Dirac-Coulomb or Dirac-Coulomb-Breit no-pair approximation is usually used for including relativistic effects [31].

b) Experiment

Theoretical advances over the past few decades have been complemented by the high-precision spectroscopy experiments with highly charged ions. The experiments have used laser-generated plasmas, beam-foil spectroscopy, highly-charged ion sources like Electron-Beam Ion traps or Electron-cyclotron resonance ion sources, and storage rings in large facilities of HITRAP facility at GSI, GANIL in Caen, France, and GSI in Darmstadt, Germany.

Modern experiments studied the impact of the strong nuclear field on bound state QED via hydrogen-like neon up to uranium along with the entire periodic table at Fig. 1.2. At low-Z ions, the experimental measurements have reached a high degree of precision. The experimental results are in perfect agreement with the theoretical values. In the middle and high-Z ions, there seems not so optimistic due to the uncertainty of 2nd order QED effects. For example, the Lamb-shift measurements of the 1s state in H-like uranium has achieved the value of 460.2 eV$\pm$4.6 eV (about 1% uncertainty) by Gumberidze et al. [64]. While the theoretical calculation result is 463.99(39) eV, with QED contribution of 265.2 eV, 2nd order QED of -1.26(33) eV, and a comparably large correction of finite nuclear-size effects of 198.54(19) eV. These results provided testing of QED at the 2% level by combining theory and experiment in the strongest stationary electromagnetic fields. Beiersdorfer et al. [65] provided the first test of two-loop Lamb shift for the 1s level in hydrogen-like U^{89+} based on passive emission spectroscopy. This experimental value obtained with the weighted-average is consistent with the theoretical value. It will be expected to make some advances in these experiments, which will make them sensitive to 2nd order QED effects in non-perturbative methods.

Fig. 1.3 and 1.4 shows the histogram of the measurements with a given accuracy in

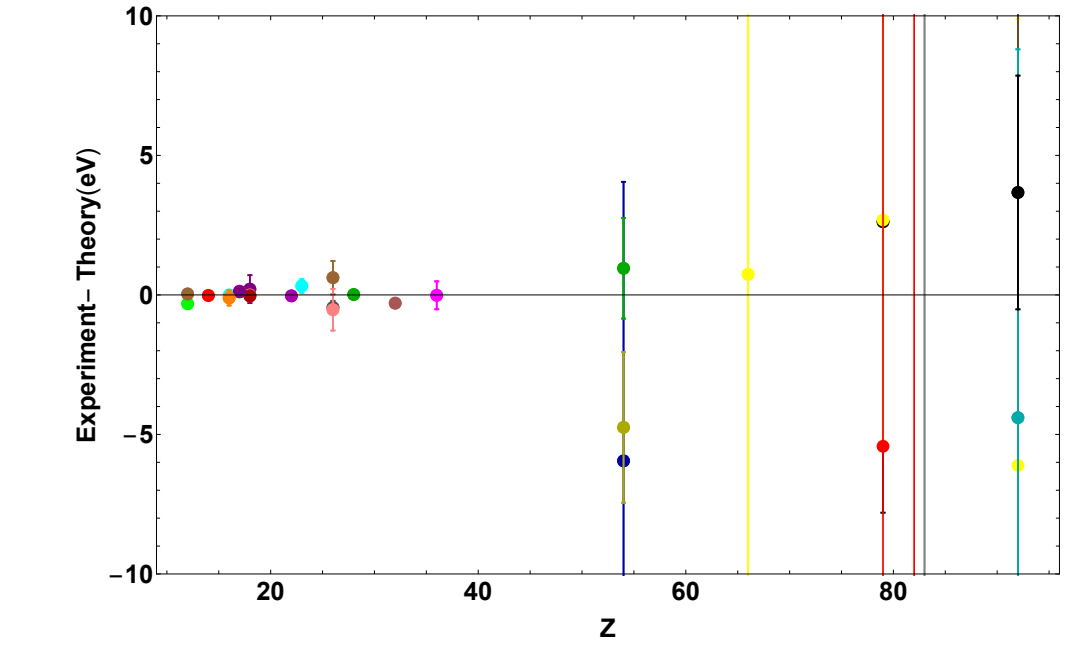

Kubiček et al. (2014) Tschischgale et al. (2002) Armour et al. (1980)
Tavernier et al. (1985) Briand et al. (1983) Briand et al. (1983) Beyer et al. (1985)
Beyer et al. (1994) Lupton et al. (1994) Beyer et al. (1995) Marmar et al. (1986)
Briand et al. (1989) Stöhlker et al. (1992) Beyer et al. (1991) Briand et al. (1990)
Stöhlker et al. (1993) Stöhlker et al. (2000) Widmann et al. (2000)
Tarbutt and Silver (2002) Chantler et al. (2007) Chantler et al. (2009)
Thorn et al. (2009) Gillaspy et al. (2010) Kraft–Bermuth et al. (2017)
Källne et al. (1984) Deslattes et al. (1985) Richard et al. (1984) Hölzer et al. (1998)
Silver et al. (1987) Gumberidze et al. (2005) Schleinkofer et al. (1982)
Beyer et al. (1993) Gassner et al. (2018)

Fig. 1.2 *Comparison between theory (Yerokhin and Shabaev 2015 [20]) and experiment for the Lyman α_1 line in hydrogen-like ions. Figure from Indelicato P [15].*
Experiments: Kubiček et al. (2014)[32], Tschischgale et al. (2002)[33], Armour et al. (1980)[34], Tavernier et al. (1985)[35], Briand et al. (1983)[36], Beyer et al. (1985)[37], Beyer et al. (1994)[38], Lupton et al. (1994)[39], Beyer et al. (1995)[40], Marmar et al. (1986)[41], Briand et al. (1989)[42], Stöhlker et al. (1992)[43], Beyer et al. (1991)[44], Briand et al. (1990)[45], Stöhlker et al. (1993)[46], Stöhlker et al. (2000)[47], Widmann et al. (2000)[48], Tarbutt and Silver (2002)[49], Chantler et al. (2007)[50], Chantler et al. (2009)[51], Thorn et al. (2009)[52], Gillaspy et al. (2010)[53], Kraft-Bermuth et al. (2017)[54], Källne et al. (1984)[55], Deslattes et al. (1985)[56], Richard et al. (1984)[57], Hölzer et al. (1998)[58], Silver et al. (1987)[59], Gumberidze et al. (2005)[60], Schleinkofer et al. (1982)[61], Beyer et al. (1993)[62], Gassner et al. (2018)[63]

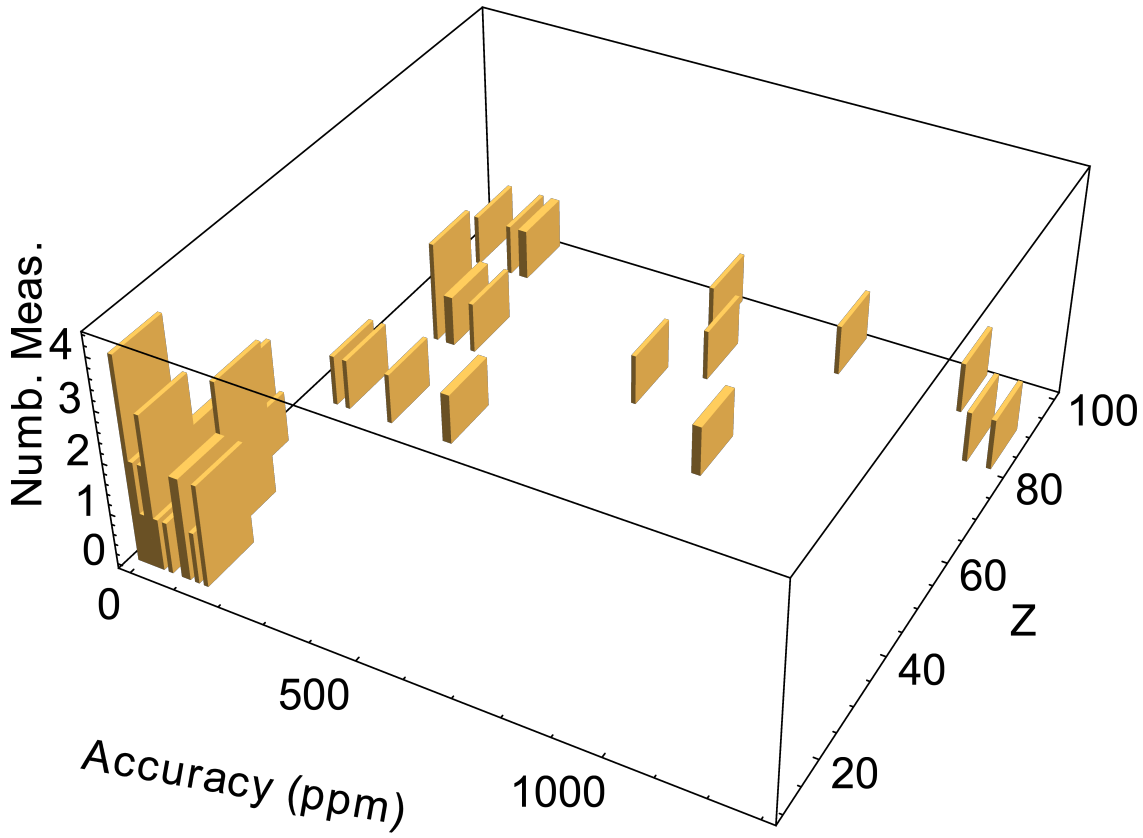

Fig. 1.3 *Histogram of the number of measurements for a given accuracy in part per million and the atomic number Z for Lyα_1 and Lyα_2. Figure from Indelicato P [15].*

part-per-million (ppm) as a function of Z for one- and two-electron ions, separately. The experimental verifications of QED prediction have mainly concentrated on a few low-Z ions with high precision, while there is lack of some accurate measurements at medium and high-Z ions. Bruhns et al. [66] measured the line of $1s2p\,^1P_1 - 1s^2\,^1S_0$ in He-like Ar^{16+} for a testing in two-photon QED corrections with a relative uncertainty of 2×10^6. The experimental result was in good agreement with theoretical calculation, also with a subsequent 1.5×10^{-6} measurement by Kubicek et al. [67].

However, there is a discrepancy of 3σ between the measurement of the w transition energy in helium-like titanium and advanced QED theory by Chantler et al. [68]. They noted that there is a general trend of Z-dependent divergence between QED predictions and average experimental data in the w line of helium-like isoelectronic sequence for $Z > 20$ at the level of about five standard errors. The evidence of the low transition energy predicted systematically suggests that there is an error term in the calculations, or the missing term is much larger than currently expected in the three-body QED calculation. Researchers have launched a heated discussion furthered by Epp [70] and Chantler et al. [69]. It seems that the interpretation is not easy to find, and further research on experiments and theories is needed. Kubiček et al. [32] present relative measurements of the resonant line in He-like Fe^{24+}, which is in perfect agreement with the advanced BSQED predictions including screening QED terms. Another measurement on spectroscopy data of Fe^{24+} by Rudolph et al. [71] are also agreement with QED theory. These evidences refute the argument that there is an obvious deviation between experiment and advanced three-body QED theory.

In 2012, Amaro et al. [72] measured the magnetic dipole transition of $1s2s\,^3S_1 - 1s^2\,^1S_0$ in helium-like argon without any energy reference. The theoretical prediction from Artemyev et al. [73] is 1.6σ smaller than this experimental value. In 2017, our group [1] measured the transition of $1s2p\,^1P_1 \rightarrow 1s^2\,^1S_0$ in He-like argon ion and ransition of $1s2s^22p\,^1P_1 \rightarrow 1s^22s^2\,^1S_0$ in Be-like argon ion adopting the same experimental device: a DCS connected to an ECRIS, the "Source d'Ions Multichargés de Paris" (SIMPA) [74], jointly operated by the Laboratoire Kastler Brossel and the Institute des Nanosciences de Paris on the Université Pierre and Marie Curie campus.

For three-electron systems, a notable example, the $2s_{1/2} - 2p_{1/2}$ transition energy of lithium-like U^{91+} was measured about 280.645(15) eV with an 0.005% uncertainty by Beiersdorfer et al. [65]. This result, which is consistant with the theoretical value of 280.71(10) eV, displays relative QED effects of up to 15% with second-order QED correction of 6%. Our group made reference-free measurements of $1s2s2p\,^2P_{1/2,3/2} - 1s^22s\,^2S_{1/2}$ transitions in lithium-like sulfur and argon, and of the $1s2s2p\,^4P_{5/2} - 1s^22s\,^2S_{1/2}$ M2 transition in sulfur using a double flat-crystal spectrometer connected to an ECRIS.

A higher accuracy of 0.6 *ppm* was obtained in $1s^22s^22p\,^2P_{3/2} - 1s^22s^22p\,^2P_{1/2}$ transition of boron-like Ar^{13+} ions by Mackel et al. [75]. The theoretical wavelength obtained can be up to 441.261(70) (*nm*, air) by Artemyev et al. [76] and consistent with the experimental value of 441.2559(1) (*nm*, air), with two orders of magnitude difference in this forbidden transition. This transition determined by QED and relativity effects is considered an excellent candidate for accurate QED tests since the two states, $p_{1/2}$ and $p_{3/2}$, are the same in non-relativistic energies. It has recently been confirmed that the demonstration of sympathetic cooling of HCIs can significantly improve the accuracy of the experiment by Schmoger et al. [77].

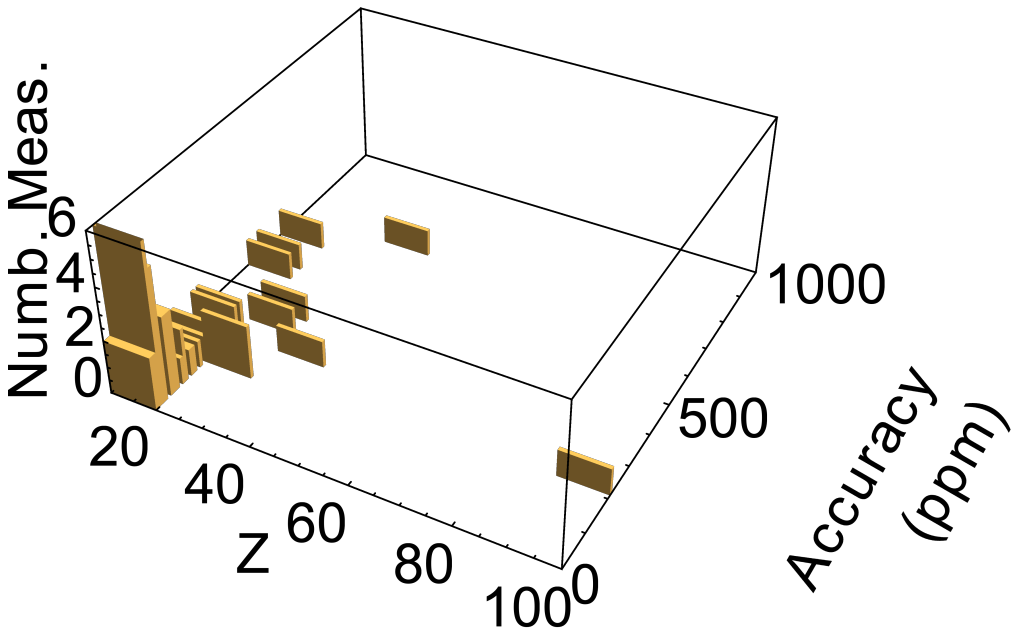

Fig. 1.4 *Histogram of the number of measurements for a given accuracy in part per million and the atomic number Z for two-electron ions. Figure from Indelicato P [15].*

The accuracy of both experiment and theory urgently needs to be improved to better test QED effects.

1.2.2 Muonic atoms

In the early days of modern physics, a series of simple atoms or ions composed only of hydrogen and after helium. Today, there are other atoms under investigation, such as the muonic atom, which is the same with hydrogen-like of two-body atoms. The orbital is much closer to the nucleus in the muonic atom than in the conventional atom with electrons, and the muonic levels are more susceptible to the nuclear structure. As a result, the muonic atom provides a unique opportunity to study the nuclear properties with high precision by spectroscopic methods, which is an approved tool for determining the nuclear radius [78].

The transition frequencies and Lamb shift of $2p_{1/2} - 2s_{1/2}$ in muonic hydrogen was measured with great accuracy by Antognini et al. [78]. The proton structural parameters were determined by the comparison with theoretical predictions. This theory is updated from the $2P-2S$ Lamb shift in the bound muonic hydrogen by Jentschura [79], using full Coulomb with Uehling potential of vacuum polarization. Indelicato [157] calculated the contributions to the Lamb shift at $n = 2$, fine structure interval and hyperfine structure of muonic hydrogen in the framework of nonrelativistic QED. A lot of contributions to the Lamb shift, fine structures, and hyperfine structures of muonic hydrogen have been evaluated in Refs. [80, 81, 82, 83, 84, 85]. Relativistic two-body effects of vacuum polarization shift and the nuclear charge distribution shape are also investigated. These radii play an important role in understanding the bound state QED of the atomic hydrogen spectrum. They also provide the information for testing quantum chromodynamics (QCD) in non-perturbative theory.

The proton radius puzzle has troubled the physics world for more than five years. The puzzles are that there exist 7 standard deviations between the experimental measurements in muonic atoms and normal atoms. This problem has led to abundant research by many groups in the world.

The discrepancy in muonic hydrogen energy of 0.42 meV is far outside the experimental uncertainty of ± 0.01 meV. Finding this difference between theoretical calculations and experimental measurements is the main driving force for further development of physics, leading to new physics to solve these deviations. In this sense, the QED method is currently regarded as the most advanced basic theory and serves as a blueprint for other new quantum field theory.

Many theoretical research in heavy muonic atom has been evaluated [86, 87, 88, 89]. Moreover, experimental measurement accuracy is increasing constantly [5, 90]. QED, recoil and nuclear polarization (NP) corrections limit the accuracy of muonic atom level energies. The calculation of the NP effect is difficult and imprecise. It is well-known to be the origin of the discrepancy between the experimental value and calculated value in the splitting energy of the $2p$ levels of Pb [92, 94].

Indelicato [157] evaluated the contributions of Lamb shift at $n = 2$ states, $2s$ hyperfine structure and fine structure interval in muonic hydrogen using accurate Dirac equation. Akihiro Haga et al. [89] reanalyzed muonic ^{90}Zr and ^{208}Pb atoms on nuclear polarization corrections using the full-electromagnetic nuclear response. They put forward to enhance the transverse nuclear polarization effects and considered newly established pygmy dipole resonances (PDR) employing collective models to reanalyze NP effects.

There are some experimental measurements for high-Z of muonic atoms, but the number of spectra measured is very small. The spectrum of the muonic ^{208}Pb is relatively complete and accurate. Bergern et al. [5] measured low-lying transition energies of muonic ^{208}Pb with a precision up to 11×10^{-6} using a Compton suppression spectrometer. There is ongoing experiment to perform muonic atom spectroscopy aiming at the precise measurement of level energies of radioactive ^{226}Ra with 0.2% relative precision at the Paul Scherrer Institute (PSI) [95].

1.3 Overview of methods

In order to achieve high precision calculation of atomic states, electron-electron correlation and QED contributions have been the focus of theoretical investigations. These effects can be evaluated using many methods, including the multiconfiguration Dirac-Fock method (MCDF), the relativistic configuration-interaction (RCI) method, relativistic many-body perturbation theory (RMBPT), the relativistic coupled-cluster method, S-Matrix method, and covariant-evolution-operator (CEO) method.

For establishing the correct relationship between multibody problems and QED method, it is necessary to begin with a no-pair Hamiltonian.

MCDF

Dirac-Fock approximation, verified as a natural and well-defined multi-body computing starting point, is based on the relativistic equivalent of the Hartree-Fock. Electrons are in the independent particle approximation, and their wave functions are treated in the Coulomb field of the nucleus and the spherical mean-field from the electrons. This method is a powerfully modern tool for relativistic atomic calculations based on the Dirac-Fock Hamiltonian and the potential approach. The calculations can be divided into two important parts. One is the Slater determinant computing all angular integrals including one-electron integrals, Breit operator, and Coulomb interaction. Another is the radial part being responsible for solving the given MCDF equations and calculating the large and small component of the wavefunctions to probe atomic properties. The foundational idea of this method is that wavefunctions are used to represent the atomic states. These functions are linear combinations of a number of configuration state functions, which are sums of products of single-electron Dirac orbitals. This method is developed by Grant and co-workers [106, 251], Desclaux [105], Gorceix and Indelicato [110].

RMBPT

In relativistic many-body perturbation theory [96, 97], the Coulomb term is replaced by a model of one-electron localized potential. This provides a complete set of single-electron eigenfunctions, including continuous eigenfunctions. Then, Breit interaction and the difference between the Coulomb term and the model potential are treated as a perturbation expansion. This method is very efficient in considering virtual core excitations.

RCI

In relativistic configuration-interaction (RCI) method [98], the total CI wavefunction $\Psi(\gamma JP)$ can be written in a linear combination of configuration state functions(CSF) as

$$\Psi(JPM) = \sum_n c_n \Phi_n(\gamma_n JPM), \tag{1.1}$$

with a total parity P, angular momentum J and angular momentum projection M. Here $\Phi(\gamma_n JPM)$ is a CSF and c_n is an expansion coefficient. The matrix elements of the DCB Hamiltonian between the CSFs,

$$\{H_{ns}\} \equiv \{\langle \gamma_n PJM \,|H_{DCB}|\, \gamma_s PJM\rangle\}\,. \tag{1.2}$$

The RCI method deals with the secular equation for a Hamiltonian matrix with respect to CSF's. This method is very successful for the explicit treatment of valence-valence interactions. This method is often used in conjunction with other methods.

Relativistic coupled-cluster

The first few terms of relativistic many-body perturbation series are sufficient for highly charged ions but are less suitable for neutral atoms, where higher orders of corrections are not negligible. It is more complex for higher-order expressions. The direct perturbation studies rarely go beyond second-order corrections or the third-order energy correction. The most promising of methods is the coupled-cluster (CC) formalism [97]. This theory takes into account correlations to all orders as a perturbation in every level of particle-hole excitation. Size extensivity is important for accurate calculations of heavy elements with significant relativistic effects. This method has high-accuracy electron correlation and is widely used in non-relativistic atomic and molecular calculations [99].

S-Matrix

In S-matrix theory, developed by Sucher [100] and used by Sapirstein and Cheng [26], the energy levels of atoms or ions are related to matrix elements of an operator which evolves the atom or ion from t $= -\infty$ to t $= \infty$,

$$S_{\epsilon,\lambda} = T\left(e^{-i\lambda\int dt e^{-\epsilon|t|}H(t)}\right), \tag{1.3}$$

through $E = E_0 + \Delta E$, where

$$\Delta E = \lim_{\epsilon\to 0}\frac{i\epsilon}{2}\lim_{\lambda\to 1}\frac{\partial}{\partial\lambda}\ln\langle\Phi_0|S_{\epsilon,\lambda}|\Phi_0\rangle, \tag{1.4}$$

and where E_0 represents the energy of the atom at times t $= -\infty$ and t $= \infty$. The interaction Hamiltonian is suppressed by the adiabatic damping factor ϵ. For the Li-like isoelectronic sequence we are treating here, the state $|\Phi_0\rangle$ can be represented by,

$$|\Phi_0\rangle = a_\nu^\dagger|0_c\rangle, \tag{1.5}$$

where ν is a valence electron and $|0_c\rangle$ is a filled helium-like core. The wave functions obeying the Dirac equation can be written as,

$$\left[c\vec{\alpha}\cdot\vec{p} + (\beta-1)mc^2 + U(r)\right]\Psi_n(\vec{x}) = \epsilon_n\Psi_n(\vec{x}). \tag{1.6}$$

in a spherically symmetric potential $U(r)$.

CEO method

One of the main problems in extending the energy-dependent perturbation theory to include electron correlation is that most methods have structures that are completely different from the energy-independent perturbation theory, which makes it difficult to exploit the latter's sophisticated methods. An available method of the CEO method developed by Lindgren Salomonson and coworkers [101, 102, 103], has a structure which is quite similar to standard energy independent MBPT. In this way, the electron correlation can be processed for the first time as an energy-dependent interaction of any order of QED type. CEO, which represents the time evolution of the relativistic wave function or state vector, can be constructed.

Chapter 2

Context and principle

The goal of this chapter is to give a general introduction to the theoretical context of our calculations. A muon can be regarded as an electron with heavy mass, so in this chapter, we only introduce the case of electronic ions and the corresponding corrections. I will present the one-loop and two-loop QED corrections and the calculations of transition energies in one and three electron ions. We also present the improvements in vacuum polarization to all orders and an effective operator approach for self-energy screening corrections.

2.1 MCDF-procedure

The MCDF method [106, 105, 110, 251] is intended to provide an approximate solution to the relativistic multibody problem, beyond the single-particle approximation. It is introduced as a direct extension of the Hartree-Fock method. This method is applied in our MCDFGME program by Desclaux [105] and developed by Indelicato [156, 177, 157].

2.1.1 Dirac equations

For an N-electron atom, the relativistic total Dirac-Coulomb-Breit (DCB) Hamiltonian is approximated by

$$H = \sum_i H_D(i) + \sum_{i<j} \left[\frac{1}{r_{ij}} + H_B(ij) \right], \tag{2.1}$$

Here $i, j = 1, \ldots, N$ are the numbers of electrons, $H_D(i)$ is the Dirac Hamiltonian of one-particle,

$$H_D(i) = c\boldsymbol{\alpha}_i \cdot \boldsymbol{p}_i + (\beta - 1)mc^2 + V_N(r), \tag{2.2}$$

Here, we make use of atomic units($\hbar$=e=m=1;$c = 1/\alpha$). $\boldsymbol{p}_i$ represents the momentum operator, and $\boldsymbol{\alpha}$ and β are the Dirac 4×4 matrices,

$$\boldsymbol{\alpha}_i = \begin{pmatrix} 0 & \boldsymbol{\sigma}_i \\ \boldsymbol{\sigma}_i & 0 \end{pmatrix}, \beta = \begin{pmatrix} I & 0 \\ 0 & -I \end{pmatrix}, \tag{2.3}$$

where σ_i represents the 2×2 Pauli matrices. I is the second-order unit matrix. $V_N(r)$ represents the nucleus Coulomb potential. This results in the Coulomb field being included in all orders when doing the evaluation of relevant quantities. The two-body part $\frac{1}{r_{ij}}$ of Eq. (2.1) represents Coulomb repulsion, H_B is the Breit parts (magnetic and retardation interaction) of the electron-electron interaction (we will introduce this part in section 2.3 below).

When evaluating the Dirac equation with finite-size nuclear corrections, QED effects and recoil effects, the energy of a given level is written [15]

$$\begin{aligned} E_{n,\kappa}(Z,A) &= E^D_{n,\kappa}(Z) + E^{(1)}_{QED}(n,\kappa,Z) + E^{(2)}_{QED}(n,\kappa,Z) \\ &\quad + E^{Nuc.}_{n,\kappa}(Z,A) + E^{Rec.}_{n,\kappa}(Z,M_A) \\ &= E^D_{n,\kappa}(Z) + \frac{\alpha}{\pi}\frac{(Z\alpha)^4}{n^3}F^{(1)}_{n,\kappa}(Z\alpha) + \frac{\alpha}{\pi}\frac{(Z\alpha)^4}{n^3}F^{(2)}_{n,\kappa}(Z\alpha) \\ &\quad + E^{Nuc.}_{n,\kappa}(Z,M_A) + E^{Rec.}_{n,\kappa}(Z,M_A) \end{aligned} \tag{2.4}$$

where $E^D_{n,\kappa}(Z)$ represents the solution of the Dirac equation, $E^{(1)}_{QED}(n,\kappa,Z)$ the first order of self-energy corrections and vacuum polarization corrections, and $E^{(2)}_{QED}(n,\kappa,Z)$ the summation of two-loop corrections. The finite nuclear correction is represented by $E^{Nuc.}_{n,\kappa}(Z,A)$, which can include nuclear polarization. The remaining correction $E^{Rec.}_{n,\kappa}(Z,M_A)$ is the recoil effects. These contributions will be introduced separately.

2.1.2 Wave functions

The total wavefunction of N-electron can be obtained by,

$$H\Psi_{\Pi,J,M}(r_1,\ldots,r_m) = E_{\Pi,J,M}\Psi_{\Pi,J,M}(r_1,\ldots,r_m), \tag{2.5}$$

The MCDF method is defined by the specific choice of function to solve Eq. (2.5) with the parity Π, total angular momentum J, and its projection M on the z axis of J_z as a linear combination of configuration-state functions (CSFs),

$$|\Psi_{\Pi,J,M}\rangle = \sum_{\nu=1}^{NCF} c_\nu |\nu\Pi JM\rangle, \tag{2.6}$$

where NCF is the number of configurations and c_ν are the configurations mixing coefficient. The label ν is all other values that are explicitly required to define CSF. As with many self-consistent field methods, the starting point for constructing an N-electron wave function is the central field of single electron orbital. In the relativistic case, the spin-orbital coupling is explicitly introduced in the Dirac Hamiltonian, so each Dirac four-spinor can be expressed as,

$$\Phi_{n\kappa m}(r,\theta,\varphi) = \frac{1}{r}\begin{bmatrix} P_{n\kappa}(r)\,\chi_{\kappa m}(\theta,\varphi) \\ iQ_{n\kappa}(r)\,\chi_{-\kappa m}(\theta,\varphi) \end{bmatrix}. \tag{2.7}$$

These spinors are simultaneous eigenfunctions of the parity operator Π, the total angular momentum operator $\boldsymbol{J^2}$ and its z-component. $P_{n\kappa}(r)$ and $Q_{n\kappa}(r)$ are large and

small radial components of the wave function respectively, n is the principal quantum number, and the quantum number kappa is defined by,

$$\kappa = \begin{cases} -l-1 & \text{if } j = l+1/2 \\ l & \text{if } j = l-1/2 \end{cases}. \tag{2.8}$$

In this expression, l represents the quantum number of the orbital and the total angular momentum j is related of

$$j = |\kappa| - 1/2. \tag{2.9}$$

The functions $\chi_{\kappa m}$ in Eq. (2.7) are the two component Pauli spherical spinors,

$$\chi_{-\kappa m}(\theta, \varphi) = \sum_{\sigma=\pm 1/2} \langle lm - \sigma\sigma | l\ 1/2\ jm \rangle\, Y_l^{m-\sigma}(\theta, \varphi)\, \phi^{\sigma}, \tag{2.10}$$

which include a spherical harmonic,

$$\phi^{1/2} = \begin{pmatrix} 1 \\ 0 \end{pmatrix}, \quad \phi^{-1/2} = \begin{pmatrix} 0 \\ 1 \end{pmatrix}. \tag{2.11}$$

For a N-electron system, a CSF is a linear combinations of Slater determinants of Dirac four-spinors,

$$|\nu \Pi J M\rangle = \sum_{i=1} d_i \begin{vmatrix} \Phi_1^i(r_1) & \cdots & \Phi_N^i(r_1) \\ \vdots & \ddots & \vdots \\ \Phi_1^i(r_N) & \cdots & \Phi_N^i(r_N) \end{vmatrix}. \tag{2.12}$$

The integro-differential equation can be reduced to [108]

$$\begin{aligned} &\begin{pmatrix} \frac{d}{dr} + \frac{\kappa_i}{r} & -\frac{2}{\alpha} + \alpha V_i(r) \\ -\alpha V_i(r) & \frac{d}{dr} - \frac{\kappa_i}{r} \end{pmatrix} \begin{pmatrix} P_i(r) \\ Q_i(r) \end{pmatrix} \\ &= \alpha \sum_j \lambda_{i,j} \begin{pmatrix} Q_j(r) \\ -P_j(r) \end{pmatrix} + \begin{pmatrix} X_Q^i(r) \\ X_P^i(r) \end{pmatrix} \end{aligned} \tag{2.13}$$

in the spherically symmetric potential, the sum of the direct Dirac-Fock potential and the nuclear potential represented by $V_i(r)$, and exchange potentials represented by $\left(X_Q^i(r), X_P^i(r)\right)$. The Lagrange parameter is $\lambda_{i,j}$.

2.1.3 Numerical methods

Most numerical methods for solving relativistic Hartree-Fock equations are derived from long-known non-relativistic cases [107]. Integral differential equations can be solved using an iterative process. Each step reduces the integral differential equation to a simple differential equation by considering the direct and exchange potential term as a given source function, which is calculated by the wave function obtained in the previous step. The iterative process then continues until a given precision is achieved between two successive iterations.

The pair of two first-order coupled differential equations in Eq.(2.13) is solved by a five-point predictor-corrector method [105, 108, 109] for the one body system and by a mixed predictor-corrector and finite difference method for the many-electron system. A linear mesh step in the variable t is defined by,

$$t_n = \ln\left(\frac{r_n}{r_0}\right) + ar_n. \tag{2.14}$$

with $t_n = t_0 + nh$, and the first point of the mesh gives $t_0 = ar_0$, corresponding to $n = 0$. The expression can also be inverted by inverting equation to obtain,

$$\begin{aligned} r_n &= \frac{W\left(ar_0 e^{t_n}\right)}{a}, \\ \frac{dr_n}{dt_n} &= \frac{W\left(ar_0 e^{t_n}\right)}{a\left[1 + W\left(ar_0 e^{t_n}\right)\right]}. \end{aligned} \tag{2.15}$$

This yield the defining equation for the W function of $f(W) = W(z)e^{W(z)}$, which represents the Lambert or the product logarithm function. The differential equation and wave function between 0 and r_0 are represented by a ten-term series expansion. Usually the first point is decided as $r_0 = 10^{-2}/Z$ and $h = 0.025$. We use the values as low as $r_0 = 10^{-7}/Z$ and $h = 0.002$ to get the best accuracy for muonic atoms. The first-order contribution to the eigenvalue is given by a mean value of an operator $\mathcal{O}$ [157],

$$\begin{aligned} \Delta E_{\mathcal{O}} &= \int_0^{\infty} dr \left[P(r)^2 + Q(r)^2\right] \mathcal{O}(r) \\ &= \int_0^{r_0} dr \left[P(r)^2 + Q(r)^2\right] \mathcal{O}(r) \\ &\quad + \int_{r_0}^{\infty} dt \frac{dr}{dt} \left[P(r)^2 + Q(r)^2\right] \mathcal{O}(r). \end{aligned} \tag{2.16}$$

This method has the advantage of being fast and accurate.

2.2 Nuclear models

Several possible models are provided for the nuclear potential. One is that the nucleus is considered to be a point charge. When it is mandatory to go beyond the point nucleus approximation for the inner shell of heavy atoms, a finite nuclear charge distribution model should be used instead of a pointlike nucleus. For example, a uniform spherical model with radius R can be assumed as the nuclear charge distribution. The nuclear potential is given by [108]

$$V_{nuc}(r) = \begin{cases} \frac{-eZ}{2R_0}\left[3 - \frac{r^2}{R_0^2}\right] & \text{if} \quad r \le R_0 \\ \frac{-eZ}{r} & \text{if} \quad r > R_0 \end{cases} \tag{2.17}$$

In the present work, a realistic description of nucleus charge distribution is given by the two-parameter Fermi model,

$$\rho_N(R) = \rho_0(1 + exp[(R - c)/a])^{-1}, \tag{2.18}$$

with normalization(uniform nuclear charge density),

$$\rho_0 = \frac{3Ze}{4\pi R_0^2}, \tag{2.19}$$

where the half-density radius is c, and R_0 is the radius of the uniform model having the same rms radius as the Fermi model,

$$R_0 = \sqrt{\frac{5}{3}\langle R^2 \rangle}, \tag{2.20}$$

Here t is the skin-thickness parameter, which indicates the distance over which the density falls from 90% to 10% of its central value. It is related to the Fermi parameters by the expression of

$$t = 4a \ln 3. \tag{2.21}$$

The $t = 2.30$ fm value is used in our calculations, and c is calculated by the formulas given in Ref. [111]. The nuclear radius of all elements come from experimental values. Since the detailed charge distribution is a key parameter for very heavy atoms, the default option for our calculations is to use a uniform charged sphere for atomic numbers below 45 and the Fermi distribution for $Z > 45$.

To the lowest order, the nucleus finite mass effect to the energy can be roughly corrected by reducing the mass. The reduced mass can be expressed by the following formula,

$$\mu = \frac{m_e M_{nuc}}{m_e + M_{nuc}}. \tag{2.22}$$

where M_{nuc} is the mass of the nucleus.

2.3 Electron-electron interaction

The effective electron-electron interaction operator is derived from the Feynman diagram in Fig. 2.1 based on a single photon exchange approximation. This operator is gauge dependent, and the contribution to the energy is also gauge dependent [110]. The Coulomb gauge should be used to avoid introducing spurious effects.

Here, we will describe the three common parts of electron-electron interactions, namely Coulomb, magnetic and delayed interactions. The corresponding interactions are shown in Fig. 2.1(b), 2.1(c) and 2.1(d), respectively. The expression representing the operator of the interaction between electrons i and j in the Coulomb gauge [156] (formulas are given in atomic units) is

$$g_{ij} = g_{ij}^{Coul} + g_{ij}^{Mag} + g_{ij}^{Ret}, \tag{2.23}$$

where the Coulomb interaction is

$$g_{ij}^{Coul} = \frac{1}{r_{ij}}, \tag{2.24}$$

The magnetic (Gaunt) interaction is

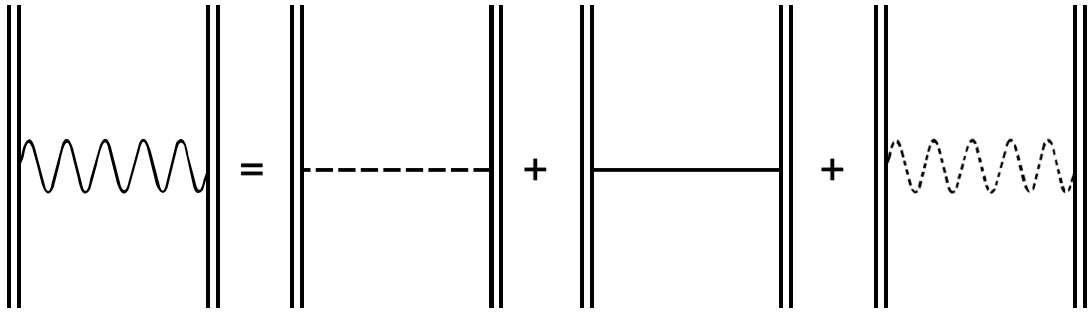

Fig. 2.1 *Feynman diagrams for the electron-electron interaction. The double lines represent the Coulomb-bound electron propagator. The wavy lines represent the virtual photon propagator.*

$$g_{ij}^{Mag} = -\frac{\boldsymbol{\alpha_1} \cdot \boldsymbol{\alpha_2}}{r_{ij}}, \tag{2.25}$$

The retardation operator is

$$\begin{aligned} g_{ij}^{Ret} = &- \boldsymbol{\alpha_1} \cdot \boldsymbol{\alpha_2} \frac{\cos(\omega_{ij} r_{ij}) - 1}{r_{ij}} \\ &+ (\boldsymbol{\alpha_1} \cdot \boldsymbol{\partial_1}) (\boldsymbol{\alpha_2} \cdot \boldsymbol{\partial_2}) \frac{\cos(\omega_{ij} r_{ij}) - 1}{\omega_{ij}^2 r_{ij}}. \end{aligned} \tag{2.26}$$

The Breit operator is

$$H_B(ij) = -\frac{\boldsymbol{\alpha_1} \cdot \boldsymbol{\alpha_2}}{r_{ij}} \cos(\omega_{ij} r_{ij}) + (\boldsymbol{\alpha_1} \cdot \boldsymbol{\partial_1}) (\boldsymbol{\alpha_2} \cdot \boldsymbol{\partial_2}) \frac{\cos(\omega_{ij} r_{ij}) - 1}{\omega_{ij}^2 r_{ij}}. \tag{2.27}$$

including the magnetic and the retardation interaction due to the finite value of the speed of light. The value of ω_{ij} represents the photon exchanged energy, $\boldsymbol{\alpha_i}$ are the Dirac matrices and r_{ij} represents the interelectronic distance. The zero-order energy is calculated by the Coulomb operator and a single configuration of the expansion from the wave function, which leads to a Coulomb contribution. We can obtain the first order of the magnetic and the retarded corrections by adopting a single-configuration wavefunction.

One difficulty is the gauge dependent of the electron-electron interaction. When the electron-electron operator is solved with the Dirac equation, the gauge invariance is lost. In QED calculations, the diagrams provide gauge-invariant results. Another difficulty is that the value of ω_{ij} can be well defined in the independent particle approximation. However, it can't decide what value to be used when evaluating the interaction operator between the correlation orbitals. Therefore there is always a problem of using the magnetic and retardation operator to evaluate the correlation energy. Our MCDFGME code allows this, which can result in a very large contribution to the correlation energy at heavy elements. This method is described by Indelicato [112]. The correlation energies are expanded in both expansions of $1/Z$ and $Z\alpha$ [113], and the nonrelativistic correlation energy is expressed as [156]

$$\Delta E_{corr}^{NR} = \Delta E_0 + \Delta E_1 \frac{1}{Z} + \Delta E_2 \frac{1}{Z^2} + \Delta E_3 \frac{1}{Z^3} + \cdots . \tag{2.28}$$

The exact nonrelativistic calculations for the ΔE_0 term come from Horak et al. [114]. The higher-order terms contribution, which is much smaller, is fitted to the nonrelativistic limit of our MCDF calculations. This method is used for the calculations.

2.4 QED Corrections

Quantum Electrodynamics (QED) describes all possible events related to charged particles as the relativistic quantum field theory of electromagnetic forces. The model of the QED operator is divided into three parts,

$$V^{QED} = V^{SE} + V_{Uehl} + V_{WK}. \tag{2.29}$$

Here, V^{SE} is the self-energy operator, V_{WK} is the Wichmann–Kroll part of vacuum polarization and V_{Uehl} is the Uëhling part of the vacuum polarization. The two parts of Uëhling and Wichmann–Kroll are local potentials. Therefore their prescription is quite forthright.

In low Z systems, the QED contributions are calculated according to the expansion in two small parameters α and $Z\alpha$. The parameter $Z\alpha$ is not small for high-Z systems. Therefore, the calculations based on the parameter $Z\alpha$ cannot be used as an expansion and should be calculated to all orders in $Z\alpha$. The developments of nonperturbative QED methods are performed by Indelicato [157].

2.4.1 One-loop QED correction

Fig. 2.2 depicts the first-order (one-loop) radiative corrections in α by Feynman diagrams. In these diagrams, the double lines signify an electron propagating in the external Coulomb field of the nucleus, and the wavy line is the photon propagator. Part (a) is the so-called self-energy, in which a photon is emitted and absorbed again by the bound electron. Part (b) indicates the vacuum polarization in which the photon mediating the interaction between the bound electron and the nucleus creates an electron-positron pair. The virtual electron-positron pair causes a change of the Coulomb potential and thus leads to energy shifts of the bound electrons.

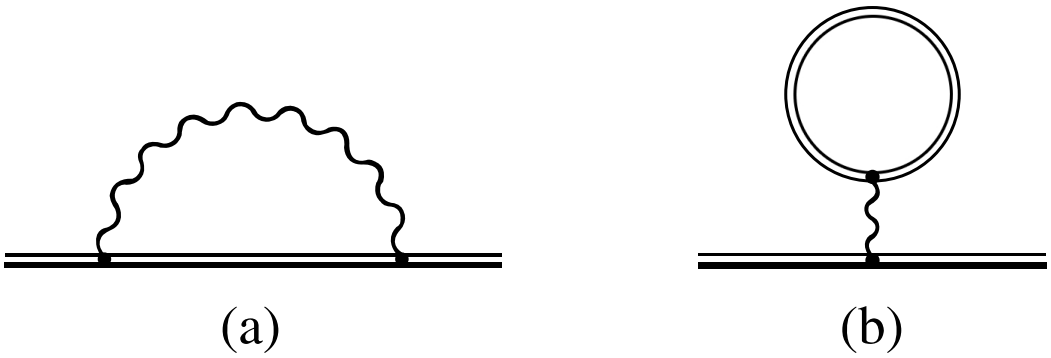

Fig. 2.2 *Feynman diagrams representing: one-loop self-energy (a) and vacuum-polarization (b) radiative corrections. The double line indicates an electron propagating in the Coulomb field of the nucleus and the wavy line signifies the photon propagator*

The one-loop self-energy contribution can be expressed as

$$\Delta E_{SE} = \left(\frac{\mu}{m_e}\right)^3 \frac{\alpha}{\pi} \frac{(Z\alpha)^4}{n^3} F(Z\alpha)\, m_e c^2, \tag{2.30}$$

where $F(Z\alpha)$ is the dimensionless function,

$$\begin{aligned} F(Z\alpha) =& A_{41} \ln(Z\alpha)^{-2} + A_{40} + A_{50}(Z\alpha) \\ &+ A_{62}(Z\alpha)^2 \ln^2(Z\alpha)^{-2} + A_{61}(Z\alpha)^2 \ln(Z\alpha)^{-2} \\ &+ G_{SE}(Z\alpha)(Z\alpha)^2. \end{aligned} \tag{2.31}$$

where $G_{SE}(Z\alpha)$ contains all remainder terms of higher-order expansion in $Z\alpha$ and the values of the coefficients A_{ij} have been listed in Ref. [115].

These diagrams must be calculated to all orders in $Z\alpha$ for highly charged ions. Desiderio and Johnson [116] first performed the nonperturbative calculation to the self-energy contribution. The first high-precision evaluation to the self-energy correction is due to Mohr [282] for the 1s level at medium and high-Z. Jentschura et al. [17, 18] performed all-order calculations at low-Z, which are very difficult, because the correction of $E^{(1)}_{QED}(n, \kappa, Z)$ from QED is formally of order $\frac{\alpha}{\pi} mc^2$ and so terms of order 1, $Z\alpha$, $(Z\alpha)^2$ and $(Z\alpha)^3$ have to be cancelled, requiring very large accuracy.

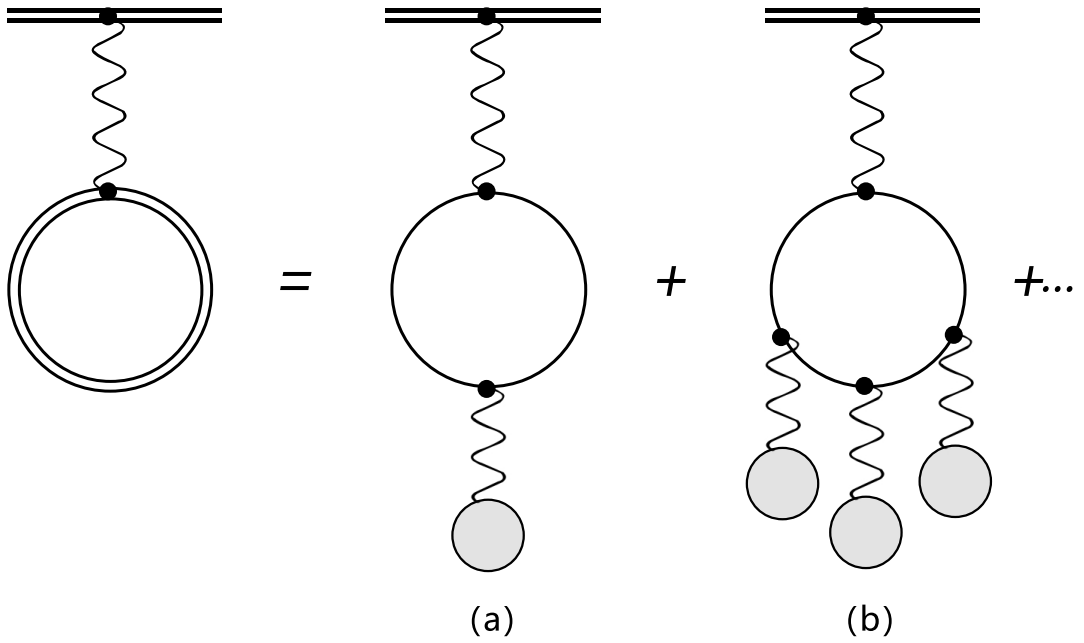

Fig. 2.3 *Feynman diagrams corresponding to the full vacuum polarization contribution and expansion in $Z\alpha$. One-loop vacuum polarization of the free electron propagator(single line). (a): Uëhling potential. (b): Wichmann and Kroll correction. Figure from Indelicato P [157].*

Indelicato P [157] evaluate the all order vacuum polarization contribution by numerical solution from the Dirac equation. Fig. 2.3 gives Feynman diagrams related to the full vacuum polarization correction. The double line represents the wavefunction in the external Coulomb field of the nucleus, and the wavy line corresponds to the Coulomb photon propagator. The single circle indicates a free electron-positron pair. The gray circle is the interaction with the nucleus. The nucleus, with a charge Ze, is considered to be a static point particle.

The Uëhling part play an important role in the one-loop vacuum polarization correction [124]. The Uëhling approximation considers the virtual e^+e^- pair to leading order of the coupling constant $Z\alpha$. The Uëhling potential, which corresponds to Fig. 2.3(a) and represents a leading contribution in the QED, is given by

$$V_{11}(r) = -\frac{2\alpha Z\alpha}{3mr}\int_0^\infty dr' r' \rho(r') \left[K_0\left(2m\left|r-r'\right|\right) - K_0\left(2m\left|r+r'\right|\right)\right], \tag{2.32}$$

where

$$K_0(x) = \int_1^\infty dt e^{-xt}\left(\frac{1}{t^3}+\frac{1}{2t^5}\right)\sqrt{t^2-1}. \tag{2.33}$$

is a modified Bessel function. When deducing the Uëhling potential, it is assumed that

the virtual electrons and the positrons are free to propagate. The remaining part is called the Wichmann–Kroll corrections, which include all terms of higher-order $Z\alpha, \sim (Z\alpha)^n$ with $n \geq 3$. Fig. 2.3(b) is higher orders of the Wichmann and Kroll corrections, which represent the main order effect of the distortion of the electron and positron wavefunctions in the nuclear Coulomb field. The explicit expression for the $\alpha(Z\alpha)^3$ term by Wichmann and Kroll [158] is,

$$V_{13}(r) = \frac{\alpha(Z\alpha)^3}{\pi r}\int_0^\infty dt\, e^{-2tr}\frac{1}{t^4}\left\{-\frac{1}{12}\pi^2\sqrt{t^2-1}\,\Theta(t-1) + \int_0^t dx\sqrt{t^2-x^2}\,f(x)\right\}. \tag{2.34}$$

in the Laplace transform of the charge density. For all r, $V_{13}(r)$ is repulsive, and the energy shift is positive, thereby reducing the binding due to the attractive Coulomb and Uëhling potentials. The evaluation of the Wichmann–Kroll contribution is not an easy task. The first nonperturbative calculations of the Wichmann-Kroll part were calculated by Soff and Mohr [11] to all orders in $Z\alpha$. The most accurate results of the vacuum-polarization diagram were obtained in Ref. [121].

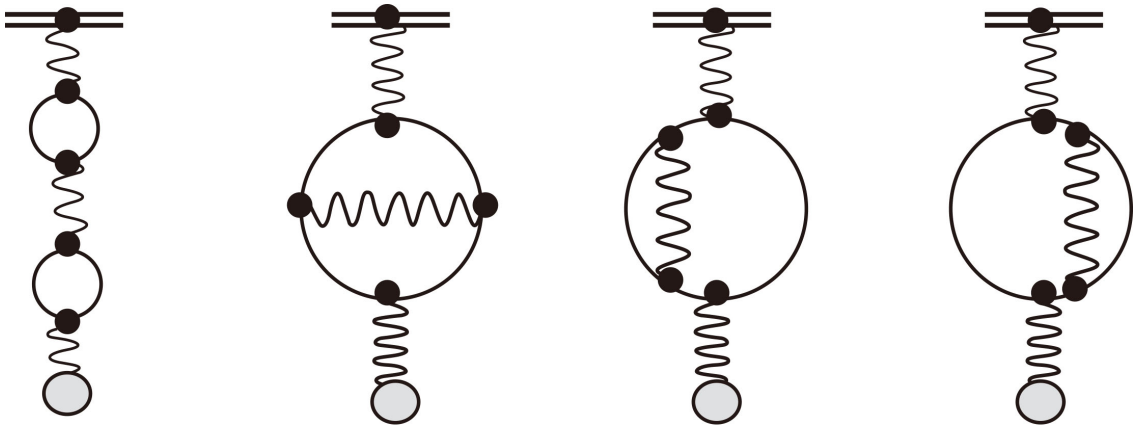

Fig. 2.4 *Feynman diagrams included in the Källén and Sabry $V_{21}(r)$ potential. Figure from Indelicato P [157].*

Fig. 2.4 corresponds to the Källén and Sabry potential with a fourth-order potential. The expression of this potential is

$$V_{21}(r) = -\frac{\alpha^2 Z\alpha}{m\pi r}\int_0^\infty dr' r'\rho(r')\left[L_0\left(2m\left|r-r'\right|\right) - L_0\left(2m\left|r+r'\right|\right)\right], \tag{2.35}$$

for a spherically symmetric nuclear charge. The series expansion for small r was provided by Blomqvist [159] and Mohr PJ et al. [308] to evaluate the function L_0 with very good precision.

The term named "VP iteration" correspond to Fig. 2.5, which can be expressed by $(\frac{\alpha}{\pi})^2(Z\alpha)^2$ and $(\frac{\alpha}{\pi})^3(Z\alpha)^2$ respectively. The Uëhling potential can be easily put in the Dirac Eq. (2.13) when it is solved numerically. This is equivalent to getting an accurate solution by inserting any number of vacuum polarization.

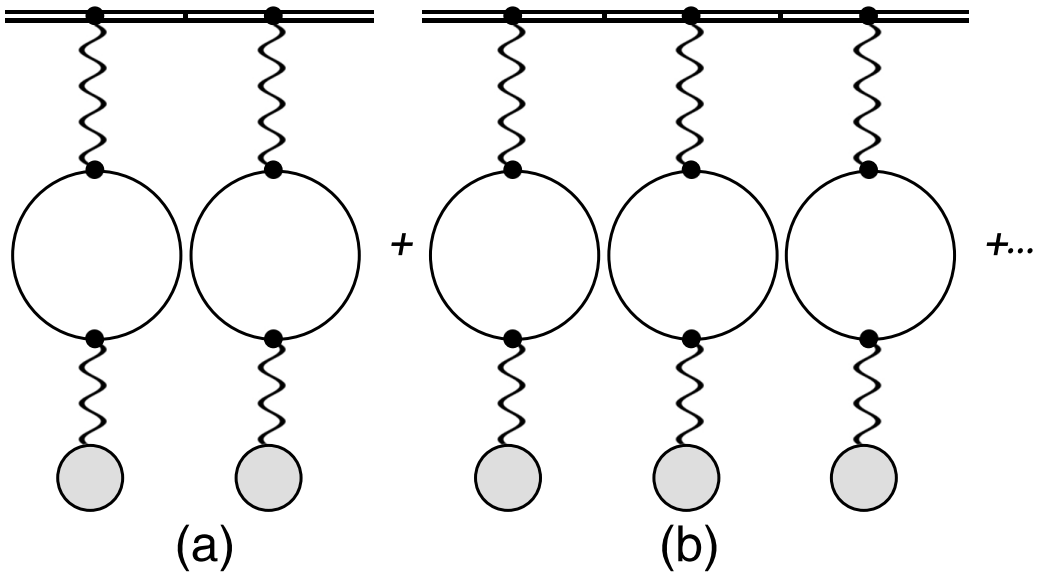

Fig. 2.5 *Feynman diagrams obtained when the Uëhling potential is added to the nuclear potential in the Dirac equation. Figure from Indelicato P [157].*

Since the vacuum polarization is included in the Dirac equation potential, the calculation of all the energy performed by using the numerical wavefunction as a disturbance includes the contribution of the higher-order. This represents that a wavefunction with a bound propagator with one or more vacuum polarization insertions can replace the original wave function. For instance, when the Källén and Sabry corrections are evaluated in this way, they include corrections of the type shown in Fig. 2.6. These corrections are part of the three-loop corrections from [160].

2.4.2 Two-loop QED correction

The two-loop QED effect is represented by

$$\Delta E_{QED2} = \left(\frac{\mu}{m_e}\right)^3 \left(\frac{\alpha}{\pi}\right)^2 \frac{(Z\alpha)^4}{n^3} F_{QED2}\,(Z\alpha)\, m_e c^2, \tag{2.36}$$

The dimensionless function $F_{QED2}\,(Z\alpha)$ is represented as an expansion in the term of $Z\alpha$ and $\ln(Z\alpha)$,

$$\begin{aligned} F_{QED2}\,(Z\alpha) =& B_{40} + B_{50}(Z\alpha) + B_{63}(Z\alpha)^2 \ln^3(Z\alpha)^{-2} \\ &+ B_{62}(Z\alpha)^2 \ln^2(Z\alpha)^{-2} + B_{61}(Z\alpha)^2 \ln(Z\alpha)^{-2} \\ &+ B_{60}(Z\alpha)^2 + \cdots . \end{aligned} \tag{2.37}$$

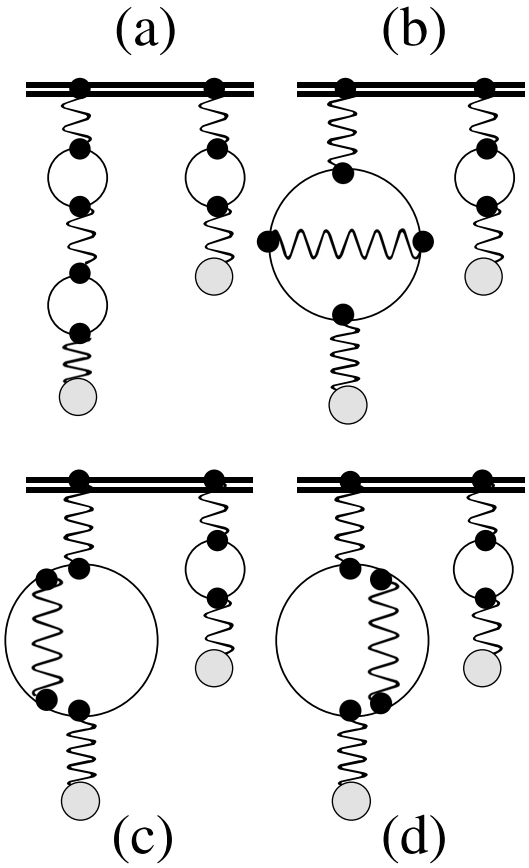

Fig. 2.6 *Lower-order Feynman diagrams included in the Källén and Sabry $V_{21}(r)$ potential, when the Uëhling potential is included in the differential equation. Figure from Indelicato P [157].*

Fig. 2.7 shows the two-loop (second-order) QED corrections in α^2 by Feynman diagrams. The two-loop QED contribution can be divided,

$$E_{QED2} = E_{SESE} + E_{VPVP} + E_{SEVP} + E_{S(VP)E} + E_{KS}, \tag{2.38}$$

where the two-loop self-energy contribution E_{SESE} is shown in Figs. 2.7(a)-2.7(c). Two kinds of Green function methods [139] can easily derive the corresponding formal expressions. The two-loop self-energy is taken from Refs. [287, 288, 289, 24, 290, 291, 292, 293]. Ones have performed a complete evaluation of the two-loop self-energy contribution in the parameter $Z\alpha$ for ground states and excited states of hydrogenlike ions. Since this correction is a major factor in the uncertainty of the theoretical ground-state Lamb shift in these systems, numerical accuracy is increased by an order of magnitude. At the same time, the improvements in extension to lower Z has also been performed.

The crossed and mixed diagrams of SEVP and S(VP)E shown in Figs. 2.7(d)–2.7(f) are obtained from Ref. [291]. In view of the first-order perturbation of vacuum polarization potential, the self-energy can be modified by the vacuum polarization in the Coulomb

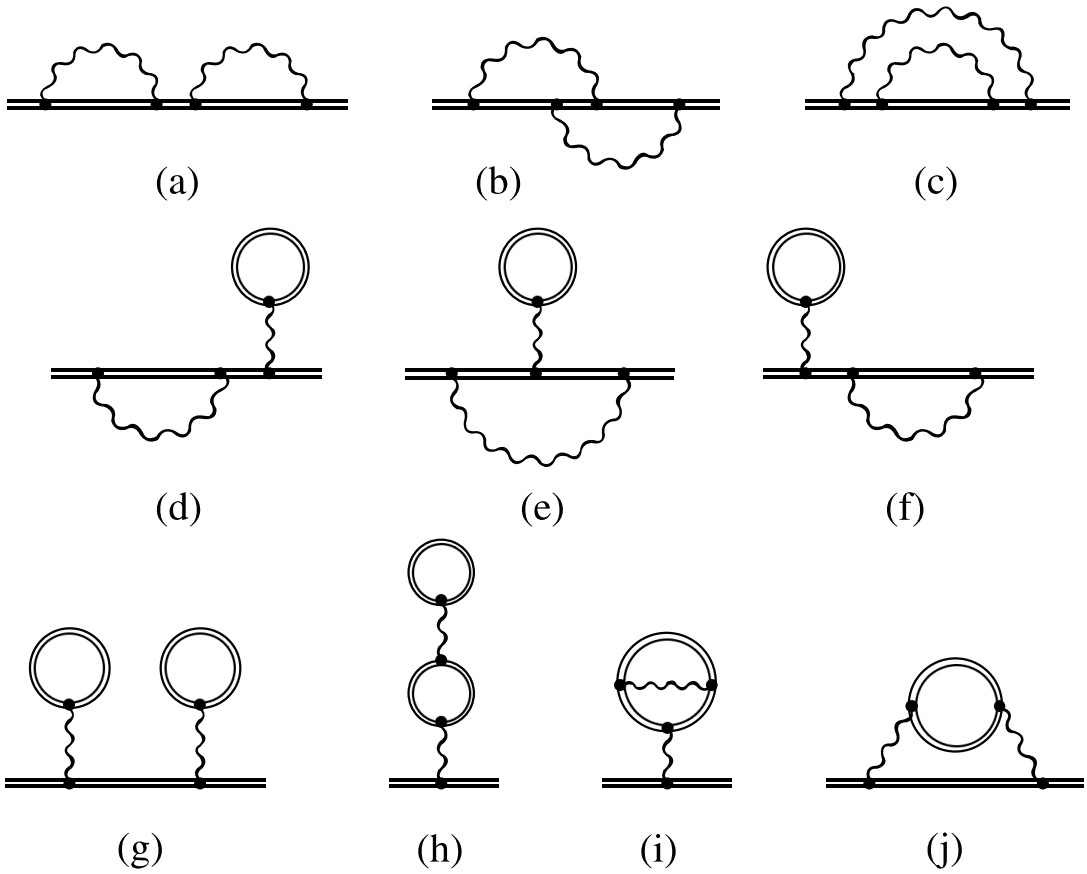

Fig. 2.7 *Feynman representing of QED: two-loop diagrams. (a), (b), (c): two-loop self-energy. (d), (e), (f): SE-VP correction. (j): S(VP)E correction. (h), (i): Källén and Sabry correction. (g): loop after loop vacuum polarization. Double line indicates an electron propagating in the Coulomb nuclear field.*

potential, where the SEVP correction can be obtained. It is the summation of the irreducible contributions, the reducible contributions, and the vertex contributions, which are given by perturbations of the reference-state wave functions, the binding energy, and the electron propagator, respectively. The insertion of vacuum polarization into the self-energy photon line is called S(VP)E correction, where the leading part of $Z\alpha$ is obtained under the free-loop approximation. Since it is a difficult problem to perform all-order calculations of S(VP)E correction beyond the free-loop approximation, this correction is just within the free-loop approximation.

The two-loop vacuum-polarization corrections are obtained from Refs. [291, 157], represented by the diagrams in Figs. 2.7(g)-2.7(i). In the evaluation, it can be split into two parts: the loop-after loop vacuum-polarization correction in Figs. 2.7(g), and Källén and Sabry correction in Figs. 2.7(h)-2.7(i). The VPVP correction is considered as the second-order correction of the one-loop VP potential of U_{VP},

$$\Delta E_{VPVP,g} = \sum_{n \neq a} \frac{\langle a | U_{VP} | n \rangle \langle n | U_{VP} | a \rangle}{\varepsilon_n - \varepsilon_a}. \tag{2.39}$$

The numerical calculation of the VPVP contribution is relatively simple. This can be performed by using a general method for solving VP potential. The sum of the Dirac spectrum is carried out by the method of dual-kinetic-balance basis set [140]. The correction of the higher-order part $(Z\alpha)^5$ can be identified by considering the $(Z\alpha)$ expansion. The correction of Källén and Sabry is written as

$$\Delta E^{KS}_{VPVP,hi} = \langle a | V_{KS} | a \rangle . \tag{2.40}$$

in the free-loop approximation. The Källén and Sabry potential is given by the reference [142] in a spherically symmetric nuclear charge distribution.

The calculations of complete non-perturbative processes described by these Feynman diagrams are an extremely difficult task due to many complicated integrals involved in these terms. The leading order of the three-loop QED correction is known in the $Z\alpha$ expansion as $\frac{\alpha^3 (Z\alpha)^4}{\pi^3 n^3}$. These contributions are very small and are only associated with very low Z ions.

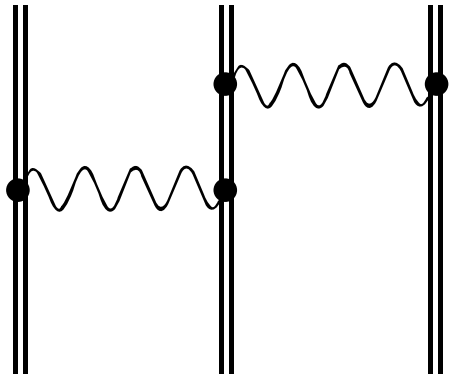

Fig. 2.8 *Three-electron interaction in QED.*

When performing calculations for atoms with more than three electrons, additional diagrams of three-body QED corrections, represented in Fig. 2.8, should be taken into account [141].

2.4.3 Screened QED corrections

For few-electron atoms or ions, the self-energy correction and vacuum-polarization correction are disturbed by an external potential, and this perturbation is caused by electron-electron interaction. We call this perturbation screened QED correlation. The self-energy

screening and vacuum-polarization screening corrections for a two-electron system are depicted in Fig. 2.9.

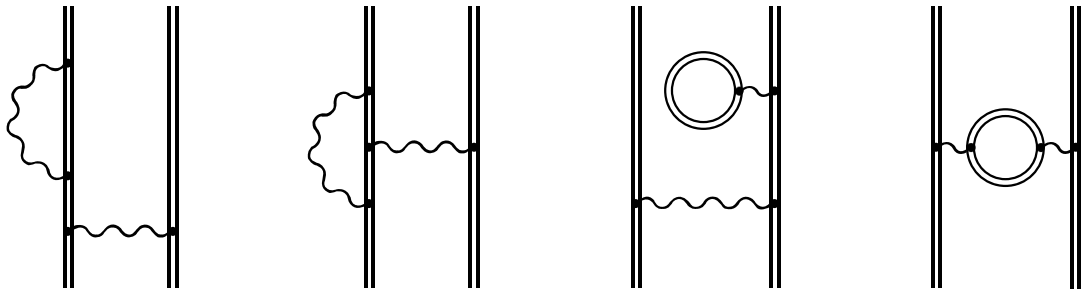

Fig. 2.9 *Feynman representing the self-energy screening diagrams and vacuum-polarization screening diagrams.*

The screening effect is considered to be a small change in the external potential relative to the total Coulomb potential [122],

$$V(x) = V_C(x) + \delta V(x). \tag{2.41}$$

Then, the perturbation theory methods may be extended to employ an effective screened potential which replaces the Coulomb one for few-electron ions. However, this method is too complicated to be directly included in the Dirac-Coulomb-Breit calculations. In the past, these corrections have been evaluated using an effective-Z parameter, which was derived by comparing the mean radius of the orbital with the radius of the hydrogenlike orbital in the same n, κ.

a) Welton picture

Indelicato et al. [155, 156] proposed to use the Welton approximation [161], which can correctly represent the lowest order of the self-energy. Then a more general scheme where the screening electron effect is considered as a first-order perturbation to the self-energy by an effective potential, has been proposed to evaluate all possible self-energy screening contributions between $1s_{1/2}$, $2s_{1/2}$, $2p_{1/2}$ and $2p_{3/2}$ states by Indelicato and Mohr [122] using the method proposed by Indelicato and Mohr [135].

An effective potential must be used to correct the lowest order part of the one-electron self-energy in $Z\alpha$ for the two-electron effects by correcting the changes of electronic density. This potential can be derived by using a more physical prescription based upon Welton's [161] semiclassical arguments. In the Welton picture, self-energy is a perturbation in the classical trajectory of electrons due to fluctuations in the vacuum electromagnetic field. Mohr et al. [118] had calculated exactly the hydrogenic self-energy corrected for finite nuclear size. This approximation for screened self-energy has been applied to the two or three electron systems.

For s orbitals, the self-energy screening correction deduced from Mohr's results leads to a relation [155, 156],

$$\delta E_{SE}^{ns} = \sum \frac{\langle ns\,|\Delta U_n(r)|\,ns\rangle_{DF}}{\langle ns\,|\Delta U_n(r)|\,ns\rangle_{Hyd}} E_{SE,ns}^{Hyd}, \tag{2.42}$$

Here, the subscript DF represents Dirac-Fock, Hyd stands for hydrogenlike wave functions, $|ns\rangle$ is a radical solution of the Dirac-Fock equation, U_n is the nuclear potential, and $E_{SE,ns}^{Hyd}$ is the self-energy of one-particle. For p, d, . . . orbitals, the screening correction proportional to the square of the wave function is canceled at the origin, and the $g-2$ diagram provides the leading correction

$$\delta E_{SE}^{nl\geq 3} = \sum \frac{\langle nl \geq 3\,|\beta\boldsymbol{\alpha}\cdot\boldsymbol{E}|\,nl \geq 3\rangle_{DF}}{\langle nl \geq 3\,|\beta\boldsymbol{\alpha}\cdot\boldsymbol{E}|\,nl \geq 3\rangle_{Hyd}} E_{SE,nl\geq 3}^{Hyd}. \tag{2.43}$$

In the above expression, E represents the nuclear electric field.

b) Model operator approach

The true self-energy operator being not local, it cannot be well approximated by a local potential. Shabaev and Tupitsyn [104] evaluated the screened self-energy corrections based on the self-energy operator model method. In this approach, the screened self-energy contributions were estimated by evaluating the total energy together with the effective operator contained in the Dirac-Fock or the Kohn-Sham equation and subtracting the related energy evaluated without this model operator and the self-energy contribution performed with the H-like wave functions. Shabaev et al. [104, 162] approximated the QED operator, which are easily included in any calculations based on the Dirac-Coulomb-Breit equation, using a sum of short-range local and nonlocal potentials. The effective self-energy operator V^{SE} in Eq. (2.29) can be divided into two parts, the local part V_{loc}^{SE} and the nonlocal part V_{nloc}^{SE},

$$V^{SE} = V_{loc}^{SE} + V_{nloc}^{SE}, \tag{2.44}$$

where V_{loc}^{SE} is written as

$$V_{loc}^{SE} = \sum_{\kappa} V_{\kappa}(r)\hat{P}_{\kappa}. \tag{2.45}$$

Here $V_{\kappa}(r)$ represents the radial part, and $\hat{P}_{\kappa}$ stands for the projector operator. The nonlocal operator V_{nloc}^{SE}, which approximates the part of the exact self-energy operator, can be defined by

$$V_{nloc}^{SE} = \sum_{i,j=1}^{n} |\phi_i\rangle\, D_{ij}\, \langle\phi_j|\,, \tag{2.46}$$

where the matrix D is expressed as

$$D_{ij} = \sum_{\kappa,l=1}^{n} \left[(S^t)^{-1}\right]_{i\kappa} \langle\psi_\kappa| \left\{\frac{1}{2}\left[\sum(\varepsilon_\kappa) + \sum(\varepsilon_l)\right] - V_{loc}^{SE}\right\} |\psi_l\rangle \, (S^{-1})_{lj}. \tag{2.47}$$

Here $\psi_i(r)$ is the hydrogen-like wavefunction, and $\phi_i(r)$ is the model of projected basis functions. $S_{i\kappa}$ stands for the overlap matrix $S_{i\kappa} = \langle\phi_i|\psi_\kappa\rangle$.

2.5 Relativistic recoil

The recoil parts and mass-dependent are usually composed of normal and specific mass shifts. This mass shift was first evaluated by Hughes and Eckart [123] for multi-electron atoms. The normal-mass-shift operator is given by

$$H_{RNMS} = \frac{1}{2M}\sum_i \left\{\boldsymbol{p}_i^2 - \frac{\alpha Z}{r_i}\left[\boldsymbol{\alpha}_i + \frac{(\boldsymbol{\alpha}_i\cdot\boldsymbol{r}_i)\boldsymbol{r}_i}{r_i^2}\right]\cdot\boldsymbol{p}_i\right\}, \tag{2.48}$$

an the specific-mass-shift operator can be written as

$$H_{RSMS} = \frac{1}{2M}\sum_{i\neq j} \left\{\boldsymbol{p}_i\cdot\boldsymbol{p}_j - \frac{\alpha Z}{r_i}\left[\boldsymbol{\alpha}_i + \frac{(\boldsymbol{\alpha}_i\cdot\boldsymbol{r}_i)\boldsymbol{r}_i}{r_i^2}\right]\cdot\boldsymbol{p}_j\right\}, \tag{2.49}$$

The specific-mass part gives a small contribution, so it can be treated in perturbation. The total recoil operator is defined by the sum of Eq. (2.48) and (2.49), which can be deduced from the recoil Hamiltonian [179, 180, 181, 182],

$$H_{RMS} = \frac{1}{2M}\sum_{i,j} \left\{\boldsymbol{p}_i\cdot\boldsymbol{p}_j - \frac{\alpha Z}{r_i}\left[\boldsymbol{\alpha}_i + \frac{(\boldsymbol{\alpha}_i\cdot\boldsymbol{r}_i)\boldsymbol{r}_i}{r_i^2}\right]\cdot\boldsymbol{p}_j\right\}. \tag{2.50}$$

Here M represents the nuclear mass, the momentum operator is described by $\boldsymbol{p}_i$, and $\boldsymbol{\alpha}_i$ is the Dirac matrix operator. The recoil correction is the expectation value of the recoil Hamiltonian on the Dirac wave function. The recoil correction is usually expressed by the form $\alpha m(Z\alpha)^n(m/M)^k$.

The higher-order relativistic corrections have been calculated by V. Shabaev [180]. For hydrogenlike atoms, Artemyev et al. [120] finally wrote the recoil contribution as,

$$\Delta E_{rr} = \Delta E^{(1)} + \Delta E^{(2)}. \tag{2.51}$$

with

$$\Delta E^{(1)} = \frac{m}{M}\frac{(\alpha Z)^2}{2N^2}mc^2, \tag{2.52}$$

and

$$\Delta E^{(2)} = \frac{m}{M}\frac{(\alpha Z)^5}{\pi n^3}P(\alpha Z)mc^2. \tag{2.53}$$

where,

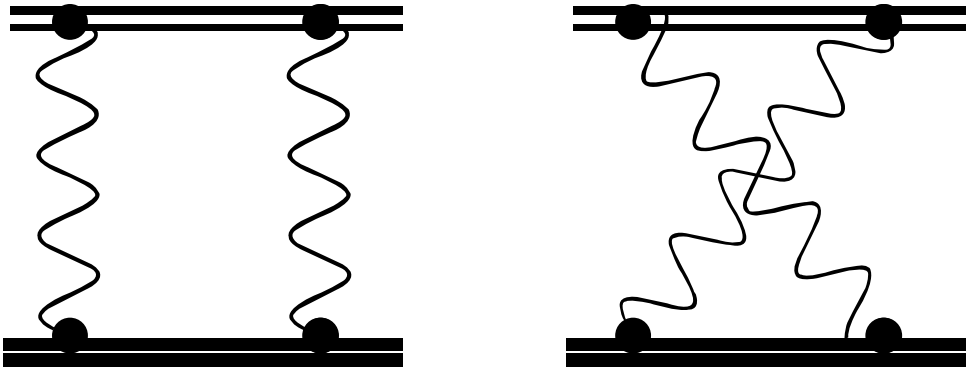

Fig. 2.10 *Feynman diagrams representing the relativistic recoil correction. The heavy double line indicates the proton wave function or propagator.*

$$
\begin{aligned}
N &= \sqrt{n^2 - 2(n - |\kappa|)(|\kappa| - \gamma)}, \\
\gamma &= \sqrt{\kappa^2 - (\alpha Z)^2}, \qquad \kappa = (-1)^{j-l+1/2}(j + \frac{1}{2}).
\end{aligned}
\tag{2.54}
$$

Eq. (2.51) corresponds to the diagrams in Fig. 2.10. The function $P(\alpha Z)$ has been evaluated numerically. The nontrivial radiative-recoil correction can be calculated up to terms of order $(\alpha Z)^6$. These corrections are the sum of one- and two-electron contributions for high-Z few-electron atoms.

2.6 Nuclear polarization

Nuclear polarization (NP) corrections are due to the interactions between the atomic electron and virtual excitation states of the nucleus. The NP correction is very small, yet it sets the ultimate precision limition which can be used to test QED corrections in highly charged ions. The uncertainty of nuclear excitation spectrum limits the determination of nuclear polarization correction. The NP energy shift can be written as

$$
\Delta E_a = \sum_{b \neq a} \frac{\langle b \,|V_R|\, a \rangle^2}{E_a - E_b}. \tag{2.55}
$$

where the state $|a\rangle$ represents an electron or muon state coupled to the nuclear ground state, and $|b\rangle$ is the entire spectrum of electron or muon and excited nuclear states. A relativistic field approach of effective photon propagators specified for collective nuclear excitations is evaluated in Ref. [125, 126]. A relation between the NP correction to the Lamb shift and bound-electron g factor is given

$$E_{NP} \approx mc^2 \frac{j(j+1)}{3\kappa^2} \delta g_{NP}, \tag{2.56}$$

where E_{NP} represents the NP contribution to the Lamb shift, which is deduced from the bound-electron g factor. The evaluation of the nuclear polarization contribution was carried out only for a few ions. We can get a conservative estimate [20],

$$E_{NP} \approx -\frac{1}{1000} E_{FNS}, \tag{2.57}$$

were E_{FNS} represents the finite nuclear-size correction.

Volotka and Plunien [127] evaluated systematic investigation on one- and few-electron high-Z ions. They presented $\Delta E_{NP}/\Delta E_{FS}(10^{-3})$ values of -0.430 for $1s$, -0.431 for $2s$, and -0.425 for $2p1/2$ in H-like ^{208}Pb and -0.947 for $1s$, -0.951 for $2s$, and -0.941 for $2p1/2$ in H-like ^{238}U, respectively. The ratio of the screened nuclear polarization and screened finite nuclear size contributions $\Delta E_{SNP}/\Delta E_{SFNS}(10^{-3})$ are -0.430 for $1s^2$ binding energy and, respectively, -0.432, -0.441, and -0.388 to the $(1s^2)2s$, $(1s^2)2p1/2$, and $(1s^2)2p3/2$ ionization energies in Li-like ^{208}Pb. For ^{238}U, this ratio is -0.948 to the $1s^2$ binding energy and -0.952 to $(1s^2)2s$, -0.955 to $(1s^2)2p1/2$, and -0.847 to $(1s^2)2p3/2$ of ionization energies respectively. These ratios appear to behave rather similarly for all the considered electron states.

2.7 Nuclear deformation

For heavy nuclei, nuclear deformations should be considered. However, it is more difficult to evaluate the corrections connected to internal nuclear structure. We used the experimental nuclear charge radius. The important parameter for the atomic calculation is the contribution of deformation to the RMS radius. For a deformed nucleus, the half-density radius c can be written as

$$c(\theta, \phi) = c_0[1 + \beta_{20} Y_{20}(\theta, \phi) + \beta_{40} Y_{40}(\theta, \phi)]. \tag{2.58}$$

where β_{20} and β_{40} are the quadrupole deformation parameters, exclusively extracted the data of the muonic X-ray experiment. The effect of nuclear deformation on the RMS radius and energy shifts are researched by Johnson et al. [88], Zumbro et al. [133, 134] and Indelicato and Lindroth[128]. Kozhedub et al. [29] have been performed the calculations in hydrogenlike and lithiumlike uranium using the approximate formulas. The contribution from this effect is about 140 meV and 26 meV for the $1s$ state and $2s$ state in $^{238}U^{91+}$ respectively, where nuclear deformation offers a 0.07% contribution. Therefore, in order to compute the accuracy of the nuclear size correction to 0.1%, it is necessary to take into account the nuclear deformation effect.

2.8 Auger shift

Another effect from a feature of these lithiumlike ion core-excited states is Auger shift since the initial level is degenerate with a continuum. The MCDF method is very inefficient to calculate the hole state of the inner shell caused by autoionization. Special methods should be used, for example, perturbation theory or complex scaling (CS) method, in order to calculate the inner-shell Auger shifts of these states. For instance, the CS method is suitable for computing light atoms [143]. Unfortunately, this method is not suitable for relativistic calculations of heavy atoms because the computation takes a long time. In the RMBPT method framework, the discretized Dirac-Fock basis sets can provide a simpler but less accurate method for estimating Auger shifts, which is described in Refs. [128, 129, 130, 144]. They noticed that the $3s$ level is the most sensitive to Auger shift.

Research on the transition of heavy atomic inner shells has become one of the most promising tools for testing QED in strong Coulomb fields. The complexity of relativistic multibody problem up to 100 electrons can be found in Refs. [128, 129, 130, 144]. These calculations are time-consuming, they are only executed on selected elements, and the results are interpolated to obtain values for other elements.

The Auger shift does not always have the same smooth Z-dependence as other many-body effects, because the mixing of the two other holes can increase dramatically as the energy difference between the sum of the energy of the holes and the original hole becomes smaller. Recently, Tupitsyn et al. [131] used the RMBPT method in the Brillouin-Wigner form to calculate the Auger shifts on neutral uranium.

2.9 Radiative transitions

We consider radiative transitions of an atom or ion from state $|i\rangle$ and $|f\rangle$ by emission of a photon γ from the S-matrix theory by Cheng [136].

In quantum electrodynamics, the Hamiltonian density is described as

$$H_{int} = -\frac{1}{c} j_\mu A^\mu, \tag{2.59}$$

which represent the interaction between the electromagnetic field and the electron-positron field. Here A^μ represents the operator of electromagnetic field and the operator of Dirac current density is described by j_μ.

An initial state of the system can be expressed by $|J_i\rangle \otimes |0\rangle$, in which $|0\rangle$ is the vacuum state of the photon field and a final state of the system can be expressed by $|J_f\rangle \otimes |1\gamma\rangle$, in which $|1\gamma\rangle$ is a one-photon state.

The matrix element of transition becomes

$$\begin{aligned} S_{i\to f} &= -\frac{i}{\hbar} \langle f, \gamma \left| H_{int} \right| i \rangle \\ &= \frac{i}{\hbar c} \int \langle f \left| j_\mu \right| i \rangle \int \langle \gamma \left| A^\mu \right| 0 \rangle \, d^4x \\ &= -\frac{e}{\hbar} \sqrt{\frac{2\pi\hbar c^2}{\omega V}} \int \bar{\psi}_f \gamma_\mu \epsilon_\mu e^{-ik_\nu x_\nu} \psi_i d^4x. \end{aligned} \tag{2.60}$$

The unperturbed electron states ψ are given by

$$\psi(x) = u(\vec{x})e^{-iEt/\hbar}. \tag{2.61}$$

Here $u(\vec{x})$ satisfies the single-particle Dirac equation in an external potential.

We reduce the multipole transition matrix element to a sum of radial integrals. The radiative transition rate between an initial state described by i with a total angular momentum of J_i and a final state described by f with total angular momentum of J_f, is written by

$$A_{if} = \alpha^2 \left|\langle J_f, 1\gamma \left| j_\mu A^\mu \right| J_i, 0\rangle\right|^2. \tag{2.62}$$

Eq. (2.62) can also be rewritten as a sum of radial integrals weighted by angular and configuration coefficients according to averaging over angles. If confined to the multipole electric component λ of the electromagnetic field operator, we can obtain [132]

$$A^\lambda_{if} = K_\lambda \Delta E_{if} \left| \sum_{n_i=1}^{N_i^{conf}} \sum_{n_f=1}^{N_f^{conf}} \sum_{m_i=1}^{N_{n_i}^{orb}} \sum_{m_f=1}^{N_{n_f}^{orb}} c_{m_i} c_{m_f} T^{m_i m_f}_{n_i n_f} R^{m_i m_f \lambda}_{n_i n_f} \right|^2, \tag{2.63}$$

with

$$K_\lambda = \frac{4\pi\alpha(2\lambda+1)e}{(\lambda+1)(2J_i+1)h}. \tag{2.64}$$

Here m_i and m_f are the orbital designation numbers in the configuration designation numbers of n_i and n_f, and the initial state is represented by the subscript i, and the final state is represented by f, and T is the reduced angular coefficient of the 2^λ-pole electric operator. The c_m represents configuration mixing coefficients, and the transition energy is denoted by ΔE_{if}. The R represents a dimensionless radial matrix element written as

$$\begin{aligned} R^{m_i m_f \lambda}_{n_i n_f} = \int_0^\infty dr \Big\{ & (\lambda+1) j_\lambda(\alpha\omega r)(P^{m_i}_{n_i} P^{m_f}_{n_f} + Q^{m_i}_{n_i} Q^{m_f}_{n_f}) \\ & - j_{\lambda+1}(\alpha\omega r)[(\kappa^{m_f}_{n_f} - \kappa^{m_i}_{n_i} - \lambda) Q^{m_i}_{n_i} P^{m_f}_{n_f} \\ & + (\kappa^{m_f}_{n_f} - \kappa^{m_i}_{n_i} + \lambda) P^{m_i}_{n_i} Q^{m_f}_{n_f}] \Big\}. \end{aligned} \tag{2.65}$$

where P^m and P^n are the large radial components, Q^m and Q^n are the small radial components of the Dirac wavefunction, j_λ is the spherical Bessel function, ω is the transition energy, and $\kappa = (l-j)(2j+1)$, in which l is the orbital angular momentum and j is total angular momentum respectively.

2.10 Auger transitions

For the initial state of $1s^1 2s^1 2p^1$, the Auger transition is considered a two-electron transition, in which an outer electron of 2s orbital jump into an inner hole of $1s$ orbital, and another outer electron of 2p orbital are simultaneously excited into a continuous state or bound state. Auger decay can be treated in time-dependent perturbation theory because the interaction between the core-hole state and Auger continuum is weak.

The basic idea in non-radiative situations is to regard the emission of Auger electrons as a resonance in single photoionization, which is considered a complete scattering process,

$$A^* = A^+ + e_A^-, \tag{2.66}$$

This equation is represented by the transition amplitude [137, 138]

$$\begin{aligned}\langle V_f \left|H - E\right| U_i\rangle = \prod_{\nu\neq 1,2} \langle \nu'|\nu\rangle \Bigg[\langle \epsilon k||12\rangle + \begin{vmatrix} \langle \epsilon \left|F\right| 1\rangle & \langle \epsilon \left|F\right| 2\rangle \\ \langle k|1\rangle & \langle k|2\rangle \end{vmatrix} \\ + \begin{vmatrix} \langle \epsilon|1\rangle & \langle \epsilon|2\rangle \\ \langle k \left|F\right| 1\rangle & \langle k \left|F\right| 2\rangle \end{vmatrix} - \xi \begin{vmatrix} \langle \epsilon|1\rangle & \langle \epsilon|2\rangle \\ \langle k|1\rangle & \langle k|2\rangle \end{vmatrix} \\ + \sum_{\mu\neq 1,2} \left(\begin{vmatrix} \langle \mu'|1\rangle & \langle \mu'|2\rangle \\ \langle \epsilon k||1\mu\rangle & \langle \epsilon k||2\mu\rangle \end{vmatrix} + \begin{vmatrix} \langle \epsilon|\mu\rangle & \langle k|\mu\rangle \\ \langle \epsilon\mu'||12\rangle & \langle k\mu'||12\rangle \end{vmatrix} \right) \Bigg] .\end{aligned} \tag{2.67}$$

where U_i is the restricted Hartree-Fock solution of the initial state and V_f is the final state. The notation $\langle ab||cd\rangle$ stands for

$$\langle ab||cd\rangle = \left\langle ab \left| \frac{1}{r_{12}} \right| cd \right\rangle - \left\langle ab \left| \frac{1}{r_{12}} \right| dc \right\rangle , \tag{2.68}$$

here the Fock-like operator

$$F = h + \sum_{\mu\neq 1,2} \langle \mu'||\mu\rangle . \tag{2.69}$$

The coefficient ξ of the quadratic overlap term is written as

$$\xi = E - \frac{1}{2} \sum_{\mu\neq 1,2} \left(\langle \mu' \left|h\right| \mu\rangle + \langle \mu' \left|F\right| \mu\rangle \right) . \tag{2.70}$$

The corrections to the lowest-order Auger amplitude, $\langle \epsilon k||12\rangle$, involve both one and two-electron interaction matrix elements in addition to a scaling factor. The initial and final states must be optimised separately and the continuum orbital solved in the field of the final doubly ionised ion.

Chapter 3

Muonic atoms

We evaluate higher-order finite-size corrections, starting from accurate numerical evaluations of the Dirac equation in a Coulomb potential within the framework of nonperturbative methods of some QED contributions for muonic atoms. In this chapter, we mainly introduce the difference between muonic atoms and electronic atoms. They can be summarized by describing muons as "heavy electrons" with a mass of 207 times of ordinary electrons. Since the mass of the muon is large, it is 207 times closer to the nucleus than an electron in the same orbital. Especially for heavy nuclei, this leads to large nuclear size corrections and a strong dependence of the bound state energy of the muon on the current distribution and nuclear charge. There is also a large relativistic effect for muonic atoms.

The theory of the muon and the electron within finite-size mechanics is the same, and corrections come from the same sources, such as relativity, recoil, QED, and proton structure effects. However, the relative importance of the various effects is not the same. More importantly, there are different QED proportions in muonic atoms due to the influence of the electron vacuum polarization, which is dominant in the QED corrections.

It should be observed that the large differences between the observed interactions of muonic and electronic atoms are not all due to differences in masses.

3.1 Wave function

Since the mass of the muon is 207 times that of the electron, the bound muon is close to the nucleus and has a relationship of $m_\mu/m_e \approx 207$ with the bound electron. The radius of the muon is smaller than the Compton wavelength of the electron $\lambda = \hbar/m_e c$ by a ratio of $m_e/\alpha m_\mu \approx 137/207$ (m_μ and m_e are the muon and electron mass, respectively).

Fig. 3.1 outlines how the muon in the low states penetrates the nucleus. The dotted line indicates the nuclear charge distribution. It can be noted that the $1s$ wave penetrates deeply into the nucleus, the $2p$ and $3p$ waves penetrate very little, and $3d$ has almost no penetration. The $2s$ wave has the greatest overlap with the nucleus next to the ground state. For the $2s$ level, the average radius of the muon wave function is 2.6 times larger than the Compton wavelength, which is the scale of QED corrections. The sensitivity of the muonic atom test to the effects of nuclear size is determined by the overlap integral $(P(r)^2 + Q(r)^2)\rho(r)r^2$, where $Q(r)$ and $P(r)$ are small and large components of the radial

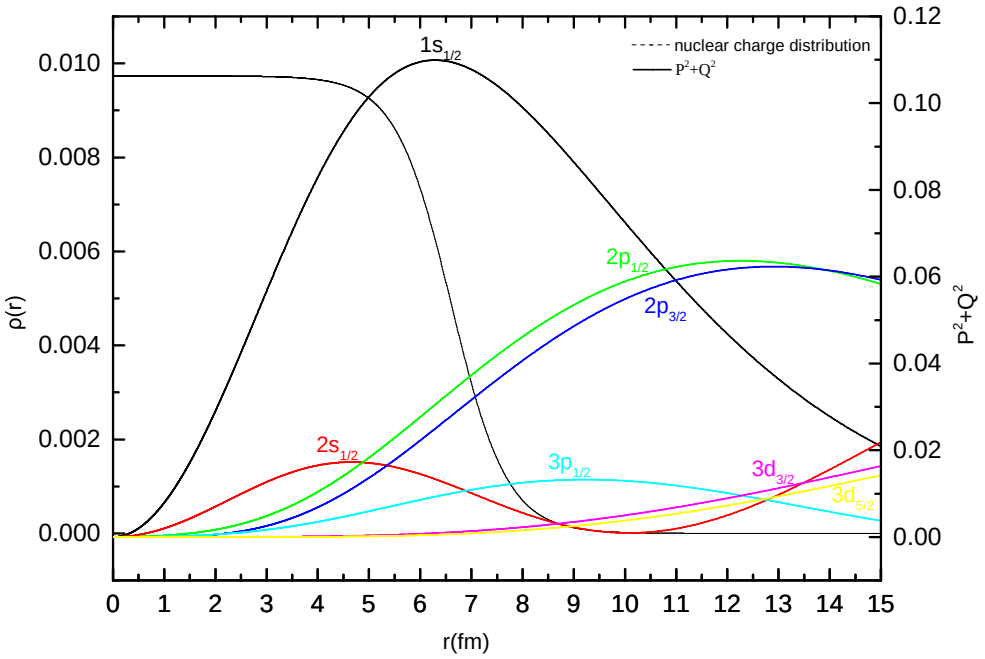

Fig. 3.1 *Muon wave function(solid lines) for relatively low-lying states, compared to the nuclear charge distributions(dashed line) from the Fermi model in muonic* ^{208}Pb.

wavefunctions to the Dirac equation, respectively.

3.2 Nuclear charge distribution models

The muonic energy levels are sensitive to the nuclear structure. In order to determine the size of the nuclei from the muonic atom transition energies, the Uniform, Fermi and 3-parameter Gaussian nuclear charge distributions are often used to solve the Dirac equation, and the nuclear parameters are adjusted to reproduce the transition energies. The analytic distributions are parameterized, so they provide the same mean square radius R. The moment of the charge distribution can be expressed as

$$\langle r^n \rangle = 4\pi \int_0^\infty r^{2+n} \rho(r) dr, \tag{3.1}$$

For a spherically symmetric charge distribution, the nuclear charge distribution $\rho(r) = \rho_N(r)/(Ze)$ can be normalized as

$$\int \rho(\vec{r}) d(\vec{r}) = 4\pi \int_0^\infty r^2 \rho(r) dr = 1, \tag{3.2}$$

where the mean square radius is $R = \sqrt{\langle r^2 \rangle}$.

The Coulomb potential of the nucleus may be expressed as

$$V_N(r) = -\frac{4\pi e}{r}\int_0^r duu^2\rho_N(u) - 4\pi e\int_r^\infty duu\rho_N(u). \tag{3.3}$$

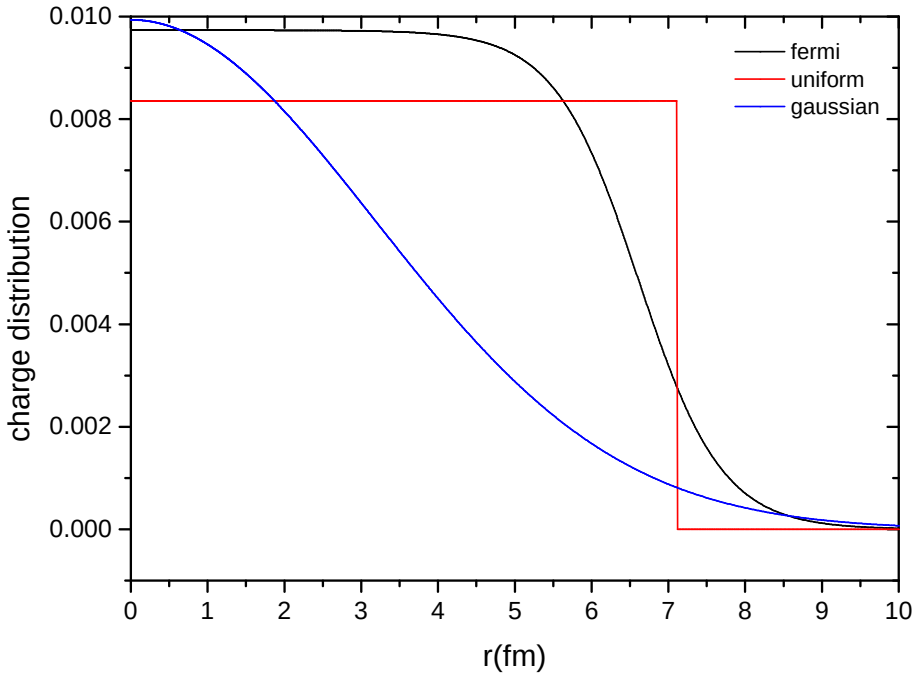

Fig. 3.2 *Nuclear charge distributions of Uniform model, Fermi model and three-parameters Gauss model in* ^{208}Pb *for a mean spherical radius of* $5.5057fm$.

We have described the nuclear charge distribution using the two-parameter Fermi distribution in Eq. (2.18). We also use the three-parameter Gauss function, which is defined as

$$\rho(r) = \rho_0\left(1+\omega\left(\frac{r}{c}\right)^2\right)\left(1+e^{\left(\frac{\left(r^2-c^2\right)}{t^2}\right)}\right)^{-1}, \tag{3.4}$$

where ω is a shape parameter.

3.3 Finite-size effect

The consequences of the large mass of the muon are obvious. Although the point charge is still good for electronic atoms, the approximation of point charges is very wrong for muonic atoms. The finite nuclear size effect is no longer correction and dominates in muonic atoms. This effect greatly reduces (two times) the binding energy of $1s$ in heavy atoms. It is well known that the energy shift caused by the finite size effect is proportional

to the charge distribution moments. The perturbation calculation shows that in the low-Z element, s state energy shift is proportional to $\langle r^2 \rangle$ and the p state to $\langle r^4 \rangle$. Because the $2p$ state of the muon in light element spend a very short time inside the nucleus, and this results in a very small energy shift at the $2p$ level. The leading order has a simple expression [115]

$$E = \frac{2}{3}\left(\frac{\mu_r}{m_\mu}\right)^3 \frac{(Z\alpha)^2}{n^3} m_\mu c^2 \left(\frac{Z\alpha R}{\lambda}\right)^2 \delta_{1,0}, \tag{3.5}$$

where R is the root-mean-square charge radius of the nucleus, and λ is the muon Compton wavelength. In addition to this leading limited size contribution, there are various relativistic and QED corrections.

For electronic atoms, the self-energy correction is much larger than the vacuum polarization correction. However, for muons, the vacuum polarization correction is dominant due to the Uëhling potential at a shorter distance. The vacuum polarization potential can be added to the Dirac equation directly with the term of $\alpha(Z\alpha)^2 m_\mu c^2$. In this way, the calculation includes all iterations of the Uëhling potential. The Uëhling correction can produce $2s - 2p$ splittings bigger than $2p_{3/2} - 2p_{1/2}$. The finite-size effects are the most prominent feature in the low levels of heavy muonic atoms.

3.4 Fine-structure splitting

The complicated nuclear structure leads to the uncertainty of the muon levels in heavy nuclei. Thus the muonic atoms become one of the tools for studying electromagnetic properties of the nucleus. However, with the continuous improvement of experimental accuracy, there is a long-term difference between the theoretical and experimental aspects of fine structure splitting in muonic heavy atoms. One of the discrepancies is that the theoretical nuclear polarization energy shift gives the opposite contribution to the predicted values from the experiment. This discrepancy was first reported by Yamazaki et al. [91, 92] in the $\Delta 2p$ splitting energy of μ^-Pd/Rh and ^{208}Pb of the muonic x-ray analysis. In that analysis, the experimental nuclear polarization correction was derived from a model-independent analysis of muonic x-ray and elastic electron scattering. The same difference is also indicated in the $2p$ level of the muonic ^{90}Zr [146]. In view of the fact that the theoretical calculations are in good agreement with the experimental measurements for μ^-Ni/Co cases [93], so the discrepancy is supposed to be due to experimental factors in heavy muon nuclei. Later, Bergern et al. [5] got the values from the experiment to consist of the calculations by a hypothesis inversion in the nuclear polarization corrections. The other difference is in the splitting energy from $3p$, which was found in the X-ray measurements of the muonic ^{208}Pb. The difference is 300-500 eV, which is of the same order of magnitude as the $2p$ splitting energy [5]. Haga et al. [89] reanalyzed this difference by adding pygmy dipole resonances to the excitation spectrum, in which the final fit of ^{208}Pb has been greatly improved. There is the same difference in ^{90}Zr, where the nuclear excitation spectrum is not sensitive to nuclear polarization. They guess that the existing discrepancy might be caused by other effects in addition to the nuclear polarization.

3.5 Nuclear polarization

The nucleus and muon will produce virtual transitions to excited intermediate states due to the electromagnetic interaction between the muon and the nucleon. This effect results in an increase in the muon binding levels. Fig. 3.3 shows diagrams contributing to nuclear polarization in lowest order.

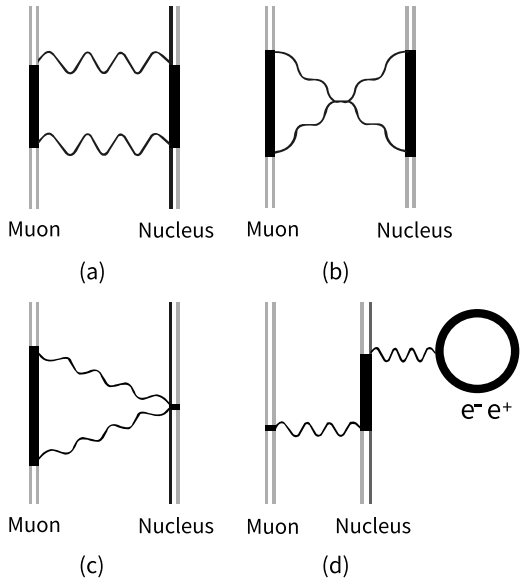

Fig. 3.3 *Feynman diagrams representing the lowest-order nuclear polarization effect to the muon binding energy. (a) ladder diagram, (b) cross diagram, (c) seagull diagram, (d) NP-VP diagram. The muon (heavy line) interacts with the nucleus (heavy line) in its state via the exchange of virtual photons (wavy lines). [89]*

We evaluate the nuclear polarization with the RURP code, which is used in the low states of the muonic atoms and developed by Rinker [147]. This method provides a general computational framework for calculating nuclear excitation in the muonic spectrum, where the states include all virtual excitations of the nuclei and the muon. The nuclear polarization calculations are defined in terms of first-order perturbation theory in which exact sums over the entire muon spectrum and certain closure approximations for the nuclear spectrum. Since the properties (such as transition matrix elements, angular momentum, and energy) of only a few low-excited states of these nuclei are known, calculating this correction ΔE_a (2.55) is complicated. Most excited states effects can only be estimated by charged particle scattering data or photonuclear reactions. The other is by using a summation rule or a specific theoretical nuclear model if they are available with sufficient accuracy. Due to the lack of experimental information and a lack of good theoretical models of these nuclei, this calculation is primarily based on the summation

rules. Various sums contain energy weighting and rules (EWSR) [148, 149],

$$\sum_f (E_f - E_0)^n B(EL; 0 \to f) = \frac{L(2L+1)^2}{4\pi} \frac{(\hbar c)^2}{2M} Z \left\langle r^{2L-2} \right\rangle \tag{3.6}$$

The monopole for $L = 0$ of the sum rules is obtained approximately by setting $B(E_0; 0 \to f) \to \left|\langle 0 \left| r^2 \right| f \rangle\right|^2$ and $L \to 2$ in Eq. (3.6). In the RURP code, this correction $\Delta B_{NP}(L)$ has been calculated for the electric monopole with $L = 0$, dipole with $L = 1$, quadrupole with $L = 2$, octupole with $L = 3$, and $L \geq 3$ excitations. The result can be seen as the Hamiltonian approximate diagonalization over the entire and infinite muon-nuclear spectrum. The determination of the nuclear-polarization correction is limited by uncertainties in the nuclear excitation spectrum. The present computation of nuclear polarization corrections corresponds to the ladder diagram of Fig. 3.3(a).

Haga et al. [89] reanalyzed the low-lying μ^-–^{90}Zr and μ^-–^{208}Pb states by using nuclear polarization with the full-electromagnetic nuclear response. In their analysis, they employed collective models, which are three forms for the transition density of Tassie-Goldhaber-Teller (TGT) [150, 151], Rinker (RIN) [94], and Jensen-Steinwedel (JS) [151, 152] models to avoid the transverse nuclear polarization correction being gauge-dependent. In addition to leading-order nuclear polarization corrections for the ladder in Fig. 3.3(a), they also considered the cross diagram in Fig. 3.3(b), seagull diagram in Fig. 3.3(c), and the nuclear polarization combined vacuum polarization in Fig. 3.3(d). Although the seagull diagram does not polarize the nucleus, it needs to be included as part of the "nuclear polarization" correction due to it playing an important role in retaining the gauge invariance of the nuclear polarization correction.

3.6 Effects of remaining electron

In heavy elements, not all atomic electrons are ionized by Auger transitions during the muonic cascade. Furthermore, empty electron orbits can be refilled during the cascade in solids or in high-pressure gases. The remaining electrons have an effect on the muon and the binding energy. In addition to the muon, we also solve the full Dirac-Fock equation with the electrons from K, L, and M shells, respectively. We define this effect in terms of $\delta E = E_{\mu+e} - E_\mu$. In the following sections, we will discuss the calculation results in detail.

One important source of uncertainty in this effect calculations is lack of information on the number of present electrons during the muonic cascade. The electronic K x-ray experiments in heavy muonic atoms have been performed by Schneuwly and Vogel [153], which showed that the internal electron shells were refilled almost immediately during the muonic cascade. It is highly probable that all ten K and L electrons are present during the radiative transition between states within $n \leq 8$ of the heavy elements [154]. The K and L electrons are responsible for more than 95% of the effective electron density. Therefore, we will consider that the electrons refill K, L, M shells, separately. The effect of the remaining electron is inevitable for solid-state targets. Modern measurement techniques have been developed to completely ionize low-Z exotic atoms in gas targets [171, 172].

Chapter 4

Computational procedure

In this chapter, our purpose is to introduce the relativistic atomic structure program and computational methods used in our calculations.

4.1 Relativistic atomic structure program

Our present calculations are performed using MCDFGME, a general multiconfiguration Dirac-Fock code, which is programmed ab initio completely to include both relativistic and correlation contributions in the calculations related to theoretical atomic structure. This code has evolved from Desclaux [105], and the new version is developed by Indelicato [1]. It can be used to evaluate level energies, including one-loop QED corrections with all-order Uëhling contribution (see section 2.4.1), two-loop QED corrections (see section 2.4.2), QED screening corrections with Welton picture (see section a)) and effective operator (see section b)), and relativistic recoil corrections (see section 2.5). This code is very versatile with numerical methods (see section 2.1.3) and allows to modify mesh grid where the wavefunctions (see section 2.1.2) are tabulated and calculate various other properties. The electron-electron interaction (see section 2.3) is evaluated by the sum of the Breit and the Coulomb parts. MCDFGME allows for an option of including a full Breit operator (Eq. 2.27) or omitting the magnetic part (Eq. 2.25) or omitting the first term of retardation (Eq. 2.26) in the self-consistent field process. The higher-order retardation (Eq. 2.26) can be treated as the first-order perturbation. All calculations are solved using the Dirac-Coulomb-Breit Hamiltonian (see section 2.1.2) with a finite nucleus model using several alternative distributions, in which the default thickness parameter of 2.3 fm or setting any values can be adopted. The nuclear radiuses are used from the experimental results compiled by Angeli [185, 186]. All calculations use the latest atomic mass tables in [184] to replace the electronic mass with the reduced mass in the Dirac equation. The radiative transition probabilities (see section 2.9) are discussed by Cheng [136]. The transition probabilities are calculated by using Dirac wavefunctions, which are obtained in a complete self-consistent process, including relaxation.

The atomic structure can be explained in an extended sense, because the program can handle not only electrons, but also several " exotic " particles that can be added to electrons, such as muons(spin 1/2 lepton), kaons(spin 0 meson), and so on. The Klein Gordon equation is solved instead of the Dirac equation when the "exotic" particle is a

boson. The muon can be regarded as an electron with heavy mass, where the process to deal with the muonic atoms [157] is the same as the Hydrogen-like systems. In addition, we take into account the nuclear polarization correction (see section 3.5) and the effects from remaining electrons (see section 3.6).

The program provides the associated energy as well as the numerical representation of the one-electron orbitals constituting the total wave function. Present, the program can directly deal with any number of electronic systems including one electron, two electrons [1, 267], three electrons [156, 267], four electrons [167, 1, 267], more electrons [167, 163] and also super-heavy elements [167, 165, 166]. From these results, the code can evaluates a variety of atomic proprieties such as the total energy of a given state either at the multiconfiguration or single configuration level, the Landé g-factor [167, 168], the Auger transition probabilities [1], the radiative transition probabilities [164], the hyperfine structure parameters [157] and so on.

4.2 Computational methods

We used optimized levels method (OLs) to calculate the energy of each state and wave function. By using this technique, the orbitals of the initial and final states are not orthogonal because they have been individually optimized. Indelicato [169, 191] use the formalism developed by Löwdin [170] to take into account this non-orthogonality effect.

The atomic states are defined as a linear combination of electronic configurations, and each electronic configuration is defined as a determinant with their occupation numbers. These configurations are listed in the form of LS coupling, using the labels of $1s$, $2s$, $2p$, etc. The program will use the labels of $1s$, $2s$, $2p^*$, $2p$, etc. to generate all jj configurations resulting from a given LS configuration. The $*$ denotes $j = l - 1/2$, while no $*$ stands for the $j = l + 1/2$.

The configuration space is occupied by all single to triple excitations from the occupied orbitals to some active sets. In this way, active variational space size is increased from all occupied shells to all virtual orbitals up to maximum $n = 5$ and $l = n - 1$. It customarily doesn't consider the type of the single excitation of $n\kappa \rightarrow n'\kappa$ (κ represents Dirac angular number), that is the configurations of electron excited to an orbital, which has the same κ with the initial orbital. In principle, this should have a zero effect on energies in non-relativistic transitions (Brillouin's theorem [173, 174]). But there would get the wrong non-relativistic limit if you do not include them, which was proved by Indelicato et al. [175] and Kim et al. [176]. So, we include the Brillouin configurations in the calculations of single excitations. The excitation is layer-by-layer enhanced, which makes it easy to monitor the convergence of various physical quantities. In the present cases of $1s2s2p^{2S+1}P_J$, each of the associated layers labeled $n = 2, 3, 4, 5$ can include s, p, d orbitals of up to $4f, 5g$ subshells. The program can excite much higher orbitals for other cases. The process of these shells will result in a lot of configurations. The MCDFGME code will automatically perform the generation of the multiple configuration expansions.

4.3 Convergence considerations

4.3.1 Wavefunctions

If WF_n^i and WF_n^f represent the initial and final values of the wavefunction respectively at the nth iteration, the estimation value of the normalized wavefunction for the $(n+1)$th iteration is considered to be [105]

$$WF_{n+1}^i = \delta WF_n^f + (1-\delta)WF_n^i \tag{4.1}$$

The coefficient δ remains fixed during the self-consistent field process, or it is determined for each orbital according to the following scheme. We take ΔWF_n as the maximum difference between ΔWF_n^i and ΔWF_n^f, if ΔWF_{n-1} and ΔWF_n have the same sign then δ is increased by 0.1. Otherwise it is decreased by the same amount provided that

$$0.1 \leq \delta \leq 0.9. \tag{4.2}$$

We also can compare the differences between successive correlation energy values obtained in different active spaces to assess the energy convergence of the calculation. Energy convergence is kept within 0.01 eV in order to ensure convergence of the calculation.

4.3.2 Weights of the configurations

The LSJ level is given by $[XLJ]\#nLSm$ where $X = 2S+1$, L and J are the total angular momenta of the orbital, S is the total spin, n is the energy ordering ($n = 1$ correspond to the lowest energy of all degenerate terms of the selected LS configuration), and LS is derived from its configuration (the mth following them are listed in the input data). The convergence will be towards an eigenstate with the greatest weight for a given LSJ level.

For a multiconfiguration calculation, the weights W_ν of the configurations are determined in the following way. We suppose that the nth step is performed using a set of coefficients W_ν^n. The diagonalization of the energy matrix provides a new set $(W_\nu^n)_d$. The $(n+1)$th step can be performed using W_ν^{n+1} coefficients, which can be described as [105],

$$W_\nu^{n+1} = \lambda(W_\nu^n)_d + (1-\lambda)W_\nu^n. \tag{4.3}$$

The damping factor λ is extremely important when a calculation converges to a high eigenvalue or excited state, rather than to the lowest eigenvalue (ground state).

Chapter 5

Results and discussion on Li-like ions

In the present chapter, we discuss diverse QED corrections, for example, the self-energy screening from the Welton model and effective operator model, respectively. We analyze the electron correlation of Coulomb, magnetic, retardation and higher-order retardation terms. Our calculations with Welton or effective operator methods are compared with other theoretical and experimental results.

5.1 Welton model and Effective operator model

Table 5.1 – The screened self-energy for the transition $1s^2\,2p\,^2P_{1/2} \rightarrow 1s^2\,2s\,^2S_{1/2}$ and $1s^2\,2p\,^2P_{3/2} \rightarrow 1s^2\,2s\,^2S_{1/2}$ of Li-like ions (in eV). The Welton (Wel) and effective operator (Eff) results are obtained by Welton picture and effective operator model. Shabaev et al. performed the calculations using the method of Kohn-Sham (KS) [104], Dirac-Fock (DF)[104] and perturbation theory (PT)[297, 281, 26] in the Kohn-Sham potential.

	$1s^2\,2p\,^2P_{1/2} \rightarrow 1s^2\,2s\,^2S_{1/2}$					$1s^2\,2p\,^2P_{3/2} \rightarrow 1s^2\,2s\,^2S_{1/2}$					
Z	Wel	Eff	KS	DF	PT	Wel	Eff	KS	DF	PT	PT
10	0.006	0.006				0.005	0.006				
11	0.008	0.008				0.007	0.007				
12	0.009	0.010				0.009	0.009				0.009
13	0.012	0.012				0.011	0.011				
14	0.014	0.015				0.013	0.014				0.013
15	0.017	0.017				0.015	0.016				
16	0.020	0.021				0.018	0.019				0.018
17	0.023	0.024				0.021	0.022				
18	0.026	0.028				0.024	0.026				0.024
19	0.030	0.032				0.027	0.030				
20	0.034	0.037	0.038	0.037	0.036 0.038	0.031	0.034	0.035	0.034	0.031 0.033	0.032
21	0.039	0.041				0.035	0.038				
22	0.044	0.047				0.040	0.043				
23	0.049	0.052				0.044	0.048				
24	0.055	0.058				0.049	0.054				

25	0.061	0.065				0.055	0.060				
26	0.067	0.072				0.060	0.066				
27	0.074	0.079				0.066	0.073				
28	0.081	0.087				0.073	0.080				
29	0.088	0.095				0.079	0.088				
30	0.096	0.104				0.086	0.096				0.086
31	0.104	0.113				0.094	0.105				
32	0.113	0.122				0.102	0.114				
33	0.123	0.133				0.110	0.123				
34	0.132	0.143				0.119	0.133				
35	0.142	0.155				0.128	0.144				
36	0.153	0.166				0.138	0.155				
39	0.188	0.195				0.170	0.182				
42	0.228	0.250				0.207	0.235				
47	0.306	0.338				0.281	0.322				
50	0.361	0.423	0.370	0.370	0.360	0.334	0.408	0.360	0.350	0.320	0.318
54	0.444	0.529				0.416	0.516				
56	0.491	0.494				0.463	0.484				
59	0.566	0.567				0.542	0.563				
60	0.593	0.593	0.600	0.580	0.550	0.571	0.591	0.600	0.590	0.530	0.532
62	0.650	0.646				0.632	0.651				
64	0.711	0.703				0.699	0.717				
66	0.775	0.763				0.773	0.788				
68	0.844	0.827				0.853	0.866				
70	0.917	0.895				0.941	0.951				0.859
74	1.077	1.042	1.010	0.990	0.930	1.145	1.141	1.130	1.120	1.020	
79	1.303	1.251				1.460	1.435				
82	1.454	1.387				1.689	1.645				
83	1.506	1.435	1.380	1.270	1.190	1.773	1.722	1.700	1.640	1.570	1.579
					1.19					1.500	
90	1.900	1.780				2.499	2.375				2.199
92	2.019	1.887	1.800	1.500	2.230	2.761	2.638	2.560	2.330	2.770	2.420
94	2.139	2.005				3.051	2.885				
96	2.255	2.039				3.378	3.160				

Table 5.2 – The screened self-energy for the transition $1s\,2s\,2p\,^2P_J \rightarrow 1s^2\,2s\,^2S_{1/2}, J = 1/2, 3/2$ and $1s\,2s\,2p\,^4P_J \rightarrow 1s^2\,2s\,^2S_{1/2}, J = 1/2, 3/2, 5/2$ of Li-like ions (in eV). The Welton (Wel) and effective operater (Eff) results are obtained by Welton picture and effective operator model.

	$^2P_{1/2} \rightarrow^2 S_{1/2}$		$^2P_{3/2} \rightarrow^2 S_{1/2}$		$^4P_{1/2} \rightarrow^2 S_{1/2}$		$^4P_{3/2} \rightarrow^2 S_{1/2}$		$^4P_{5/2} \rightarrow^2 S_{1/2}$	
Z	Wel	Eff	Wel	Eff	Wel	Eff	Wel	Eff	Wel	Eff
10	0.020	0.021	0.020	0.021	0.022	0.023	0.022	0.023	0.022	0.023
11	0.025	0.027	0.026	0.027	0.029	0.030	0.029	0.030	0.028	0.030
12	0.032	0.033	0.032	0.034	0.036	0.038	0.036	0.038	0.035	0.037

13	0.039	0.041	0.039	0.041	0.044	0.046	0.044	0.046	0.043	0.046
14	0.047	0.049	0.047	0.050	0.053	0.056	0.053	0.056	0.052	0.055
15	0.055	0.058	0.057	0.059	0.063	0.066	0.063	0.066	0.063	0.066
16	0.065	0.068	0.067	0.070	0.075	0.078	0.074	0.078	0.074	0.077
17	0.075	0.078	0.078	0.082	0.087	0.091	0.087	0.091	0.086	0.090
18	0.086	0.090	0.091	0.095	0.100	0.105	0.100	0.105	0.099	0.104
19	0.098	0.102	0.105	0.109	0.115	0.121	0.115	0.120	0.114	0.120
20	0.111	0.115	0.120	0.125	0.131	0.138	0.131	0.137	0.130	0.136
21	0.125	0.129	0.136	0.142	0.149	0.156	0.148	0.155	0.147	0.154
22	0.139	0.144	0.153	0.160	0.167	0.175	0.167	0.174	0.165	0.173
23	0.155	0.160	0.173	0.180	0.187	0.196	0.187	0.195	0.185	0.193
24	0.171	0.176	0.193	0.202	0.209	0.218	0.208	0.217	0.206	0.215
25	0.188	0.194	0.215	0.224	0.232	0.241	0.231	0.241	0.229	0.239
26	0.206	0.212	0.239	0.248	0.256	0.266	0.256	0.266	0.253	0.263
27	0.225	0.231	0.264	0.275	0.282	0.293	0.282	0.293	0.278	0.290
28	0.245	0.251	0.291	0.303	0.309	0.321	0.309	0.321	0.306	0.318
29	0.266	0.272	0.320	0.332	0.339	0.351	0.339	0.351	0.335	0.347
30	0.288	0.294	0.351	0.363	0.370	0.382	0.370	0.382	0.365	0.378
31	0.312	0.317	0.383	0.396	0.402	0.415	0.403	0.415	0.398	0.411
32	0.337	0.342	0.417	0.431	0.437	0.450	0.437	0.450	0.432	0.446
33	0.363	0.367	0.453	0.468	0.474	0.487	0.474	0.487	0.468	0.482
34	0.390	0.394	0.491	0.506	0.512	0.525	0.513	0.525	0.506	0.520
35	0.419	0.422	0.531	0.543	0.553	0.566	0.554	0.566	0.546	0.560
36	0.449	0.452	0.573	0.589	0.595	0.608	0.597	0.608	0.589	0.602
39	0.550	0.548	0.714	0.723	0.737	0.747	0.739	0.748	0.730	0.741
42	0.665	0.657	0.868	0.889	0.900	0.905	0.901	0.907	0.892	0.899
47	0.896	0.871	1.186	1.205	1.227	1.216	1.230	1.220	1.221	1.212
50	1.061	1.021	1.424	1.443	1.461	1.434	1.472	1.440	1.457	1.434
54	1.314	1.247	1.785	1.746	1.823	1.767	1.839	1.775	1.826	1.773
56	2.515	2.462	1.989	1.935	2.029	1.953	2.046	1.963	2.036	1.964
59	1.694	1.578	2.340	2.332	2.371	2.260	2.399	2.273	2.387	2.281
60	1.780	1.651	2.463	2.361	2.495	2.370	2.523	2.384	3.098	3.000
62	1.961	1.801	2.724	2.595	2.757	2.597	2.786	2.615	3.429	3.292
64	2.157	1.965	3.030	2.852	3.042	2.844	3.075	2.866	3.788	3.613
66	2.369	2.141	3.344	3.131	3.351	3.112	3.404	3.138	4.180	3.965
68	2.597	2.335	3.679	3.437	3.686	3.404	3.739	3.436	4.605	4.354
70	2.844	2.538	4.070	3.765	4.049	3.715	4.123	3.753	5.068	4.768
74	3.397	2.980	4.926	4.496	4.866	4.401	4.971	4.455	5.022	4.557
79	4.217	3.634	6.250	5.608	6.089	5.423	6.247	5.506	6.355	5.683
82	8.845	8.041	7.194	6.385	6.947	6.122	7.148	6.228	7.308	6.471
83	4.993	4.225	7.565	6.665	7.256	6.371	7.475	6.487	7.654	6.755
90	6.656	5.393	10.436	8.965	9.801	8.341	10.181	8.545	10.546	9.085
92	7.214	5.810	11.477	9.811	10.667	9.040	11.112	9.279	11.556	9.930
94	7.816	6.222	12.591	10.703	15.230	13.380	12.127	10.043	15.230	13.380
96	8.467	6.693	13.825	11.825	16.683	14.699	13.239	10.906	16.683	14.699

The previous MCDFGME code used the Welton approximation (see section a)) to evaluate the self-energy screening correction. Recently, Indelicato has modified the code using the model operator method (see section b)) developed by the St. Petersburg group [104, 162]. The new code is covered in detail in the theoretical part of Chapter 4.

In Table 5.1, the self-energy screening energies for the transition $1s^2\,2p\,^2P_{1/2} \rightarrow 1s^2\,2s\,^2S_{1/2}$ and $1s^2\,2p\,^2P_{3/2} \rightarrow 1s^2\,2s\,^2S_{1/2}$ of Li-like ions are presented and are compared with results of other calculations. The present results of the Welton (Wel) and effective (Eff) are obtained by Welton picture and effective model operator, respectively. In early works, Blundell's screened self-energy and vacuum polarization energies [279] already included estimates of contributions of one-loop Lamb-shift added to the MBPT results, whose screened calculations start from the core-Hartree potential, but the vertex-exchange terms were not calculated.

The St. Petersburg group [104, 281, 297] considered the screened self-energy correction using the model of SE operator technique, which can be expressed as the Kohn-Sham (KS) or Dirac-Fock (DF) equation in total energy. The DF and KS potentials are constructed self-consistently in consideration of the valence state. The calculations by the perturbation theory (PT) with the Kohn-Sham potential is obtained by YS Kozhedub [281] using the CI method and J. Sapirstein [26] using the S-matrix method. The screened self-energy from our results fits well with St. Petersburg group for the iso-electronic sequence. This also verifies the accuracy of our calculations on screened self-energy. Our results obtained employing the model SE operator approach are in rough agreement with the results obtained with the perturbation theory. Perturbation theory values are a little smaller than DF values.

We can compare the different values as an example to evaluate the reliability of this technique for calculating self-energy screening. For example, the $2p_{1/2} - 2s$ transition in Li-like calcium from the St. Petersburg group [104] has a QED value of 0.038 eV, and Ref.[26] has a QED value of 0.038 eV. The Welton technique provides 0.034 eV, and the implementation of effective operator technique achieves a result of 0.037 eV, which is closer to St. Petersburg's calculations. Therefore, for the effective operator and the Welton operator technique, we can evaluate them by assuming an uncertainty of 0.001 eV and 0.004 eV, respectively. The same procedure applied to the tungsten ion transition gives the following data, respectively, 1.010 eV from St. Petersburg [104], 0.930 eV from Ref.[26], 1.042 eV from the effective operator method, and 1.077 eV from the Welton method. While, uranium ion transition provides 2.019 eV for the Welton method, 1.887 eV for the effective operator method, 1.800 eV using St. Petersburg [104] and 1.500 eV using Ref.[26].

In Table 5.2, the self-energy screening energies for core-excited transitions $1s\,2s\,2p\,^2P_J \rightarrow 1s^2\,2s\,^2S_{1/2}, J = 1/2, 3/2$ and $1s\,2s\,2p\,^4P_J \rightarrow 1s^2\,2s\,^2S_{1/2}, J = 1/2, 3/2, 5/2$ of Li-like ions are also presented. The deviation between Welton method and effective operator method in valence-excited transitions is 0.2 eV at Li-like curium, while this deviation has reached 2 eV in core-excited transitions.

Table 5.3 – Individual contributions to $1s^2\,2p\,^2P_{3/2} \rightarrow 1s^2\,2s\,^2S_{1/2}$ transition energies on selected lithiumlike ions, are evaluated with the MCDFGME code. All energies are given in eV.

Contribution	Z=10	Z=26	Z=56	Z=79	Z=92
Coulomb+ Uelhing	16.225	65.281	571.480	2279.666	4530.514
Magnetic	0.000	0.062	0.492	-0.512	-3.956
Retardation	-0.005	-0.132	-1.402	-3.684	-5.316
Higher-order Retardation	0.000	-0.011	-0.577	-3.262	-6.963
Self-energy	-0.020	-0.559	-7.952	-29.239	-56.546
Sef-energy screening	0.006	0.066	0.484	1.435	2.638
Uelhing (muon pairs)	0.000	0.000	0.000	0.001	0.003
Electronic density Uelhing	0.000	0.000	-0.007	-0.030	-0.068
Wichmann and Kroll	0.000	0.000	-0.026	-0.239	-0.709
Källèn and Sabry	0.000	0.000	0.009	0.049	0.117
Two-loop self-energy	0.000	0.000	0.007	-0.119	0.278
SEVP	0.000	-0.004	-0.008	-0.426	-0.204
S(VP)E	0.000	0.000	-0.002	-0.056	-0.025
Normal mass shift	0.000	-0.001	-0.002	-0.004	-0.004
Specific mass shift	-0.004	-0.012	-0.023	-0.030	-0.031
Relativistic Recoil	0.000	0.000	-0.003	-0.013	-0.022
Coulomb correlation	-0.109	-0.124	-0.130	-0.150	-0.176
Magnetic correlation	0.001	0.013	0.090	0.289	0.523
Retardation correlation	0.000	-0.001	-0.013	-0.054	-0.105
Higher-order ret. Corr.	0.000	0.001	0.015	0.021	-0.005
Total	16.092	64.579	562.433	2243.641	4459.942

5.2 QED contribution

We now mainly discuss the calculation results for radiation corrections. Table 5.3 and Table 5.4 present the breakdown of individual radiative contributions of $1s^2\,2p\,^2P_{3/2} \rightarrow 1s^2\,2s\,^2S_{1/2}$ transition and $1s\,2s\,2p\,^2P_{3/2} \rightarrow 1s^2\,2s\,^2S_{1/2}$ transition in selected lithiumlike ions. One-electron radiative corrections are exact QED calculations. The self-consistent field process includes Uëhling potential and full Breit interaction.

Next, we consider the one-loop QED corrections, which are the largest effects. They are determined by the self-energy and vacuum-polarization corrections and are presently well described. We present the details in Sec. 2.4.1. The one-electron self-energy is taken from the work of Mohr and co-workers [282, 283, 284, 285, 286], and corrected for finite nuclear size. The Uëhling part of the vacuum-polarization contribution, which is the exact contribution of the Uëhling potential with Dirac wave functions including the finite nuclear size, is calculated in the present works from Ref. [124]. The expression of the Uëhling potential relates to the charge density. Here, we calculate a correction in which the nuclear charge density is replaced by the charge density of the electron. This correction is very small, except for very high-Z ions. The vacuum polarization due to the creation of virtual

Table 5.4 – Individual contributions to the $1s\,2s\,2p\,^2P_{3/2} \rightarrow 1s^2\,2s\,^2S_{1/2}$ transitions energies on selected lithiumlike ions, as evaluated with the MCDFGME code. All energies are given in eV.

Contribution	Z=10	Z=26	Z=56	Z=79	Z=92
Coulomb+ Uelhing	908.056	6671.882	33102.521	70584.687	101002.176
Magnetic	-0.332	-6.585	-67.854	-203.327	-340.466
Retardation	0.011	0.237	0.627	0.488	0.200
Higher-order Retardation	0.000	0.009	0.113	0.175	0.123
Self-energy	-0.156	-4.259	-56.915	-192.355	-346.156
Sef-energy screening	0.021	0.248	1.935	5.608	9.811
Uelhing (muon pairs)	0.000	0.000	0.001	0.005	0.015
Electronic density Uelhing	0.000	-0.004	-0.049	-0.174	-0.336
Wichmann and Kroll	0.000	-0.002	-0.198	-1.638	-4.455
Källèn and Sabry	0.000	0.003	0.067	0.318	0.696
Two-loop self-energy	0.000	0.003	0.121	0.667	1.556
SEVP	0.000	-0.001	-0.060	-0.421	-1.129
S(VP)E	0.000	0.000	-0.011	-0.056	-0.135
Normal mass shift	-0.025	-0.065	-0.123	-0.164	-0.165
Specific mass shift	0.003	0.011	0.006	0.002	0.000
Relativistic Recoil	0.000	-0.001	-0.021	-0.074	-0.126
Coulomb correlation	0.572	0.452	0.236	-0.063	-0.345
Magnetic correlation	0.038	0.290	1.705	3.850	5.748
Retardation correlation	-0.011	-0.081	-0.434	-0.930	-1.357
Higher-order ret. Corr.	0.000	0.001	0.011	-0.043	-0.166
Total	908.178	6662.136	32981.676	70196.554	100325.490

muon pairs is listed in the Table 5.3 and 5.4, which is very small and even in the high-Z ions, and the order of magnitude is only 0.001 eV for the $1s^2\,2p\,^2P_{3/2} \rightarrow 1s^2\,2s\,^2S_{1/2}$ transition. The Wichmann-Kroll part of the vacuum-polarization contribution is also evaluated from Ref. [158].

The next effects are the screened QED contributions from other electrons. The evaluation of the screened QED corrections is introduced in Sec. 2.4.3 following [128, 130, 156, 155, 117]. Here we compare the self-energy screening obtained using the Welton approximation [156, 155] and the approach from Ref. [104, 162]. We have made a detailed discussion in Sec. 5.1 for this contribution.

Another correction that leads to the largest theoretical uncertainty of middle- and high-Z ions comes from nuclear recoil. The evaluation of the recoil effect is described in Sec. 2.5. This calculation significantly improves the accuracy of theoretical simulation of $2p_j - 2s$ transition energy for Li-like ions. The relativistic correction with the nuclear movement is treated as a relativistic-recoil correction. In the calculation, all orders in m/M and the lowest order leading term in $Z\alpha$ are considered. We obtain the calculations of normal mass shift and specific mass shift evaluating the reduced mass correction. Their contributions are presented in the Table 5.3 and Table 5.4 separately. We have observed

that for the valence-excited transitions, the specific mass shift dominates in the recoil correlation, and the normal mass shift is equal to zero at low-Z ions. While for core-excited transitions, the normal mass shift dominates the recoil correlation and the specific mass shift is equal to zero at high-Z ions. We also notice that the relativistic recoil is equal to zero in all the transitions in low-Z ions.

Finally, we account for the two-loop QED effects. They are called SEVP, VPVP, and S(VP)E contributions, which are evaluated in Sec. 2.4.2. Yerokhin, Indelicato and Shabaev [24] performed all-order calculations for the two-loop one electron QED corrections of $n = 2$ states for several ions with $Z \geq 60$ at first. We used the values from this reference within the Z range covered. The remaining two-loop self-energy correction (the "SESE" subset), which is taken from Refs. [287, 288, 289, 24, 290, 291, 292, 293]. The SEVP and S(VP)E corrections are obtained from Ref. [291]. The indicated error bars are due to the free-loop approximation used in evaluating the VPVP and S(VP)E subsets, which Ref. [24] gives the details. The Kallen and Sabry potential is also included, as described in Ref. [157].

The current level of experimental accuracy requires a rigorous QED calculation for the two-photon exchange contribution in Li-like ions. At the same time, no strict QED calculations have been performed for more photon exchange contributions so far. For few-electron ions with high-Z, the evaluation of these contributions within the Breit approximation is usually not sufficient.

The nuclear polarization correction for Li-like thorium was 0.02 eV and Li-like uranium was 0.03 eV for $2p_{1/2} - 2s$ transition, which were studied by Plunien [295] and by Nefiodov [296].

5.3 Electron correlation

In a relativistic calculation, the correlation contribution is composed of the Breit part of the electron-electron interaction and pure Coulomb interaction between the electrons. The Breit interaction is separated into the magnetic interaction, the first term of the retardation and the higher-order retardation of the electromagnetic field. As already discussed in section 2.3, the total instantaneous $g^{ins} = (1 - \boldsymbol{\alpha_1} \cdot \boldsymbol{\alpha_2})/R$ and the complete retardation g^{ω} can be added in the self-consistent Dirac-Fock method. This will improve the results of the heavy ions, where the retardation interaction is no longer a small perturbation compared to the Coulomb repulsion. While these interactions become small compared to the nuclear potential, the wave functions become more hydrogenic, as Z increases. In Tables .10, .11, .12, .13, .14, .15, .16 of Appendix A (6.5), we provide individual values of the Coulomb, magnetic, retardation and higher-order retardation correlations, which are obtained using a wavefunction built up from all configurations with $n = 1, 2, 3, 4$ and 5 for Z=10 to 96.

The retardation correlation is more intricate, so it leads to yet unsolved fundamental problems. The definition of ω (Equation. 2.26) is terms of one-electron energies. Koopmans' theorem can be used to provide estimates of single-particle energies for a single configuration, while there is no single-particle parameter being identified as an approximation one-electron energy in the case of MCDF.

We also plot the individual correlations of Coulomb and Breit electron-electron interac-

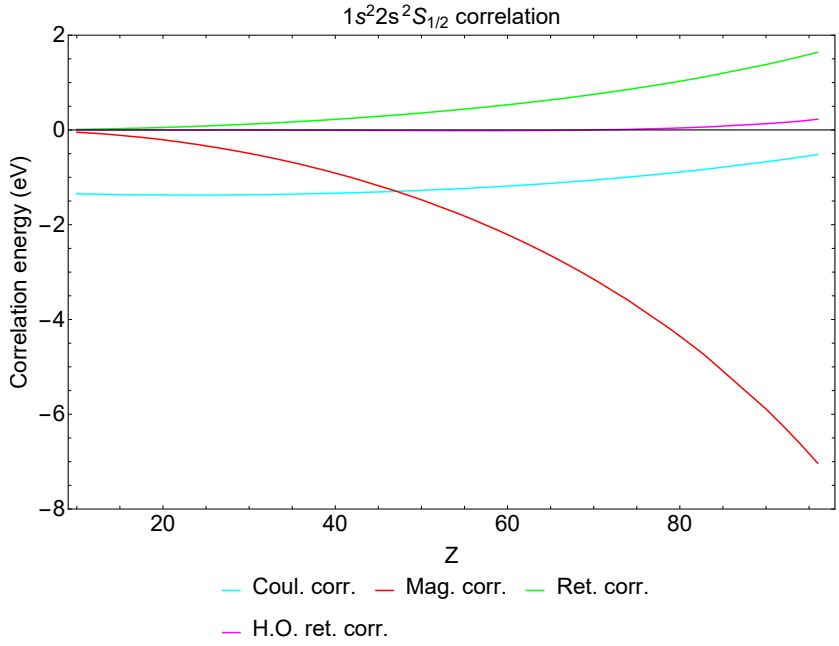

Fig. 5.1 *Correlation from Coulomb, magnetic, retardation, and higher order retardation part on ground state of* $1s^2\,2s\,^2S_{1/2}$

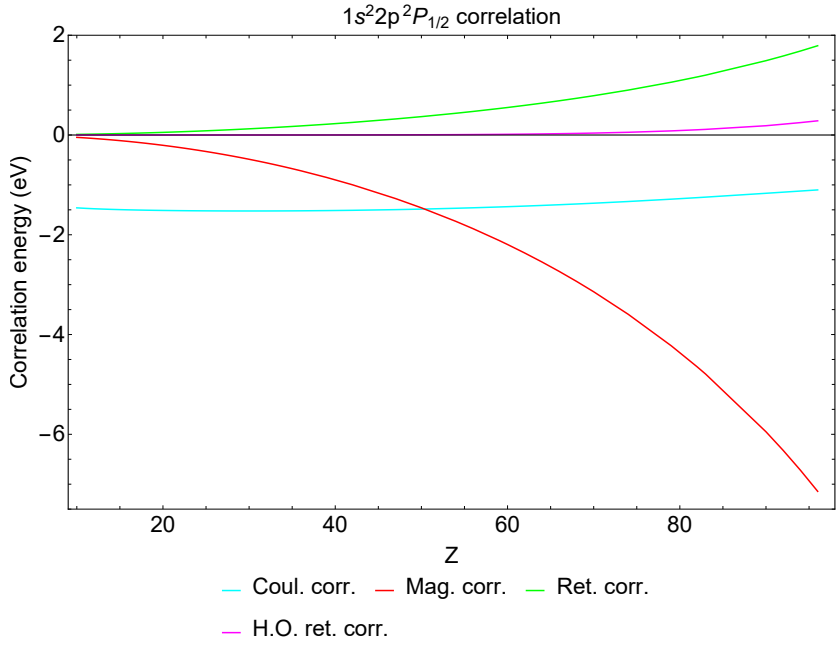

Fig. 5.2 *Correlation from Coulomb, magnetic, retardation, and higher order retardation on excited state of* $1s^2\,2p\,^2P_{1/2}$

tions to level energies for the ground state of $1s^2\,2p\,^2S_{1/2}$, the excited state of $1s^2\,2p\,^2P_{1/2}$ and core-excited state of $1s\,2s\,2p\,^2P_{3/2}$ in Li-like ions in Fig. 5.1, Fig. 5.2 and Fig. 5.3,

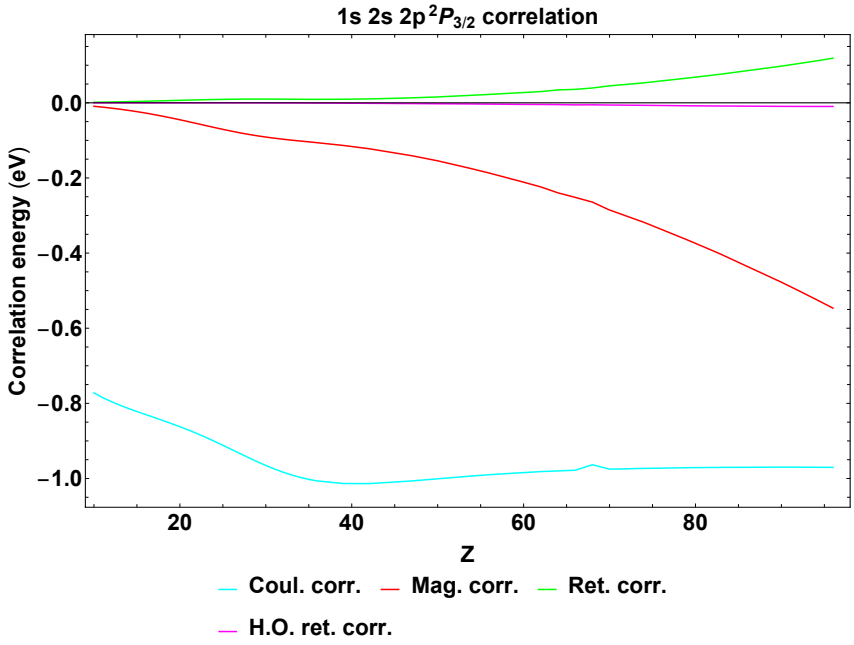

Fig. 5.3 *Correlation from Coulomb, magnetic, retardation, and higher order retardation on excited state of* $1s\,2s\,2p\,^2P_{3/2}$

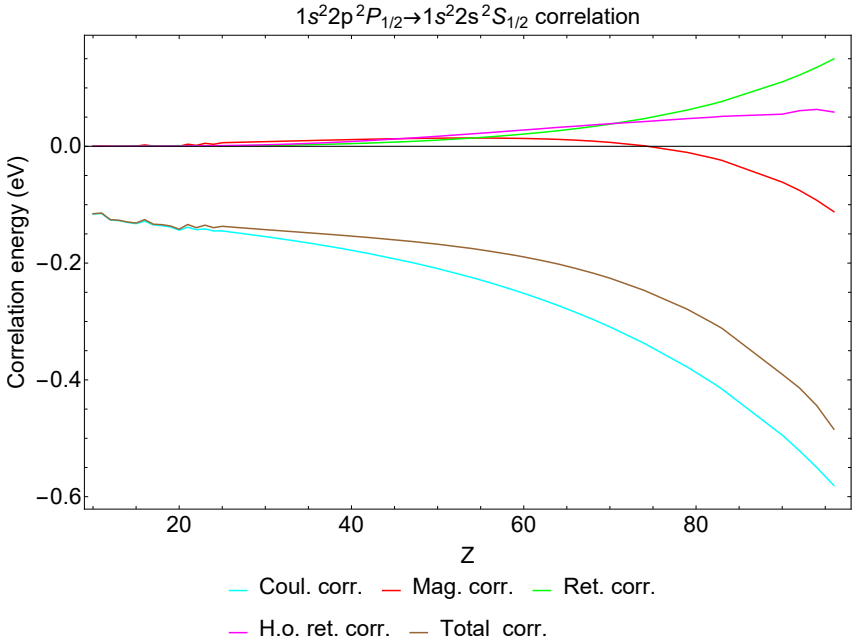

Fig. 5.4 *The difference correlation from Coulomb, magnetic, retardation, and higher order retardation between* $1s^2\,2s\,^2S_{1/2}$ *and* $1s^2\,2p\,^2P_{1/2}$

respectively. The blue line indicates the Coulomb correlation, the red line represents the magnetic correlation, the green line stands for the retardation correlation, and the pink

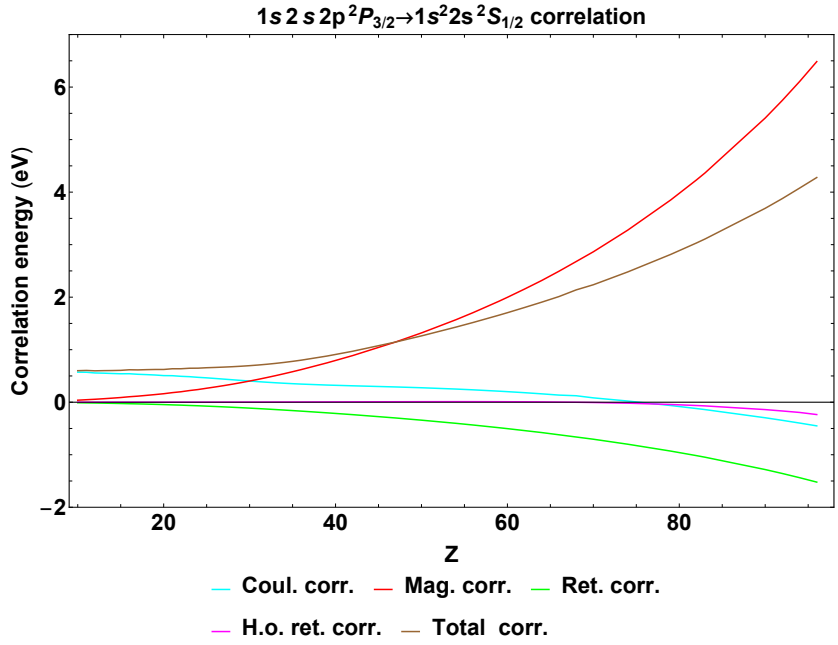

Fig. 5.5 *The difference correlation from Coulomb, magnetic, retardation, and higher order retardation between* $1s^2\,2s\,^2S_{1/2}$ *and* $1s\,2s\,2p\,^2P_{3/2}$

line represents the higher-order retardation correlation of the Breit interaction. Correlation corrections of the magnetic interaction start being the same size as Coulomb correlation at Z=47 and to be ten times larger at Z=92 for the ground state of three-electron systems. In the excited state of $1s^2\,2p\,^2P_J, J = 1/2, 3/2$, there is a similar trend consistent with the two-electron systems [294]. Although the Coulomb correlation has always been larger than the magnetic correlation for the core-excited state in the isoelectronic sequence of Li-like ions, the magnetic correlation energy gives a sizable contribution(about -0.6 eV) at high-Z. The results of the higher-order correlation are estimated to be less than 0.1 eV due to their scaling as $1/Z$ compared to the leading correlation contribution, while at high-Z, its value is higher than 0.1 eV seeing Fig. 5.1.

In Fig. 5.4 and Fig. 5.5, we also plot the individual contributions of Coulomb and Breit electron-electron interactions to transition energies for the $1s^2\,2p\,^2P_{1/2} \rightarrow 1s^2\,2s\,^2S_{1/2}$ and $1s\,2s\,2p\,^2P_{3/2} \rightarrow 1s^2\,2s\,^2S_{1/2}$ transitions in Li-like ions. We note that the Coulomb correlation dominates the contributions and is consistent with the trend of total correlations in the valence-excited transition. However, for core-excited transition, the magnetic correlation energy is consistent with the trend of total correlations, because the magnetic correlation energy is so large in the middle- and high-Z ions.

5.4 Total transition energy and transition probability

We have evaluated the valence-excited transitions of the $1s^2\,2p\,^2P_J \rightarrow 1s^2\,2s\,^2S_{1/2}, J = 1/2, 3/2$, core-excited transitions of the $1s\,2s\,2p\,^2P_J \rightarrow 1s^2\,2s\,^2S_{1/2}, J = 1/2, 3/2$, $1s\,2s\,2p\,^4P_J \rightarrow 1s^2\,2s\,^2S_{1/2}, J = 1/2, 3/2, 5/2$, and Auger transitions of the $1s\,2s\,2p\,^2P_J \rightarrow 1s^2\,^1S_0, J =$

Table 5.5 – Convergence of radiative and Auger transition energies for the transition of $1s\,2s\,2p\,^2P_{3/2} \rightarrow 1s^2\,2s\,^2S_{1/2}$ in Li-like neon and uranium. All energies are in eV.

	Radiative				Auger			
	Welton		Model operator		Welton		Model operator	
Max.n	10	92	10	92	10	92	10	92
DF	907.58	100323.28	907.58	100321.61	668.63	67486.95	668.63	67485.39
2	908.22	100325.51	908.22	100323.83	669.63	67490.54	669.63	67488.99
3	908.23	100326.81	908.23	100325.16	669.26	67490.30	669.26	67488.75
4	908.21	100327.02	908.21	100325.38	669.16	67490.30	669.16	67488.75
5	908.18	100327.10	908.19	100325.47	669.11	67490.30	669.11	67488.79

$1/2, 3/2$, $1s\,2s\,2p\,^4P_J \rightarrow 1s^2\,^1S_0, J = 1/2, 3/2$ in Li-like from neon (Z=10) to uranium (Z=92). For some of these transitions, we calculate to curium (Z=96) with convergence allowed. We perform these calculations using the multiconfiguration Dirac-Fock approach, which is implemented in the relativistic MCDF code (MCDFGME), written by Indelicato and Desclaux [105, 156, 155]. We used the new version of the code, which takes into account the most-recent two-loop self-energy corrections calculations [287], although their effects are very small here. A complete description of the approach and code can be found in Refs. [105, 106, 177]. This approach also evaluates specific and normal mass shifts after [178, 179, 180] as described in [183]. All of the calculations are performed taking into account the finite nucleus with fermi model. The atomic masses are taken from tables in Ref. [184] and the nuclear radii from [185, 186], respectively.

The most important feature of the MCDF code is to include a lot of electronic correlations with a limited number of configurations [187, 189, 190]. The calculations are rather difficult for the excited states $1s2s2p$, when the $1s2s$ core acquires a $^1S_0$ component. In this case, the off-diagonal Lagrange multiplier that is used to maintain the orthogonality between the two orbitals tend to become very small, and the $2s$ orbital tends to become identical to the $1s$. Here, we give three sets of $(1s)2(2p)1$, $(1s)1(2s)1(2p)1$, and $(2s)2(2p)1$ as reference configurations and use the method of $2s$ as frozen orbital to solve the Dirac equation. The presence of the $1s^2$ orbital can prevent the $2s$ electron to become $1s$ orbital. The self-consistent field process includes Uëhling potential and full Breit interaction. The projection operator has been taken into account [177] to avoid coupling with the negative energy continuum.

Here, for Li-like ions, the correlation contributions are obtained by taking into account all single-electron, double-electron and triple-electron excitations containing $n = 1$ and $n = 2$ electrons in the undisturbed configuration until $n = 5$. For $1s^2\,2s\,^2S_{1/2}$ ground state, it is related to the 1463 configurations and for $1s\,2s\,2p\,^2P_{3/2}$ core-excited state to 2478 configurations. The convergence of the radiative and Auger transition energies for the transition of $1s\,2s\,2p\,^2P_{3/2} \rightarrow 1s^2\,2s\,^2S_{1/2}$ in Li-like neon and uranium can be found in Table 5.5, which allows us to make a detailed estimate of the reliability of the MCDF calculation. We had to employ virtual orbitals to ensure the convergence of the MCDF calculation results.

5.4.1 $1s^2\,2p\,^2P_J \rightarrow 1s^2\,2s\,^2S_{1/2}, J = 1/2, 3/2$ transition

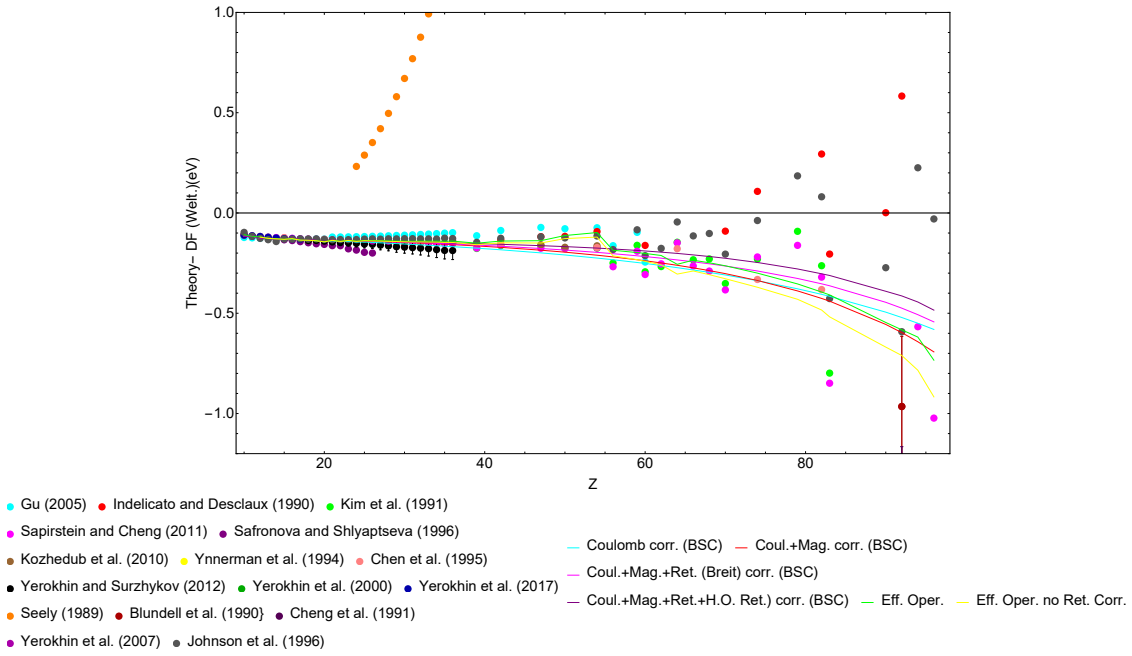

Fig. 5.6 *Comparison of the transition energy between theoretical values and the present MCDF calculations for the* $1s^2\,2p\,^2P_{1/2} \rightarrow 1s^2\,2s\,^2S_{1/2}$ *transition. The reference value is obtained with the DF Welton unperturbed method. Theoretical works: Gu (2005)[258], Indelicato and Desclaux (1990)[156], Kim et al. (1991)[252], Sapirstein and Cheng (2011)[26], Safronova and Shlyaptseva (1996)[256], Kozhedub et al. (2010)[281], Ynnerman et al. (1994)[253], Chen et al. (1995)[254], Yerokhin and Surzhykov (2012)[192], Yerokhin et al. (2000)[257], Yerokhin et al. (2017)[193], Seely (1989)[249], Blundell et al. (1990)[250], Cheng et al. (1991)[218], Yerokhin et al. (2007)[25], Johnson et al. (1996)[255]. Our calculations: Coulomb corr.: Coulomb correlation; Mag.corr: magnetic correlation; Ret.: retardation; H.O.Ret.: higher-order retardation; Eff.Oper.:Effective Operator; DF:single-configuration Dirac Fock model.*

Table 5.6 – Comparison of the transition energy between experiment and the present MCDF calculations using Welton model and effective operators, respectively, for the $1s^2\,2p\,^2P_{1/2} \rightarrow 1s^2\,^1S_0$ transition. The other theory is from Sapirstein and Cheng [26]. Energies are in eV.

			$1s^2\,2p\,^2P_{1/2} \rightarrow 1s^2\,^1S_0$			
Z	Experiment	Error	Diff. Welt.	Diff. Effec.	Diff.Th.	Ref.
10	15.88870	0.00025	-0.00688	0.00015	-0.00110	Edlén (1983) [209]
10	15.88881	0.00020	-0.00699	0.00004	-0.00121	Bockasten et al. (1963) [210]
11	17.86141	0.00037	-0.00117	-0.00241	-0.00081	Edlén (1983) [209]
11	17.86140	0.00100	-0.00116	-0.00240	-0.00080	Nikolic et al. (2004) [223]

12	19.83938	0.00063	-0.00965	-0.00400	-0.00118	Widing and Purcell (1976) [195]
12	19.83896	0.00037	-0.00923	-0.00358	-0.00076	Edlén (1983) [209]
13	21.82271	0.00050	-0.00728	-0.00717	-0.00081	Edlén (1983) [209]
14	23.81015	0.00091	-0.00522	-0.00384	0.00215	Widing and Purcell (1976) [195]
14	23.81253	0.00037	-0.00760	-0.00622	-0.00023	Edlén (1983) [209]
15	25.80979	0.00149	-0.00541	-0.00467	0.00201	Edlén (1983) [209]
16	27.81723	0.00125	0.00267	0.00122	0.00257	Widing and Purcell (1976) [195]
16	27.81871	0.00074	0.00119	-0.00026	0.00109	Edlén (1983) [209]
17	29.8379	0.0015	-0.0055	-0.0065	0.0001	Edlén (1983) [209]
18	31.86353	0.00164	-0.00067	-0.00178	0.00457	Widing and Purcell (1976) [195]
18	31.86642	0.00087	-0.00356	-0.00467	0.00168	Edlén (1983) [209]
18	31.86370	0.00057	-0.00084	-0.00195	0.00440	Biedermann et al. (2007) [300]
18	31.86714	0.00124	-0.00428	-0.00539	0.00096	Peacock et al. (1984) [216]
20	35.9625	0.0021	-0.0106	-0.0105	-0.0002	Widing and Purcell (1976) [195]
20	35.9614	0.0010	-0.0095	-0.0094	0.0009	Edlén (1983) [209]
21	38.020	0.040	0.009	0.009	0.011	Suckewer et al. (1980) [213]
22	40.11590	0.00195	-0.00879	-0.00899	-0.00350	Hinnov et al. (1989) [208]
22	40.1150	0.0010	-0.0079	-0.0081	-0.0026	Edlén (1983) [209]
22	40.1150	0.0012	-0.0079	-0.0081	-0.0026	Peacock et al. (1984) [216]
24	44.3291	0.0032	-0.0098	-0.0093	-0.0082	Widing and Purcell (1976) [195]
24	44.3230	0.0032	-0.0036	-0.0031	-0.0021	Hinnov et al. (1989) [208]
24	44.3276	0.0037	-0.0082	-0.0077	-0.0067	Edlén (1983) [209]
25	46.4569	0.0035	-0.0038	-0.0028	-0.0064	Widing and Purcell (1976) [195]
25	46.4586	0.0050	-0.0055	-0.0045	-0.0081	Edlén (1983) [209]
26	48.6022	0.0038	-0.0019	-0.0003	-0.0033	Widing and Purcell (1976) [195]
26	48.6003	0.0038	0.0001	0.0017	-0.0014	Denne and Hinnov (1987) [202]
26	48.6001	0.0019	0.0002	0.0018	-0.0012	Knize (1991) [206]
26	48.6033	0.0019	-0.0030	-0.0014	-0.0044	Hinnov et al. (1989) [208]
26	48.6012	0.0031	-0.0008	0.0008	-0.0023	Edlén (1983) [209]
28	52.9395	0.0045	0.0114	0.0143	0.0112	Widing and Purcell (1976) [195]
28	52.9530	0.0045	-0.0021	0.0007	-0.0023	Denne and Hinnov (1987) [202]
28	52.9467	0.0038	0.0042	0.0070	0.0040	Staude et al. (1998) [205]
28	52.9496	0.0023	0.0013	0.0041	0.0011	Hinnov et al. (1989) [208]
28	52.960	0.014	-0.009	-0.006	-0.009	Zacarias et al. (1988) [211]
29	55.1531	0.0049	0.0037	0.0073	0.0027	Denne and Hinnov (1987) [202]
29	55.1595	0.0027	-0.0027	0.0009	-0.0037	Knize (1991) [206]
29	55.1543	0.0025	0.0025	0.0060	0.0015	Hinnov et al. (1989) [208]
30	57.3839	0.0029	-0.0009	0.0034	-0.0018	Staude et al. (1998) [205]
32	61.8992	0.0062	0.0058	0.0116	0.0043	Denne and Hinnov (1987) [202]
32	61.9008	0.0019	0.0043	0.0100	0.0027	Knize (1991) [206]
32	61.9023	0.0031	0.0027	0.0085	0.0012	Hinnov et al. (1989) [208]
34	66.5294	0.0071	-0.0071	0.0001	-0.0098	Denne and Hinnov (1987) [202]
34	66.5294	0.0025	-0.0071	0.0001	-0.0098	Knize (1991) [206]
34	66.5240	0.0054	-0.0018	0.0055	-0.0044	Hinnov et al. (1989) [208]
36	71.241	0.011	0.001	0.011	-0.001	Denne et al. (1989) [199]
36	71.235	0.033	0.007	0.016	0.005	Kukla et al. (2005) [201]

36	71.243	0.012	-0.001	0.008	-0.003	Denne and Hinnov (1987) [202]
36	71.2430	0.0080	-0.0012	0.0083	-0.0031	Madzunkov et al. (2002) [203]
36	71.284	0.016	-0.042	-0.033	-0.044	Martin et al. (1990) [301]
36	71.241	0.011	0.001	0.011	-0.001	Hinnov et al. (1989) [208]
39	78.5396	0.0045	0.0135	0.0180	-0.0061	Silwal et al. (2017) [215]
42	86.101	0.012	0.003	0.022	0.003	Denne et al. (1989) [197]
42	86.101	0.012	0.003	0.022	0.003	Hinnov et al. (1989) [208]
47	99.4379	0.0072	-0.0150	0.0141	-0.0238	Bosselman et al. (1999) [194]
50	107.9109	0.0075	-0.0088	0.0513	-0.0139	Feili et al. (2000) [200]
54	119.811	0.012	0.003	0.086	0.010	Träbert et al. (2003) [196]
54	119.816	0.042	-0.002	0.081	0.005	Bernhardt et al. (2015) [198]
54	119.8204	0.0081	-0.0066	0.0766	0.0006	Feili et al. (2000) [200]
56	126.112	0.013	-0.116	0.040	-0.043	Reader et al. (2014) [217]
79	216.134	0.096	-0.052	-0.108	0.084	Brandau et al. (2003) [212]
82	230.650	0.081	0.105	0.036	0.110	Brandau et al. (2003) [212]
92	280.59	0.10	0.95	0.81	0.06	Schweppe et al. (1991) [207]
92	280.516	0.099	1.028	0.886	0.136	Brandau et al. (2003) [212]
92	280.645	0.015	0.899	0.757	0.007	Beiersdorfer et al. (2005) [65]

Table 5.7 – Comparison of the transition energy between experiment and the present MCDF calculations using Welton model and effective operators, respectively, for the $1s^2\,2p\,^2P_{3/2} \rightarrow 1s^2\,^1S_0$ transition. The theory is from Sapirstein and Cheng [26]. Energies are in eV.

	$1s^2\,2p\,^2P_{3/2} \rightarrow 1s^2\,^1S_0$					
Z	Experiment	Error	Diff. Welt.	Diff. Effec.	Diff.Th.	Ref.
10	16.09330	0.00010	-0.00100	0.00667	-0.00050	Bockasten et al. (1963) [210]
10	16.09315	0.00035	-0.00085	0.00682	-0.00035	Edlén (1983) [209]
11	18.18761	0.00053	0.01931	0.01041	-0.00091	Edlén (1983) [209]
11	18.18700	0.00100	0.01992	0.01102	-0.00030	Nikolic et al. (2004) [223]
12	20.33228	0.00067	0.00121	-0.00596	-0.00078	Widing and Purcell [195]
12	20.33180	0.00053	0.00169	-0.00548	-0.00030	Edlén (1983) [209]
13	22.54132	0.00070	0.00106	-0.00418	-0.00102	Edlén (1983) [209]
14	24.82514	0.00099	0.00124	0.00399	0.00066	Widing and Purcell [195]
14	24.82635	0.00053	0.00003	0.00278	-0.00055	Edlén (1983) [209]
15	27.2050	0.0021	-0.0015	0.0010	-0.0024	Edlén (1983) [209]
16	29.6847	0.0014	-0.0058	-0.0180	0.0003	Widing and Purcell [195]
16	29.6863	0.0011	-0.0073	-0.0196	-0.0013	Edlén (1983) [209]
17	32.2891	0.0021	0.0074	0.0051	0.0016	Edlén (1983) [209]
18	35.0357	0.0020	0.0049	0.0059	0.0014	Widing and Purcell [195]
18	35.03803	0.00061	0.00249	0.00354	-0.00093	Peacock et al. (1984) [216]
18	35.0369	0.0012	0.0036	0.0046	0.0002	Edlén (1983) [209]
18	35.03160	0.00059	0.00892	0.00997	0.00550	Biedermann et al. (2007) [300]
20	41.0286	0.0027	-0.0032	-0.0006	-0.0044	Widing and Purcell [195]
20	41.0261	0.0014	-0.0007	0.0018	-0.0019	Edlén (1983) [209]

21	44.30943	0.00020	0.00954	0.01150	-0.00103	Lestinsky et al. (2008) [226]
21	44.312	0.035	0.007	0.009	-0.004	Suckewer et al. (1980) [213]
21	44.3107	0.0019	0.0083	0.0102	-0.0023	Kieslich et al. (2004) [214]
22	47.8150	0.0037	0.0027	0.0052	-0.0002	Hinnov et al. (1989) [208]
22	47.82012	0.00074	-0.00250	0.00005	-0.00532	Peacock et al. (1984) [216]
22	47.8201	0.0014	-0.0025	0.0001	-0.0053	Edlén (1983) [209]
24	55.5983	0.0050	-0.0021	0.0019	-0.0065	Widing and Purcell [195]
24	55.5958	0.0050	0.0004	0.0044	-0.0040	Hinnov et al. (1989) [208]
24	55.5936	0.0015	0.0027	0.0066	-0.0018	Knize (1991) [206]
24	55.5992	0.0053	-0.0030	0.0010	-0.0074	Edlén (1983) [209]
25	59.9247	0.0058	-0.0014	0.0029	-0.0105	Widing and Purcell [195]
25	59.9275	0.0070	-0.0042	0.0000	-0.0133	Edlén (1983) [209]
26	64.5617	0.0067	0.0099	0.0149	0.0003	Widing and Purcell [195]
26	64.5583	0.0067	0.0133	0.0182	0.0037	Denne and Hinnov (1987) [202]
26	64.5711	0.0067	0.0005	0.0055	-0.0091	Hinnov et al. (1989) [208]
26	64.5596	0.0030	0.0119	0.0169	0.0024	Knize (1991) [206]
26	64.5665	0.0044	0.0051	0.0100	-0.0045	Edlén (1983) [209]
28	74.9620	0.0091	0.0031	0.0096	-0.0072	Denne and Hinnov (1987) [202]
28	74.9575	0.0068	0.0076	0.0141	-0.0027	Staude et al. (1998) [205]
28	74.9620	0.0045	0.0031	0.0096	-0.0072	Hinnov et al. (1989) [208]
28	74.976	0.011	-0.011	-0.004	-0.021	Büttner et al. (1995) [302]
29	80.7694	0.0053	0.0043	0.0117	-0.0062	Brown et al. (1987) [224]
29	80.766	0.011	0.007	0.015	-0.003	Denne and Hinnov (1987) [202]
29	80.768	0.011	0.006	0.013	-0.005	Hinnov et al. (1989) [208]
29	80.7683	0.0032	0.0054	0.0128	-0.0051	Knize (1991) [206]
30	87.0303	0.0037	0.0038	0.0122	-0.0072	Staude et al. (1998) [205]
32	101.022	0.016	0.032	0.042	0.022	Denne and Hinnov (1987) [202]
32	101.042	0.016	0.011	0.022	0.002	Hinnov et al. (1989) [208]
32	101.0425	0.0049	0.0112	0.0217	0.0015	Knize (1991) [206]
34	117.298	0.022	0.030	0.042	0.019	Denne and Hinnov (1987) [202]
34	117.314	0.022	0.014	0.027	0.003	Hinnov et al. (1989) [208]
36	136.173	0.037	0.012	0.027	0.001	Denne et al. (1989) [199]
36	136.246	0.045	-0.062	-0.046	-0.072	Martin et al. (1990) [301]
36	136.198	0.036	-0.014	0.002	-0.024	Podpaly et al. (2014) [221]
36	136.216	0.090	-0.032	-0.016	-0.042	Kukla et al. (2005) [201]
36	136.157	0.030	0.028	0.043	0.017	Denne and Hinnov (1987) [202]
36	136.173	0.037	0.012	0.027	0.001	Hinnov et al. (1989) [208]
39	170.135	0.014	-0.010	-0.001	-0.038	Silwal et al. (2017) [215]
42	211.942	0.072	0.047	0.075	0.040	Denne et al. (1989) [197]
42	211.942	0.072	0.047	0.075	0.040	Hinnov et al. (1989) [208]
47	303.667	0.030	-0.001	0.039	0.000	Bosselman et al. (1999) [194]
54	492.174	0.052	0.032	0.131	0.032	Bernhardt et al. (2015) [198]
74	1697.3	1.0	-1.4	-1.5	-1.2	Podpaly et al. (2009) [222]
74	1696.20	0.50	-0.31	-0.32	-0.10	Clementson et al. (2011) [225]
82	2642.26	0.10	-0.26	-0.21	-0.09	Zhang et al. (2008) [227]
83	2788.139	0.039	0.298	0.241	-0.099	Beiersdorfer et al. (1998) [219]

90	4025.230	0.152	0.668	0.539	0.020	Beiersdorfer et al. (1995) [220]
92	4459.370	0.269	0.689	0.541	0.090	Beiersdorfer et al. (1993) [276]
92	4460.9	2.2	-0.8	-1.0	-1.4	Nakano et al. (2013) [303]

In three-electron systems, the valence-excited transitions of $1s^2\,2p\,^2P_J \rightarrow 1s^2\,2s\,^2S_{1/2}, J = 1/2, 3/2$ in Li-like ions can be well used to test QED effects and relativistic multi-body effects. A great deal of research has been done in both experiment and theory. For the experiment, generating a basic state $1s^2\,2s\,^2S_{1/2}$ becomes possible in the heavy ion source such as EBIT. However, it is still impossible to generate and stimulate this state for one and two-electron ions so far, since the production rate of the heavy elements is low [244, 245, 246]. At the same time, the experiments have been able to measure the transition energies very accurately using low energy X-ray or deep UV spectroscopy. Therefore, researchers have more measurements with higher accuracy. Accurate measurements of the valence-excited transitions in three-electronic systems can also be used to measure and compare isotope shifts and to obtain the discrepancy of nuclear radii among different isotopes. For example, this was used for different isotopes of Nd^{57+} [247].

Theoretical calculations for the valence-excited transitions have been performed in diverse methods. Johnson et al. [248] carried out an MBPT calculation with second- and third-order correlation contributions, and without QED contributions. Whereafter, Seely [249] made a systematic calculation (from Z=24 to 54) with approximate QED contributions, which are calculated using grasp package with MCDF method [251]. Indelicato and Desclaux [156] performed an MCDF calculation using MCDFGME code developed by themselves, with the Welton method for screened self-energy corrections. At high-Z ions, these results look very large with lack of some mixed two-photon QED. Kim et al. [252] deduced relativistic correlation energies by comparing the MBPT method from Johnson et al. [248] and DF results from Indelicato and Desclaux [156]. The total transition energies were obtained by combining these correlation energies, DF energies, and approximate QED screening corrections. These results look consistent with Sapirstein and Cheng [26] in low- and middle-Z ions. Ynnerman et al. [253] carried out the coupled-cluster single- and double-excited approximation with the inclusion of higher-order Breit contributions on Li-like U, which is about 0.15 eV lower than Sapirstein and Cheng [26]. Chen et al. [254] also used the coupled-cluster method and solved the Dirac equation by using B-spline as a basis set to evaluate nuclear deformation and higher-order Breit contributions. Later, Johnson [255] extended this method to more ions and added third-order many-body perturbation theory correlations. Safronova and Shlyaptseva [256] employed the $1/Z$ perturbation theory method with QED and relativistic corrections for $9 \leq Z \leq 26$. Their calculation results are about 0.07 eV smaller than others. St. Petersburg group [257, 24, 25, 281] successfully performed the calculations using screened self-energy corrections, two-loop QED corrections, two-photon exchange diagrams, and higher-order correlations. Yerokhin et al. [25] calculated the electronic-structure for $3 \leq Z \leq 92$. Gu [258] evaluated the level energies of $1s^2nl$ states for ions with $Z \leq 60$ combining CI and MBPT approach. Cheng et al. [280] made relativistic CI calculations of the transition $1s^22p^2P_{3/2} - 1s^22s^2S_{1/2}$ on Li-like Bi, Th, and U using the Dirac-Kohn-Sham (DKS) potentials in QED calculations. Sapirstein and Cheng [23] evaluated Li-like Bi with Furry or extended Furry representation QED. Finally, Sapirstein and Cheng [26] performed the calculations for all $10 \leq Z \leq 100$ using the S-matrix method together with the DKS po-

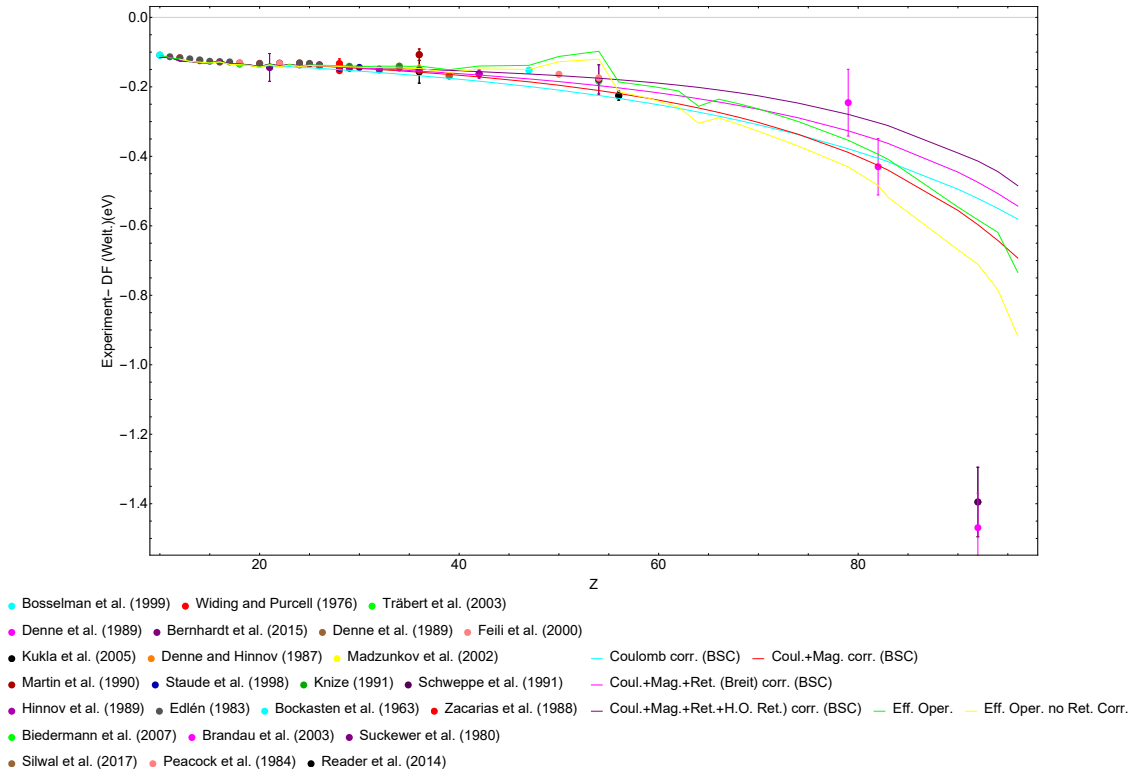

Fig. 5.7 *Comparison of the transition energy between experiment and the present MCDF calculations, using effective operators for the* $1s^2\,2p\,^2P_{1/2} \rightarrow 1s^2\,2s\,^2S_{1/2}$ *transition. Experiments: Bosselman et al. (1999)[194], Widing and Purcell (1976)[195], Träbert et al. (2003)[196], Denne et al. (1989)[197], Bernhardt et al. (2015)[198], Denne et al. (1989)[199], Feili et al. (2000)[200], Kukla et al. (2005)[201], Denne and Hinnov (1987)[202], Madzunkov et al. (2002)[203], Martin et al. (1990)[204], Staude et al. (1998)[205], Knize (1991)[206] Schweppe et al. (1991)[207], Hinnov et al. (1989)[208], Edlén (1983)[209], Bockasten et al. (1963)[210], Zacarias et al. (1988)[211], Biedermann et al. (2007) Brandau et al. (2003)[212], Suckewer et al. (1980)[213], Silwal et al. (2017)[215], Peacock et al. (1984)[216], Reader et al. (2014)[217].*

tentials. Currently, this result can be compared to our calculation results as a complete reference.

A detailed comparison between our works and other different calculations mentioned above is shown in Fig. 5.6 and Fig. 5.8. The references are single-configuration Dirac Fock (DF). In these figures, we present our calculations with Welton model, effective operator model, and different electronic correlations, respectively. We can notice that the results for lack of proper QED corrections from Seely [249] are quite far away from other calculations. This difference gets more and more significant with the increase of Z. The results of different calculations are in good agreement in low- and middle-Z ions. Notably, the transition energies coming from Sapirstein and Cheng [26] appear to scatter around our calculations in heavy lithium-like ions (Z=90 and 92) and the deviation is as large as

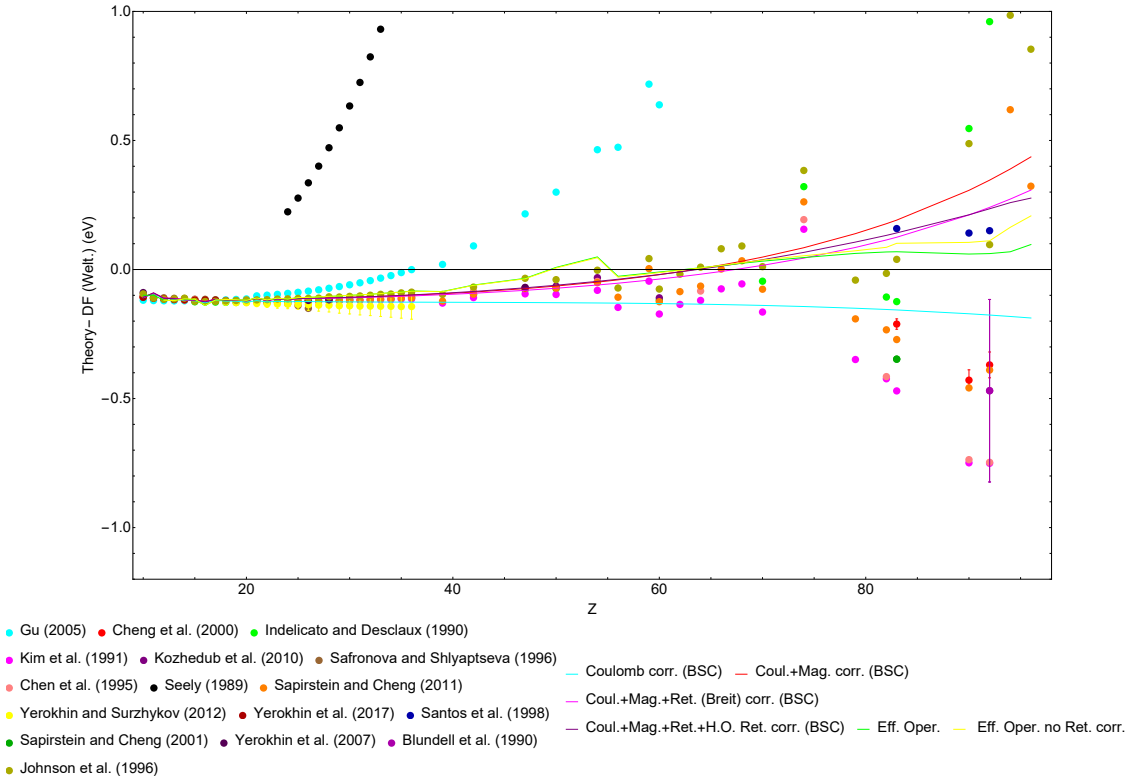

Fig. 5.8 *Comparison of the transition energy between theoretical values and the present MCDF calculations for the* $1s^2\,2p\,^2P_{3/2} \rightarrow 1s^2\,2s\,^2S_{1/2}$ *transition. The reference value is obtained with the DF Welton method. Theoretical works: Yerokhin et al. (2007)[25], Johnson et al. (1996)[255], Gu (2005)[258], Cheng et al. (2000)[280], Indelicato and Desclaux (1990)[156], Kim et al. (1991)[252], Kozhedub et al. (2010)[281], Safronova and Shlyaptseva (1996)[256], Chen et al. (1995)[254], Seely (1989)[249], Sapirstein and Cheng (2011)[26], Yerokhin and Surzhykov (2012)[192], Yerokhin et al. (2017)[193], Santos et al. (1998)[188], Sapirstein and Cheng (2001)[23], Yerokhin et al. (2007)[25], Blundell et al. (1990)[250], Johnson et al. (1996)[255]*

0.52 eV at Z=90 for the $1s^22p^2P_{3/2} - 1s^22s^2S_{1/2}$ transition. Sapirstein and Cheng [26] also added the nuclear polarization effects [295], which can lead to a shift of 0.02 eV at Z=90 and 0.03 eV at Z=92. They used the root-mean-square nuclear radii from Johnson and Soff [10], except thorium (Z=90) from Ref. [133] and uranium (Z=92) from Ref. [134]. Our works are from the tabulation of Angeli [185, 186]. The finite nuclear sizes are uncertain, and they can actually result in a large difference. The deviation reduces to 0.36 eV at Z=90 when we used the same radii with them. Different calculation results are affected by the same limitations from nuclear size, with or without second-order QED contributions and which electron correlation involved. All of these contributions can lead to differences in a few eV.

The comparison of total transition energies are carried out between our calculations and experimental works in Fig. 5.7 for the $1s^22p^2P_{1/2} - 1s^22s^2S_{1/2}$ transition and Fig.

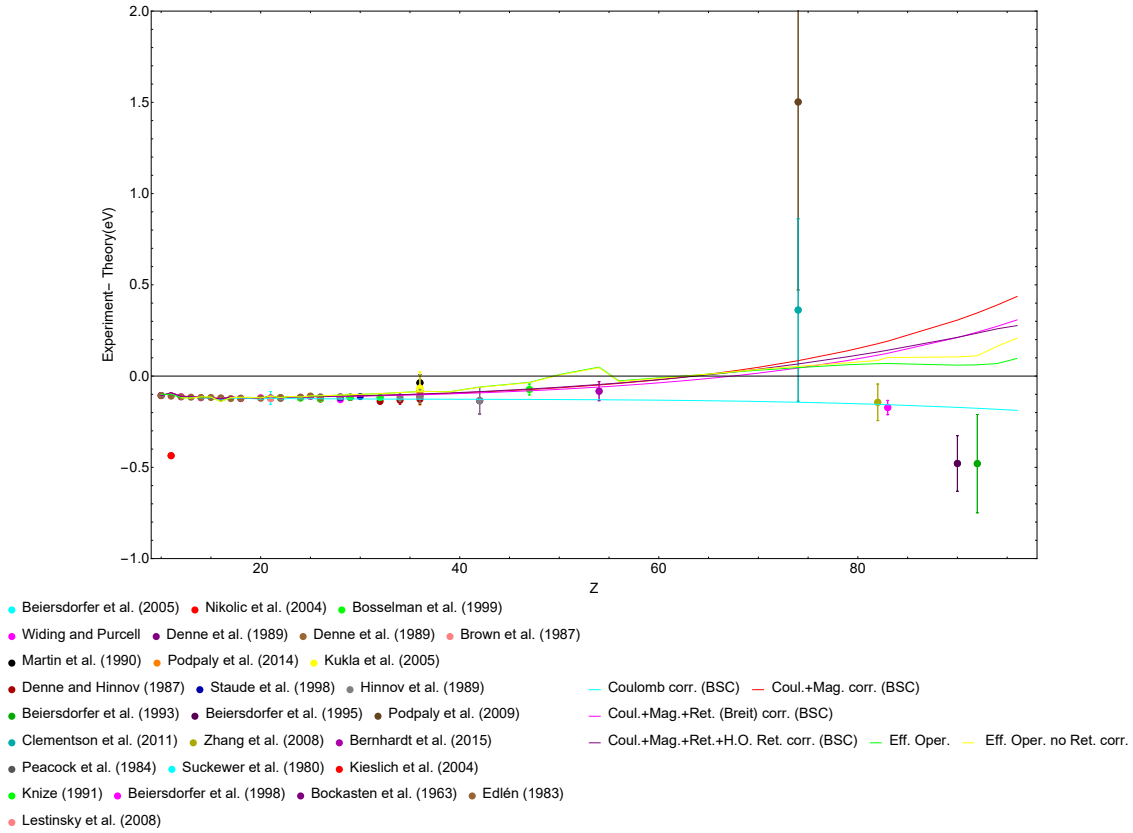

Fig. 5.9 *Comparison of the transition energy between experiment and the present MCDF calculations, using effective operators for the* $1s^2\,2p\,^2P_{3/2} \rightarrow 1s^2\,2s\,^2S_{1/2}$ *transition. Experiments: Beiersdorfer et al. (2005)[65], Nikolic et al. (2004)[223], Bosselman et al. (1999)[194], Widing and Purcell (1976)[195], Denne et al. (1989)[197], Denne et al. (1989)[199], Brown et al. (1987)[224], Martin et al. (1990)[204], Podpaly et al. (2014)[221], Kukla et al. (2005)[201], Denne and Hinnov (1987)[202], Staude et al. (1998)[205], Hinnov et al. (1989)[208], Beiersdorfer et al. (1993)[276], Beiersdorfer et al. (1995)[220], Podpaly et al. (2009)[222], Clementson et al. (2011)[225], Zhang et al. (2008)[227], Bernhardt et al. (2015)[198], Peacock et al. (1984)[216], Suckewer et al. (1980)[213], Kieslich et al. (2004)[214], Knize (1991)[206], Beiersdorfer et al. (1998)[219], Bockasten et al. (1963)[210], Edlén (1983)[209], Lestinsky et al. (2008)[226]*

5.9 for the $1s^22p^2P_{3/2} - 1s^22s^2S_{1/2}$ transition. All experimental results, error bars, and discrepancy with theory are presented in Table 5.6 and Table 5.7, in which the other theory is from Sapirstein and Cheng [26]. Various techniques have been used in experimental development. Widing and Purcell [195] provided accurate astrophysical observations in solar flares. The TFR tokamak was used by T.F.R. group et al. (1985) [299] to measure core-excited ions. Some middle-ions results comes from beam-foil excited measurements [194, 200, 302]. Some available results come from EBIT experiments [227, 220, 65, 276] at high-Z ions. Recently, ECRIS connected with a vacuum double crystal spectrometer can provide reference-free measurements [1]. There are some precise measurements in the

middle- and high-Z ions, which are meaningfully compared with the theory. Our results, whether with Welton models or effective operator model generally agree well with the experiment, except for Z=90 and Z=92. The difference is as large as 0.53 eV with the experimental error bar of 0.152 eV at Z=90.

Different electron correlation effects are also shown in all the figures corresponding to the Table .10 and Table .11 in Appendix A 6.5. The comparison between DF calculations with MCDF values shows that the total correlation effects reduce the transition energies. At low-Z ions, the size of total correlation is within -0.2 eV and this contribution can reach -0.48 eV at high-Z ions in transition $1s^2 2p^2 P_{1/2} - 1s^2 2s^2 S_{1/2}$. While the correlation no longer causes the transition energy to decrease after Z=70 of transition $1s^2 2p^2 P_{3/2} - 1s^2 2s^2 S_{1/2}$. This is because the magnetic correlation, which increases the transition energies, begins to get larger than other correlations.

5.4.2 $1s\,2s\,2p\,^2P_J \rightarrow 1s^2\,2s\,^2S_{1/2}, J = 1/2, 3/2$ and $1s\,2s\,2p\,^4P_J \rightarrow 1s^2\,2s\,^2S_{1/2}, J = 1/2, 3/2, 5/2$ transitions

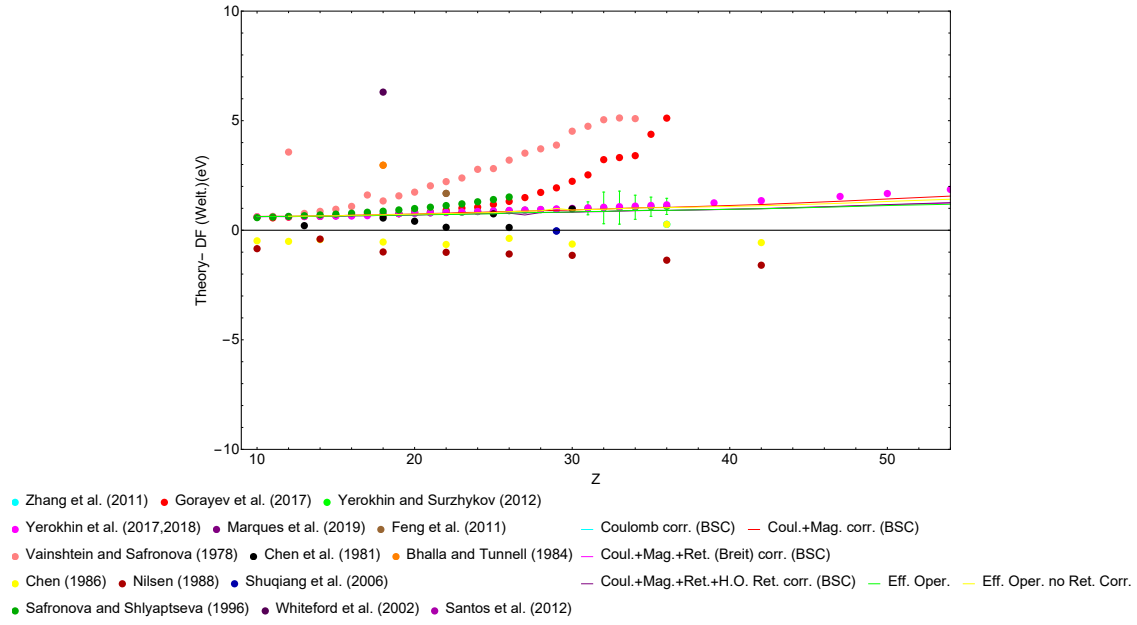

Fig. 5.10 *Comparison of the transition energy between theoretical values and the present MCDF calculations for the* $1s\,2s\,2p\,^2P_{1/2} \rightarrow 1s^2\,2s\,^2S_{1/2}$ *transition. The reference value is obtained with the new effective operator method. Theoretical works: Zhang et al. (2011)[238], Gorayev et al. (2017)[263], Yerokhin and Surzhykov (2012)[192], Yerokhin et al. (2017,2018)[193, 298], Marques et al. (2019), Feng et al. (2011)[261], Vainshtein and Safronova (1978)[259], Chen et al. (1981)[266], Bhalla and Tunnell (1984)[268], Chen (1986)[264], Nilsen (1988)[239], Shuqiang et al. (2006)[260], Safronova and Shlyaptseva (1996)[256], Whiteford et al. (2002)[240], Santos et al. (2012)[265]*

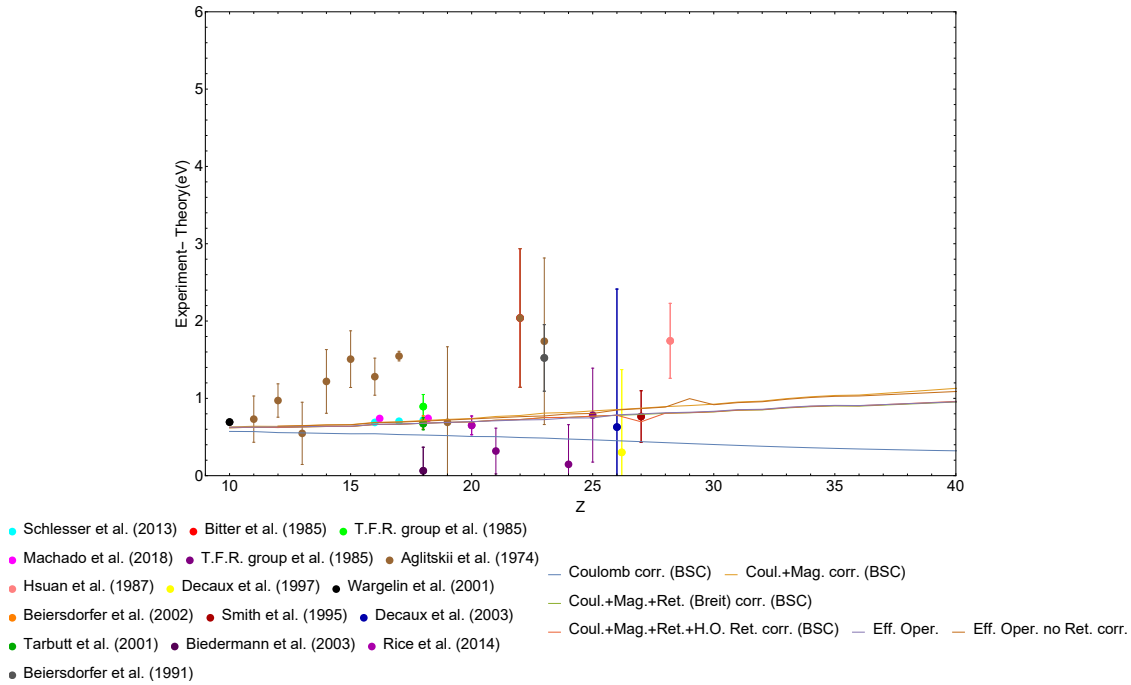

Fig. 5.11 *Comparison of the transition energy between experiment and the present MCDF calculations, using effective operators for the* $1s\,2s\,2p\,^2P_{1/2} \rightarrow 1s^2\,2s\,^2S_{1/2}$ *transition. Experiments: Schlesser et al. (2013)[228], Bitter et al. (1985)[229], T.F.R. group et al. (1985)[273], Machado et al. (2018)[1], Aglitskii et al. (1974)[269], Hsuan et al. (1987)[230], Decaux et al. (1997)[270], Wargelin et al. (2001)[231], Beiersdorfer et al. (2002)[272], Smith et al. (1995)[232], Decaux et al. (2003)[233], Tarbutt et al. (2001)[234], Biedermann et al. (2003)[235], Rice et al. (2014)[236], Beiersdorfer et al. (1991)[237], Rudolph et al. (2013)[71], Rice et al. (1995)[274]*

Table 5.8 – Comparison of the transition energy between experiment and the present MCDF calculations using Welton model and effective operators, respectively, for the $1s\,2s\,2p\,^2P_{1/2} \rightarrow 1s^2\,^1S_0$ transition. The theory is from Yerokhin et al. (2017,2018)[193, 298].

		$1s\,2s\,2p\,^2P_{1/2} \rightarrow 1s^2\,^1S_0$				
Z	Experiment	Error	Diff. Welt.	Diff. Effec.	Diff.Th.	Ref.
10	908.123	0.027	-0.075	-0.065	-0.079	Wargelin et al. (2001) [231]
11	1111.47	0.30	-0.11	-0.10	-0.11	Aglitskii et al. (1974) [269]
12	1335.58	0.22	-0.35	-0.34	-0.35	Aglitskii et al. (1974) [269]
13	1579.62	0.40	0.08	0.09	0.08	Aglitskii et al. (1974) [269]
14	1845.39	0.41	-0.58	-0.58	-0.59	Aglitskii et al. (1974) [269]
15	2131.45	0.37	-0.87	-0.87	-0.86	Aglitskii et al. (1974) [269]
16	2437.115	0.005	-0.028	-0.025	-0.041	Schlesser et al. (2013) [228]
16	2437.166	0.011	-0.079	-0.076	-0.092	Machado et al. (2019)
16	2437.71	0.24	-0.62	-0.62	-0.63	Aglitskii et al (1974) [269]

17	2764.378	0.005	-0.040	-0.036	-0.039	Schlesser et al. (2013) [228]
17	2765.22	0.06	-0.88	-0.88	-0.88	Aglitskii et al. (1974) [269]
18	3112.451	0.002	-0.042	-0.041	0.017	Schlesser et al. (2013) [228]
18	3112.63	0.16	-0.22	-0.22	-0.16	T.F.R. group et al. (1985) [299]
18	3112.4737	0.0071	-0.0646	-0.0636	-0.0060	Machado et al. (2019)
18	3112.42	0.09	-0.01	-0.01	0.05	Beiersdorfer et al. (2002) [272]
18	3112.405	0.078	0.004	0.005	0.063	Tarbutt et al. (2001) [234]
18	3111.795	0.305	0.614	0.615	0.672	Biedermann et al. (2003) [235]
19	3481.33	0.98	0.00	0.00	0.06	Aglitskii et al. (1974) [269]
20	3871.12	0.12	0.04	0.05	0.12	Rice et al. (2014) [236]
21	4281.58	0.30	0.40	0.39	0.48	T.F.R. group et al. (1985) [273]
21	4281.67	0.15	0.32	0.31	0.39	Rice et al. (1995) [274]
22	4715.12	0.18	-1.31	-1.32	-1.22	Bitter et al. (1985) [229]
22	4715.12	0.90	-1.31	-1.32	-1.22	Aglitskii et al. (1974) [269]
23	5165.05	0.43	1.69	1.67	1.78	T.F.R. group et al. (1985) [273]
23	5167.73	1.08	-0.99	-1.01	-0.90	Aglitskii et al. (1974) [269]
23	5167.52	0.43	-0.77	-0.80	-0.69	Beiersdorfer et al. (1991) [237]
24	5640.19	0.51	0.61	0.60	0.71	T.F.R. group et al. (1985) [273]
25	6136.11	0.61	-0.01	-0.04	0.10	T.F.R. group et al. (1985) [273]
26	6652.2	1.1	0.5	0.5	0.6	Decaux et al. (1997) [270]
26	6652.51	1.78	0.15	0.16	0.28	Decaux et al. (2003) [233]
26	6652.826	0.069	-0.163	-0.156	-0.038	Rudolph et al. (2013) [71]
27	7190.57	0.33	-0.07	0.03	0.16	Smith et al. (1995) [232]
28	7750.92	0.48	-0.94	-0.93	-0.79	Hsuan et al. (1987) [230]

Table 5.9 – Comparison of the transition energy between experiment and the present MCDF calculations using Welton model and effective operators, respectively, for the $1s\,2s\,2p\,^2P_{3/2} \rightarrow 1s^2\,^1S_0$ transition. The theory is from Yerokhin et al. (2017,2018)[193, 298].

	$1s\,2s\,2p\,^2P_{3/2} \rightarrow 1s^2\,^1S_0$					
Z	Experiment	Error	Diff. Welt.	Diff. Effec.	Diff.Th.	Ref.
10	908.123	0.027	0.053	0.062	0.046	Wargelin et al. (2001) [231]
11	1111.47	0.30	0.09	0.08	0.08	Aglitskii et al. (1974) [269]
12	1335.58	0.22	-0.07	-0.07	-0.07	Aglitskii et al. (1974) [269]
13	1579.62	0.40	0.48	0.48	0.48	Aglitskii et al. (1974) [269]
14	1845.39	0.41	-0.03	-0.03	-0.04	Aglitskii et al. (1974) [269]
14	1845.83	0.27	-0.47	-0.47	-0.48	Träbert et al. (1979) [242]
15	2131.45	0.37	-0.11	-0.12	-0.12	Aglitskii et al. (1974) [269]
16	2438.106	0.003	-0.019	-0.016	-0.040	Schlesser et al. (2013) [228]
16	2438.162	0.010	-0.075	-0.072	-0.096	Machado et al. (2019)
17	2765.678	0.003	-0.031	-0.040	-0.044	Schlesser et al. (2013) [228]
18	3114.122	0.002	-0.024	-0.019	0.021	Schlesser et al. (2013) [228]
18	3114.1493	0.0071	-0.0510	-0.0463	-0.0067	Machado et al. (2019)
18	3114.19	0.08	-0.09	-0.09	-0.05	T.F.R. group et al. (1985) [299]

18	3114.132	0.078	-0.034	-0.029	0.010	Tarbutt et al. (2001) [234]
18	3114.08	0.09	0.02	0.03	0.06	Beiersdorfer et al. (2002) [272]
18	3113.968	0.117	0.130	0.135	0.174	Biedermann et al. (2003) [235]
20	3874.540	0.000	-0.650	-0.659	-0.594	Suleiman et al. (1994) [241]
20	3874.02	0.12	-0.13	-0.14	-0.08	Rice et al. (2014) [236]
21	4285.28	0.30	0.11	0.11	0.16	T.F.R. group et al. (1985) [273]
21	4281.67	0.15	3.73	3.72	3.78	Rice et al. (1995) [274]
22	4719.25	0.18	-1.20	-1.21	-1.14	Bitter et al. (1985) [229]
23	5171.73	0.43	0.24	0.24	0.30	T.F.R. group et al. (1985) [273]
23	5172.47	0.22	-0.50	-0.51	-0.45	Beiersdorfer et al. (1991) [237]
24	5647.39	0.51	-0.17	-0.18	-0.11	T.F.R. group et al. (1985) [273]
25	6143.71	0.30	0.20	0.21	0.26	T.F.R. group et al. (1985) [273]
26	6661.9	1.1	0.3	0.3	0.3	Decaux et al. (1997) [270]
26	6662.20	1.79	-0.07	-0.06	-0.01	Decaux et al. (2003) [233]
26	6662.240	0.069	-0.114	-0.103	-0.052	Rudolph et al. (2013) [71]
27	7203.11	0.46	-1.12	-1.12	-1.05	Smith et al. (1995) [232]
28	7765.00	0.49	-1.40	-1.40	-1.33	Hsuan et al. (1987) [230]
59	36886.8	8.5	-5.9	-5.9	-5.9	Thorn et al. (2008) [243]

Table 5.10 – Comparison of the transition energy between the present MCDF calculations using Welton model and effective operators and other calculation, for the $1s\,2s\,2p\,^4P_J \rightarrow 1s^2\,^1S_0, J = 1/2, 3/2, 5/2$ transition. The other theory is from Yerokhin et al. (2017,2018)[193, 298].

	$1s\,2s\,2p\,^4P_{1/2} \rightarrow 1s^2\,2s\,^2S_{1/2}$			$1s\,2s\,2p\,^4P_{3/2} \rightarrow 1s^2\,2s\,^2S_{1/2}$			$1s\,2s\,2p\,^4P_{3/2} \rightarrow 1s^2\,2s\,^2S_{1/2}$		
		Difference			Difference			Difference	
Z	Effec.	Welt.	Th.	Effec.	Welt.	Th.	Effec.	Welt.	Th.
10	895.951	-0.009	0.009	895.999	-0.010	0.009	896.144	-0.010	0.010
11	1097.672	-0.002	0.012	1097.752	-0.002	0.012	1097.978	-0.002	0.013
12	1319.942	-0.009	0.009	1320.069	-0.009	0.009	1320.406	-0.009	0.011
13	1562.795	-0.004	0.012	1562.983	-0.004	0.011	1563.470	-0.004	0.013
14	1826.265	-0.006	0.007	1826.535	-0.006	0.007	1827.216	-0.006	0.009
15	2110.392	-0.006	0.006	2110.766	-0.006	0.006	2111.695	-0.006	0.009
16	2415.215	-0.004	-0.003	2415.719	-0.004	-0.003	2416.963	-0.004	0.000
17	2740.768	-0.005	0.001	2741.430	-0.005	0.000	2743.066	-0.005	0.003
18	3087.086	-0.006	0.084	3087.938	-0.006	0.084	3090.055	-0.006	0.086
19	3454.258	-0.006	0.087	3455.334	-0.006	0.087	3458.039	-0.006	0.089
20	3842.321	-0.007	0.089	3843.658	-0.007	0.088	3847.072	-0.007	0.090
21	4251.334	-0.008	0.090	4252.969	-0.008	0.090	4257.233	-0.008	0.093
22	4681.347	-0.009	0.091	4683.321	-0.009	0.092	4688.596	-0.009	0.096
23	5132.428	-0.010	0.094	5134.779	-0.010	0.094	5141.250	-0.010	0.097
24	5604.639	-0.010	0.094	5607.405	-0.010	0.094	5615.284	-0.010	0.099
25	6098.055	-0.011	0.096	6101.274	-0.011	0.095	6110.797	-0.011	0.101
26	6612.786	-0.012	0.055	6616.493	-0.012	0.055	6627.931	-0.012	0.059
27	7148.830	0.310	0.055	7153.057	-0.013	0.055	7166.710	-0.013	0.060

28	7706.304	-0.014	0.056	7711.079	-0.014	0.057	7727.282	-0.014	0.061
29	8285.299	-0.014	0.057	8290.645	-0.014	0.058	8309.773	-0.014	0.063
30	8885.896	-0.015	0.058	8891.830	-0.015	0.058	8914.296	-0.015	0.064
31	9508.194	-0.015	0.058	9514.728	-0.015	0.057	9541.155	-0.015	-0.103
32	10152.282	-0.016	0.059	10159.423	-0.016	0.057	10190.108	-0.016	-0.068
33	10818.263	-0.016	0.057	10826.011	-0.016	0.056	10861.534	-0.016	-0.070
34	11506.245	-0.016	0.057	11514.596	-0.015	0.056	11555.546	-0.016	-0.073
35	12216.326	-0.016	0.057	12225.271	-0.016	0.055	12272.287	-0.014	-0.076
36	12948.636	-0.016	0.056	12958.160	-0.015	0.053	13011.783	-0.016	0.065
39	15280.082	-0.015	0.052	15291.213	-0.013	0.048	15369.713	-0.018	0.066
42	17816.032	-0.011	0.042	17828.516	-0.011	0.039	17939.965	-0.006	0.065
47	22507.852	0.003	0.024	22521.878	0.002	0.021	22710.674	0.004	-0.084
50	25609.372	0.018	0.025	25623.852	0.024	0.022	25872.543	0.028	2.628
54	30089.516	0.046	-0.009	30104.003	0.054	-0.005	30462.306	0.051	-0.275
56	32481.219	0.065	-0.008	32495.450	0.072	-0.021	32918.459	0.065	-0.111
59	36263.695	0.099	-0.020	36277.191	0.115	-0.033	36811.925	0.097	2.032
60	37577.531	0.113	-0.036	37590.680	0.127	-0.042			
62	40286.033	0.147	-0.039	40298.346	0.158	-0.052			
64	43104.916	0.183	-0.040	43116.183	0.194	-0.055			
66	46036.543	0.224	-0.007	46046.538	0.251	-0.016			
68	49083.760	0.264	-0.093	49092.249	0.287	-0.092			
70	52249.180	0.315	-0.108	52255.933	0.353	-0.113			
74	58948.285	0.445	-0.124	58950.761	0.496	-0.150	60465.865	0.486	0.855
79	68049.218	0.639	-0.195	68044.685	0.717	-0.233	70100.025	0.668	0.424
82	73921.812	0.795	-0.299	73912.038	0.893	-0.349	76362.150	0.793	0.210
83	75951.502	0.855	-0.183	75939.826	0.959	-0.262	78535.175	-0.059	0.041
90	91234.444	1.419	-0.231	91206.203	1.595	-0.331			
92	95969.999	1.593	0.165	95935.903	1.798	0.056			
94				100845.167	2.046				
96				105940.644	2.314				

The precise knowledge of core-excited is necessary to explain astrophysics spectrum, and the states benefit the prominent K-shell emission lines, which can be observed in the spectra of almost all types of cosmic x-ray sources [275]. Another important objective in the study of K-shell emission [276, 277] is its use in the thermal laboratory plasma diagnosis, especially those in magnetic confinement fusion studies. For the study of core-excited states $1s\,2s\,2p$, there are not much reference results in theory, especially in the experiment. The exact theoretical description and calculation to the transitions involving core-excited states are complicated by the following two aspects. The first is a huge contribution from the QED effects. In fact, QED contributions are the strongest for K shell electrons, so they are also strong for the K shell transition. The second can be summarized as core-excited states are mainly the autoionizing states. This represents an intensive mixing of reference state with a tight continuous continuum of a single excited state, for example consisting of a continuous closed core and electrons. In theoretical calculations, the interaction with the continuum cannot be accurately calculated and described [259, 264, 239, 192, 298].

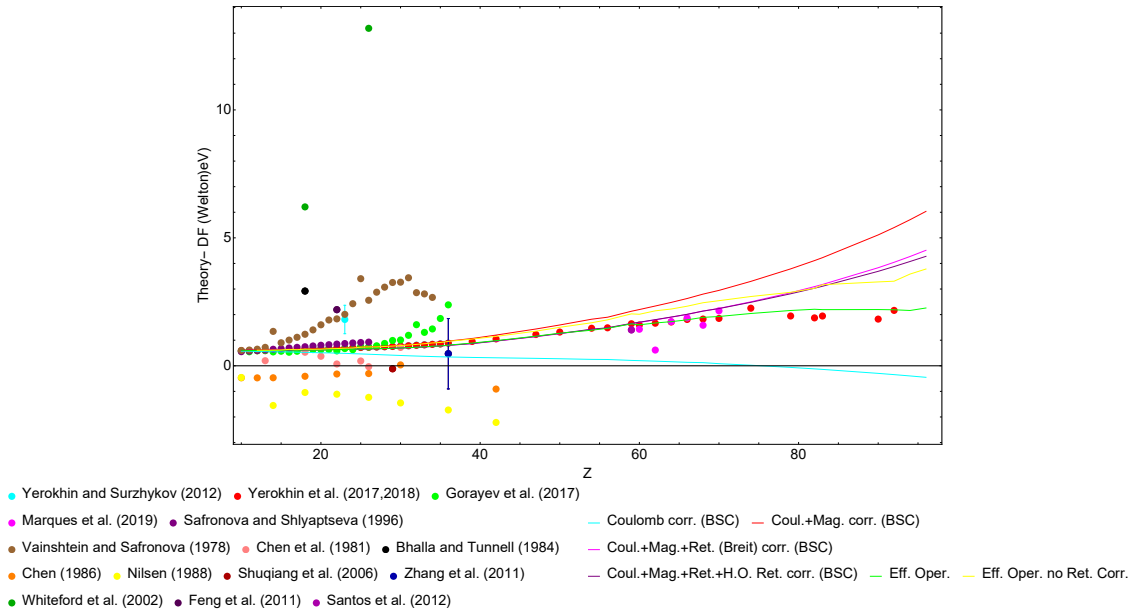

Fig. 5.12 *Comparison of the transition energy between theoretical values and the present MCDF calculations for the* $1s\,2s\,2p\,^2P_{3/2} \rightarrow 1s^2\,2s\,^2S_{1/2}$ *transition. The reference value is obtained with the new effective operator method. Theoretical works: Yerokhin and Surzhykov (2012)[192], Yerokhin et al. (2017,2018)[193, 298], Gorayev et al. (2017)[263], Marques et al. (2019), Safronova and Shlyaptseva (1996)[256], Vainshtein and Safronova (1978)[259], Chen et al. (1981)[266], Bhalla and Tunnell (1984)[268], Chen (1986)[264], Nilsen (1988)[239], Shuqiang et al. (2006)[260], Zhang et al. (2011)[238], Whiteford et al. (2002)[240], Feng et al. (2011)[261], Santos et al. (2012)[265]*

Vainshtein and Safronova [259] were the first to obtain core-excited states of Li-like ions for atomic numbers Z=4 to 34 within the $1/Z$ expansion method. Bhalla and Tunnell [268] calculated the excited electron configurations of lithiumlike argon without QED and Breit interaction. Later, Chen et al. [266, 264] addressed $1s2s2p$ configuration of Li-like ions ($13 \leq Z \leq 30$) using MCDF approach and the Moller two-electron operator with a generalized Breit and QED corrections, which results show smaller than others. Later, Safronova and Shlyaptseva [256] calculated the inner-shell excitation for the nuclear charge Z=6-54 by using the $1/Z$ perturbation theory method with relativistic and first and second-order corrections. More recently, these calculations have been reevaluated by Gorayev et al. [263] for $6 \leq Z \leq 36$ based on the same method by considering the first-order correction to the power of $1/Z$. The results of $1/Z$ perturbation methods are still far from those of other methods. Then, Safronova and Shlyaptseva [278] addressed RMBPT, including second-order Breit–Coulomb interactions. These states were addressed by Gang Jing group [260, 261, 262], who calculated Li-like-Cu, Ti, and Kr using GRASPVU within the MCDF approach. Santos et al. [265] calculated Li-like-praseodymium using MDFGME code developed by Desclaux and Indelicato [105, 156, 155]. Yerokhin and Surzhykov [192] calculated all $n = 2$ core-excited states with a relativistic CI method for lithiumlike ions starting from argon (Z=18) and ending with krypton (Z=36). Then, Yerokhin et al. [193]

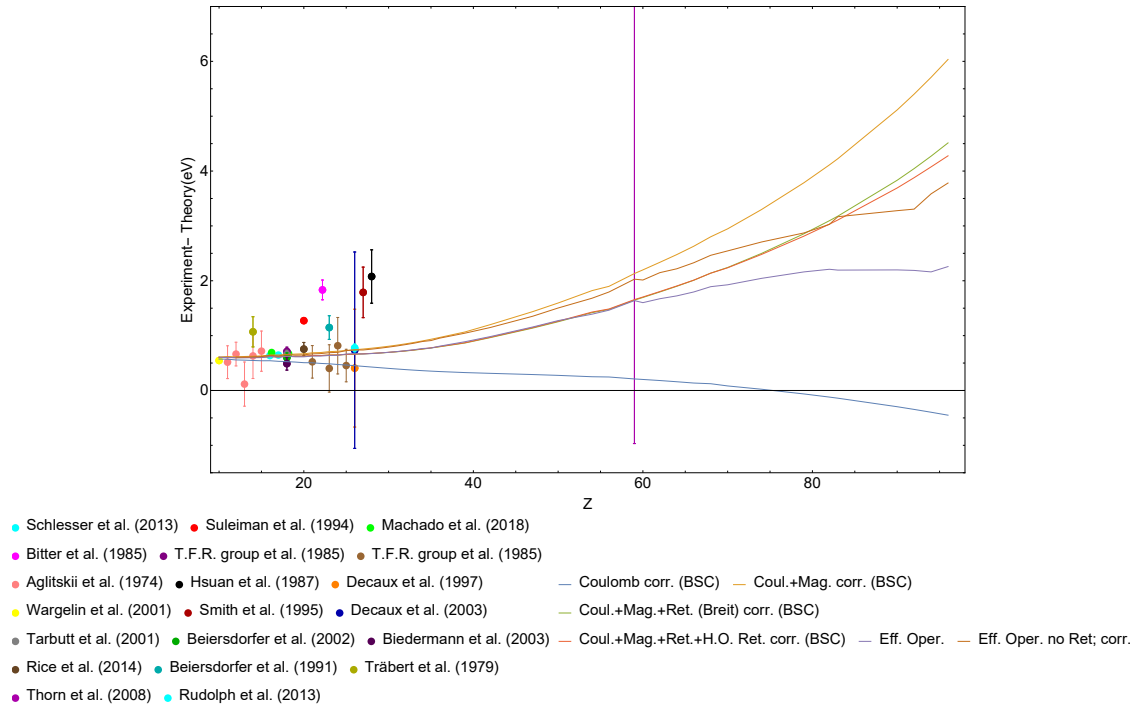

Fig. 5.13 *Comparison of the transition energy between experiment and the present MCDF calculations, using effective operators for the* $1s\,2s\,2p\,^2P_{3/2} \rightarrow 1s^2\,2s\,^2S_{1/2}$ *transition. Experiments: Schlesser et al. (2013)[228], Suleiman et al. (1994)[241], Machado et al. (2018)[1], Bitter et al. (1985)[229], T.F.R. group et al. (1985)[273], Aglitskii et al. (1974)[269], Hsuan et al. (1987)[230], Decaux et al. (1997)[270], Wargelin et al. (2001)[231], Smith et al. (1995)[232], Decaux et al. (2003)[233], Tarbutt et al. (2001)[234], Beiersdorfer et al. (2002)[272], Biedermann et al. (2003)[235], Rice et al. (2014)[236], Beiersdorfer et al. (1991)[237], Träbert et al. (1979)[242], Thorn et al. (2008)[243], Rudolph et al. (2013)[71]*

used the same method to calculate energy levels of the $1s^22l$ and $1s2l2l'$ states of ions along the lithium isoelectronic sequence from carbon to chlorine. In 2018, Yerokhin and Surzhykov [298] supplemented new calculations of Li-like ions from argon to uranium using the CI method with two-loop QED and nuclear recoil in QED part. Marques et al. [267] calculated Li-like Nd, Sm, Gd, Dy, Er, and Yb with Welton model using the same code with us.

We perform the comparisons between different calculations are shown in Fig. 5.10, 5.12 for the $1s\,2s\,2p\,^2P_J \rightarrow 1s^2\,2s\,^2S_{1/2}, J = 1/2, 3/2$ transition with DF Welton model as references and Fig. 5.14, 5.16, 5.18 for the $1s\,2s\,2p\,^4P_J \rightarrow 1s^2\,2s\,^2S_{1/2}, J = 1/2, 3/2, 5/2$ transitions with effective operator as references. Our calculations start from neon (Z=10) to uranium (Z=92) with missing some ions in core-excited transiton of $1s\,2s\,2p\,^2P_{1/2} \rightarrow 1s^2\,2s\,^2S_{1/2}$ due to bad converge. The corresponding tables are also listed in Tables 5.8, 5.9, 5.11, 5.10. It is noticed that the results from $1/Z$ perturbation method [259, 263] are far away from the CI and MCDF methods and the size of difference can reach as large as 4 eV at Z=36. Another large difference comes from Chen et al. [266, 264] and

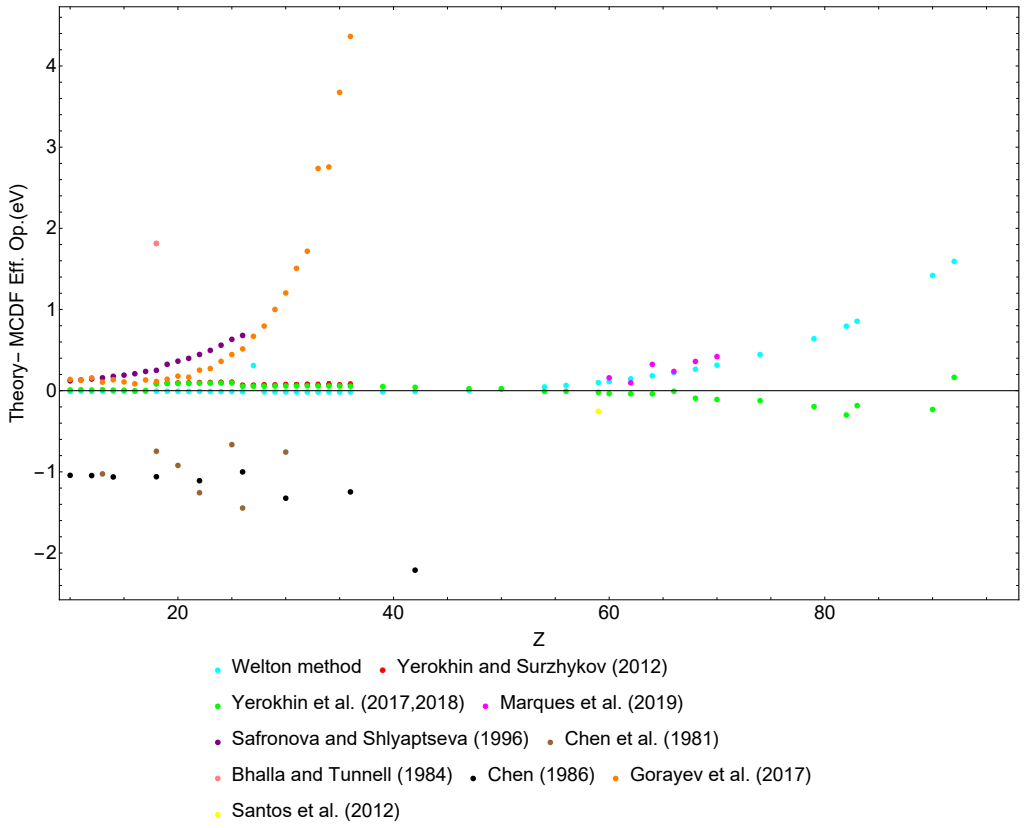

Fig. 5.14 *Comparison of the transition energy between theoretical values from others and the MCDF calculations of the present work for the* $1s\,2s\,2p\,^4P_{1/2} \rightarrow 1s^2\,2s\,^2S_{1/2}$ *transitions. Theoretical works: Yerokhin and Surzhykov (2012)[192], Yerokhin et al. (2017,2018)[193, 298], Marques et al. (2019), Safronova and Shlyaptseva (1996)[256], Chen et al. (1981)[266], Bhalla and Tunnell (1984)[268], Chen (1986)[264], Gorayev et al. (2017)[263], Santos et al. (2012)[265]*

Nilsen et al. [239] with generalized Breit interaction and QED corrections, which are about 2 eV smaller than those of other calculations. Except for these deviations, other calculations generally agree with each other. We also give a detailed comparison with the CI calculations described by Yerokhin et al. [192, 193, 298], which are considered accurate and complete evaluations to the core-excited states. Our calculations have a good agreement with the latest results of Yerokhin et al. [193, 298]. There is just a shift of 0.4 eV at high-Z ions, within the uncertainty of 0.5 eV for their theory error. We use the same method for the screened QED and the same nucleus size, expect for Z=90 with the difference of nuclear radius of 0.0002 fm. They also provided the uncertainty of 0.95 eV from the nuclear size at Z=90. Our calculations of transition $1s\,2s\,2p\,^4P_{5/2} \rightarrow 1s^2\,2s\,^2S_{1/2}$ compare with Yerokhin's results shown in Table 5.11, in which deviations are 2.6 eV at Z=50 and 1.9 eV at Z=59. This is because the convergence is not achieved at n=5, with errors of 0.56 eV and 4.7 eV, respectively.

The results of Welton model are almost identical to the results of the new effective operator method. However, at Z=50, the value of Welton model starts to move away from

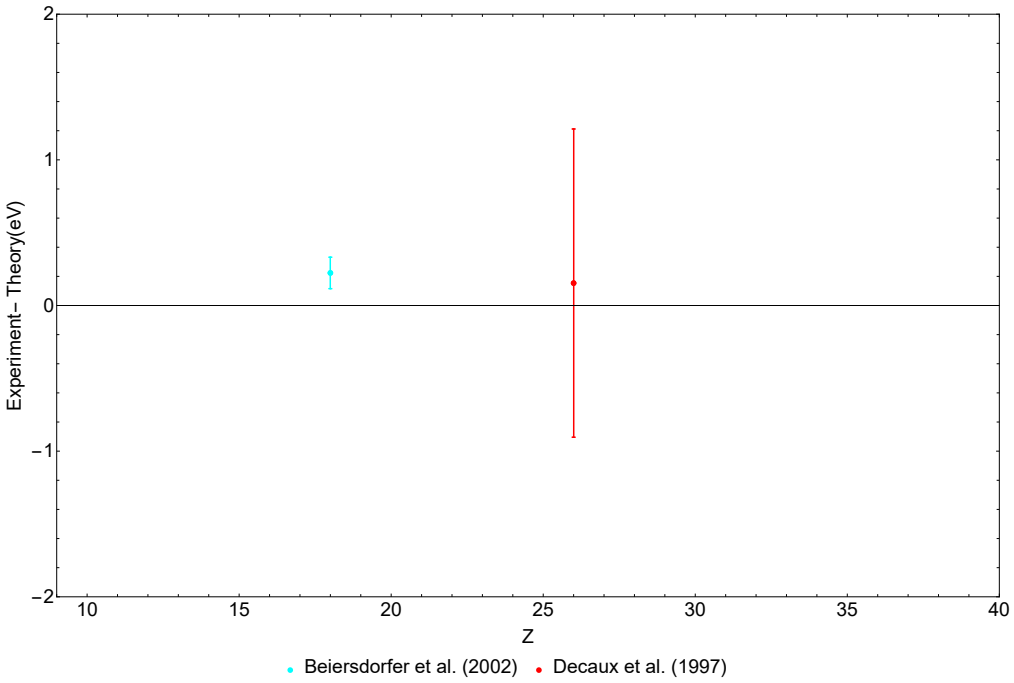

Fig. 5.15 *Comparison of the transition energy between experimental values and the MCDF calculation of the present work for the* $1s\,2s\,2p\,^4P_{1/2} \rightarrow 1s^2\,2s\,^2S_{1/2}$ *transitions. The MCDF value with effective operator for the self-energy is used. Experiments are from: Beiersdorfer et al. (2002)[272], Decaux et al. (1997)[270]*

the effective operator method following the increase with Z. The results show that the effective operator model is in better agreement with the experimental results at high-Z ions for valence-excited transitions. But for core-excited transitions, we can't judge which model is better because there is no experiment as a reference in the high-Z ions.

In experiments, all measurements are concentrated between Z=10 and Z=30, except that only praseodymium ion has been measured with a large uncertainty of 8.5 eV using SuperEBIT. Aglitskii et al. [269] give observations of Li-like Z=11-23 using laser plasmas. Schlesser et al. [228] obtained transition energies in Li-like Z=16-18 within the accuracy of 10 ppm. Li-like Fe is identified by Decaux et al. [270] using EBIT technique. The experimental values of several other elements of lithiumlike ions of Ar^{15+}, Sc^{18+}, V^{20+}, Cr^{21+}, and Mn^{23+} from T.F.R. group et al. [273], Sc^{18+} from Rice et al. [274] with accurate to $\pm 0.1\text{m}\mathring{A}$ and Fe^{23+} from Rudolph et al. [71] with the 60 meV energy error bar. For the forbidden M2 transition of $1s\,2s\,2p\,^4P_{5/2} \rightarrow 1s^2\,2s\,^2S_{1/2}$, only Li-like Ar been measured by Dohmann et al. [271, 272]. Recently, our group measured this transition in both Li-like S and Ar with a double-flat crystal spectrometer without the use of any reference line. The transition energy measurements are performed with accuracies ranging from 2.3 ppm to 6.4 ppm depending on the element and line intensity. Our theoretical values are in agreement with our experimental value.

The comparison of core-excited transitions between the available experimental results and calculations are presented in Table 5.8, 5.9 and 5.11. There is a shift in some ions

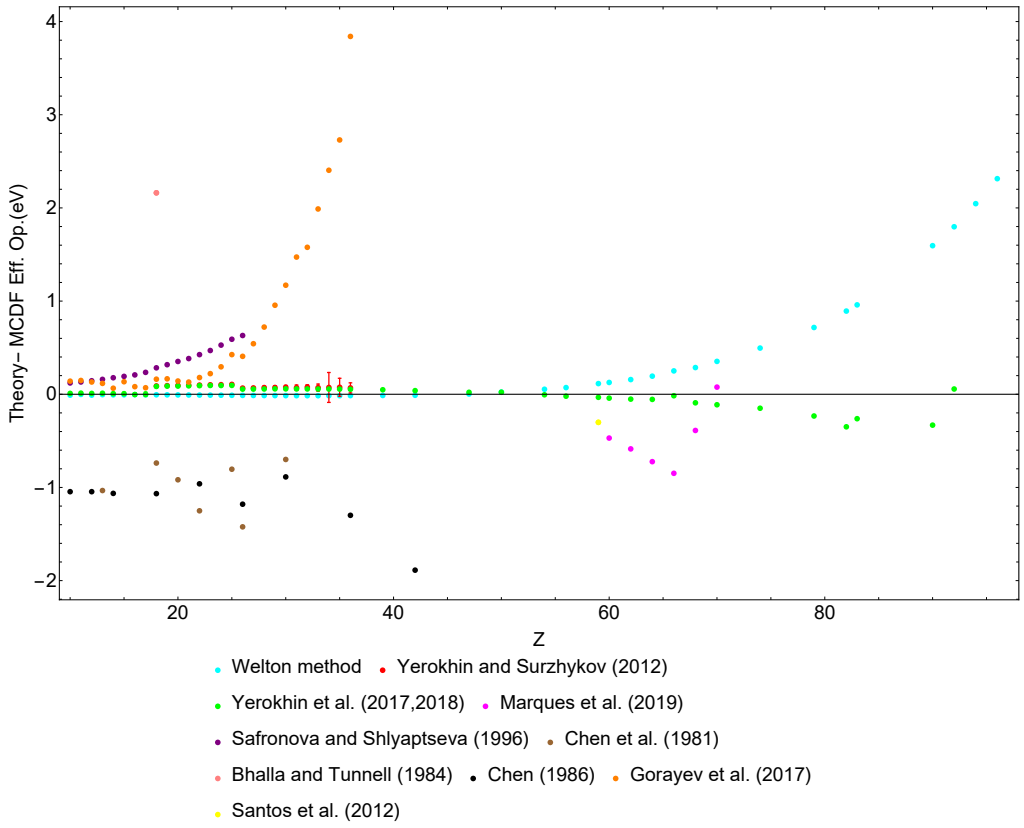

Fig. 5.16 *Comparison of the transition energy theoretical values and the present MCDF calculations for the* $1s\,2s\,2p\,^4P_{3/2} \rightarrow 1s^2\,2s\,^2S_{1/2}$ *transition. The reference value is obtained with the new effective operator method. Theoretical works: Yerokhin and Surzhykov (2012)[192], Yerokhin et al. (2017,2018)[193, 298], Marques et al. (2019), Safronova and Shlyaptseva (1996)[256], Chen et al. (1981)[266], Bhalla and Tunnell (1984)[268], Chen (1986)[264], Gorayev et al. (2017)[263], Santos et al. (2012)[265].*

between measurements and calculations. Especially, the experimental values from Tarbutt et al. [49] and Biedermann et al. [235], which are 3.8 eV and 3.3 eV larger than the theory calculations at transition $1s\,2s\,2p\,^4P_{3/2} \rightarrow 1s^2\,2s\,^2S_{1/2}$ of Ar^{15+} ion.

In the low- and middle-Z ions, all theories are in good agreement with each other, except for $1/Z$ expansion method, which is far away from other theories. It can be seen that the present MCDF calculation results have a small shift with the values from the advanced RMBPT, RCI and S-matrix methods at high-Z ions due to different finite nuclear sizes, nuclear polarization and the errors from our calculation convergence. Comparing the current works with other calculations for the different contributions to the transition energy shows the importance of the QED screening correction for rigorous processing. The difference between Welton model and effective operator model becomes larger in core-excited states of $1s2s2p$ than $1s^22p$ at high-Z ions.

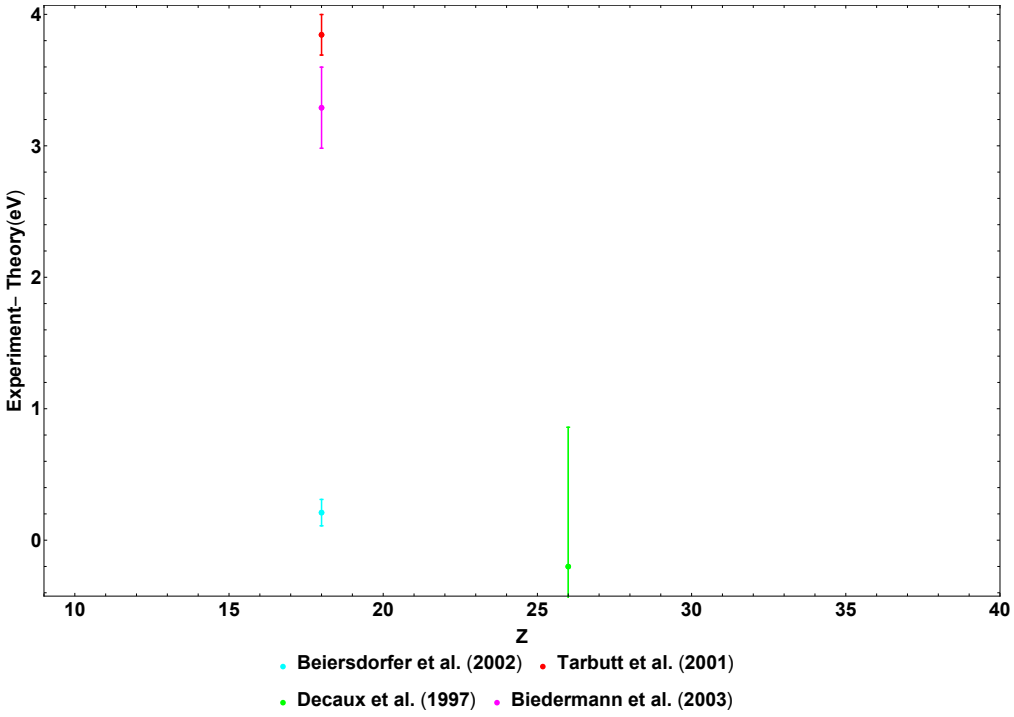

Fig. 5.17 *Comparison of the transition energy experimental values and the MCDF calculation of the present work for the* $1s\,2s\,2p\,^4P_{3/2} \rightarrow 1s^2\,2s\,^2S_{1/2}$ *transitions. The MCDF value with effective operator for the self-energy is used. Experiments are from: Beiersdorfer et al. (2002)[272], Tarbutt et al. (2001)[234], Decaux et al. (1997)[270], Biedermann et al. (2003)[235].*

5.4.3 $1s\,2s\,2p\,^4P_J \rightarrow 1s^2\,^1S_0, J = 1/2, 3/2$ transition

This thesis follows the technique described in the reference [137] and calculates the Auger transition energy (see section 2.10) at the $1s2l2l'$ level by using the MCDFGME code. We combine this technique with a fully correlated wave function until $n = 5$. The table 5.5 gives the convergence of the transition energy.

Table 5.12 gives the comparison of present works of the effective operator and Welton picture, respectively, with the CI method from Yerokhin et al. [298] of $1s2l2l'$ states to ground state in Li-like Z from 18 to 92. The results of Auger transitions show the same trend as the radiative transitions. The Welton models are still 1.2 eV higher than the effective operator model at Li-like Uranium. At high-Z ions, the deviation is reached 0.2 eV with the results of Yerokhin et al. [298].

5.4.4 Radiative transition probability

Radiative transition probabilities are evaluated using the multipole expansion of the matrix element, as mentioned in section 2.9, for Li-like system. The initial and final state orbitals are fully relaxed, we use final-state channel mixing and take into account the non-orthogonality between the fully relaxed orbitals in the initial and final state, following [191, 170].

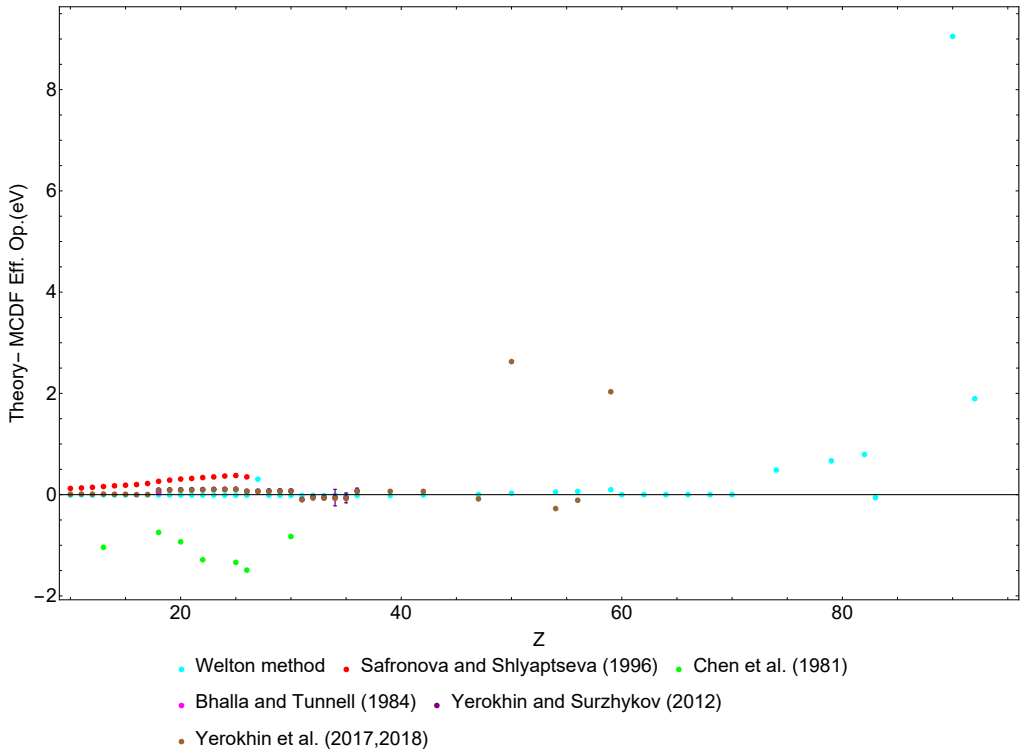

Fig. 5.18 *Comparison of the transition energy theoretical values and the present MCDF calculations for the* $1s\,2s\,2p\,^4P_{5/2} \rightarrow 1s^2\,2s\,^2S_{1/2}$ *transition. The reference value is obtained with the new effective operator method. Theoretical works: Safronova and Shlyaptseva (1996)[256], Chen et al. (1981)[266], Bhalla and Tunnell (1984)[268], Yerokhin and Surzhykov (2012)[192], Yerokhin et al. (2017,2018)[193, 298].*

The radiative transition probabilities are plotted in Fig. 5.20 and Fig. 5.21. The single-configuration(DF) and multi-configuration(MCDF) with $n = 2, 3, 4, 5$ are presented separately in the figures. We adopt singly, doubly, and triply excited configurations up to 5g orbitals in order to ensure the convergence of MCDF calculation results. The comparison of DF and MCDF shows that multi-configurations do not cause big shifts to the radiative transition probabilities.

5.5 Errors and uncertainty

The numerical accuracy of the MCDF method can be easily controlled by changing the self-consistency criteria and mesh size. For all results given here, the numerical error is less than 0.003 eV [156]. When we increase the correlation orbitals n to the maximum, the convergence of the correlated energy is kept within 0.1 eV. From the comparison between our calculations and experiments, we have found that the effective operator model can improve the accuracy of the total transition energy by 0.002% for high-Z ions at valence-excited transitions.

The uncertainties of the calculated transition energies come from the omitted high-

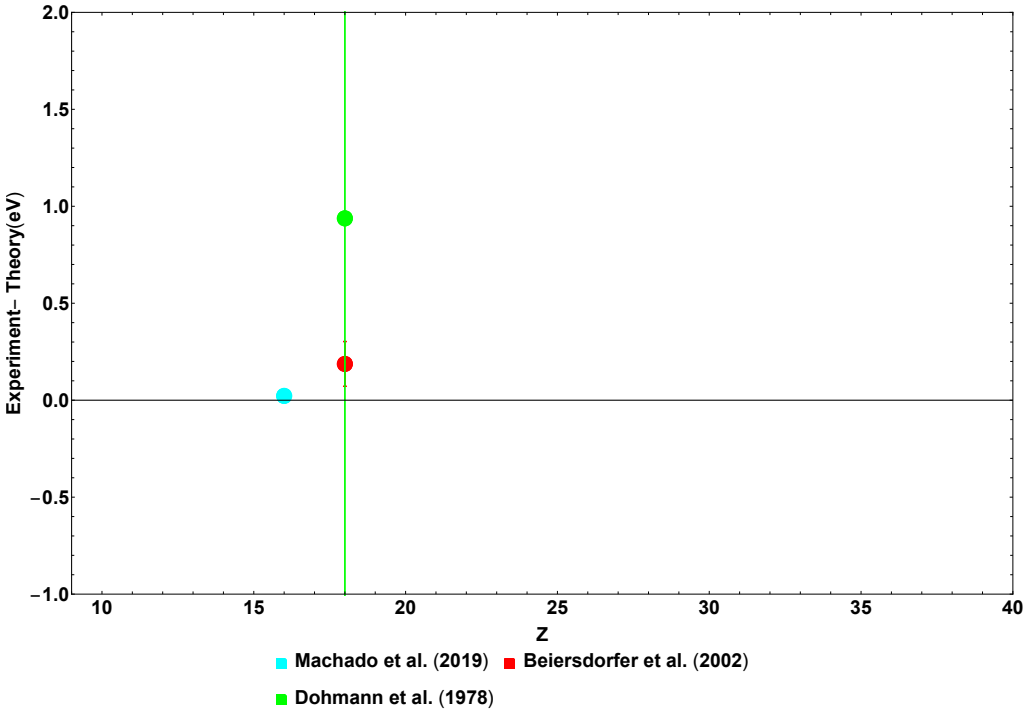

Fig. 5.19 *Comparison of the transition energy between experimental values and the MCDF calculation of the present work for the* $1s\,2s\,2p\,^4P_{5/2} \rightarrow 1s^2\,2s\,^2S_{1/2}$ *transitions. The MCDF value with effective operator for the self-energy is used. Experiments are from: Machado et al. (2019), Beiersdorfer et al. (2002)[272], Dohmann et al. (1978)[271].*

order QED effects, for example, the incomplete three- and more-photon correlations, in addition to the uncertainty of the Dirac-Coulomb-Breit energy. At middle- to high-Z, the main sources of uncertainty are due to uncertainties in the nuclear radii.

Table 5.11 – Comparison of the transition energy between experiment and the present MCDF calculations using Welton model and effective operators, respectively, for the $1s\,2s\,2p\,^4P_J \rightarrow 1s^2\,^1S_0, J = 1/2, 3/2, 5/2$ transition. The other theory is from Yerokhin et al. (2017,2018)[193, 298].

			$1s\,2s\,2p\,^4P_{1/2} \rightarrow 1s^2\,^1S_0$			
Z	Experiment	Error	Diff. Welt.	Diff. Effec.	Diff. OtherTh.	Ref.
18	3087.31	0.11	-0.23	-0.22	-0.14	Beiersdorfer et al. (2002)[272]
26	6612.9	1.1	-0.2	-0.2	-0.1	Decaux et al. (1997)[270]
			$1s\,2s\,2p\,^4P_{3/2} \rightarrow 1s^2\,^1S_0$			
18	3088.15	0.10	-0.22	-0.21	-0.13	Beiersdorfer et al. (2002)[272]
18	3091.783	0.154	-3.850	-3.845	-3.760	Tarbutt et al. (2001)[234]
18	3091.228	0.308	-3.295	-3.290	-3.205	Biedermann et al. (2003)[235]
26	6616.3	1.1	0.2	0.2	0.3	Decaux et al. (1997)[270]
			$1s\,2s\,2p\,^4P_{5/2} \rightarrow 1s^2\,^1S_0$			
16	2416.997	0.011	-0.038	-0.034	-0.034	Machado et al. (2019)
18	3090.25	0.12	-0.20	-0.19	-0.11	Beiersdorfer et al. (2002)[272]
18	3091	2	-1	-1	-1	Dohmann et al. (1978)[271]

Table 5.12 – Comparision of Auger transition energy between present works with effective operator and Welton picture, respectively and the CI method from Yerokhin et al. [298] of $1s2l2l'$ states in Li-like Z from 18 to 92. Transition energies are in eV.

	$1s\,2s\,2p\,^2P_{3/2} \rightarrow 1s^2\,^1S_0$			$1s\,2s\,2p\,^4P_{3/2} \rightarrow 1s^2\,^1S_0$		
Z	Effective operator	Welton	CI theory	Effective operator	Welton	CI theory
18	2195.743	2195.740	2195.755	2169.606	2169.603	2169.634
19	2448.966	2448.963	2448.981	2420.836	2420.832	2420.865
30	6170.608	6170.605	6170.643	6109.834	6109.830	6109.868
42	12275.674	12275.688	12275.705	12115.312	12115.329	12115.327
54	20712.650	20712.713	20712.654	20293.599	20293.669	20293.571
62	27779.406	27779.548	27779.369	27035.487	27035.675	27035.424
74	40867.826	40868.244	40867.719	39263.962	39264.411	39263.812
83	52981.238	52982.066	52981.031	50282.792	50283.708	50282.587
90	64031.991	64033.316	64031.738	60083.145	60084.225	60082.985
92	67488.787	67490.297	67488.863	63099.171	63100.396	63099.367
	$1s\,2s\,2p\,^4P_{1/2} \rightarrow 1s^2\,^1S_0$					
Z	Effective operator	Welton	CI theory			
18	2168.755	2168.751	2168.782			
19	2419.760	2419.757	2419.789			
30	6103.901	6103.896	6103.936			
42	12102.830	12102.844	12102.848			
54	20279.109	20279.183	20279.081			
62	27023.181	27023.354	27023.124			
74	39261.483	39261.933	39261.363			

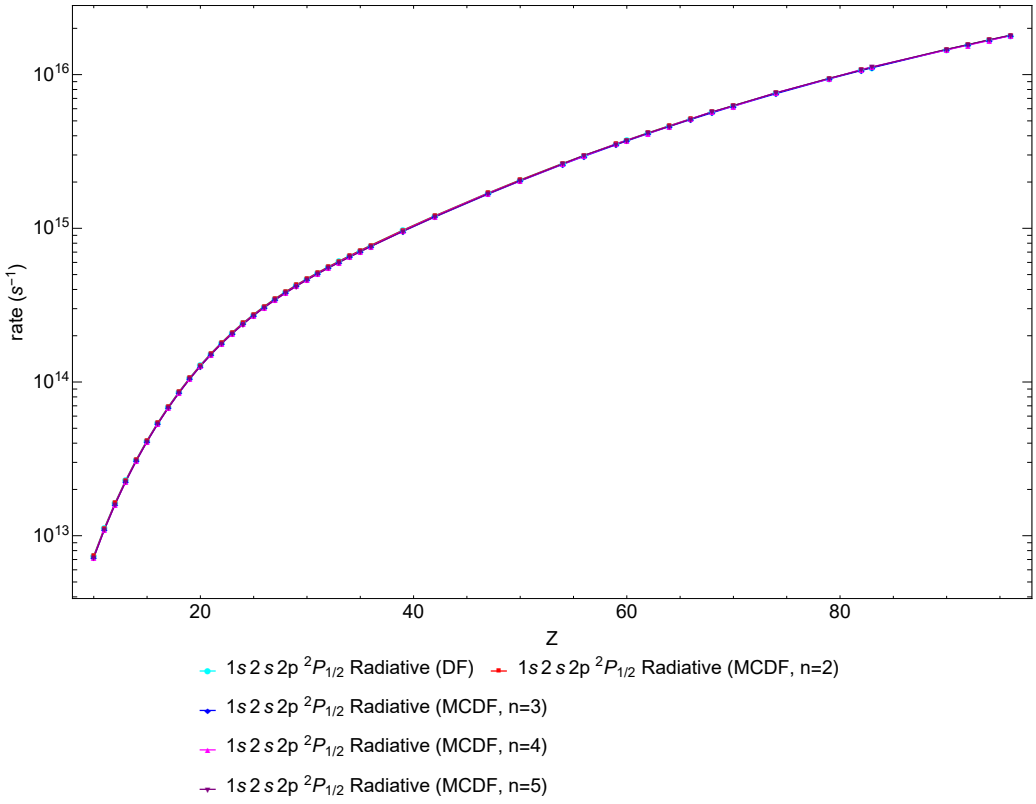

Fig. 5.20 *Radiative transition probabilities for the transition of* $1s\,2s\,2p\,^2P_{1/2} \rightarrow 1s^2\,2s\,^2S_{1/2}$. *DF: single-configuration calculations. MCDF: multi-configurations calculations with excited configurations up to 2p, 3d, 4f, 5g, respectively.*

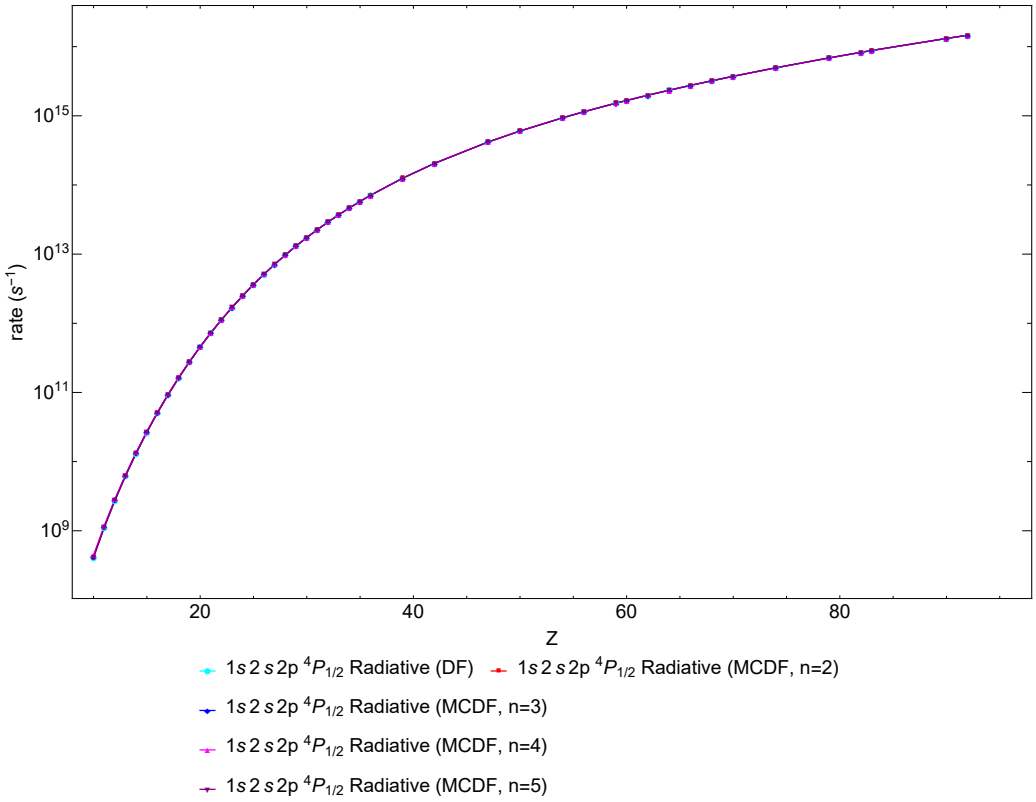

Fig. 5.21 *Radiative transition probabilities for the transition of* $1s\,2s\,2p\,^4P_{1/2} \rightarrow 1s^2\,2s\,^2S_{1/2}$. *DF: single-configuration calculations. MCDF: multi-configurations calculations with excited configurations up to 2p, 3d, 4f, 5g, respectively.*

Chapter 6

Analysis for muonic atoms

The nuclear charge-density distribution can be determined by the experiments of electron scattering and muonic x-rays or simultaneous analyses of the two experimental data, which can improve the nuclear information significantly.

There will be an upcoming experiment to perform precise measurement of the absolute nuclear charge radii of radioactive ^{226}Ra with a level of 0.2% relative precision by muonic x-rays at the Paul Scherrer Institute(PSI). Therefore, in order to prepare theoretical data for muonic ^{226}Ra and ^{248}Cm, we first analyze muonic ^{208}Pb in detail to test the reliability of our theory.

This section gives theoretical calculations for the transition energies of heavy muonic atoms and analyzes the corresponding contributions. This calculation can be used to determine and further improve nuclear parameter values combined with experimental data. The calculations take into account the finite size effects and QED effects. In addition, the effects of the surrounding atomic electrons and nuclear polarization are also considered.

For the analysis of the nuclear charge distribution in the two-parameter Fermi model, the half density parameter c and surface thickness parameter t, are varied around 6.6 fm and 2.3 fm, respectively, until a minimum χ^2 fit between theoretical and experimental transition energies are obtained.

6.1 Energy levels

When the nuclear charge parameters are fitted to the experimental transition energy, it is necessary to evaluate the QED corrections and the nuclear polarization correction. Then we study a set of muonic energy levels with the finite nuclear size. The calculations include all one-loop and the main two-loop QED contributions. A description of the method is given in Ref.[157]. These energies can be evaluated by exact numerical solution of the Dirac equation, which includes the lowest order vacuum polarization potential of order $\alpha(Z\alpha)$. Table 6.3 lists the energy levels and radiation corrections. The maximum relative size of QED corrections to the energies is about 0.6% at $1s$ level for muonic lead. As the level becomes higher, the QED contributions get smaller.

In particular, the vacuum polarization is caused by the virtual electron-positron pair, which modifies electric interaction between the nucleus and muon. The electron loop part

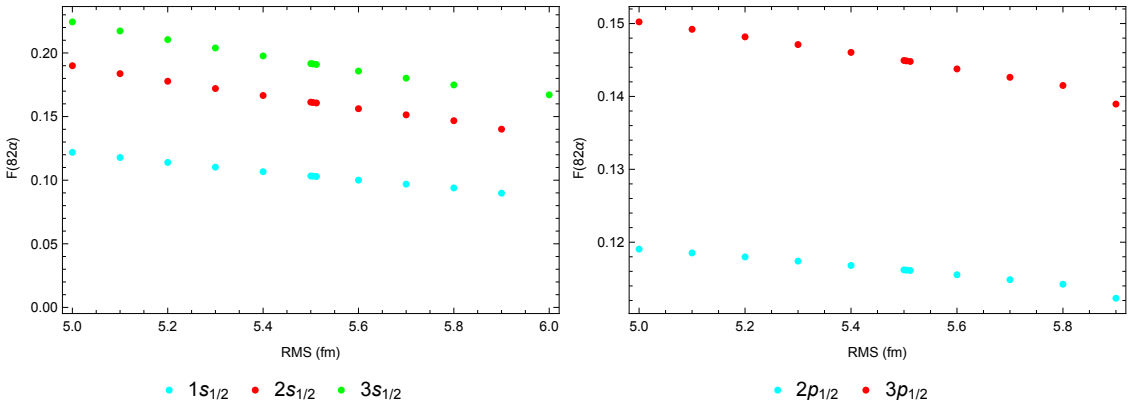

Fig. 6.1 *Self-energy with finite size correction in muonic lead. From Indelicato and Mohr(2018). [304]*

Table 6.1 – Self-energy corrections for muonic ^{208}Pb. All energies are in keV.

	Indelicato and Mohr(2018) [304]	Akihiro Haga [89]		
	self-energy with finite size	leading self-energy	higher-order self-energy	total self-energy
1s1/2	3.249	3.220	0.153	3.373
2s1/2	0.634	0.696	0.025	0.721
2p1/2	0.457	0.348	0.065	0.413
3p1/2	0.223			
3p1/2	0.169	0.149	0.021	0.170

causes a considerable correction to the energy levels. The correction is called Wichmann and Kroll correction (see section 2.4), which decreases the transition energies. This correction accounts for about 1% to 1.8% of the total vacuum polarization for these states listed in Table 6.3 for the muonic lead. We study the contributions of Kallen and Sabry (see section 2.4), a fourth-order potential of $\alpha^2 (Z\alpha)$ using our numerical wave functions with good accuracy. We also consider the vacuum polarization due to the generation of the virtual muon positron pairs. The term named loop after loop Uëhling (see section 2.4) only accounts for 0.4% of the Uëhling correction.

Concerning the muonic self-energy correction, Indelicato and Mohr [304] have calculated the exact one-loop self-energy with the finite-size contribution in the framework of nonrelativistic prescription for the first time. Semianalytic expansion of $F(Z\alpha)$ as the RMS dependence is plotted in Fig. 6.1. They have extended the work described in Refs. [118, 307, 308] to muonic atoms. In Table 6.1, we listed their calculation of self-energy corrections with leading order $\alpha (Z\alpha)^4$ and compared with the results of Akihiro Haga et al. [89]. In their estimation, self-energy correction can be divided into two contributions, namely a low-energy term with the nonrelativistic multipole expansion and a high-energy term with only the lowest order of the external field using the mean value method. The result from Indelicato and Mohr [304] is 0.1 keV higher than Akihiro Haga at $2p_{1/2}$ level. The self-energy generally increases the energy level, which is around 3.2 keV for the lowest

Table 6.2 – Nuclear polarization corrections for muonic ^{208}Pb. This work is calculated using RURP code from Rinker and Speth [94]. All energies are in keV.

	This work			Akihiro Haga [89]			P. Bergern [5]
	L =0,1,2,3	L >3	Total	TGT model	RIN model	JS model	Best fit
1s1/2	-3.749	-0.175	-3.924	-2.727	-3.599	-5.721	-4.252
2s1/2	-0.713	-0.015	-0.728	-0.463	-0.611	-0.930	-0.964
2p1/2	-1.484	-0.082	-1.566	-1.357	-1.590	-2.178	-1.307
2p3/2	-1.355	-0.074	-1.429	-1.425	-1.656	-2.214	-1.534
3p1/2	-0.459	-0.023	-0.482	-0.561	-0.690	-0.929	-0.525
3p3/2	-0.449	-0.022	-0.471	-0.749	-0.914	-1.118	-0.855
3d3/2	-0.130	-0.005	-0.135	-0.226	-0.239	-0.280	-0.240
3d5/2	-0.110	-0.004	-0.114	-0.043	-0.042	-0.038	-0.045

state of ^{208}Pb. The higher-order $\alpha^2\,(Z\alpha)$ combined vacuum-polarization correction has been considered in their analysis. The relativistic recoil corrections were considered with order $(Z\alpha)^5$ and to all orders in $\frac{m_u}{m_p}$ by performing the direct numerical evaluation for the Dirac equation, the same method as we do.

However, the largest theoretical uncertainty comes from the calculation of nuclear polarization. Akihiro Haga also reanalyzed the nuclear polarization in ^{90}Zr and ^{208}Pb. They used three forms of transition densities, including Jensen-Steinwedel (JS) [151, 125, 126], Rinker (RIN) [94] and Tassie-Goldhaber-Teller (TGT) [150, 151] models, in which the calculation results of the JS model are reasonable. So we choose the JS result as a reference. We also calculate the densities using the program of RURP from Rinker and Speth [94], which is described in detail in section 2.7. Bergern et al. [5] give a set of best-fit nuclear polarization correction values of the low-lying muonic level, which are very suitable for experimental transition energies. The comparison of our calculations and other two theoretical results are presented in Table 6.2. For ^{208}Pb, we obtain -3.924 keV for the 1s orbital. This is consistent with the RIN model value of -3.599 keV, and the JS model gave a lower value of -5.721 keV. Bergern also gives a value of -4.252 keV, which is lower than our result, including nuclear excited states of both continuous (high-lying) and discrete (low-lying). They fixed the 1s correction at its theoretical fit. In addition, the nuclear polarization values of the two 3d states are also fixed due to the small shifts. At the same time, the nuclear polarization of 2s level is shown of -0.964 keV, slightly above the estimated value of -0.816 keV, which is adjusted simultaneously for nuclear polarization in the 2p and 3p levels. The nuclear polarization effects decrease the energy levels as a relatively large correction.

However, with the improvement of measurement accuracy, there is a certain difference between the calculation result in the nuclear polarization correction and experimental value. The difference in nuclear polarization correction for the muonic x-ray is that this correction of $p_{1/2}$ is larger than the $p_{3/2}$ levels in theory predicts, while the analysis from experiments gives the opposite result. The consistency between the measured and calculated transition energies requires the magnitude of the corresponding nuclear polarization

Table 6.3 – Corrections to muonic energy levels in ^{208}Pb with r =5.5057 fm. All energies are in keV.

^{208}Pb	1s1/2	2s1/2	2p1/2	2p3/2
Dirac energy	-10526.651	-3581.248	-4781.507	-4599.336
Uelhing (electron loop)	-67.121	-19.342	-32.273	-29.740
Uelhing (muon loop)	-0.490	-0.122	-0.023	-0.005
Loop after loop Uelhing	-0.084	-0.039	-0.094	-0.083
Wichmann and Kroll	1.014	0.347	0.482	0.447
Källen and Sabry (electrons)	-0.554	-0.150	-0.252	-0.230
Recoil 1	-0.290	-0.033	-0.060	-0.055
Relat. Recoil	3.523	0.568	-0.054	-0.054
Self-energy [89]	3.373	0.721	0.413	0.707
Nuclear polarization [89]	-5.721	-0.930	-2.178	-2.214
	3p1/2	3p3/2	3d3/2	3d5/2
Dirac energy	-2128.299	-2081.349	-2162.376	-2120.312
Uelhing (electron loop)	-10.754	-10.222	-10.493	-9.839
Uelhing (muon loop)	-0.008	-0.002	0.000	0.000
Loop after loop Uelhing	-0.027	-0.026	-0.034	-0.030
Wichmann and Kroll	0.195	0.186	0.202	0.193
Källen and Sabry (electrons)	-0.082	-0.077	-0.076	-0.071
Recoil 1	-0.012	-0.011	-0.012	-0.012
Relat. Recoil	-0.015	-0.015	-0.003	-0.003
Self-energy [89]	0.170	0.244	-0.036	0.057
Nuclear polarization [89]	-0.929	-1.179	-0.280	-0.038

value to be inverted. Furthermore, the same phenomenon can be found in the $2p$ state, and the $3p$ state and is also presented in both papers of Haga and Bergem. The same kind of discrepancies are discovered not only in the muonic ^{208}Pb but also in the muonic ^{90}Zr. The difference of nuclear polarization energy shift is about 0.036 keV for the $2p$ level, whereas the difference is 0.2 keV for the $3p$ level. We find that in the fitting data of Bergem, there is the same magnitude of influence in the $3p$ and $2p$ splittings.

In view of the large theoretical uncertainties, the nuclear polarization calculations can only give orders of magnitude, not exact results.

6.2 Effects from remaining electrons

Effects caused by the electrons refilling the orbitals should also be taken into account. The static electron effect dominates these corrections between the muon and the nucleus. Table 6.4 shows the effects on the transition energy of the muon by the surrounding atomic electrons. Small results of electron effects show that muon is less constrained by the presence of the effect. Since the wave function of the $1s$ electron has the largest overlap with the muon, it contributes to the main effect.

Table 6.4 – The effects from remaining electrons to the transition energies in muonic ^{208}Pb. For the superscript (1), only the 1s electrons are considered, while for (1+2), all electrons from the first and second shells are considered, for (1+2+3), all electrons from the first, second and third shells are considered. All energies are in keV.

muon transition	ΔE(1)	ΔE(1+2)	ΔE(1+2+3)
2p3/2-1s1/2	-0.005	-0.006	-0.007
2p1/2-1s1/2	-0.005	-0.006	-0.006
3d3/2-2p1/2	-0.019	-0.022	-0.022
3d5/2-2p3/2	-0.019	-0.022	-0.023
3d3/2-2p3/2	-0.018	-0.021	-0.022
3p3/2-2s1/2	-0.022	-0.026	-0.027
3p1/2-2s1/2	-0.021	-0.024	-0.025
2s1/2-2p1/2	-0.009	-0.011	-0.011
2s1/2-2p3/2	-0.009	-0.010	-0.011
5f5/2-3d3/2	-0.144	-0.167	-0.172
5f7/2-3d5/2	-0.144	-0.168	-0.173
5f5/2-3d5/2	-0.142	-0.165	-0.171
4f5/2-3d3/2	-0.041	-0.048	-0.050
4f7/2-3d5/2	-0.041	-0.048	-0.050
4f5/2-3d5/2	-0.040	-0.047	-0.048
4d3/2-3p1/2	-0.049	-0.057	-0.059
4d5/2-3p3/2	-0.028	-0.033	-0.034
4d3/2-3p3/2	-0.048	-0.056	-0.058

The effect of remaining electrons is a basic electromagnetic effect and easy to calculate in principle. The key issue comes from the lack of an in-depth understanding of the state of the electrons in the muonic atoms during the X-ray transitions. This Auger transitions may occur, leading to ionization and excitation, and thus an unknown resultant electronic configuration. In addition to relying on the X-ray and Auger transition rates, the atomic ionization state relies on the formation of atoms and the ability of this system to regain the lost electrons from the surrounding environment. As a result, it is difficult to judge how many electrons are filled in the electronic shells.

The effects of remaining electrons to the 1s to 5f energy levels for muonic ^{208}Pb with the muon and 2, 10, 18 electrons has been obtained in Table 6.4, separately. For example, the effects to the transition $5f5/2 - 3d3/2$, $5f7/2 - 3d5/2$, and $5f5/2 - 3d5/2$ are, respectively, -0.172 keV, -0.173 keV, and -0.171 keV in row 10 and 11, and 12 when 18 electrons are included. The effects for three of the transitions are significant due to the large effect on level 5f. However, there is only -0.006 keV value on transition $2p1/2-1s1/2$. It can be found that for low-level muonic states, the effects are very small. The effect from K-shell occupies approximately 80% in this total effect, each L shell electrons 14%, and each M shell only 4% in the muonic lead.

Table 6.5 – Muonic ^{208}Pb transition energies (keV) in Fermi, Uniform and three parameter Gauss models with the same r =5.5057fm. Diff. represent the differences of Uniform and Gauss models with Fermi model. The Gauss parameter (c,t,w)=(6.1819,2.9071,0.38).

	Fermi model	Uniform model	Diff.	Gaussian 3 model	Diff.
2p3/2-1s1/2	5962.475	5905.583	-56.892	5959.467	-3.008
2p1/2-1s1/2	5777.495	5722.397	-55.098	5774.642	-2.853
3d3/2-2p1/2	2642.414	2644.953	2.539	2641.860	-0.554
3d5/2-2p3/2	2500.487	2504.914	4.427	2500.084	-0.403
3d3/2-2p3/2	2457.434	2461.767	4.333	2457.035	-0.398
3p3/2-2s1/2	1507.801	1491.239	-16.562	1507.369	-0.432
3p1/2-2s1/2	1460.492	1444.738	-15.753	1460.100	-0.392
2s1/2-2p1/2	1215.276	1233.434	18.157	1215.303	0.027
2s1/2-2p3/2	1030.296	1050.248	19.952	1030.478	0.182
5f5/2-3d3/2	1404.877	1405.190	0.313	1404.884	0.007
5f7/2-3d5/2	1366.535	1366.755	0.220	1366.547	0.011
5f5/2-3d5/2	1361.824	1362.043	0.219	1361.835	0.011
4f5/2-3d3/2	972.029	972.341	0.312	972.034	0.005
4f7/2-3d5/2	938.150	938.370	0.220	938.159	0.010
4f5/2-3d5/2	928.976	929.195	0.219	928.985	0.009
4d3/2-3p1/2	921.419	921.690	0.270	921.239	-0.181
4d5/2-3p3/2	891.831	892.958	1.127	891.687	-0.144
4d3/2-3p3/2	874.110	875.189	1.079	873.969	-0.141

6.3 Best fit nuclear parameter values

Firstly, in Table 6.5, we list the transition energies for the uniform sphere and Gaussian models compared with the Fermi model with the same RMS radius. The value of the three-parameter Gaussian model is very close to the Fermi model. In contrast, the uniform model has a big difference, more than 50 keV for the $2p_{1/2} - 1s_{1/2}$ transition, in which the $1s$ and $2s$ states are very sensitive to the internal part of nuclear charge distribution.

As a first step, we select a few sets of meaningful nuclear parameters according to the RMS given by Angeli [185], and corresponding to some sets of calculated transition energies for two-parameter fermi and three gauss models. Next, we give a fit and analysis using these energies combined with the experimental data. Our fit includes 18 transition energies, namely nine M-lines, five L-lines, two K_α-lines, and two transitions concerning $2s$ level. These data include 14 energy levels from $1s$ to $5f$. We report on the nuclear parameters that minimize the weighted theory-experiment distance. This experiment [5] obtained an accuracy of up to 11 ppm, which is a factor of five improvements over the result of Kessler et al. [90].

The values of nuclear polarization effects and self-energy correction calculated by Haga are adopted directly. We have also calculated them respectively introduced in section 6.1. For the two-parameter Fermi model, we performed a polynomial fit comparing with the experimental values. When the parameters are r = 5.5057 fm, and t = 2.3919 fm, the

Table 6.6 – Muonic ^{208}Pb transition energies(keV) with the minimum value of χ^2 of two-parameter Fermi and three-parameter gauss models. The superscript (1) represents the effects of 2 electrons, and superscript (1+2+3) represents 18 electrons. The nuclear polarization uncertainties are from JS and RIN models. The Fermi model is evaluated with r =5.5057 fm, and t =2.3950 fm. The Three parameter gauss model is evaluated with c =6.1778 fm, t =2.9706 fm, and w =0.3790 fm, corresponding to r =5.5031 fm

.

	Experiment		Fermi		Fermi+ΔE(1)		Fermi+ΔE(1+2+3)		Gaussian		Uncertainty
	Energy	Error	Theory	Diff.	Theory	Diff.	Theory	Diff.	Theory	Diff.	JS-RIN
2p3/2-1s1/2	5962.854	0.09	5962.475	-0.379	5962.470	-0.384	5962.468	-0.386	5962.428	-0.426	-1.564
2p1/2-1s1/2	5778.058	0.1	5777.495	-0.563	5777.490	-0.568	5777.489	-0.569	5777.451	-0.607	-1.534
3d3/2-2p1/2	2642.332	0.03	2642.414	0.082	2642.395	0.063	2642.392	0.060	2642.421	0.089	-0.547
3d5/2-2p3/2	2500.59	0.03	2500.487	-0.103	2500.467	-0.123	2500.463	-0.127	2500.499	-0.091	-0.562
3d3/2-2p3/2	2457.569	0.07	2457.434	-0.135	2457.416	-0.153	2457.412	-0.157	2457.444	-0.125	-0.517
3p3/2-2s1/2	1507.754	0.05	1507.801	0.047	1507.778	0.024	1507.774	0.020	1507.830	0.076	-0.054
3p1/2-2s1/2	1460.558	0.032	1460.492	-0.066	1460.471	-0.087	1460.467	-0.091	1460.522	-0.036	-0.080
2s1/2-2p1/2	1215.33	0.03	1215.276	-0.054	1215.267	-0.063	1215.265	-0.065	1215.273	-0.057	-0.269
2s1/2-2p3/2	1030.543	0.027	1030.296	-0.247	1030.287	-0.256	1030.285	-0.258	1030.296	-0.247	-0.239
5f5/2-3d3/2	1404.659	0.02	1404.877	0.218	1404.734	0.075	1404.705	0.046	1404.897	0.238	-0.041
5f7/2-3d5/2	1366.347	0.019	1366.535	0.188	1366.391	0.044	1366.362	0.015	1366.554	0.207	0.004
5f5/2-3d5/2	1361.748	0.25	1361.824	0.076	1361.682	-0.066	1361.653	-0.095	1361.842	0.094	0.004
4f5/2-3d3/2	971.974	0.017	972.029	0.055	971.987	0.013	971.979	0.005	972.047	0.073	-0.041
4f7/2-3d5/2	938.096	0.018	938.150	0.054	938.108	0.012	938.100	0.004	938.167	0.071	0.004
4f5/2-3d5/2	928.883	0.014	928.976	0.093	928.936	0.053	928.928	0.045	928.992	0.109	0.004
4d3/2-3p1/2	920.959	0.028	921.419	0.460	921.370	0.411	921.360	0.401	921.413	0.454	-0.239
4d5/2-3p3/2	891.383	0.022	891.831	0.448	891.803	0.420	891.797	0.414	891.825	0.442	-0.265
4d3/2-3p3/2	873.761	0.063	874.110	0.349	874.063	0.302	874.053	0.292	874.104	0.343	-0.265

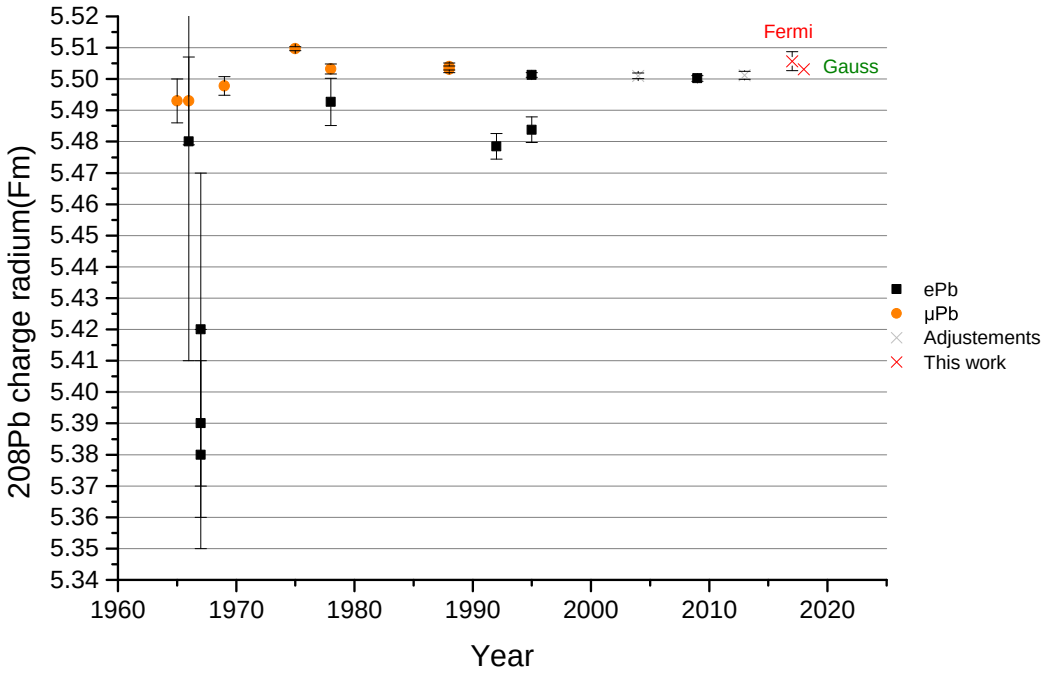

Fig. 6.2 *The trend of nuclear charge radius from experiments in the past 50 years and compared with our calculation data on muonic lead.*
Electron scattering: Van Niftrik et al.(1966) [310], Bellicard et al.(1967) [309], Euteneuer et al. [314], Frickeet al.(1995) [317], Wasowicz(2009) [316].
Muonic x-ray : Acker et al.(1965) [311], Anderson et al.(1966) [312], Anderson et al.(1969) [313], Kessler et al.(1975) [315], Euteneuer et al.(1978) [314], Bergern et al.(1988) [5].
Adjustements: Angeli(2004) [185], Angeli et al. (2013) [186].

minimum of the chi-square is $\chi^2 = 1160.63$ for 14 degrees of freedom. The error bars are $r_{error} = 0.003$ fm and $t_{error} = 0.026$ fm. The errors obtained in the fitting come from the combination of theoretical uncertainties and experimental error bars. The fit of the data is not good. This leads to doubts about the model dependence from the charge distribution of the nucleus when one tries to fit the data. So, we continue to fit with three gauss model, in which the RMS radius is drastically improved. Our fit results are $c = 6.1778$ fm, $t = 2.9706$ fm, and $w = 0.3790$ fm, with $r = 5.5031$ fm. This agrees with the experimental result (5.5031(11) fm) given by Bergern, but the transition energies are still not consistent with the experiment. So, we continue to consider the effects from 2 and 18 remaining electrons, respectively. The transition energies have been greatly improved for high-state, but it is useless for low-state. It has been found that the largest deviation between the experiment and calculation values occurs in the Kα transition. In our current work, this deviation reached 0.6 keV. Another discrepancy is 0.45 keV for the $4d - 3p$ transitions.

Table 6.7 – Theoretical and experimental fine structure splitting(Δp) energies in muonic ^{208}Pb(keV).

^{208}Pb level	This work	Akihiro Haga [89]			P. Bergern [5]		
		TGT model	RIN model	JS model	Fit	Best fit	Exp.
Δ2p	184.981	184.858	184.846	184.829	185.112	184.776	184.788(27)
Δ3p	47.308	47.231	47.208	47.225	47.531	47.196	47.197(45)

Although the radius is improved from Gauss model fit, it does not provide any improvement for the transition energy. In addition, χ^2 in both fits turn out to be very large. One reason might be some important effects of nuclear polarization. In Table 6.6, we give the uncertainty of nuclear polarization between JS model and RIN model. The deviations of the calculation results from the two models are within the uncertainty of nuclear polarization at low-states. Another reason is that too many energy levels involved in the fitting fail to achieve convergence. In addition to nuclear polarization shifts, which must be applied to the muonic energy levels, other corrections of first-order vacuum polarization can be excluded, due to accurate calculation. The self-energy would affect the $2p$ levels by 0.7 keV, and the $3p$ levels by 0.2 keV, while nuclear polarization amounts to -2.2 keV and -1.2 keV, respectively. Regarding higher-order vacuum polarization corrections, these values are just 0.4 keV. In addition, it may be important to consider high-order corrections of nuclear polarization.

P. Bergern et al. [5] obtained charge moments and nuclear polarization from precise experimental measurements of muonic X-rays. The fit just using Fermi charge distribution as free parameters is very poor, in which the χ^2 is 187 for ^{208}Pb. If fitting includes more free variables of eight nuclear polarization parameters, 13 low-lying lines, and two charge parameters matching the experimental transition energies, the χ^2 value is reduced to 0.19 per degree of freedom. Finally, they obtained the RMS radius of $\langle r^2 \rangle^{1/2} = 5.5031(11)$ fm, which is consistent with the elastic electron scattering value 5.503(6) fm. However, the latest data is 5.5012 fm compiled by Angeli [185].

It is needed to recalculate the $2p$ and $3p$ splitting energy considering such large χ^2 value. In table 6.7, we compare the fine structure splitting(Δp) in the χ^2 minimum with the experimental results. We can notice that the calculated the fine structure splitting(Δp) of $2p$ and $3p$ are not within the scope of the experimental error bars. The discrepancies are less than 0.2 keV in the present calculation comparing with the experiment. The effects of two electrons from the $1s$ orbital are only 0.6 eV to $2p$ splitting and 1.5 eV to $3p$ splitting.

Although the present theoretical evaluation provides some large deviations, the nuclear radius is reproduced combining with the experimental results.

6.4 Energy levels of Muonic Radium and Curium

The charge radius of a nucleus is a fundamental parameter and important for understanding the strong interactions in the nucleus. Accurate measurements of the charge radius of

Table 6.8 – Corrections to muonic energy levels in ^{226}Ra and ^{248}Cm (keV). The parameters (c, t) = (5.7211, 2.25) and (5.8687, 2.25) in the Fermi-charge distribution are used for ^{226}Ra and ^{248}Cm, respectively.

^{226}Ra	1s1/2	2s1/2	2p1/2	2p3/2	3p1/2	3p3/2	3d3/2	3d5/2
Dirac energy	-11442.285	-4004.708	-5442.702	-5234.869	-2432.399	-2379.564	-2499.601	-2444.595
Uelhing (electron loop)	-71.431	-21.648	-36.810	-34.060	-12.445	-11.880	-12.705	-11.838
Uelhing (muon loop)	-0.534	-0.143	-0.029	-0.006	-0.010	-0.002	0.000	0.000
Loop after loop Uelhing	-0.082	-0.044	-0.100	-0.091	-0.030	-0.029	-0.043	-0.036
Wichmann and Kroll	1.268	0.451	0.629	0.584	0.258	0.246	0.273	0.259
Källen and Sabry (electrons)	-0.588	-0.168	-0.289	-0.265	-0.095	-0.090	-0.093	-0.086
Källen and Sabry (muons)	0.000	0.000	0.000	0.000	0.000	0.000	0.000	0.000
Recoil 1	-0.315	-0.038	-0.071	-0.066	-0.014	-0.014	-0.015	-0.014
Recoil 2	0.000	0.000	0.094	-0.047	0.028	-0.014	0.008	-0.006
Relat. Recoil	4.529	0.733	-0.071	-0.071	-0.020	-0.020	-0.004	-0.004
Self-energy	3.378	0.668	0.582		0.211			
Nuclear polarization	-4.309	-0.866	-1.992	-1.845	-0.634	-0.633	-0.237	-0.206
Total	-11510.369	-4025.762	-5480.759	-5270.736	-2445.150	-2391.999	-2512.416	-2456.526
^{248}Cm	1s1/2	2s1/2	2p1/2	2p3/2	3p1/2	3p3/2	3d3/2	3d5/2
Dirac energy	-12801.914	-4622.116	-6384.953	-6136.963	-2868.806	-2806.463	-2989.529	-2913.275
Uelhing (electron loop)	-78.610	-25.214	-43.359	-40.242	-14.947	-14.313	-16.053	-14.835
Uelhing (muon loop)	-0.617	-0.180	-0.039	-0.008	-0.014	-0.003	0.000	0.000
Loop after loop Uelhing	-0.083	-0.051	-0.111	-0.101	-0.035	-0.034	-0.055	-0.047
Wichmann and Kroll	1.688	0.628	0.875	0.811	0.365	0.348	0.396	0.373
Källen and Sabry (electrons)	-0.648	-0.195	-0.342	-0.315	-0.114	-0.109	-0.118	-0.108
Källen and Sabry (muons)	0.000	0.000	0.000	0.000	0.000	0.000	0.000	0.000
Recoil 1	-0.359	-0.047	-0.089	-0.083	-0.018	-0.017	-0.020	-0.019
Recoil 2	0.000	0.000	0.111	-0.055	0.033	-0.016	0.010	-0.007
Relat. Recoil	6.226	1.013	-0.100	-0.100	-0.028	-0.028	-0.006	-0.006
Self-energy	3.646	0.737	0.763		0.273			
Nuclear polarization	-4.816	-1.099	-2.626	-2.482	-0.919	-0.949	-1.997	
Total	-12875.487	-4646.523	-6429.870	-6179.538	-2884.210	-2821.583	-3007.372	-2927.923

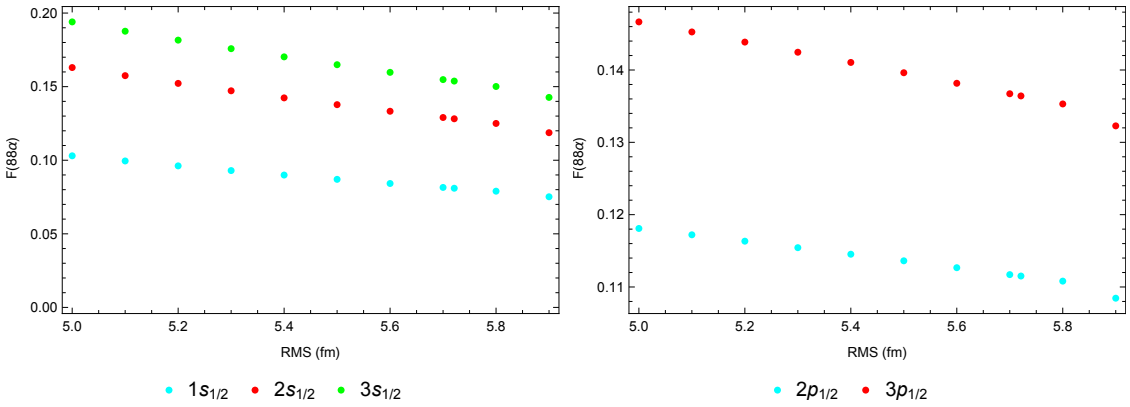

Fig. 6.3 *Self-energy with finite size correction in muonic radium. From Indelicato and Mohr(2018) [304].*

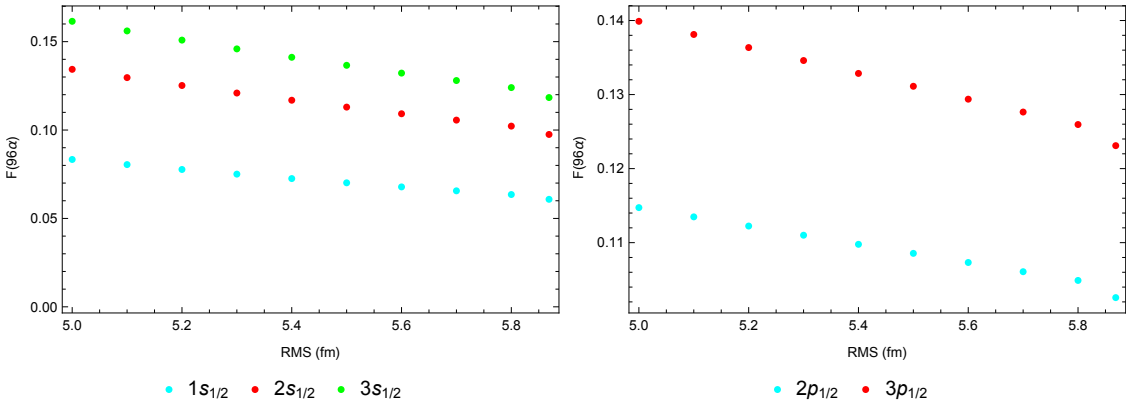

Fig. 6.4 *Self-energy with finite size correction in muonic curium. From Indelicato and Mohr(2018) [304].*

radioactive atoms are essential. An upcoming measurement in PSI [95] will be performed to measure atomic parity violation in single Ra^+ ion. There, various levels of radium can be drawn from the exact spectrum of the emitted muonic X rays. The extraction of charge radius is to be performed with the accuracy of 0.2%. The charge radius of ^{226}Ra, ^{248}Cm can be extracted by combining the transition energies from measurement with the calculation results as we test on lead.

With the upcoming experiments on high Z muonic radium and curium and the expected improvement in experimental precision, correct treatment is necessary of all relevant effects including QED corrections with vacuum polarization to leading order and second-order terms and finite-nuclear size corrected self-energy, nuclear polarization, deformation, nuclear excitations and so on. The precise theoretical calculation is very important for the extraction of nuclear parameters from future experiments.

We calculate muonic radium and curium using the same prescription of exact QED corrections, which were discussed above. Although there were some uncertainties for the nuclear polarization in the present analysis due to the uncertainties in the nuclear

excitation spectrum, we can provide the correction as an order-of-magnitude estimation. In view of the precise calculations of the element lead, we can provide reliable values for the upcoming experiment.

All corrections causing the energy shifts are listed in Table 6.8 for muonic ^{226}Ra and ^{248}Cm levels with $n \leq 3$. The χ^2 analysis with nuclear charge parameters will be performed after the experimental results are obtained.

6.5 Finite nuclear size

The measurements of the Lamb shift in light muonic atoms and the proton radius puzzle prompt ones to conduct a large number of new studies on muonic atoms. The accuracy of determining the nuclear radii depends on the precision of the experiments, and on the exactness of the QED calculations and nuclear structure evaluations.

In Table 6.9, the level energies for muonic ^{208}Pb, ^{226}Ra, and ^{248}Cm are shown with pointlike nucleus size, finite size, QED corrections. For heavy nuclei, the finite nuclear size correction can amount up to 50% in the total energy. The leading-order effects of Uëhling potential dominate more than 95% in the QED corrections. One can see that the finite size corrections are 100 times larger than QED corrections. It seems that such low-level transitions are suitable for extraction of the nuclear structure information, owing to the huge contribution from the nucleus.

Table 6.9 – The level energies on muonic ^{208}Pb, ^{226}Ra and ^{248}Cm of the pointlike nucleus, finite nuclear size and QED effects are presented. The nuclear radius of 5.5057 fm for ^{208}Pb, 5.7211 fm for ^{226}Ra and 5.8687 fm for ^{248}Cm are adopted in the Fermi-charge distribution. All energies are in keV.

	State	Pointlike	Finite size	QED
^{208}Pb	1s1/2	-20992.35	-10479.64	-67.23
	2s1/2	-5385.41	-3573.09	-19.31
	2p1/2	-5385.41	-4780.70	-32.16
	2p3/2	-4837.24	-4598.27	-29.61
	3p1/2	-2329.93	-2127.99	-10.68
	3p3/2	-2166.53	-2091.57	-10.14
	3d3/2	-2166.53	-2162.41	-10.40
	3d5/2	-2121.97	-2120.24	-9.75
	4d3/2	-1216.32	-1213.85	-4.49
	4d5/2	-1197.37	-1196.33	-4.25
	4f5/2	-1197.37	-1197.37	-3.71
	4f7/2	-1188.30	-1188.28	-3.61
	5f5/2	-766.38	-766.37	-1.86
	5f7/2	-761.71	-761.70	-1.81
^{226}Ra	1s1/2	-24652.01	-11380.31	-71.37
	2s1/2	-6354.17	-3993.56	-21.55
	2p1/2	-6354.17	-5441.30	-36.60
	2p3/2	-5591.71	-5233.38	-33.84
	3p1/2	-2734.89	-2431.88	-12.32
	3p3/2	-2507.49	-2379.06	-11.75
	3d3/2	-2507.49	-2499.64	-12.57
	3d5/2	-2447.78	-2444.50	-11.70
	4d3/2	-1407.30	-1402.63	-5.45
	4d5/2	-1381.89	-1379.91	-5.13
	4f5/2	-1381.89	-1381.88	-4.53
	4f7/2	-1369.80	-1369.78	-4.38
	5f5/2	-884.49	-884.48	-2.28
	5f7/2	-878.27	-878.25	-2.21
^{248}Cm	1s1/2	-12804.68	-12713.03	-78.27
	2s1/2	-4623.00	-4605.30	-25.01
	2p1/2	-6384.85	-6382.15	-42.98
	2p3/2	-6136.73	-6134.73	-39.86
	3p1/2	-2868.82	-2867.80	-14.75
	3p3/2	-2806.42	-2805.69	-14.11
	3d3/2	-2989.49	-2989.57	-15.83
	3d5/2	-2913.25	-2913.14	-14.62
	4d3/2	-1676.60	-1676.63	-6.91
	4d5/2	-1645.54	-1645.49	-6.47
	4f5/2	-1649.46	-1649.48	-5.77
	4f7/2	-1632.27	-1632.25	-5.55
	5f5/2	-1055.76	-1055.76	-2.93
	5f7/2	-1046.91	-1046.90	-2.83

Conclusions and Perspectives

In this thesis, we use the MCDF method to perform theoretical calculations, which include the valence-excited transitions of $1s^2\,2p^{\,2}P_J \rightarrow 1s^2\,2s^{\,2}S_{1/2}, J = 1/2, 3/2$, core-excited transitions of $1s\,2s\,2p^{\,2}P_J \rightarrow 1s^2\,2s^{\,2}S_{1/2}, J = 1/2, 3/2$ and $1s\,2s\,2p^{\,4}P_J \rightarrow 1s^2\,2s^{\,2}S_{1/2}, J = 1/2, 3/2, 5/2$, and Auger transitions of $1s\,2s\,2p^{\,2}P_J \rightarrow 1s^{2\,1}S_0$ and $1s\,2s\,2p^{\,4}P_J \rightarrow 1s^{2\,1}S_0, J = 1/2, 3/2$ in the lithium isoelectronic sequence from neon (Z=10) to uranium (Z=96). These energies are calculated by taking into account the QED effects and contributions from electronic correlation. In addition, radiative corrections, as well as all-order vacuum polarization and Breit corrections, are also included with fully optimized active set wave functions.

The Welton approximation and the effective operator methods are used for the self-energy screening contributions. We note that the results from the two models are almost identical to each other at low-Z ions. However, from $Z = 50$, the value of the Welton model begins to move away from the effective operator method following the increase with Z. In the high-Z regions, the values of the Welton picture method are bigger than the effective operator method. The deviation reaches 0.2 eV at curium for valence-excited transitions, while this deviation has reached 2 eV in core-excited transitions. The effective operator model can improve the accuracy of the total transition energy by 0.002% for high-Z ions in valence-excited transitions. However, for core-excited transitions, we can't judge which model is better because there is no experiment as a reference in the heavy nuclear.

We also provide individual values of the Coulomb, Magnetic, Retardation, and higher-order Retardation correlations of electron-electron interaction correction. These correlations are obtained using a wavefunction built up from all configurations with single, double, and triple excitations to 5g orbitals. The Magnetic correlation corrections start being the same size as Coulomb correlation at Z=47 and being ten times larger than Coulomb part at Z=92 for the ground state of three-electron systems. The magnetic and retardation part can lead to a very large contribution to the correlation energy at high-Z. For example, the Magnetic correlation corrections are consistent with the trend of total correlations in core-excited transitions because the Magnetic parts dominate in the correlation contributions at middle- and high-Z ions.

It is very necessary to perform rigorous QED calculations. In the low- and middle-Z ions, diverse calculations are in good agreement with each other, except for $1/Z$ expansion method, which is far away from other theories. It can be seen that the present MCDF calculation results have a small shift with the values from the advanced RMBPT, RCI and S-matrix methods at high-Z ions due to different finite nuclear sizes, with or without nuclear polarization and the theoretical errors. The differences of many kinds of methods come from the uncertainty on the finite nuclear size and their evolution over time,

from whether some second-order QED corrections included or not, from what part of the electron-electron operator included in the correlation energy evaluation, and from Auger shift.

A number of measurements are performed using Tokamaks, ECRIS or astrophysics plasmas. Recently, our group measured He-, Li- and Be-like sulfur and argon ions with a double-flat crystal spectrometer without the use of any reference line. The transition energy measurements are performed with accuracies ranging from 2.3 ppm to 6.4 ppm depending on the element and line intensity. At low- and middle-Z, it clearly shows a generally good agreement between successive experiments and the most advanced theoretical calculations from the present work.

An upcoming experiment will be performed for muonic atom spectroscopy aiming at a precise measurement of the absolute nuclear charge radii of radioactive ^{226}Ra with a level of 0.2% relative precision at PSI. Extensive theoretical calculations are needed to deduce nuclear size. The muonic transition energies are also calculated numerically using Dirac wave functions with constant self-energy, including the QED contributions and finite nuclear size. Firstly, we give a detailed test on the muonic lead due to many experimental lines with high accuracy, double-magic property, and having a well-know radius. Muonic energy levels are highly sensitive to nuclear charge distribution due to large overlap with nuclear.

Nuclear parameters that minimize the weighted theory-experiment distance are found in the muonic ^{208}Pb with two-parameter Fermi model and three-parameter Gauss model, including 18 transition lines. We obtain r=5.5057 fm in the Fermi model and r=5.5031 in Gauss model by polynomial-fitting with large chi-square values. Many energy levels involved in the fitting fail to achieve convergence. Gauss model agrees with the experimental result (5.5031(11) fm) given by Bergern [5], and disagrees with the adjustment result (5.5012(13) fm) compiled by Angeli et al. [186]. Although the nuclear radius is improved from Gauss model fit, it did not provide any improvement for the transition energy.

One reason is that the effects caused by the electrons refilling the orbitals should be also taken into account. The effect from K-shell occupies approximately 80% in this total effect, each L shell electrons 14%, and each M shell only 4% in the muonic lead. The transition energies have been greatly improved by adding this effect for high-state, but it is useless for low-state.

Another reason is the large uncertainty of nuclear polarization due to the nuclear excitation spectrum. The deviations of the calculation results from the two models are within the uncertainty of nuclear polarization at low-states.

For tansition energies of heavy nuclei, the finite nuclear size corrections can amount up to 50%, which are more than 100 times larger than QED corrections. It seems that such low-levels are suitable for the extraction of nuclear structure information, owing to the huge contribution from the nucleus.

Finally, we also perform the calculations of the muonic ^{226}Ra and ^{248}Cm using the same prescription of exact QED corrections. The precise theoretical calculations are very important for the extraction of nuclear parameters from future experiments. We provide a rigorous QED calculation, except that the nuclear polarizations give an order-of-magnitude estimation.

Perspectives

The next step, I will continue to complete the calculations of the Auger transitions of $1s\,2s\,2p\,^2P_{1/2} \rightarrow 1s^2\,^1S_0$ and $1s\,2s\,2p\,^4P_{5/2} \rightarrow 1s^2\,^1S_0$, and it is difficult to achieve convergence for some free wavefunctions at $n = 5$. In some ions, numerical problems prevent us from doing calculations for a sufficiently large basis set, especially for the core-excited levels such as $1s\,2s\,2p$. It is hard to correlate those core excited states as the correlation wavefunctions need to have a part at the $1s$ distance and a part at the $2s$ and $2p$ distance at the same time. We plan to place constraints on the energy with the way that the orbitals are generated, for example from the $1s^22p$ in place of $1s2s2p$ when it changes the list of Brillouin configurations. The Auger rate is performed by using the Aberg method with multichannel exit. Normally all possible wave functions are equivalent, and the energy is the same at the end. Yet, it could happen that it is not true for the Auger rate, and the extra matrix elements could change the cross-section when the wavefunction rotates between those equivalent states. The radiative rates should be immune to such problems.

Before, one had to use the same configuration generation methods for the initial and final state in our MCDFGME code. So, one would enter for the $1s^2$ double excitation and single ones including Brillouin. CF Fischer showed that normally, one should only use of $1s^2 + 2s^2 + 2p^2 + 3s^2 + ...$ due to symmetries but also get with singles of $1s2s, 2s3s, 2p3p$ and so forth. One can get rid of those by doing local unitary transformations in the Hamiltonian, which preserve the norm. In the version of 2019v2, Indelicato has been changed the code so that one can use the "build" option for generating configurations automatically for one state and the "given" one for the other configuration, which allows entering the configurations by hand.

In view of the fact that nuclear polarization has high uncertainty. Next, I will conduct the fitting of nuclear polarization corrections by combining experimental results. The best-fit nuclear polarization will be very suitable for the experimental transition energies. therefore, I will try to deduce nuclear size using the three-parameter Fermi model in the muonic lead, because the three-parameter model can provide good improvements for the nuclear radius. Once the experiment of ^{226}Ra is completed, we can perform a fitting by extensive theoretical calculations with different nuclear parameters deriving the nuclear size of ^{226}Ra and ^{248}Cm.

It is very difficult to conduct a full QED evaluation beyond the two-photon exchange, which requires the development of some methods being able to contain higher orders. Another difficulty with the use of all-order methods lies in the photon energy of ω_{ij} exchanged between two electrons when the interaction operators are calculated in the correlation orbitals. Our MCDFGME code can perform it with the help of introduction the diagonal Lagrange multipliers, and this can result in a large contribution to the correlation contributions of magnetic and retardation part at high-Z.

The experiments have been performed in He-, Li- and Be-like sulfur and argon ions by our group using a double-crystal spectrometer from ions produced in an ECRIS without

the use of any reference line. Based on the experimental results, I would like to continue to study four and five electrons systems to analyze the QED contributions and nuclear effects. As the number of electrons increases, the characters of QED approximate become more and more challenging to evaluate.

The uncertainty of the nucleus, including finite nuclear size correction, nuclear polarization, and nuclear deformation limit the understanding of QED theory. Therefore, for a long-term goal, there is clearly a need to improve our knowledge of nuclear structures and their interactions with electrons. This may require combining the measurements of " exotic " particles, for example, muonic atoms, pionic atoms, and so on. Another important issue is the need to improve the accuracy of constants, including electron mass and the fine structure constant.

Appendix A

Table .10 – Correlations from Coulomb, magnetic, retardation, and higher order retardation part for the $1s^2\,2p\,^2P_{1/2} \rightarrow 1s^2\,^1S_0$ transition. Energies are in eV.

$1s^2\,2p\,^2P_{1/2} \rightarrow 1s^2\,^1S_0$					
Z	Coulomb corr.	Magnetic corr.	Retardation corr.	Higher-order Retardation corr.	Total corr.
10	-0.11596	0.00031	0.00013	0.00005	-0.11547
11	-0.11522	0.00090	0.00005	0.00003	-0.11424
12	-0.12617	0.00014	0.00028	0.00017	-0.12558
13	-0.12718	0.00011	0.00037	0.00007	-0.12663
14	-0.13044	0.00023	0.00044	0.00016	-0.12961
15	-0.13241	0.00030	0.00050	0.00020	-0.13141
16	-0.12821	0.00237	0.00012	0.00017	-0.12555
17	-0.13468	0.00037	0.00072	0.00023	-0.13336
18	-0.13595	0.00075	0.00074	0.00030	-0.13416
19	-0.13823	0.00051	0.00094	0.00037	-0.13641
20	-0.14357	0.00018	0.00115	0.00032	-0.14192
21	-0.13858	0.00362	0.00047	0.00058	-0.13391
22	-0.14277	0.00160	0.00111	0.00071	-0.13935
23	-0.14147	0.00510	0.00048	0.00085	-0.13504
24	-0.14492	0.00348	0.00104	0.00102	-0.13938
25	-0.14495	0.00612	0.00063	0.00121	-0.13699
26	-0.14685	0.00656	0.00074	0.00142	-0.13813
27	-0.14876	0.00689	0.00090	0.00165	-0.13932
28	-0.15070	0.00726	0.00107	0.00191	-0.14046
29	-0.15269	0.00765	0.00125	0.00223	-0.14156
30	-0.15469	0.00794	0.00148	0.00257	-0.14270
31	-0.15675	0.00832	0.00169	0.00297	-0.14377
32	-0.15888	0.00874	0.00190	0.00339	-0.14485
33	-0.16103	0.00906	0.00216	0.00385	-0.14596
34	-0.16326	0.00943	0.00244	0.00438	-0.14701
35	-0.16553	0.00977	0.00276	0.00489	-0.14811
36	-0.16789	0.01014	0.00307	0.00550	-0.14918
39	-0.17535	0.01112	0.00420	0.00748	-0.15255
42	-0.18357	0.01214	0.00550	0.00977	-0.15616
47	-0.19894	0.01344	0.00838	0.01420	-0.16292

50	-0.20933	0.01396	0.01057	0.01717	-0.16763
54	-0.22477	0.01428	0.01407	0.02138	-0.17504
56	-0.23319	0.01411	0.01615	0.02346	-0.17947
59	-0.24687	0.01369	0.01965	0.02683	-0.18670
60	-0.25173	0.01345	0.02095	0.02791	-0.18942
62	-0.26188	0.01276	0.02373	0.03010	-0.19529
64	-0.27269	0.01189	0.02674	0.03245	-0.20161
66	-0.28411	0.01056	0.03012	0.03438	-0.20905
68	-0.29628	0.00890	0.03385	0.03656	-0.21697
70	-0.30919	0.00678	0.03793	0.03869	-0.22579
74	-0.33748	0.00090	0.04739	0.04235	-0.24684
79	-0.37812	-0.01051	0.06209	0.04740	-0.27914
82	-0.40568	-0.02036	0.07283	0.05000	-0.30321
83	-0.41556	-0.02408	0.07674	0.05131	-0.31159
90	-0.49445	-0.06123	0.11030	0.05500	-0.39038
92	-0.52122	-0.07542	0.12201	0.06097	-0.41366
94	-0.54984	-0.09230	0.13509	0.06319	-0.44386
96	-0.58072	-0.11199	0.14961	0.05864	-0.48446

Table .11 – Correlations from Coulomb, magnetic, retardation, and higher order retardation part for the $1s^2\,2p\,^2P_{3/2} \rightarrow 1s^2\,^1S_0$ transition. Energies are in eV.

$1s^2\,2p\,^2P_{3/2} \rightarrow 1s^2\,^1S_0$					
Z	Coulomb corr.	Magnetic corr.	Retardation corr.	Higher-order Retardation corr.	Total corr.
10	-0.10937	0.00120	-0.00017	0.00003	-0.10831
11	-0.09374	0.00256	-0.00042	0.00121	-0.09039
12	-0.11255	0.00199	-0.00026	-0.00074	-0.11156
13	-0.11399	0.00223	-0.00025	-0.00109	-0.11310
14	-0.11938	0.00233	-0.00019	0.00012	-0.11712
15	-0.12104	0.00269	-0.00021	0.00017	-0.11839
16	-0.12841	0.00486	-0.00068	-0.00100	-0.12523
17	-0.11942	0.00379	-0.00029	0.00073	-0.11519
18	-0.12237	0.00407	-0.00026	0.00022	-0.11834
19	-0.12278	0.00507	-0.00038	0.00028	-0.11781
20	-0.12652	0.00593	-0.00049	0.00021	-0.12087
21	-0.12056	0.00978	-0.00131	0.00042	-0.11167
22	-0.12565	0.00590	-0.00028	0.00051	-0.11952
23	-0.12316	0.00974	-0.00105	0.00062	-0.11385
24	-0.12532	0.00857	-0.00064	0.00073	-0.11666
25	-0.12394	0.01179	-0.00125	0.00088	-0.11252
26	-0.12432	0.01284	-0.00136	0.00102	-0.11182
27	-0.12467	0.01393	-0.00147	0.00118	-0.11103
28	-0.12497	0.01509	-0.00159	0.00138	-0.11009
29	-0.12525	0.01634	-0.00172	0.00161	-0.10902
30	-0.12551	0.01764	-0.00186	0.00187	-0.10786

31	-0.12570	0.01901	-0.00201	0.00215	-0.10655
32	-0.12592	0.02049	-0.00219	0.00248	-0.10514
33	-0.12608	0.02200	-0.00236	0.00281	-0.10363
34	-0.12622	0.02352	-0.00251	0.00315	-0.10206
35	-0.12637	0.02525	-0.00272	0.00354	-0.10030
36	-0.12651	0.02703	-0.00294	0.00398	-0.09844
39	-0.11324	-0.10832	0.03094	0.00518	-0.18544
42	-0.12727	0.03989	-0.00467	0.00692	-0.08513
47	-0.12797	0.05403	-0.00679	0.00981	-0.07092
50	-0.12858	0.06444	-0.00848	0.01166	-0.06096
54	-0.12964	0.08080	-0.01127	0.01415	-0.04596
56	-0.04766	-0.52743	0.13382	0.02345	-0.41782
59	-0.13156	0.10619	-0.01589	0.01720	-0.02406
60	-0.08807	-0.21102	0.05958	0.02268	-0.21683
62	0.02379	-0.98759	0.24207	0.04664	-0.67509
64	0.08081	-1.36798	0.33041	0.06655	-0.89021
66	0.10864	-1.54773	0.37175	0.08012	-0.98722
68	0.10018	-1.47894	0.35554	0.08281	-0.94041
70	0.21280	-2.26070	0.53465	0.13185	-1.38140
74	-0.14339	0.22779	-0.04039	0.02235	0.06636
79	-0.15006	0.28904	-0.05350	0.02081	0.10629
82	-0.15485	0.33231	-0.06292	0.01771	0.13225
83	-0.15665	0.34807	-0.06639	0.01671	0.14174
90	-0.17147	0.47821	-0.09542	0.00065	0.21197
92	-0.17644	0.52267	-0.10547	-0.00548	0.23528
94	-0.18195	0.57128	-0.11651	-0.01376	0.25906
96	-0.18787	0.62418	-0.12857	-0.03104	0.27670

Table .12 – Correlations from Coulomb, magnetic, retardation, and higher order retardation part for the $1s\,2s\,2p\,^2P_{1/2} \rightarrow 1s^2\,^1S_0$ transition. Energies are in eV.

$1s\,2s\,2p\,^2P_{1/2} \rightarrow 1s^2\,^1S_0$					
Z	Coulomb corr.	Magnetic corr.	Retardation corr.	Higher-order Retardation corr.	Total corr.
10	0.59072	0.03861	-0.01034	0.00005	0.61904
11	0.59159	0.04775	-0.01276	0.00003	0.62661
12	0.58107	0.05645	-0.01512	0.00017	0.62257
13	0.58106	0.06679	-0.01783	0.00007	0.63009
14	0.57878	0.07807	-0.02079	0.00016	0.63622
15	0.57013	0.08956	-0.02384	0.00019	0.63604
16	0.584	0.10548	-0.02786	0.00016	0.66178
17	0.57856	0.11762	-0.03101	0.00022	0.66539
18	0.57919	0.13328	-0.03498	0.00027	0.67776
19	0.57862	0.14921	-0.03894	0.00035	0.68924
20	0.57279	0.16601	-0.04314	0.00028	0.69594
21	0.57781	0.18784	-0.04846	0.00052	0.71771

22	0.5729	0.20552	-0.05271	0.00065	0.72636
23	0.57875	0.23033	-0.05844	0.0008	0.75144
24	0.56642	0.2502	-0.06323	0.00094	0.75433
25	0.56206	0.27582	-0.0692	0.00112	0.7698
26	0.55425	0.30031	-0.07489	0.00133	0.781
27	0.54686	0.32583	-0.08075	-0.095	0.69694
28	0.54047	0.35279	-0.08685	0.0018	0.80821
29	0.52713	0.37947	-0.09322	0.00213	0.81551
30	0.51655	0.40792	-0.09982	0.00246	0.82711
31	0.51352	0.4388	-0.10663	0.00289	0.84858
32	0.49712	0.46699	-0.11358	0.00326	0.85379
33	0.49593	0.50048	-0.12075	0.00375	0.87941
34	0.48813	0.53227	-0.128	0.00431	0.89671
35	0.47341	0.56394	-0.1356	0.00473	0.90648
36	0.44873	0.59409	-0.14355	0.00523	0.9045
39	0.41141	0.69578	-0.16807	0.00717	0.94629
42	0.37174	0.8024	-0.19451	0.00921	0.98884
47	0.32994	0.99416	-0.24111	0.01269	1.09568
50	0.30598	1.12078	-0.27176	0.01508	1.17008
54	0.26432	1.29309	-0.31573	0.01702	1.2587
59	0.24183	1.53853	-0.37485	0.02046	1.42597
60	0.55319	1.83706	-0.44671	0.02446	1.968

Table .13 – Correlations from Coulomb, magnetic, retardation, and higher order retardation part for the $1s\,2s\,2p\,^2P_{3/2} \rightarrow 1s^2\,^1S_0$ transition. Energies are in eV.

$1s\,2s\,2p\,^2P_{3/2} \rightarrow 1s^2\,^1S_0$					
Z	Coulomb corr.	Magnetic corr.	Retardation corr.	Higher-order Retardation corr.	Total corr.
10	0.57222	0.03844	-0.01052	0.00005	0.60019
11	0.57047	0.04747	-0.01299	0.00003	0.60498
12	0.55695	0.05603	-0.01541	0.00017	0.59774
13	0.55315	0.06617	-0.01819	0.00007	0.60120
14	0.54691	0.07729	-0.02129	0.00015	0.60306
15	0.54163	0.08923	-0.02461	0.00020	0.60645
16	0.54225	0.10409	-0.02867	0.00016	0.61783
17	0.53155	0.11558	-0.03199	0.00021	0.61535
18	0.52562	0.13042	-0.03615	0.00027	0.62016
19	0.51801	0.14556	-0.04045	0.00035	0.62347
20	0.50666	0.16157	-0.04504	0.00029	0.62348
21	0.50493	0.18234	-0.05083	0.00053	0.63697
22	0.49320	0.19877	-0.05564	0.00064	0.63697
23	0.48617	0.22193	-0.06209	0.00077	0.64678
24	0.47367	0.24123	-0.06768	0.00091	0.64813
25	0.46396	0.26622	-0.07466	0.00108	0.65660
26	0.45195	0.29040	-0.08145	0.00125	0.66215

27	0.43963	0.31606	-0.08859	0.00143	0.66853
28	0.42724	0.34343	-0.09618	0.00165	0.67614
29	0.41493	0.37249	-0.10417	0.00188	0.68513
30	0.40293	0.40322	-0.11254	0.00215	0.69576
31	0.39142	0.43560	-0.12127	0.00243	0.70818
32	0.38056	0.46961	-0.13034	0.00274	0.72257
33	0.37048	0.50516	-0.13974	0.00306	0.73896
34	0.36120	0.54226	-0.14945	0.00343	0.75744
35	0.35279	0.58090	-0.15950	0.00377	0.77796
36	0.34520	0.62074	-0.16971	0.00418	0.80041
39	0.32641	0.73993	-0.20126	0.00508	0.87016
42	0.31238	0.88814	-0.23687	0.00682	0.97047
47	0.29055	1.14694	-0.30021	0.00904	1.14632
50	0.27539	1.31926	-0.34193	0.01011	1.26283
54	0.25060	1.56980	-0.40172	0.01098	1.42966
56	0.24596	1.65246	-0.42205	0.00939	1.48576
59	0.21037	1.92125	-0.48517	0.00983	1.65628
60	0.20100	1.99728	-0.50327	0.00915	1.70416
62	0.18135	2.15493	-0.54049	0.00782	1.80361
64	0.15924	2.31808	-0.57791	0.00586	1.90527
66	0.13555	2.49381	-0.62015	0.00237	2.01158
68	0.12322	2.67831	-0.66234	-0.00077	2.13842
70	0.08286	2.86398	-0.70461	-0.00581	2.23642
74	0.02259	3.27612	-0.79971	-0.01868	2.48032
79	-0.06314	3.85034	-0.93043	-0.04296	2.81381
82	-0.12045	4.23200	-1.01700	-0.06292	3.03163
83	-0.14060	4.36606	-1.04732	-0.07014	3.10800
90	-0.29607	5.41070	-1.28220	-0.14054	3.69189
92	-0.34523	5.74780	-1.35747	-0.16585	3.87925
94	-0.39672	6.10532	-1.43704	-0.19532	4.07624
96	-0.45047	6.48492	-1.52120	-0.23561	4.27764

Table .14 – Correlations from Coulomb, magnetic, retardation, and higher order retardation part for the $1s\,2s\,2p\,^4P_{1/2} \rightarrow 1s^2\,^1S_0$ transition. Energies are in eV.

	$1s\,2s\,2p\,^4P_{1/2} \rightarrow 1s^2\,^1S_0$				
Z	Coulomb corr.	Magnetic corr.	Retardation corr.	Higher-order Retardation corr.	Total corr.
10	0.99610	0.04504	-0.01097	0.00005	1.03022
11	1.00322	0.05572	-0.01356	0.00003	1.04541
12	0.99743	0.06614	-0.01613	0.00018	1.04762
13	1.00064	0.07832	-0.01907	0.00007	1.05996
14	1.00084	0.09171	-0.02232	0.00015	1.07038
15	1.00168	0.10612	-0.02582	0.00019	1.08217
16	1.00814	0.12361	-0.03002	0.00016	1.10189
17	1.00345	0.13810	-0.03353	0.00021	1.10823

18	1.00349	0.15606	-0.03785	0.00027	1.12197
19	1.00209	0.17449	-0.04228	0.00034	1.13464
20	0.99721	0.19393	-0.04696	0.00028	1.14446
21	1.00228	0.21821	-0.05279	0.00051	1.16821
22	0.99773	0.23817	-0.05757	0.00064	1.17897
23	0.99827	0.26478	-0.06391	0.00077	1.19991
24	0.99368	0.28735	-0.06929	0.00092	1.21266
25	0.99208	0.31533	-0.07595	0.00109	1.23255
26	0.98827	0.34215	-0.08231	0.00129	1.24940
27	0.98403	0.37009	-0.08892	0.32460	1.58980
28	0.97943	0.39915	-0.09580	0.00174	1.28452
29	0.97444	0.42935	-0.10293	0.00203	1.30289
30	0.96910	0.46068	-0.11031	0.00235	1.32182
31	0.96342	0.49315	-0.11797	0.00271	1.34131
32	0.95742	0.52677	-0.12587	0.00310	1.36142
33	0.95114	0.56150	-0.13404	0.00352	1.38212
34	0.94455	0.59743	-0.14247	0.00400	1.40351
35	0.93773	0.63448	-0.15115	0.00446	1.42552
36	0.93066	0.67271	-0.16012	0.00499	1.44824
39	0.90834	0.79424	-0.18859	0.00669	1.52068
42	0.88476	0.92605	-0.21948	0.00851	1.59984
47	0.84390	1.16817	-0.27639	0.01169	1.74737
50	0.81910	1.32645	-0.31381	0.01341	1.84515
54	0.79403	1.54879	-0.36765	0.01525	1.99042
56	0.76984	1.67112	-0.39623	0.01558	2.06031
59	0.76122	1.83832	-0.44063	0.01562	2.17453
60	0.73665	1.92320	-0.45699	0.01523	2.21809
62	0.73614	2.03318	-0.48820	0.01459	2.29571
64	0.72251	2.16443	-0.52122	0.01322	2.37894
66	0.69496	2.31993	-0.55665	0.01091	2.46915
68	0.65809	2.49446	-0.59418	0.00836	2.56673
70	0.66567	2.60791	-0.62973	0.00403	2.64788
74	0.64366	2.90323	-0.70817	-0.00526	2.83346
79	0.61590	3.29932	-0.81485	-0.02520	3.07517
82	0.56769	3.60592	-0.88690	-0.04196	3.24475
83	0.60405	3.62239	-0.90708	-0.05044	3.26892
90	0.56731	4.27759	-1.08989	-0.10600	3.64901
92	0.55097	4.49031	-1.14756	-0.12555	3.76817

Table .15 – Correlations from Coulomb, magnetic, retardation, and higher order retardation part for the $1s\,2s\,2p\,^4P_{3/2} \rightarrow 1s^2\,^1S_0$ transition. Energies are in eV.

$1s\,2s\,2p\,^4P_{3/2} \rightarrow 1s^2\,^1S_0$					
Z	Coulomb corr.	Magnetic corr.	Retardation corr.	Higher-order Retardation corr.	Total corr.
10	0.99652	0.04566	-0.01097	0.00006	1.03127

11	1.00366	0.05651	-0.01358	0.00003	1.04662
12	0.99784	0.06710	-0.01614	0.00017	1.04897
13	1.00099	0.07949	-0.01910	0.00007	1.06145
14	1.00104	0.09309	-0.02234	0.00015	1.07194
15	1.00164	0.10775	-0.02587	0.00019	1.08371
16	1.00772	0.12548	-0.03007	0.00015	1.10328
17	1.00244	0.14022	-0.03359	0.00022	1.10929
18	1.00165	0.15844	-0.03794	0.00027	1.12242
19	0.99909	0.17715	-0.04238	0.00035	1.13421
20	0.99265	0.19687	-0.04706	0.00029	1.14275
21	0.99567	0.22143	-0.05290	0.00052	1.16472
22	0.98846	0.24166	-0.05770	0.00065	1.17307
23	0.98563	0.26852	-0.06403	0.00079	1.19091
24	0.97686	0.29136	-0.06942	0.00093	1.19973
25	0.97019	0.31956	-0.07605	0.00112	1.21482
26	0.96029	0.34662	-0.08239	0.00132	1.22584
27	0.94889	0.37480	-0.08899	0.00153	1.23623
28	0.93600	0.40410	-0.09583	0.00179	1.24606
29	0.92159	0.43457	-0.10292	0.00208	1.25532
30	0.90569	0.46622	-0.11027	0.00241	1.26405
31	0.88842	0.49908	-0.11789	0.00278	1.27239
32	0.86983	0.53320	-0.12579	0.00318	1.28042
33	0.85014	0.56856	-0.13395	0.00361	1.28836
34	0.82941	0.60527	-0.14241	0.00410	1.29637
35	0.80792	0.64329	-0.15115	0.00456	1.30462
36	0.78577	0.68271	-0.16022	0.00512	1.31338
39	0.71736	0.80934	-0.18926	0.00685	1.34429
42	0.64890	0.94884	-0.22117	0.00868	1.38525
47	0.54073	1.21047	-0.28071	0.01175	1.48224
50	0.48032	1.38538	-0.32029	0.01335	1.55876
54	0.40417	1.64038	-0.37765	0.01483	1.68173
56	0.36744	1.77753	-0.40835	0.01505	1.75167
59	0.31327	1.99603	-0.45703	0.01484	1.86711
60	0.29531	2.07240	-0.47397	0.01437	1.90811
62	0.25937	2.23057	-0.50898	0.01325	1.99421
64	0.22315	2.39640	-0.54557	0.01172	2.08570
66	0.18645	2.57012	-0.58374	0.00900	2.18183
68	0.14880	2.75246	-0.62362	0.00565	2.28329
70	0.10949	2.94446	-0.66547	0.00123	2.38971
74	0.02870	3.35522	-0.75464	-0.01086	2.61842
79	-0.07582	3.92043	-0.87646	-0.03370	2.93445
82	-0.13967	4.28881	-0.95541	-0.05293	3.14080
83	-0.16440	4.42018	-0.98323	-0.05991	3.21264
90	-0.33147	5.41211	-1.19302	-0.12820	3.75942
92	-0.37925	5.72331	-1.25864	-0.15260	3.93282
94	-0.41781	6.03865	-1.32650	-0.17937	4.11497

96	-0.46326	6.37600	-1.39764	-0.21749	4.29761

Table .16 – Correlations from Coulomb, magnetic, retardation, and higher order retardation part for the $1s\,2s\,2p\,^4P_{5/2} \rightarrow 1s^2\,^1S_0$ transition. Energies are in eV.

$1s\,2s\,2p\,^4P_{5/2} \rightarrow 1s^2\,^1S_0$					
Z	Coulomb corr.	Magnetic corr.	Retardation corr.	Higher-order Retardation corr.	Total corr.
10	0.99685	0.04623	-0.01098	0.00005	1.03215
11	1.00419	0.05721	-0.01358	0.00004	1.04786
12	0.99866	0.06797	-0.01615	0.00017	1.05065
13	1.00219	0.08053	-0.01912	0.00008	1.06368
14	1.00276	0.09433	-0.02238	0.00016	1.07487
15	1.00404	0.10921	-0.02590	0.00019	1.08754
16	1.01104	0.12721	-0.03014	0.00015	1.10826
17	1.00696	0.14222	-0.03367	0.00021	1.11572
18	1.00776	0.16077	-0.03805	0.00027	1.13075
19	1.00724	0.17985	-0.04253	0.00033	1.14489
20	1.00340	0.19998	-0.04727	0.00028	1.15639
21	1.00967	0.22502	-0.05317	0.00052	1.18204
22	1.00650	0.24580	-0.05805	0.00063	1.19488
23	1.00862	0.27329	-0.06448	0.00076	1.21819
24	1.00581	0.29684	-0.06998	0.00091	1.23358
25	1.00621	0.32583	-0.07677	0.00108	1.25635
26	1.00460	0.35380	-0.08329	0.00126	1.27637
27	1.00276	0.38296	-0.09009	0.31959	1.61522
28	1.00074	0.41336	-0.09716	0.00172	1.31866
29	0.99850	0.44500	-0.10452	0.00198	1.34096
30	0.99606	0.47788	-0.11215	0.00230	1.36409
31	1.15748	0.52393	-0.12536	-0.00086	1.55519
32	1.12431	0.55822	-0.13267	-0.00340	1.54646
33	1.12217	0.59576	-0.14147	-0.00254	1.57392
34	1.11944	0.63465	-0.15059	-0.00089	1.60260
35	1.11608	0.67480	-0.15996	0.00153	1.63245
36	0.97689	0.70259	-0.16409	0.00490	1.52029
39	0.96773	0.83362	-0.19435	0.00671	1.61371
42	0.94954	0.97587	-0.22685	0.00780	1.70636
47	1.05356	1.26753	-0.29709	0.00678	2.03078
54	1.04086	1.73101	-0.40644	0.15326	2.51869
56	0.98556	1.86297	-0.43397	0.03276	2.44732

Résumé en français

Dans cette thèse, nous utilisons la méthode multi-configuration Dirac-Fock (MCDF) pour effectuer un calcul précis des énergies des transitions entre les niveaux de structure fine et le niveau fondamental $1s^2\ 2p\ ^2P_J\ \rightarrow 1s^2\ 2s\ ^2S_{1/2}, J = 1/2, 3/2$ des ions de la sequence isoélectronique du lithium. Nous évaluons également l'énergie des transitions à partir de niveaux excités en couche internes $1s\ 2s\ 2p\ ^2P_{1/2}\ \rightarrow 1s^2\ 2s\ ^2S_{1/2}, J = 1/2, 3/2$ et $1s\ 2s\ 2p\ ^4P_J\ \rightarrow 1s^2\ 2s\ ^2S_{1/2}, J = 1/2, 3/2, 5/2$ dans la même séquence isoélectronique. Nous avons aussi évalué les énergies des transitions Auger $1s\ 2s\ 2p\ ^2P_J\ \rightarrow 1s^2\ ^1S_0$ et $1s\ 2s\ 2p\ ^4P_J\ \rightarrow 1s^2\ ^1S_0, J = 1/2, 3/2$ correspondantes. Ces calculs ont effectués pour des ions de numéro atomique $10 \leq Z \leq 96$. Nous avons utilisé la version 2018 du code relativiste MCDF (MCDFGME), écrit par Jean-Paul Desclaux et Paul Indelicato. Les énergies ci-dessus sont calculées en prenant en compte les effets d'électrodynamique quantique du premier ordre et la corrélation inter-électronique, en incluant les effets magnétiques et de retard. L'écrantage de la self-énergie et les corrections radiatives du deuxième ordre sont également incluses.

L'énergie de corrélation est évaluée en prenant en compte les excitations simples, doubles et triples de la configuration non perturbée vers les niveaux virtuels avec un nombre quantique principal $n = 5$. Pour l'état fondamental $1s^2\ 2s\ ^2S_{1/2}$ cela conduit à 1463 configurations et pour les états $1s\ 2s\ 2p\ ^2P_{3/2}$ à 2478 configurations. Toutes les orbitales ont étés totalement relaxées. Cela a permis d'obtenir une convergence des energies vérifiée en comparant leur évolution en fonction du niveau virtuel maximal utilisé dans le calcul.

La précision de l'écrantage de la self-énergie est évaluée en comparant les résultats obtenu en utilisant m'approximation de Welton à ceux obtenus par la méthode de l'opérateur effectif développée récemment par l'équipe de Saint Petersbourg. Les résultats du modèle de Welton sont en bon accords avec ceux de méthode d'opérateur effectif pour les ions jusqu'à $Z = 50$, mais au delà les valeurs du modèle de Welton commencent à s'éloigner de celles de la méthode de l'opérateur effectif. Dans la région de Z élevé, la valeur de la méthode d'image Welton est supérieure à celle de la méthode de Saint Petersbourg L'écart atteint un maximum de 0.13 eV à $Z = 92$ pour les transitions $1s^2\ 2p\ ^2P_J\ \rightarrow 1s^2\ 2s\ ^2S_{1/2}, J = 1/2, 3/2$ et 1.6 eV dans les transitions à partir des niveaux excités en couches internes ($1s\ 2s\ 2p\ ^{2S+1}P_J$).

Les corrections de corrélation dues à l'interaction magnétique commencent à être de la même taille que la corrélation de Coulomb à partir de $Z = 47$ et sont dix fois plus grandes à $Z = 92$ pour l'état fondamental des ions lithiumoïdes. Pour les transitions à partir des niveaux $1s\ 2s\ 2p\ ^{2S+1}P_J$, les énergies de corrélation magnétique dominent l'énergie de corrélation, et définissent donc l'évolution des correlations pour des numéros

atomiques moyens et élevés.

Les résultats de nos calculs sont comparés à l'ensembles des résultats expérimentaux existants et à l'ensemble des valeurs théoriques connues. Pour les éléments de numéro atomique faible et moyen, la comparaison montre une concordance généralement bonne entre les expériences et les calculs théoriques les plus avancés, et en particulier ceux présentés dans cette thèse. Les énergies de transition théoriques comportant les corrections d'électrodynamique quantique montrent une certaine dispersion pour les éléments lourds, liées en partie à l'utilisation de paramètres nucléaires un peu différents. L'écart est cependant inférieur à 0.2 eV pour $Z \approx 90$ pour les transitions à partir de niveaux excités en couches internes.

Dans une deuxième partie, nous étudions les effets d'électrodynamique quantique et de taille finie du noyau pour le plomb muonique. L'objectif de cette étude est de préparer l'analyse des résultats pour le radium et le curium qui sont en train d'être mesurés à l'Institut Paul Scherrer pour mesurer le rayon de charge du noyau. Les énergies des transitions muoniques sont calculées avec le programme MCDFGME. Ces calculs incluent la self-énergie, la polarisation du vide (potentiel de Uehling) à tous les ordres, le terme de Whichmann et Kroll, et certaines corrections d'ordre deux d'électrodynamique quantique (potentiel de Källèn et Sabry). La plus grandes incertitude théorique provient de la polarisation nucléaire dont nous ne pouvons fournir que l' ordre de grandeur. La correction de taille finie du noyau a été faite avec deux modèles différents (Fermi et Gauss à trois paramètres).

Nus avons déterminé les paramètres nucléaires qui minimisent l'écart pondéré entre la théorie et l'expérience pour l'ensemble des énergies des transitions mesurées pour le modèle de Fermi à deux paramètres et le modèle de Gauss à trois paramètres. Nous obtenons ainsi 5.5057 fm pour le rayon quadratique moyen sphérique et 2.3919 fm pour le paramètre d'épaisseur dans le modèle de Fermi et $r = 5.5031$ dans le modèle de Gauss. Le modèle de Gauss à trois paramètre ne donne cependant pas d'amélioration sur l'accord théorie-expérience.

Pour permettre d'analyser les expériences à venir sur le ^{226}Ra et le ^{248}Cm muoniques nous avons également effectué des calculs des énergies de transitions correspondantes en utilisant les mêmes corrections d'électrodynamiques quantiques que pour le plomb. Un calcul théorique précis est en effet essentiel pour permettre l'extraction des paramètres nucléaires à partir de ces expériences futures.

Bibliography

[1] J. Machado, C. I. Szabo, J. P. Santos, P. Amaro, M. Guerra, A. Gumberidze, G. Bian, J. Isac & P. Indelicato; «High-precision measurements of $n = 2 \rightarrow n = 1$ transition energies and level widths in He-and Be-like argon ions»; Phys. Rev. A **97**, p. 032 517 (2018)https://journals.aps.org/pra/abstract/10.1103/PhysRevA.97.032517. v, 9, 43, 44, 65, 67, 72

[2] R. Engfer, H. Schneuwly, J. L. Vuilleumier, H. K. Walter & A. Zehnder; «Charge-distribution parameters, isotope shifts, isomer shifts, and magnetic hyperfine constants from muonic atoms»; Atomic Data and Nuclear Data Tables **14**, p. 509–597 (1974)https://www.sciencedirect.com/science/article/pii/S0092640X74800033. v

[3] G. Fricke, K. Heilig & H. F. Schopper; «Nuclear charge radii»; Springer Berlin (2004)http://cds.cern.ch/record/790765/files/3540428291_TOC.pdf. v

[4] A. Adamczak, A. Antognini, N. Berger, T. E. Cocolios, R. Dressler, A. Eggenberger, R. Eichler, P. Indelicato, K. Jungmann, K. Kirch *et al.*; «Nuclear structure with radioactive muonic atoms»; p. 04014 (2018). https://www.epj-conferences.org/articles/epjconf/abs/2018/28/epjconf_fission2017_04014/epjconf_fission2017_04014.html. v

[5] P. Bergem, G. Piller, A. Rueetschi, L. A. Schaller, L. Schellenberg & H. Schneuwly; «Nuclear polarization and charge moments of Pb 208 from muonic x rays»; Phys. Rev. C **37**, p. 2821 (1988)https://journals.aps.org/prc/abstract/10.1103/PhysRevC.37.2821. v, 11, 40, 85, 88, 90, 91, 98

[6] C. D. Anderson & S. H. Neddermeyer; «Cloud chamber observations of cosmic rays at 4300 meters elevation and near sea-level»; Physical Review **50**, p. 263 (1936)https://journals.aps.org/pr/pdf/10.1103/PhysRev.50.263. 1

[7] S. Devons & I. Duerdoth; *Muonic Atoms, Advances in Nuclear Physic*; tome 2 (Plenum Press, New York) (1969). https://link.springer.com/chapter/10.1007/978-1-4684-8343-7_5. 2, 3

[8] T. G. Trippe, A. Barbaro-Galtieri, R. L. Kelly, A. Rittenberg, A. H. Rosenfeld, G. P. Yost, N. Barash-Schmidt, C. Bricman, R. J. Hemingway, M. J. Losty *et al.*; «Review of particle properties»; Reviews of Modern Physics **48**, p. S1 (1976)https://journals.aps.org/rmp/pdf/10.1103/RevModPhys.48.S1. 1

[9] P. J. Mohr; «Energy levels of hydrogen-like atoms predicted by quantum electrodynamics, 10≤ Z ≤ 40»; Atomic Data and Nuclear Data Tables **29**, p. 453–466 (1983)http://inspirehep.net/record/14256/. 4

[10] W. R. Johnson & G. Soff; «The lamb shift in hydrogen-like atoms, 1≤ Z ≤ 110»; Atomic Data and Nuclear Data Tables **33**, p. 405–446 (1985)https://www.sciencedirect.com/science/article/pii/0092640X85900105. 4, 64

[11] G. Soff & P. J. Mohr; «Vacuum polarization in a strong external field»; Phys. Rev. A **38**, p. 5066 (1988)https://journals.aps.org/pra/abstract/10.1103/PhysRevA.38.5066. 4, 24

[12] K. Pachucki; «Complete two-loop binding correction to the Lamb shift»; Physical review letters **72**, p. 3154 (1994)https://journals.aps.org/prl/abstract/10.1103/PhysRevLett.72.3154. 4

[13] K. Pachucki & U. D. Jentschura; «Two-loop Bethe-logarithm correction in hydrogenlike atoms»; Physical review letters **91**, p. 113 005 (2003)https://journals.aps.org/prl/abstract/10.1103/PhysRevLett.91.113005. 4

[14] U. D. Jentschura, A. Czarnecki & K. Pachucki; «Nonrelativistic QED approach to the Lamb shift»; Phys. Rev. A **72**, p. 062 102 (2005)https://journals.aps.org/pra/abstract/10.1103/PhysRevA.72.062102. 4

[15] P. Indelicato; «QED tests with highly charged ions»; J. Phys. B: At. Mol. Opt. Phys. (2019)https://iopscience.iop.org/article/10.1088/1361-6455/ab42c9/meta. 5, 7, 8, 10, 16

[16] K. T. Cheng & W. R. Johnson; «Self-energy corrections to the K-electron binding in heavy and superheavy atoms»; Phys. Rev. A **14**, p. 1943 (1976)https://journals.aps.org/pra/abstract/10.1103/PhysRevA.14.1943. 4

[17] U. D. Jentschura, P. J. Mohr & G. Soff; «Calculation of the electron self-energy for low nuclear charge»; Physical review letters **82**, p. 53 (1999)https://journals.aps.org/prl/abstract/10.1103/PhysRevLett.82.53. 4, 22

[18] U. D. Jentschura, P. J. Mohr & G. Soff; «Electron self-energy for the K and L shells at low nuclear charge»; Phys. Rev. A **63**, p. 042 512 (2001)https://journals.aps.org/pra/abstract/10.1103/PhysRevA.63.042512. 22

[19] V. A.Yerokhin & V. M. Shabaev; «Nuclear Recoil Effect in the Lamb Shift of Light Hydrogenlike Atoms»; Phys. Rev. Lett. **115**, p. 233 002 (2015)http://link.aps.org/doi/10.1103/PhysRevLett.115.233002. 4

[20] V. A. Yerokhin & V. M. Shabaev; «Lamb Shift of N = 1 and N = 2 States of Hydrogen-Like Atoms, 1 ≤ Z ≤ 110»; Journal of Physical and Chemical Reference Data **44**, p. 033 103 (2015)http://scitation.aip.org/content/aip/journal/jpcrd/44/3/10.1063/1.4927487. 4, 7, 33

[21] V. A. Yerokhin, A. N. Artemyev, V. M. Shabaev, M. M. Sysak, O. M. Zherebtsov & G. Soff; «Evaluation of the Two-Photon Exchange Graphs for the $2p_{1/2} - 2s$ Transition in Li-Like Ions»; Phys. Rev. A **64**, p. 032 109 (2001)http://link.aps.org/doi/10.1103/PhysRevA.64.032109. 5

[22] V. A. Yerokhin, A. N. Artemyev, V. M. Shabaev, M. M. Sysak, O. M. Zherebtsov & G. Soff; «Two-Photon Exchange Corrections to the 2p1/2-2s Transition Energy in Li-Like High-Z Ions»; Phys. Rev. Lett. **85**, p. 4699–4702 (2000)http://link.aps.org/doi/10.1103/PhysRevLett.85.4699. 5

[23] J. Sapirstein & K. T. Cheng; «Determination of the Two-Loop Lamb Shift in Lithiumlike Bismuth»; Phys. Rev. A **64**, p. 022 502 (2001)https://journals.aps.org/pra/abstract/10.1103/PhysRevA.64.022502. 5, 62, 64

[24] V. A. Yerokhin, P. Indelicato & V. M. Shabaev; «Nonperturbative Calculation of the Two-Loop Lamb Shift in Li-Like Ions»; Phys. Rev. Lett. **97**, p. 253 004–4 (2006)http://link.aps.org/abstract/PRL/v97/e253004. 5, 26, 53, 62

[25] V. A. Yerokhin, A. N. Artemyev & V. M. Shabaev; «QED Treatment of Electron Correlation in Li-Like Ions»; Phys. Rev. A **75**, p. 062 501 (2007)http://journals.aps.org/pra/abstract/10.1103/PhysRevA.75.062501. 6, 58, 62, 64

[26] J. Sapirstein & K. T. Cheng; «S-Matrix Calculations of Energy Levels of the Lithium Isoelectronic Sequence»; Phys. Rev. A **83**, p. 012 504 (2011)http://link.aps.org/doi/10.1103/PhysRevA.83.012504. 6, 13, 47, 50, 58, 60, 62, 63, 64, 65

[27] A. V. Volotka, D. A. Glazov, G. Plunien & V. M. Shabaev; «Progress in quantum electrodynamics theory of highly charged ions»; Annalen der Physik **525**, p. 636–646 (2013)https://onlinelibrary.wiley.com/doi/full/10.1002/andp.201300079. 6

[28] V. M. Shabaev, A. N. Artemyev, V. A. Yerokhin, O. M. Zherebtsov & G. Soff; «Towards a Test of QED in Investigations of the Hyperfine Splitting in Heavy Ions»; Phys. Rev. Lett. **86**, p. 3959–3962 (2001)https://link.aps.org/doi/10.1103/PhysRevLett.86.3959. 6

[29] Y. S. Kozhedub, O. V. Andreev, V. M. Shabaev, I. I. Tupitsyn, C. Brandau, C. Kozhuharov, G. Plunien & T. Stöhlker; «Nuclear Deformation Effect on the Binding Energies in Heavy Ions»; Phys. Rev. A **77**, p. 032 501 (2008)http://link.aps.org/doi/10.1103/PhysRevA.77.032501. 6, 33

[30] J. S. M. Ginges & J. C. Berengut; «QED radiative corrections and many-body effects in atoms: vacuum polarization and binding energy shifts in alkali metals»; **49**, p. 095 001 (2016)https://iopscience.iop.org/article/10.1088/0953-4075/49/9/095001/pdf. 6

[31] E. A. Konovalova & M. G. Kozlov; «Correlation, Breit, and QED effects in spectra of Mg-like ions»; Phys. Rev. A **92**, p. 042 508 (2015)https://journals.aps.org/pra/pdf/10.1103/PhysRevA.92.042508. 6

[32] K. Kubiçek, P. H. Mokler, V. Mäckel, J. Ullrich & J. R. Crespo López-Urrutia; «Transition energy measurements in hydrogenlike and heliumlike ions strongly supporting bound-state QED calculations»; Phys. Rev. A **90**, p. 032 508 (2014)http://link.aps.org/doi/10.1103/PhysRevA.90.032508. 7, 9

[33] J. Tschischgale, D. Klöpfel, P. Beiersdorfer, G. V. Brown, E. Förster, H. Schulte-Schrepping & S. B. Utter; «Absolute wavelength measurement of the Lyman-α transition of hydrogen-like silicon»; Canadian journal of physics **80**, p. 867–874 (2002)https://www.nrcresearchpress.com/doi/pdf/10.1139/p02-011. 7

[34] I. A. Armour, J. D. Silver, E. Trabert & B. C. Fawcett; «X-ray spectra and satellite classification of foil-excited Mg and Al»; Journal of Physics B: Atomic and Molecular Physics **13**, p. 2701 (1980)https://iopscience.iop.org/article/10.1088/0022-3700/13/14/010/meta. 7

[35] M. Tavernier, J. P. Briand, P. Indelicato, D. Liesen & P. Richard; «Measurement of the (1s) Lamb shift of hydrogen-like krypton»; Journal of Physics B: Atomic and Molecular Physics **18**, p. L327 (1985)https://iopscience.iop.org/article/10.1088/0022-3700/18/11/004/meta. 7

[36] J. P. Briand, J. P. Mosse, P. Indelicato, P. Chevallier, D. Girard-Vernhet, A. Chetioui, M. T. Ramos & J. P. Desclaux; «Spectroscopy of Hydrogenlike and Heliumlike Argon»; Phys. Rev. A **28**, p. 1413–1417 (1983)https://link.aps.org/doi/10.1103/PhysRevA.28.1413. 7

[37] H. F. Beyer, R. D. Deslattes, F. Folkmann & R. E. LaVilla; «Determination of the 1s Lamb shift in one-electron argon recoil ions»; Journal of Physics B: Atomic and Molecular Physics **18**, p. 207 (1985)https://iopscience.iop.org/article/10.1088/0022-3700/18/2/008/meta. 7

[38] H. F. Beyer, D. Liesen, F. Bosch, K. D. Finlayson, M. Jung, O. Klepper, R. Moshammer, K. Beckert, H. Eickhoff, B. Franzke *et al.*; «X rays from radiative electron capture of free cooling electrons for precise Lamb-shift measurements at high Z: Au78+»; Physics Letters A **184**, p. 435–439 (1994)https://www.sciencedirect.com/science/article/pii/0375960194905193. 7

[39] J. H. Lupton, D. D. Dietrich, C. J. Hailey, R. E. Stewart & K. P. Ziock; «Measurement of the Ground-State Lamb-Shift and Electron-Correlation Effects in Hydrogenlike and Heliumlike Uranium»; Phys. Rev. A **50**, p. 2150–2154 (1994)http://journals.aps.org/pra/abstract/10.1103/PhysRevA.50.2150. 7

[40] H. F. Beyer, G. Menzel, D. Liesen, A. Gallus, F. Bosch, R. Deslattes, P. Indelicato, T. Stöhlker, O. Klepper, R. Moshammer *et al.*; «Measurement of the ground-state lambshift of hydrogenlike uranium at the electron cooler of the ESR»; Zeitschrift für Physik D Atoms, Molecules and Clusters **35**, p. 169–175 (1995)https://link.springer.com/article/10.1007/BF01437066. 7

[41] E. S. Marmar, J. E. Rice, K. Kallne, J. Kallne & R. E. LaVilla; «Precision measurement of the 1s Lamb shift in hydrogenlike argon»; Physical Review A **33**, p. 774 (1986)https://journals.aps.org/pra/abstract/10.1103/PhysRevA.33.774. 7

[42] J. P. Briand, P. Indelicato, A. Simionovici, V. San Vicente, D. Liesen & D. Dietrich; «Spectroscopic study of hydrogenlike and heliumlike xenon ions»; EPL (Europhysics Letters) **9**, p. 225 (1989)https://iopscience.iop.org/article/10.1209/0295-5075/9/3/007/meta. 7

[43] T. Stöhlker, P. H. Mokler, H. Geissel, R. Moshammer, P. Rymuza, E. M. Bernstein, C. L. Cocke, C. Kozhuharov, G. Münzeberg, F. Nickel *et al.*; «Ground state transitions in one-and two-electron Bi projectiles»; Physics Letters A **168**, p. 285–290 (1992)https://www.sciencedirect.com/science/article/pii/037596019291133C. 7

[44] H. F. Beyer, P. Indelicato, K. D. Finlayson, D. Liesen & R. D. Deslattes; «Measurement of the 1s Lamb shift in hydrogenlike nickel»; Physical Review A **43**, p. 223 (1991)https://journals.aps.org/pra/abstract/10.1103/PhysRevA.43.223. 7

[45] J. P. Briand, P. Chevallier, P. Indelicato, K. P. Ziock & D. D. Dietrich; «Observation and Measurement of n=2 → n=1 Transitions of Hydrogenlike and Heliumlike Uranium»; Phys. Rev. Lett. **65**, p. 2761–2764 (1990)https://link.aps.org/doi/10.1103/PhysRevLett.65.2761. 7

[46] T. Stöhlker, P. H. Mokler, K. Beckert, F. Bosch, H. Eickhoff, B. Franzke, M. Jung, Y. Kandler, O. Klepper, C. Kozhuharov *et al.*; «Ground-state Lamb shift for hydrogenlike uranium measured at the ESR storage ring»; Physical review letters **71**, p. 2184 (1993)https://journals.aps.org/prl/abstract/10.1103/PhysRevLett.71.2184. 7

[47] T. Stöhlker, P. H. Mokler, F. Bosch, R. W. Dunford, F. Franzke, O. Klepper, C. Kozhuharov, T. Ludziejewski, F. Nolden, H. Reich, P. Rymuza, Z. Stachura, M. Steck, P. Swiat & A. Warczak; «1s Lamb Shift in Hydrogenlike Uranium Measured on Cooled, Decelerated Ion Beams»; Phys. Rev. Lett. **85**, p. 3109–3112 (2000)https://link.aps.org/doi/10.1103/PhysRevLett.85.3109. 7

[48] K. Widmann, P. Beiersdorfer, G. V. Brown, J. R. Crespo López-Urrutia, A. L. Osterheld, K. J. Reed, J. H. Scofield & S. B. Utter; «High-Resolution Measurements of the K-Shell Spectral Lines of Hydrogenlike and Heliumlike Xenon»; dans «X-RAY AND INNER-SHELL PROCESSES», , tome 506p. 444–66 (Chicago, Illinois (USA)) (2000). https://aip.scitation.org/doi/abs/10.1063/1.1302773. 7

[49] M. R. Tarbutt & J. D. Silver; «Measurement of the ground-state Lamb shift of hydrogen-like Ti21+»; Journal of Physics B: Atomic, Molecular and Optical Physics **35**, p. 1467 (2002)https://iopscience.iop.org/article/10.1088/0953-4075/35/6/305/meta. 7, 75

[50] C. T. Chantler, J. M. Laming, D. D. Dietrich, W. A. Hallett, R. McDonald & J. D. Silver; «Hydrogenic Lamb shift in iron Fe 25+ and fine-structure Lamb shift»; Physical Review A **76**, p. 042 116 (2007)https://journals.aps.org/pra/abstract/10.1103/PhysRevA.76.042116. 7

[51] C. T. Chantler & J. A. Kimpton; «Recent developments in X-ray tests of quantum electrodynamics»; Can. J. Phys. **87**, p. 763–772 (2009)http://www.nrcresearchpress.com/doi/abs/10.1139/P09-019. 7

[52] D. B. Thorn, M. F. Gu, G. V. Brown, P. Beiersdorfer, F. S. Porter, C. A. Kilbourne & R. L. Kelley; «Precision Measurement of the K-Shell Spectrum from Highly Charged Xenon with an Array of X-Ray Calorimeters»; Phys. Rev. Lett. **103**, p. 163 001 (2009)http://link.aps.org/doi/10.1103/PhysRevLett.103.163001. 7

[53] J. D. Gillaspy, C. T. Chantler, D. Paterson, L. T. Hudson, F. G. Serpa & E. Takacs; «First measurement of Lyman alpha x-ray lines in hydrogen-like vanadium: results and implications for precision wavelength metrology and tests of QED»; Journal of Physics B: Atomic, Molecular and Optical Physics **43**, p. 074 021 (2010)https://iopscience.iop.org/article/10.1088/0953-4075/43/7/074021/meta. 7

[54] S. Kraft-Bermuth, V. Andrianov, A. Bleile, A. Echler, P. Egelhof, P. Grabitz, S. Ilieva, O. Kiselev, C. Kilbourne, D. McCammon *et al.*; «Precise determination of the 1s Lamb shift in hydrogen-like lead and gold using microcalorimeters»; Journal of Physics B: Atomic, Molecular and Optical Physics **50**, p. 055 603 (2017)https://ntrs.nasa.gov/search.jsp?R=20170009125. 7

[55] E. Kallne, J. Kallne, P. Richard & M. Stockli; «Precision measurement of the H-like x-ray spectrum of Cl and the 1s Lamb shift»; Journal of Physics B: Atomic and Molecular Physics **17**, p. L115 (1984)https://iopscience.iop.org/article/10.1088/0022-3700/17/5/002/pdf. 7

[56] R. D. Deslattes, R. Schuch & E. Justiniano; «Application of decelerated bare nuclei to precision spectroscopy of one-electron ions»; Physical Review A **32**, p. 1911 (1985)https://journals.aps.org/pra/abstract/10.1103/PhysRevA.32.1911. 7

[57] P. Richard, M. Stockli, R. D. Deslattes, P. Cowan, R. E. La Villa, B. Johnson, K. Jones, M. Meron, R. Mann & K. Schartner; «Measurement of the 1 s Lamb shift in hydrogenlike chlorine»; Physical Review A **29**, p. 2939 (1984)https://journals.aps.org/pra/abstract/10.1103/PhysRevA.29.2939. 7

[58] G. Hölzer, E. Förster, D. Klöpfel, P. Beiersdorfer, G. V. Brown, J. R. C. López-Urrutia & K. Widmann; «Absolute wavelength measurement of the Lyman-α transitions of hydrogenic Mg 1 1+»; Physical Review A **57**, p. 945 (1998)https://journals.aps.org/pra/abstract/10.1103/PhysRevA.57.945. 7

[59] J. D. Silver, A. F. McClelland, J. M. Laming, S. D. Rosner, G. C. Chandler, D. D. Dietrich & P. O. Egan; «Simultaneous observation of Lyman-α and Balmer-β transitions in hydrogenic iron, Fe 2 5+: A novel technique for 1 s Lamb-shift measurement»; Physical Review A **36**, p. 1515 (1987)https://journals.aps.org/pra/abstract/10.1103/PhysRevA.36.1515. 7

[60] A. Gumberidze, T. Stöhlker, D. Banaś, K. Beckert, P. Beller, H. F. Beyer, F. Bosch, S. Hagmann, C. Kozhuharov, D. Liesen *et al.*; «Quantum electrodynamics in strong electric fields: the ground-state lamb shift in hydrogenlike uranium»; Physical review letters **94**, p. 223 001 (2005)https://journals.aps.org/prl/abstract/10.1103/PhysRevLett.94.223001. 7

[61] L. Schleinkofer, F. Bell, H. D. Betz, G. Trolman & J. Rothermel; «Precision Wavelength Determination of 2 1P1-1 1S0 and 2 3P1-1 1S0 transitions in heliumlike sulfur»; Physica Scripta **25**, p. 917–923 (1982)http://dx.doi.org/10.1088/0031-8949/25/6B/004. 7

[62] H. F. Beyer, K. D. Finlayson, D. Liesen, P. Indelicato, C. T. Chantler, R. D. Deslattes, J. Schweppe, F. Bosch, M. Jung, O. Klepper *et al.*; «X-ray transitions associated with electron capture into bare dysprosium»; Journal of Physics B: Atomic, Molecular and Optical Physics **26**, p. 1557 (1993)https://iopscience.iop.org/article/10.1088/0953-4075/26/9/004. 7

[63] T. Gassner, R. Trassinelli, Mand Heß, U. Spillmann, D. Banaś, K. H. Blumenhagen, F. Bosch, C. Brandau, W. Chen, C. Dimopoulou *et al.*; «Wavelength-dispersive spectroscopy in the hard x-ray regime of a heavy highly-charged ion: The 1s Lamb shift in hydrogen-like gold»; New Journal of Physics **20**, p. 073 033 (2018)https://iopscience.iop.org/article/10.1088/1367-2630/aad01d/meta. 7

[64] A. Gumberidze, T. Stöhlker, D. Banaś, K. Beckert, P. Beller, H. F. Beyer, F. Bosch, S. Hagmann, C. Kozhuharov, D. Liesen, F. Nolden, X. Ma, P. H. Mokler, M. Steck, D. Sierpowski & S. Tashenov; «Quantum Electrodynamics at Strong Electric Fields: The Ground State Lamb Shift in Hydrogenlike Uranium»; Phys. Rev. Lett. **94**, p. 223 001 (2005)http://link.aps.org/doi/10.1103/PhysRevLett.94.223001. 6

[65] P. Beiersdorfer, H. Chen, D. B. Thorn & E. Träbert; «Measurement of the Two-Loop Lamb Shift in Lithiumlike U[Sup 89+]»; Phys. Rev. Lett. **95**, p. 233 003–4 (2005)http://link.aps.org/abstract/PRL/v95/e233003. 6, 9, 60, 65

[66] H. Bruhns, J. Braun, K. Kubiçek, J. R. Crespo López-Urrutia & J. Ullrich; «Testing QED Screening and Two-Loop Contributions with He-Like Ions»; Phys. Rev. Lett. **99**, p. 113 001 (2007). https://link.aps.org/doi/10.1103/PhysRevLett.99.113001. 9

[67] K. Kubiçek, J. Braun, H. Bruhns, J. R. Crespo López-Urrutia, P. H. Mokler & J. Ullrich; «High-precision laser-assisted absolute determination of x-ray

diffraction angles»; Rev. Sci. Instrum. **83**, p. 013 102 (2012)http://link.aip.org/link/?RSI/83/013102/1http://dx.doi.org/10.1063/1.3662412. 9

[68] C. T. Chantler, M. N. Kinnane, J. D. Gillaspy, L. T. Hudson, A. T. Payne, L. F. Smale, A. Henins, J. M. Pomeroy, J. N. Tan, J. A. Kimpton, E. Takacs & K. Makonyi; «Testing Three-Body Quantum Electrodynamics with Trapped Ti^{20+} Ions: Evidence for a Z-dependent Divergence Between Experiment and Calculation»; Phys. Rev. Lett. **109**, p. 153 001 (2012)http://link.aps.org/doi/10.1103/PhysRevLett.109.153001. 9

[69] C. T. Chantler, M. N. Kinnane, J. D. Gillaspy, L. T. Hudson, A. T. Payne, L. F. Smale, A. Henins, J. M. Pomeroy, J. A. Kimpton, E. Takacs *et al.*; «Chantler et al. Reply»; Phys. Rev. Lett. **110**, p. 159 302 (2013)https://journals.aps.org/prl/pdf/10.1103/PhysRevLett.110.159302. 9

[70] S. W. Epp; «Comment on "Testing Three-Body Quantum Electrodynamics with Trapped Ti 20+ Ions: Evidence for a Z-Dependent Divergence Between Experiment and Calculation"»; Phys. Rev. Lett. **110**, p. 159 301 (2013)https://journals.aps.org/prl/pdf/10.1103/PhysRevLett.110.159301. 9

[71] J. K. Rudolph, S. Bernitt, S. W. Epp, R. Steinbrügge, C. Beilmann, G. V. Brown, S. Eberle, A. Graf, Z. Harman, N. Hell, M. Leutenegger, A. Müller, K. Schlage, H. C. Wille, H. Yavaş, J. Ullrich & J. R. Crespo López-Urrutia; «X-Ray Resonant Photoexcitation: Linewidths and Energies of K alpha Transitions in Highly Charged Fe Ions»; Phys. Rev. Lett. **111**, p. 103 002 (2013)https://link.aps.org/doi/10.1103/PhysRevLett.111.103002. 9, 67, 68, 69, 72, 74

[72] P. Amaro, S. Schlesser, M. Guerra, E. O. Le Bigot, J.-M. Isac, P. Travers, J. P. Santos, C. I. Szabo, A. Gumberidze & P. Indelicato; «Absolute Measurement of the Relativistic Magnetic Dipole Transition Energy in Heliumlike Argon»; Phys. Rev. Lett. **109**, p. 043 005 (2012)https://link.aps.org/doi/10.1103/PhysRevLett.109.043005. 9

[73] A. N. Artemyev, V. M. Shabaev, V. A. Yerokhin, G. Plunien & G. Soff; «QED calculation of the n = 1 and n = 2 energy levels in He-like ions»; Phys. Rev. A **71**, p. 062 104–26 (2005)http://link.aps.org/abstract/PRA/v71/e062104. 9

[74] A. Gumberidze, M. Trassinelli, N. Adrouche, C. I. Szabo, P. Indelicato, F. Haranger, J. M. Isac, E. Lamour, E. O. Le Bigot, J. Merot, C. Prigent, J. P. Rozet & D. Vernhet; «Electronic temperatures, densities, and plasma x-ray emission of a 14.5 GHz electron-cyclotron resonance ion source»; Rev. Sci. Instrum. **81**, p. 033 303–033 310 (2010)http://aip.scitation.org/doi/10.1063/1.3316805. 9

[75] V. Mäckel, R. Klawitter, G. Brenner, J. C. López-Urrutia & J. Ullrich; «Laser spectroscopy on forbidden transitions in trapped highly charged Ar 13+ ions»; Phys. Rev. Lett. **107**, p. 143 002 (2011)https://journals.aps.org/prl/pdf/10.1103/PhysRevLett.107.143002. 9

[76] A. N. Artemyev, V. M. Shabaev, I. I. Tupitsyn, G. Plunien & V. A. Yerokhin; «QED Calculation of the 2 p 3/2- 2 p 1/2 Transition Energy in Boron-like Argon»; Physical review letters **98**, p. 173 004 (2007)https://journals.aps.org/prl/pdf/10.1103/PhysRevLett.98.173004. 9

[77] L. Schmoger, O. O. Versolato, M. Schwarz, M. Kohnen, A. Windberger, B. Piest, S. Feuchtenbeiner, J. Pedregosa-Gutierrez, T. Leopold, P. Micke *et al.*; «Coulomb crystallization of highly charged ions»; Science **347**, p. 1233–1236 (2015). 9

[78] A. Antognini, F. Nez, K. Schuhmann, F. D. Amaro, F. Biraben, J. M. R. Cardoso, D. S. Covita, A. Dax, S. Dhawan, M. Diepold, L. M. P. Fernandes, A. Giesen, A. L. Gouvea, T. Graf, T. W. Hänsch, P. Indelicato, L. Julien, C.-Y. Kao, P. Knowles, F. Kottmann, E. O. Le Bigot, Y.-W. Liu, J. A. M. Lopes, L. Ludhova, C. M. B. Monteiro, F. Mulhauser, T. Nebel, P. Rabinowitz, J. M. F. dos Santos, L. A. Schaller, C. Schwob, D. Taqqu, J. F. C. A. Veloso, J. Vogelsang & R. Pohl; «Proton Structure from the Measurement of 2S-2P Transition Frequencies of Muonic Hydrogen»; Science **339**, p. 417–420 (2013)http://www.sciencemag.org/content/339/6118/417.abstract. 10, 11

[79] U. D. Jentschura; «Lamb shift in muonic hydrogen-II. Analysis of the discrepancy of theory and experiment»; Annals of Physics **326**, p. 516–533 (2011)https://www.sciencedirect.com/science/article/pii/S0003491610002009. 11

[80] K. Pachucki; «Theory of the Lamb shift in muonic hydrogen»; Phys. Rev. A **53**, p. 2092 (1996)https://journals.aps.org/pra/pdf/10.1103/PhysRevA.53.2092. 11

[81] K. Pachucki; «Proton structure effects in muonic hydrogen»; Phys. Rev. A **60**, p. 3593 (1999)https://journals.aps.org/pra/pdf/10.1103/PhysRevA.60.3593. 11

[82] A. Veitia & K. Pachucki; «Nuclear recoil effects in antiprotonic and muonic atoms»; Phys. Rev. A **69**, p. 042 501 (2004)https://journals.aps.org/pra/abstract/10.1103/PhysRevA.69.042501. 11

[83] M. I. Eides, H. Grotch & V. A. Shelyuto; «Theory of light hydrogenlike atoms»; Physics Reports **342**, p. 63–261 (2001)https://www.sciencedirect.com/science/article/pii/S0370157300000776. 11

[84] E. Borie; «Lamb shift in muonic hydrogen»; Phys. Rev. A **71**, p. 032 508 (2005)https://journals.aps.org/pra/abstract/10.1103/PhysRevA.71.032508. 11

[85] A. P. Martynenko; «2 S Hyperfine splitting of muonic hydrogen»; Phys. Rev. A **71**, p. 022 506 (2005)https://journals.aps.org/pra/abstract/10.1103/PhysRevA.71.022506. 11

[86] N. Michel, N. S. Oreshkina & C. H. Keitel; «Theoretical prediction of the fine and hyperfine structure of heavy muonic atoms»; Phys. Rev. A **96**, p. 032 510 (2017)https://journals.aps.org/pra/pdf/10.1103/PhysRevA.96.032510. 11

[87] J. M. Dong, W. Zuo, H. F. Zhang, W. Scheid, J. Z. Gu & Y. Z. Wang; «Correlation between muonic levels and nuclear structure in muonic atoms»; Phys. Lett. B **704**, p. 600–603 (2011)https://www.sciencedirect.com/science/article/pii/S0370269311011300. 11

[88] M. W. Johnson, E. B. Shera, M. V. Hoehn, R. A. Naumann, J. D. Zumbro & C. E. Bemis; «241am and 243am Charge Distributions from Muonic X-Ray Spectroscopy and the Quadrupole Moment of the 240am Fission Isomer»; Physics Letters **161B**, p. 75–78 (1985)http://dx.doi.org/10.1016/0370-2693(85)90612-4. 11, 33

[89] A. Haga, Y. Horikawa & H. Toki; «Reanalysis of muonic Zr 90 and Pb 208 atoms»; Phys. Rev. C **75**, p. 044 315 (2007)https://journals.aps.org/prc/pdf/10.1103/PhysRevC.75.044315. 11, 40, 41, 42, 84, 85, 86, 91

[90] D. Kessler, H. Mes, A. C. Thompson, H. L. Anderson, M. S. Dixit, C. K. Hargrove & R. J. McKee; «Muonic x rays in lead isotopes»; Phys. Rev. C **11**, p. 1719 (1975)https://journals.aps.org/prc/pdf/10.1103/PhysRevC.11.1719. 11, 88

[91] T. Yamazaki, R. S. Hayano, Y. Kuno, J. Imazato, K. Nagamine, S. E. Kohn & C. Y. Huang; «Giant hyperfine anomaly between bound negative muon and Rh nucleus in Pd metal»; Phys. Rev. Lett. **42**, p. 1241 (1979)https://journals.aps.org/prl/abstract/10.1103/PhysRevLett.42.1241. 40

[92] Y. Yamazaki, H. D. Wohlfahrt, E. B. Shera, M. V. Hoehn & R. M. Steffen; «Discrepancy between Theory and Experiment in Nuclear Polarization Corrections of Muonic Pb 208»; Phys. Rev. Lett. **42**, p. 1470 (1979)https://journals.aps.org/prl/pdf/10.1103/PhysRevLett.42.1470. 11, 40

[93] A. J. Freeman, J. V. Mallow, J. P. Desclaux & M. Weinert; «Theory of hyperfine anomalies in muonic atoms»; Hyperfine Interactions **19**, p. 865–872 (1984)https://link.springer.com/article/10.1007/BF02066131. 40

[94] G. A. Rinker & J. Speth; «Nuclear polarization in muonic 204, 206, 207, 208Pb in the random-phase approximation»; Nucl. Phys. A **306**, p. 360–396 (1978)https://www.sciencedirect.com/science/article/pii/0375947478904700. 11, 42, 85

[95] A. Antognini, N. Berger, D. V. Bruch, P. Indelicato, K. Jungmann5, K. Kirch, A. Knecht, A. Papa, R. Pohl, M. Pospelov, E. Rapisarda, N. Severijns, F. Wauters, & L. Willmann; «Measurement of the charge radius of radium (Proposal for BVR 47)»; (2016). 11, 93

[96] I. Lindgren & J. Morrison; *Atomic many-body theory*; tome 3 (Springer Science & Business Media) (2012). 12

[97] I. Shavitt & R. J. Bartlett; *Many-body methods in chemistry and physics: MBPT and coupled-cluster theory* (Cambridge university press) (2009). 12, 13

[98] T. Kagawa, Y. Honda & S. Kiyokawa; «Relativistic configuration-interaction theory for atomic systems»; Physical Review A **44**, p. 7092 (1991)https://journals.aps.org/pra/pdf/10.1103/PhysRevA.44.7092. 12

[99] E. Eliav, U. Kaldor & Y. Ishikawa; «Open-shell relativistic coupled-cluster method with Dirac-Fock-Breit wave functions: Energies of the gold atom and its cation»; Phys. Rev. A **49**, p. 1724 (1994)https://journals.aps.org/pra/pdf/10.1103/PhysRevA.49.1724. 13

[100] J. Sucher; «S-matrix formalism for level-shift calculations»; Physical Review **107**, p. 1448 (1957)https://journals.aps.org/pr/abstract/10.1103/PhysRev.107.1448. 13

[101] I. Lindgren, S. Salomonson & B. Åsén; «The covariant-evolution-operator method in bound-state QED»; Physics Reports **389**, p. 161–261 (2004)https://www.sciencedirect.com/science/article/pii/S0370157303003831. 13

[102] I. Lindgren, S. Salomonson & D. Hedendahl; «Many-body procedure for energy-dependent perturbation: Merging many-body perturbation theory with QED»; Physical Review A **73**, p. 062 502 (2006)https://journals.aps.org/pra/abstract/10.1103/PhysRevA.73.062502. 13

[103] I. Lindgren, S. Salomonson & D. Hedendahl; «Combining Many-Body Perturbation and Quantum Electrodynamics»; Journal of Atomic, Molecular, and Optical Physics **2011** (2011)http://dx.doi.org/10.1155/2011/723574. 13

[104] V. M. Shabaev, I. I. Tupitsyn & V. A. Yerokhin; «Model operator approach to the Lamb shift calculations in relativistic many-electron atoms»; Phys. Rev. A **88**, p. 012 513 (2013)http://link.aps.org/doi/10.1103/PhysRevA.88.012513. 30, 47, 50, 52

[105] J. P. Desclaux; «A Multiconfiguration Relativistic Dirac-Fock Program»; Comp. Phys. Commun. **9**, p. 31–45 (1975)http://linkinghub.elsevier.com/retrieve/pii/0010465575900545. 5, 12, 15, 18, 43, 45, 57, 71

[106] I. P. Grant; «Relativistic Calculation of Atomic Structures»; Advances in Physics **19**, p. 747–811 (1970)http://dx.doi.org/10.1080/00018737000101191. 12, 15, 57

[107] C. Froese Fischer; *The Hartree-Fock Method for Atoms* (Wiley, New York) (1977). https://www.osti.gov/biblio/5156729. 17

[108] J. P. Desclaux; «A relativistic multiconfiguration Dirac-Fock package»; Methods and techniques in computational chemistry p. 253 (1993)https://dirac.spectro.jussieu.fr/mcdf/mcdf_theory/Mettec/mettec.html. 5, 17, 18

[109] J. P. Desclaux, J. Dolbeault, M. J. Esteban, P. Indelicato & E. Sere; «Computational approaches of relativistic models in quantum chemistry»; Handbook of Numerical Analysis **10**, p. 453–483 (2003)https://www.sciencedirect.com/science/article/pii/S1570865903100063. 5, 18

[110] O. Gorceix & P. Indelicato; «Effect of the complete Breit interaction on two-electron ion energy levels»; Phys. Rev. A **37**, p. 1087 (1988)https://journals.aps.org/pra/pdf/10.1103/PhysRevA.37.1087. 12, 15, 19

[111] F. A. Parpia & A. K. Mohanty; «Relativistic basis-set calculations for atoms with Fermi nuclei»; Physical Review A **46**, p. 3735 (1992)https://journals.aps.org/pra/abstract/10.1103/PhysRevA.46.3735. 19

[112] P. Indelicato; «Multiconfiguration Dirac-Fock calculations of transition energies in two electron ions with $10 \leq Z \leq 92$»; Nuclear Instruments and Methods in Physics Research Section B: Beam Interactions with Materials and Atoms **31**, p. 14–20 (1988)https://www.sciencedirect.com/science/article/pii/0168583X88903886. 21

[113] D. Layzer & J. Bahcall; «Relativistic Z-dependent theory of many-electron atoms»; Annals of Physics **17**, p. 177–204 (1962)https://www.sciencedirect.com/science/article/pii/0003491662900246. 21

[114] Z. J. Horak, M. N. Lewis, A. Dalgarno & P. Blanchard; «Correlation Energies of the $1s^2 3l^2 L$ States of the Lithium Sequence»; Physical Review **185**, p. 21 (1969)https://journals.aps.org/pr/abstract/10.1103/PhysRev.185.21. 21

[115] P. J. Mohr, D. B. Newell & B. N. Taylor; «CODATA recommended values of the fundamental physical constants: 2014»; Journal of Physical and Chemical Reference Data **45**, p. 043 102 (2016)https://aip.scitation.org/doi/abs/10.1063/1.4954402. 22, 40

[116] A. M. Desiderio & W. R. Johnson; «Lamb shift and binding energies of K electrons in heavy atoms»; Phys. Rev. A **3**, p. 1267 (1971)https://journals.aps.org/pra/pdf/10.1103/PhysRevA.3.1267. 22

[117] P. Indelicato & P. J. Mohr; «6s and 8d state self-energy for hydrogen-like ions and new results on the self-energy screening»; Hyp. Int. **114**, p. 147 (1998)http://link.springer.com/10.1023/A:1012622505367. 4, 52

[118] P. J. Mohr & G. Soff; «Nuclear Size Correction to the Electron Self-Energy»; Phys. Rev. Lett. **70**, p. 158–161 (1993)https://link.aps.org/doi/10.1103/PhysRevLett.70.158. 4, 30, 84

[119] V. A. Yerokhin & V. M. Shabaev; «One-loop self-energy correction to the 1s and 2s hyperfine splitting in H-like systems»; Phys. Rev. A **64**, p. 012 506 (2001). https://link.aps.org/doi/10.1103/PhysRevA.64.012506. 4

[120] A. N. Artemyev, V. M. Shabaev & V. A. Yerokhin; «Relativistic nuclear recoil corrections to the energy levels of hydrogenlike and high-Z lithiumlike atoms in all

orders in αZ»; Phys. Rev. A **52**, p. 1884 (1995)https://journals.aps.org/pra/abstract/10.1103/PhysRevA.52.1884. 4, 31

[121] J. Sapirstein & K. T. Cheng; «Vacuum polarization calculations for hydrogen-like and alkali-metal-like ions»; Physical Review A **68**, p. 042 111 (2003)https://journals.aps.org/pra/pdf/10.1103/PhysRevA.68.042111. 24

[122] P. Indelicato & P. J. Mohr; «Coordinate-space approach to the bound-electron self-energy: Self-Energy screening calculation»; Physical Review A **63**, p. 052 507 (2001)https://journals.aps.org/pra/pdf/10.1103/PhysRevA.63.052507. 29

[123] D. S. Hughes & C. Eckart; «The effect of the motion of the nucleus on the spectra of Li I and Li II»; Physical Review **36**, p. 694 (1930)https://journals.aps.org/pr/pdf/10.1103/PhysRev.36.694. 31

[124] E. A. Uehling; «Polarization effects in the positron theory»; Physical Review **48**, p. 55 (1935)https://journals.aps.org/pr/pdf/10.1103/PhysRev.48.55. 23, 51

[125] G. Plunien, B. Müller, W. Greiner & G. Soff; «Nuclear polarization contribution to the Lamb shift in heavy atoms»; Phys. Rev. A **39**, p. 5428–5431 (1989)http://journals.aps.org/pra/abstract/10.1103/PhysRevA.39.5428. 33, 85

[126] G. Plunien, B. Müller, W. Greiner & G. Soff; «Nuclear Polarization in Heavy Atoms and Superheavy Quasiatoms»; Phys. Rev. A **43**, p. 5853–5866 (1991)http://link.aps.org/doi/10.1103/PhysRevA.43.5853. 33, 85

[127] A. V. Volotka & G. Plunien; «Nuclear polarization study: New frontiers for tests of QED in heavy highly charged ions»; Physical review letters **113**, p. 023 002 (2014)https://journals.aps.org/prl/abstract/10.1103/PhysRevLett.113.023002. 33

[128] P. Indelicato & E. Lindroth; «Relativistic Effects, Correlation, and QED Corrections on K_α Transitions in Medium to Very Heavy Atoms»; Phys. Rev. A **46**, p. 2426–2436 (1992)https://journals.aps.org/pra/abstract/10.1103/PhysRevA.46.2426. 33, 34, 52

[129] T. Mooney, E. Lindroth, P. Indelicato, E. Kessler & R. D. Deslattes; «Precision Measurements of K and L Transitions in Xenon: Experiment and Theory for the K, L and M Levels»; Phys. Rev. A **45**, p. 1531–1543 (1992)http://link.aps.org/doi/10.1103/PhysRevA.45.1531. 34

[130] P. Indelicato, S. Boucard & E. Lindroth; «Relativistic and many-body effects in K, L, and M shell ionization energy for elements with $10 \leq Z \leq 100$ and the determination of the 1s Lamb shift for heavy elements»; Eur. Phys. J. D **3**, p. 29–41 (1998)http://link.springer.com/article/10.1007/s100530050146. 34, 52

[131] I. I. Tupitsyn, N. A. Zubova, V. M. Shabaev, G. Plunien & T. Stöhlker; «Relativistic calculations of x-ray transition energies and isotope shifts in heavy

atoms»; Physical Review A **98**, p. 022 517 (2018)https://journals.aps.org/pra/abstract/10.1103/PhysRevA.98.022517. 34

[132] P. Indelicato, F. Parente & R. Marrus; «Effect of the hyperfine structure on the 2 3P1 and the 2 3P1 lifetime in heliumlike ions»; Phys. Rev. A **40**, p. 3505–3514 (1989)https://link.aps.org/doi/10.1103/PhysRevA.40.3505. 35

[133] J. D. Zumbro, R. A. Naumann, M. V. Hoehn, W. Reuter, E. B. Shera, C. E. B. Jr. & Y. Tanaka; «E2 and E4 Deformations in 232th and 239,240,242pu»; Physics Letters **167B**, p. 383–387 (1986)http://dx.doi.org/10.1016/0370-2693(86)91285-2. 33, 64

[134] J. D. Zumbro, E. B. Shera, Y. Tanaka, J. C. E. Bemis, R. A. Naumann, M. V. Hoehn, W. Reuter & R. M. Steffen; «E2 and E4 Deformations in 233,234,235,238u»; prl **53**, p. 1888–92 (1984)http://dx.doi.org/10.1103/PhysRevLett.53.1888. 33, 64

[135] P. Indelicato & P. J. Mohr; «Quantum electrodynamic effects in atomic structure»; Theoretica chimica acta **80**, p. 207–214 (1991)https://link.springer.com/article/10.1007/BF01119620. 29

[136] K. T. Cheng; «Relativistic formulas for multipole-transition probabilities»; Rapport technique (1977). 34, 43

[137] G. Howat, T. Åberg & O. Goscinski; «Relaxation and final-state channel mixing in the Auger effect»; Journal of Physics B: Atomic and Molecular Physics **11**, p. 1575 (1978)https://iopscience.iop.org/article/10.1088/0022-3700/11/9/011/meta. 36, 76

[138] T. Åberg & G. Howat; «Theory of the Auger effect»; Handbuch der Physik **31**, p. 469–619 (1982). 36

[139] V. M. Shabaev; «Two-time Green's function method in quantum electrodynamics of high-Z few-electron atoms»; Physics Reports **356**, p. 119–228 (2002)https://www.sciencedirect.com/science/article/pii/S0370157301000242. 26

[140] M. I. Eides, H. Grotch & D. A. Owen; «Coulomb line vacuum polarization corrections to Lamb shift of order $\alpha 2$ (Zα) 5m»; Physics Letters B **294**, p. 115–119 (1992)https://www.sciencedirect.com/science/article/pii/037026939291649T. 28

[141] M. H. Mittleman; «Structure of heavy atoms: Three-body potentials»; Physical Review A **4**, p. 893 (1971)https://journals.aps.org/pra/abstract/10.1103/PhysRevA.4.893. 28

[142] L. W. Fullerton & G. A. Rinker Jr; «Accurate and efficient methods for the evaluation of vacuum-polarization potentials of order Z α and Z α 2»; Physical Review A **13**, p. 1283 (1976)https://journals.aps.org/pra/abstract/10.1103/PhysRevA.13.1283. 28

[143] Y. Sajeev, M. K. Mishra, N. Vaval & S. Pal; «Fock space multireference coupled cluster calculations based on an underlying bivariational self-consistent field on Auger and shape resonances»; The Journal of chemical physics **120**, p. 67–72 (2004)https://aip.scitation.org/doi/abs/10.1063/1.1630025. 34

[144] R. D. Deslattes, E. G. Kessler Jr., P. Indelicato, L. de Billy, E. Lindroth & J. Anton; «X-Ray Transition Energies: New Approach to a Comprehensive Evaluation»; Rev. Mod. Phys. **75**, p. 35–99 (2003)https://journals.aps.org/rmp/abstract/10.1103/RevModPhys.75.35. 34

[145] S. G. Karshenboim; «Precision physics of simple atoms: QED tests, nuclear structure and fundamental constants»; Physics reports **422**, p. 1–63 (2005)https://www.sciencedirect.com/science/article/pii/S0370157305003637.

[146] T. Q. Phan, P. Bergem, A. Rüetschi, L. A. Schaller & L. Schellenberg; «Nuclear polarization in muonic Zr 90»; Physical Review C **32**, p. 609 (1985)https://journals.aps.org/prc/abstract/10.1103/PhysRevC.32.609. 40

[147] G. A. Rinker; «Static and dynamic muonic-atom codes-MUON and RURP»; Computer Physics Communications **16**, p. 221–242 (1979)https://inis.iaea.org/search/search.aspx?orig_q=RN:10459764. 41

[148] A. Bohr & M. B. R.; «Nuclear Structure Vol. I»; Reading, Massachussetts: WA Benjamin (1969). 42

[149] A. Bohr & M. B. R.; «Nuclear Structure Vol. II»; (1975). 42

[150] L. J. Tassie; «A Model of Nuclear Shape Oscillations for g? Transitions and Electron Excitation»; Australian Journal of physics **9**, p. 407–418 (1956)http://www.publish.csiro.au/PH/PH560407. 42, 85

[151] A. Bohr & B. R. Mottelson; «Nuclear Structure»; Benjamin, New York **2**, p. 561 (1975). 42, 85

[152] G. Plunien, B. Müller, W. Greiner & G. Soff; «Nuclear polarization in heavy atoms and superheavy quasiatoms»; Physical Review A **43**, p. 5853 (1991)https://journals.aps.org/pra/abstract/10.1103/PhysRevA.43.5853. 42

[153] H. Schneuwly & P. Vogel; «Electronic K x-ray energies in heavy muonic atoms»; Physical Review A **22**, p. 2081 (1980)https://journals.aps.org/pra/abstract/10.1103/PhysRevA.22.2081. 42

[154] E. Borie & G. A. Rinker; «The energy levels of muonic atoms»; Reviews of Modern Physics **54**, p. 67 (1982)https://journals.aps.org/rmp/abstract/10.1103/RevModPhys.54.67. 42

[155] P. Indelicato, O. Gorceix & J. P. Desclaux; «MCDF studies of two electron ions II: Radiative corrections and comparison with experiment.»; J. Phys. B: At. Mol. Opt. Phys. **20**, p. 651 (1987)http://dx.doi.org/10.1088/0022-3700/20/4/007. 5, 29, 30, 52, 57, 71

[156] P. Indelicato & J. P. Desclaux; «Multiconfiguration Dirac-Fock Calculations of Transition Energies with QED Corrections in Three-Electron Ions»; Phys. Rev. A **42**, p. 5139–5149 (1990)http://journals.aps.org/pra/abstract/10.1103/PhysRevA.42.5139. 5, 15, 19, 21, 29, 30, 44, 52, 57, 58, 62, 64, 71, 77

[157] P. Indelicato; «Nonperturbative Evaluation of Some QED Contributions to the Muonic Hydrogen N=2 Lamb Shift and Hyperfine Structure»; Phys. Rev. A **87**, p. 022 501 (2013)http://link.aps.org/doi/10.1103/PhysRevA.87.022501. 5, 11, 15, 18, 21, 23, 24, 25, 26, 27, 44, 53, 83

[158] E. H. Wichmann & N. M. Kroll; «Vacuum polarization in a strong Coulomb field»; Physical Review **101**, p. 843 (1956)https://journals.aps.org/pr/pdf/10.1103/PhysRev.101.843. 24, 52

[159] J. Blomqvist; «Vacuum polarization in exotic atoms»; Nucl. Phys. B **48**, p. 95–103 (1972)https://www.sciencedirect.com/science/article/pii/055032137290051X. 24

[160] V. G. Ivanov, E. Y. Korzinin & S. G. Karshenboim; «Second-order corrections to the wave function at the origin in muonic hydrogen and pionium»; Phys. Rev. D **80**, p. 027 702 (2009)https://journals.aps.org/prd/pdf/10.1103/PhysRevD.80.027702. 25

[161] T. A. Welton; «Some observable effects of the quantum-mechanical fluctuations of the electromagnetic field»; Physical Review **74**, p. 1157 (1948)https://journals.aps.org/pr/pdf/10.1103/PhysRev.74.1157. 29, 30

[162] V. M. Shabaev, I. I. Tupitsyn & V. A. Yerokhin; «QEDMOD: Fortran program for calculating the model Lamb-shift operator»; Comp. Phys. Commun. **189**, p. 175–181 (2015)http://www.sciencedirect.com/science/article/pii/S0010465514004081. 30, 50, 52

[163] J. P. Marques, P. Indelicato & F. Parente; «Relativistic multiconfiguration calculations of the 2s 2 2p 2 P 3/2 level lifetime along the boron isoelectronic sequence»; The European Physical Journal D **66**, p. 324 (2012)https://link.springer.com/article/10.1140/epjd/e2012-30338-3. 44

[164] J. M. Sampaio, T. I. Madeira, M. Guerra, F. Parente, J. P. Santos, P. Indelicato & J. P. Marques; «Dirac-Fock calculations of K-, L-, and M-shell fluorescence and Coster-Kronig yields for Ne, Ar, Kr, Xe, Rn, and Uuo»; Physical Review A **91**, p. 052 507 (2015)https://journals.aps.org/pra/abstract/10.1103/PhysRevA.91.052507. 44

[165] P. Indelicato, J. Bieroń & P. Jönsson; «Are MCDF calculations 101% correct in the super-heavy elements range?»; Theoretical Chemistry Accounts **129**, p. 495–505 (2011)https://link.springer.com/article/10.1007/s00214-010-0887-3. 44

[166] P. Indelicato; «Effects of the Breit interaction on the 1s binding energy of superheavy elements»; Journal of Physics B: Atomic and Molecular Physics **19**, p.

1719 (1986)https://iopscience.iop.org/article/10.1088/0022-3700/19/12/012/meta. 44

[167] P. Indelicato, J. P. Santos, S. Boucard & J.-P. Desclaux; «QED and relativistic corrections in superheavy elements»; The European Physical Journal D **45**, p. 155–170 (2007)https://link.springer.com/article/10.1140/epjd/e2007-00229-y. 44

[168] J. P. Marques, P. Indelicato, F. Parente, J. M. Sampaio & J. P. Santos; «Ground-state Landé g factors for selected ions along the boron isoelectronic sequence»; Physical Review A **94**, p. 042 504 (2016)https://journals.aps.org/pra/abstract/10.1103/PhysRevA.94.042504. 44

[169] P. Indelicato; «Correlation and Negative Continuum effects for the relativistic M1 transition in two-electron ions using the multiconfiguration Dirac-Fock method»; Phys. Rev. Lett. **77**, p. 3323–3326 (1996)http://link.aps.org/doi/10.1103/PhysRevLett.77.3323. 44

[170] P. O. Löwdin; «Quantum theory of many-particle systems. I. Physical interpretations by means of density matrices, natural spin-orbitals, and convergence problems in the method of configurational interaction»; Physical Review **97**, p. 1474 (1955)https://journals.aps.org/pr/abstract/10.1103/PhysRev.97.1474. 44, 76

[171] R. Bacher, P. Blüm, D. Gotta, K. Heitlinger, M. Schneider, J. Missimer & L. M. Simons; «Relevance of ionization and electron refilling to the observation of the M1 transition (γM1: 2s-1s) in light muonic atoms»; Phys. Rev. A **39**, p. 1610 (1989)https://journals.aps.org/pra/abstract/10.1103/PhysRevA.39.1610. 42

[172] S. Lenz, G. Borchert, H. Gorke, D. Gotta, T. Siems, D. F. Anagnostopoulos, M. Augsburger, D. Chatellard, J. P. Egger, D. Belmiloud *et al.*; «A new determination of the mass of the charged pion»; Physics Letters B **416**, p. 50–55 (1998)https://www.sciencedirect.com/science/article/pii/S0370269397013373. 42

[173] J. Bauche & M. Klapisch; «Remarks on Brillouin's theorem in the atomic variational approach»; Journal of Physics B: Atomic and Molecular Physics **5**, p. 29 (1972)https://iopscience.iop.org/article/10.1088/0022-3700/5/1/012/meta. 44

[174] M. Godefroid, J. Liévin & J. Y. Metz; «Brillouin's theorem for complex atomic configurations»; Journal of Physics B: Atomic and Molecular Physics **20**, p. 3283 (1987)https://iopscience.iop.org/article/10.1088/0022-3700/20/14/004/meta. 44

[175] P. Indelicato, E. Lindroth & J. P. Desclaux; «Nonrelativistic limit of Dirac-Fock codes: The role of Brillouin configurations»; Physical review letters **94**, p. 013 002 (2005)https://journals.aps.org/prl/abstract/10.1103/PhysRevLett.94.013002. 44

[176] Y.-K. Kim, F. Parente, J. P. Marques, P. Indelicato & J. P. Desclaux; «Failure of multiconfiguration Dirac-Fock wave functions in the nonrelativistic limit»; Physical Review A **58**, p. 1885 (1998)https://journals.aps.org/pra/abstract/10.1103/PhysRevA.58.1885. 44

[177] P. Indelicato; «Projection operators in Multiconfiguration Dirac-Fock calculations. Application to the ground state of heliumlike ions.»; Phys. Rev. A **51**, p. 1132–1145 (1995)https://link.aps.org/doi/10.1103/PhysRevA.51.1132. 5, 15, 57

[178] V. M. Shabaev; «Mass corrections in a strong nuclear field»; Theoretical and Mathematical Physics **63**, p. 588–596 (1985)http://link.springer.com/10.1007/BF01017505. 57

[179] V. M. Shabaev & A. N. Artemyev; «Relativistic nuclear recoil corrections to the energy levels of multicharged ions»; J. Phys. B: At. Mol. Opt. Phys. **27**, p. 1307–1314 (1994)https://iopscience.iop.org/article/10.1088/0953-4075/27/7/006/meta. 31, 57

[180] V. M. Shabaev; «QED theory of the nuclear recoil effect in atoms»; Phys. Rev. A **57**, p. 59–67 (1998)https://link.aps.org/doi/10.1103/PhysRevA.57.59. 31, 57

[181] J. Li, C. Nazé, M. Godefroid, S. Fritzsche, G. Gaigalas, P. Indelicato & P. Jönsson; «Mass-and field-shift isotope parameters for the 2 s- 2 p resonance doublet of lithiumlike ions»; Physical Review A **86**, p. 022 518 (2012)https://journals.aps.org/pra/abstract/10.1103/PhysRevA.86.022518. 31

[182] E. Gaidamauskas, C. Nazé, P. Rynkun, G. Gaigalas, P. Jönsson & M. Godefroid; «Tensorial form and matrix elements of the relativistic nuclear recoil operator»; Journal of Physics B: Atomic, Molecular and Optical Physics **44**, p. 175 003 (2011)https://iopscience.iop.org/article/10.1088/0953-4075/44/17/175003/meta. 31

[183] J. M. Sampaio, F. Parente, C. Nazé, M. Godefroid, P. Indelicato & J. P. Marques; «Relativistic calculations of 1s 2 2s2p level splitting in Be-like Kr»; Physica Scripta **2013**, p. 014 015 (2013)http://stacks.iop.org/1402-4896/2013/i=T156/a=014015. 57

[184] G. Audi, A. H. Wapstra & C. Thibault; «The AME2003 atomic mass evaluation:(II). Tables, graphs and references»; Nucl. Phys. A **729**, p. 337–676 (2003)http://linkinghub.elsevier.com/retrieve/pii/S0375947403018098. 43, 57

[185] I. Angeli; «A consistent set of nuclear rms charge radii: properties of the radius surface R (N, Z)»; At. Data, Nucl. Data Tab. **87**, p. 185 (2004)http://linkinghub.elsevier.com/retrieve/pii/S0092640X04000166. 43, 57, 64, 88, 90, 91

[186] I. Angeli & K. P. Marinova; «Table of experimental nuclear ground state charge radii: An update»; At. Data Nucl. Data Tables **99**, p. 69–95 (2013)http://www.

sciencedirect.com/science/article/pii/S0092640X12000265. 43, 57, 64, 90, 98

[187] J. P. Santos, J. P. Marques, F. Parente, E. Lindroth, P. Indelicato & J. P. Desclaux; «Relativistic 2s1/2 (L1) atomic subshell decay rates and fluorescence yields for Yb and Hg»; J. Phys. B: At. Mol. Phys. **32**, p. 2089 (1999)https://iopscience.iop.org/article/10.1088/0953-4075/32/9/304/meta. 57

[188] J. P. Santos, J. P. Marques, F. Parente, E. Lindroth, S. Boucard & P. Indelicato; «Multiconfiguration Dirac-Fock calculation of transition energies in highly ionized bismuth, thorium, and uranium»; The European Physical Journal D-Atomic, Molecular, Optical and Plasma Physics **1**, p. 149–163 (1998)https://link.springer.com/article/10.1007/s100530050075. 64

[189] J. P. Santos, G. C. Rodrigues, J. P. Marques, F. Parente, J. P. Desclaux & P. Indelicato; «Relativistic correlation correction to the binding energies of the ground configuration of beryllium-like, neon-like, magnesium-like and argon-like ions»; Eur. Phys. J. D **37**, p. 201 – 207 (2006)https://link.springer.com/article/10.1140/epjd/e2006-00002-x. 57

[190] M. C. Martins, J. P. Marques, A. M. Costa, J. P. Santos, F. Parente, S. Schlesser, E. O. Le Bigot & P. Indelicato; «Production and decay of sulfur excited species in an electron-cyclotron-resonance ion-source plasma»; Phys. Rev. A **80**, p. 032 501 (2009)https://link.aps.org/doi/10.1103/PhysRevA.80.032501. 57

[191] P. Indelicato; «Radiative de-excitation of the 1s22s3p 3P0 level in beryllium-like ions: A competition between a E2 and a two-electron one-photon E1 transitions»; Hyperfine Interaction **108**, p. 39–49 (1997)http://link.springer.com/10.1023/A:1012621620562. 44, 76

[192] V. A. Yerokhin & A. Surzhykov; «Relativistic Configuration-Interaction Calculation of Energy Levels of Core-Excited States in Lithiumlike Ions: Argon through Krypton»; Phys. Rev. A **86**, p. 042 507 (2012)http://link.aps.org/doi/10.1103/PhysRevA.86.042507. 58, 64, 66, 70, 71, 73, 75, 77

[193] V. A. Yerokhin, A. Surzhykov & A. Müller; «Relativistic configuration-interaction calculations of the energy levels of the 1 s 2 2 l and 1 s 2 l 2 l' states in lithiumlike ions: Carbon through chlorine»; Phys. Rev. A **96**, p. 042 505 (2017)https://journals.aps.org/pra/abstract/10.1103/PhysRevA.96.042505. 58, 64, 66, 67, 68, 69, 71, 73, 75, 77, 79

[194] P. Bosselmann, U. Staude, D. Horn, K.-H. Schartner, F. Folkmann, A. E. Livingston & P. H. Mokler; «Measurements of 2s 2s1/2-2p 2p1/2,3/2 Transition Energies in Lithiumlike Heavy Ions. Ii. Experimental Results for Ag44 + and Discussion Along the Isoelectronic Series»; Phys. Rev. A **59**, p. 1874–1883 (1999)https://journals.aps.org/pra/abstract/10.1103/PhysRevA.59.1874. 60, 61, 63, 65

[195] K. G. Widing & J. D. Purcell; «The lithium-like 2s 2S-2p 2P transition in solar flares»; The Astrophysical Journal **204**, p. L151–L153 (1976)http://adsabs.harvard.edu/full/1976ApJ...204L.151W. 59, 60, 61, 63, 65

[196] E. Träbert, P. Beiersdorfer, J. K. Lepson & H. Chen; «Extreme ultraviolet spectra of highly charged Xe ions»; Phys. Rev. A **68**, p. 042 501 (2003)https://journals.aps.org/pra/abstract/10.1103/PhysRevA.68.042501. 60, 63

[197] B. Denne, G. Magyar & J. Jacquinot; «Berylliumlike Mo XXXIV and Lithiumlike Mo XL Observed in the JET Tokamak»; Phys. Rev. A **40**, p. 3702–3705 (1989)https://journals.aps.org/pra/abstract/10.1103/PhysRevA.40.3702. 60, 61, 63, 65

[198] D. Bernhardt, C. Brandau, Z. Harman, C. Kozhuharov, S. Böhm, F. Bosch, S. Fritzsche, J. Jacobi, S. Kieslich, H. Knopp, F. Nolden, W. Shi, Z. Stachura, M. Steck, T. Stöhlker, S. Schippers & A. Müller; «Electron-Ion Collision Spectroscopy: Lithium-Like Xenon Ions»; Phys. Rev. A **91**, p. 012 710 (2015)http://link.aps.org/doi/10.1103/PhysRevA.91.012710. 60, 61, 63, 65

[199] B. Denne, E. Hinnov, J. Ramette & B. Saoutic; «Spectrum Lines of Kr XXVIII-Kr XXXIV Observed in the JET Tokamak»; Phys. Rev. A **40**, p. 1488 (1989)https://journals.aps.org/pra/abstract/10.1103/PhysRevA.40.1488. 59, 61, 63, 65

[200] D. Feili, P. Bosselmann, K.-H. Schartner, F. Folkmann, A. E. Livingston, E. Träbert, X. Ma & P. H. Mokler; «Measurements of 2s2 S1/2 –2p2 P1/2 Transition Energies in Lithiumlike Heavy Ions. Iii. Experimental Results for Sn47+ and Xe51+»; Phys. Rev. A **62**, p. 022 501 (2000)http://journals.aps.org/pra/abstract/10.1103/PhysRevA.62.022501. 60, 63, 65

[201] K. W. Kukla, A. E. Livingston, C. M. V. Vogt, H. G. Berry, R. W. Dunford, L. J. Curtis & S. Cheng; «Extreme-Ultraviolet Wavelength and Lifetime Measurements in Highly Ionized Krypton»; Can. J. Phys. **83**, p. 1127–1139 (2005)http://www.nrcresearchpress.com/doi/abs/10.1139/p05-066. 59, 61, 63, 65

[202] B. Denne & E. Hinnov; «Spectral Lines of Highly-ionized Atoms for the Diagnostics of Fusion Plasmas»; Phys. Scr. **35**, p. 811–818 (1987)https://iopscience.iop.org/article/10.1088/0031-8949/35/6/009/meta. 59, 60, 61, 63, 65

[203] S. Madzunkov, E. Lindroth, N. Eklöw, M. Tokman, A. Paál & R. Schuch; «QED effects in lithiumlike krypton»; Phys. Rev. A **65**, p. 032 505 (2002)https://journals.aps.org/pra/abstract/10.1103/PhysRevA.65.032505. 60, 63

[204] S. Martin, J. P. Buchet, M. C. Buchet-Poulizac, A. Denis, J. Desesquelles, M. Druetta, J. P. Grandin, D. Hennecart, X. Husson & D. Lecler; «Measurements of 2 s -2 p Transition Wavelengths in Helium- and Lithium-Like Xenon»; EPL (Europhysics Letters) **10**, p. 645 (1989)http://stacks.iop.org/0295-5075/10/i=7/a=007. 63, 65

[205] U. Staude, P. Bosselmann, R. Büttner, D. Horn, K.-H. Schartner, F. Folkmann, A. E. Livingston, T. Ludziejewsk & P. H. Mokler; «Measurements of 2s 2s1/2–2p 2p3/2,1/2 Transition Energies in Lithiumlike Heavy Ions: Experiments

and Results for Ni25 + and Zn27 +»; Phys. Rev. A **58**, p. 3516–3523 (1998)https://journals.aps.org/pra/abstract/10.1103/PhysRevA.58.3516. 59, 61, 63, 65

[206] R. J. Knize; «Measurement of QED Effects in Z=24 to 34 Lithium-Like Ions»; Phys. Rev. A **43**, p. 1637–1639 (1991)https://journals.aps.org/pra/abstract/10.1103/PhysRevA.43.1637. 59, 61, 63, 65

[207] J. Schweppe, A. Belkacem, L. Blumenfeld, N. Claytor, B. Feynberg, H. Gould, V. Kostroun, L. Levy, S. Misawa, R. Mowat & M. Prior; «Measurement of the Lamb Shift in Lithiumlike Uranium (U89+)»; Phys. Rev. Lett. **66**, p. 1434–1437 (1991)https://journals.aps.org/prl/abstract/10.1103/PhysRevLett.66.1434. 60, 63

[208] E. Hinnov & B. Denne; «Empirical Evaluation of Three-Electron Quantum-Electrodynamics Effects from Lithiumlike Resonance Lines of Elements Z=22-42 in the Tokamak Fusion Test Reactor and Joint European Torus Tokamaks»; Phys. Rev. A **40**, p. 4357–4360 (1989)https://link.aps.org/doi/10.1103/PhysRevA.40.4357. 59, 60, 61, 63, 65

[209] B. Edlén; «Comparison of Theoretical and Experimental Level Values of the N = 2 Complex in Ions Isoelectronic with Li, Be, O and F»; Physica Scripta **28**, p. 51 (1983)http://stacks.iop.org/1402-4896/28/i=1/a=007. 58, 59, 60, 61, 63, 65

[210] K. Bockasten, R. Hallin & T. P. Hughes; «The Spectra of Highly Ionized Light Elements in a High Temperature Plasma»; Proceedings of the Physical Society **81**, p. 522 (1963)http://stacks.iop.org/0370-1328/81/i=3/a=321. 58, 60, 63, 65

[211] A. S. Zacarias, A. E. Livingston, Y. N. Lu, R. F. Ward, H. G. Berry & R. W. Dunford; «Measurements of 2s–2p transition energies in helium-like and lithium-like nickel»; Nuclear Instruments and Methods in Physics Research Section B: Beam Interactions with Materials and Atoms **31**, p. 41–42 (1988)https://www.sciencedirect.com/science/article/pii/0168583X88903928. 59, 63

[212] C. Brandau, C. Kozhuharov, A. Müller, W. Shi, S. Schippers, T. Bartsch, S. Böhm, C. Böhme, A. Hoffknecht, H. Knopp, N. Grün, W. Scheid, T. Steih, F. Bosch, B. Franzke, P. H. Mokler, F. Nolden, M. Steck, T. Stöhlker & Z. Stachura; «Precise Determination of the 2s1/2–2p1/2 Splitting in Very Heavy Lithiumlike Ions Utilizing Dielectronic Recombination»; Phys. Rev. Lett. **91**, p. 073 202 (2003)http://link.aps.org/doi/10.1103/PhysRevLett.91.073202. 60, 63

[213] S. Suckewer, J. Cecchi, S. Cohen, R. Fonck & E. Hinnov; «Tracer element injection into PDX tokamak for spectral line identification and localized doppler temperature measurement»; Physics Letters A **80**, p. 259–262 (1980)http://adsabs.harvard.edu/abs/1980PhLA...80..259S. 59, 61, 63, 65

[214] S. Kieslich, S. Schippers, W. Shi, A. Müller, G. Gwinner, M. Schnell, A. Wolf, E. Lindroth & M. Tokman; «Determination of the 2 s-2 p excitation energy of lithiumlike scandium using dielectronic recombination»; Physical

Review A **70**, p. 042 714 (2004)https://journals.aps.org/pra/abstract/10.1103/PhysRevA.70.042714. 61, 65

[215] R. Silwal, E. Takacs, J. Dreiling, J. Gillaspy & Y. Ralchenko; «Identification and plasma diagnostics study of extreme ultraviolet transitions in highly charged yttrium»; Atoms **5**, p. 30 (2017)https://www.mdpi.com/2218-2004/5/3/30. 60, 61, 63

[216] N. J. Peacock, M. F. Stamp & J. D. Silver; «Highly-ionized atoms in fusion research plasmas»; Physica Scripta **1984**, p. 10 (1984)https://iopscience.iop.org/article/10.1088/0031-8949/1984/T8/002/meta. 59, 60, 61, 63, 65

[217] J. Reader, J. D. Gillaspy, D. Osin & Y. Ralchenko; «Extreme ultraviolet spectra and analysis of $\Delta n = 0$ transitions in highly charged barium»; Journal of Physics B: Atomic, Molecular and Optical Physics **47**, p. 145 003 (2014)http://stacks.iop.org/0953-4075/47/i=14/a=145003. 60, 63

[218] K. T. Cheng, W. R. Johnson & J. Sapirstein; «Screened Lamb shift calculations for lithiumlike uranium, sodiumlike platinum, and copperlike gold»; Physical review letters **66**, p. 2960 (1991)https://journals.aps.org/prl/abstract/10.1103/PhysRevLett.66.2960. 58

[219] P. Beiersdorfer, A. L. Osterheld, J. H. Scofield, J. R. C. López-Urrutia & K. Widmann; «Measurement of QED and Hyperfine Splitting in the 2 s 1/2-2 p 3/2 X-Ray Transition in Li-like B 209 i 8 0+»; Physical review letters **80**, p. 3022 (1998)https://journals.aps.org/prl/abstract/10.1103/PhysRevLett.80.3022. 61, 65

[220] P. Beiersdorfer, A. Osterheld, S. R. Elliott, M. H. Chen, D. Knapp & K. Reed; «Structure and Lamb shift of 2 s1/2-2 p3/2levels in lithiumlike Th87+through neonlike Th80+»; Phys. Rev. A **52**, p. 2693–2706 (1995)https://journals.aps.org/pra/abstract/10.1103/PhysRevA.52.2693. 62, 65

[221] Y. A. Podpaly, J. D. Gillaspy, J. Reader & Y. Ralchenko; «Euv Measurements of Kr Xxi–Kr Xxxiv and the Effect of a Magnetic-Dipole Line on Allowed Transitions»; J. Phys. B: At. Mol. Opt. Phys. **47**, p. 095 702 (2014)http://stacks.iop.org/0953-4075/47/i=9/a=095702. 61, 65

[222] Y. Podpaly, J. Clementson, P. Beiersdorfer, J. Williamson, G. V. Brown & M. F. Gu; «Spectroscopy of 2 S1/2 -2 P3/2 Transitions in W65+ through W71+»; Phys. Rev. A **80**, p. 052 504 (2009)http://link.aps.org/doi/10.1103/PhysRevA.80.052504. 61, 65

[223] D. Nikolic, E. Lindroth, S. Kieslich, C. Brandau, S. Schippers, W. Shi, A. Müller, G. Gwinner, M. Schnell & A. Wolf; «Dielectronic recombination resonances in Na8+»; Physical Review A **70** (2004)http://adsabs.harvard.edu/abs/2004PhRvA..70f2723N. 58, 60, 65

[224] C. M. Brown, J. O. Ekberg, U. Feldman, J. F. Seely, M. C. Richardson, F. J. Marshall & W. E. Behring; «Transitions in Lithiumlike Cu26+ and Berylliumlike Cu25+ of Interest for X-Ray Laser Research»; Journal of the Optical Society of America B **4**, p. 533–538 (1987)http://josab.osa.org/abstract.cfm?URI=josab-4-4-533. 61, 65

[225] J. Clementson, P. Beiersdorfer, G. V. Brown, M. F. Gu, H. Lundberg, Y. Podpaly & E. Träbert; «Tungsten spectroscopy at the Livermore electron beam ion trap facility»; Canadian Journal of Physics **89**, p. 571–580 (2011)https://www.nrcresearchpress.com/doi/pdf/10.1139/p11-028. 61, 65

[226] M. Lestinsky, E. Lindroth, D. A. Orlov, E. W. Schmidt, S. Schippers, S. Böhm, C. Brandau, F. Sprenger, A. S. Terekhov, A. Müller *et al.*; «Screened radiative corrections from hyperfine-split dielectronic resonances in lithiumlike scandium»; Physical review letters **100**, p. 033 001 (2008)https://journals.aps.org/prl/abstract/10.1103/PhysRevLett.100.033001. 61, 65

[227] X. M. Zhang, N. Nakamura, C. Y. Chen, M. Andersson, Y. Liu & S. Ohtani; «Measurement of the QED energy shift in the 1 s 2 2 p 3/ 2–1 s 2 2 s 1/ 2 x-ray transition in Li-like Pb 79+ 208»; Physical Review A **78**, p. 032 504 (2008)https://journals.aps.org/pra/abstract/10.1103/PhysRevA.78.032504. 61, 65

[228] S. Schlesser, S. Boucard, D. S. Covita, J. M. F. dos Santos, H. Fuhrmann, D. Gotta, A. Gruber, M. Hennebach, A. Hirtl, P. Indelicato *et al.*; «High-accuracy x-ray line standards in the 3-keV region»; Physical Review A **88**, p. 022 503 (2013)https://journals.aps.org/pra/abstract/10.1103/PhysRevA.88.022503. 67, 68, 72, 74

[229] M. Bitter, K. W. Hill, M. Zarnstorff, S. von Goeler, R. Hulse, L. C. Johnson, N. R. Sauthoff, S. Sesnic, K. M. Young, M. Tavernier, F. Bely-Dubau, P. Faucher, M. Cornille & J. Dubau; «Satellite spectra for heliumlike titanium. II»; Phys. Rev. A **32**, p. 3011–3029 (1985)https://journals.aps.org/pra/abstract/10.1103/PhysRevA.32.3011. 67, 68, 69, 72

[230] H. Hsuan, M. Bitter, K. W. Hills, S. von Goeler, B. Grek, D. Johnson, L. C. Johnson, S. Sesnic, C. P. Bhalla, K. R. Karim, F. Bely-Dubau & P. Faucher; «Satellite spectra of heliumlike nickel»; Phys. Rev. A **35**, p. 4280–4285 (1987)http://journals.aps.org/pra/abstract/10.1103/PhysRevA.35.4280. 67, 68, 69, 72

[231] B. J. Wargelin, S. M. Kahn & P. Beiersdorfer; «Dielectronic Satellite Contributions to Ne Viii and Ne Ix K-Shell Spectra»; Phys. Rev. A **63**, p. 022 710 (2001)https://link.aps.org/doi/10.1103/PhysRevA.63.022710. 67, 68, 72

[232] A. J. Smith, P. Beiersdorfer, V. Decaux, K. Widmann, A. Osterheld & M. Chen; «Measurement of Doubly Excited Levels in Lithiumlike and Berylliumlike Cobalt»; Phys. Rev. A **51**, p. 2808 (1995)http://link.aps.org/doi/10.1103/PhysRevA.51.2808. 67, 68, 69, 72

[233] V. Decaux, V. L. Jacobs, P. Beiersdorfer, D. A. Liedahl & S. M. Kahn; «Modeling of high-resolution K α emission spectra from Fe XVIII through Fe XXIV»; pra **68**, p. 012 509 (2003)https://link.aps.org/doi/10.1103/PhysRevA.68.012509. 67, 68, 69, 72

[234] M. R. Tarbutt, R. Barnsley, N. J. Peacock & J. D. Silver; «Wavelength Measurements of the Satellite Transitions to the N = 2 Resonance Lines of Helium-Like Argon»; J. Phys. B: At. Mol. Opt. Phys. **34**, p. 3979–3991 (2001)https://iopscience.iop.org/article/10.1088/0953-4075/34/20/309. 67, 68, 69, 72, 76, 79

[235] C. Biedermann, R. Radtke & K. Fournier; «Line Ratios and Wavelengths of Helium-Like Argon N=2 Satellite Transitions and Resonance Lines»; Nucl. Instr. Methods B **205**, p. 255–259 (2003)http://www.sciencedirect.com/science/article/pii/S0168583X02019730. 67, 68, 69, 72, 75, 76, 79

[236] J. E. Rice, M. L. Reinke, J. M. A. Ashbourn, C. Gao, M. M. Victora, M. A. Chilenski, L. Delgado-Aparicio, N. T. Howard, A. E. Hubbard, J. W. Hughes & J. H. Irby; «X-ray observations of Ca 19 + , Ca 18 + and satellites from Alcator C-Mod tokamak plasmas»; J. Phys. B: At. Mol. Opt. Phys. **47**, p. 075 701 (2014)http://stacks.iop.org/0953-4075/47/i=7/a=075701. 67, 68, 69, 72

[237] P. Beiersdorfer, M. H. Chen, R. E. Marrs, M. B. Schneider & R. S. Walling; «Dielectronic satellite spectrum of heliumlike vanadium»; Phys. Rev. A **44**, p. 396 (1991)http://link.aps.org/abstract/PRA/v44/p396. 67, 68, 69, 72

[238] Z. Li, J. Gang, H. Lianghuan & D. Banglin; «Relativistic configuration interaction calculations on Kα x-ray satellites of krypton»; Phys. Scr. **83**, p. 025 302 (2011)https://iopscience.iop.org/article/10.1088/0031-8949/83/02/025302/meta. 66, 71

[239] J. Nilsen; «Dielectronic Satellite Spectra for Helium-Like Ions»; At. Data, Nucl. Data Tab. **38**, p. 339–379 (1988)http://www.sciencedirect.com/science/article/B6WBB-4DBJ6CP-44/2/b08d317acbf37d974f86941a43fb9bf4. 66, 70, 71, 73

[240] A. D. Whiteford, N. R. Badnell, C. P. Ballance, S. D. Loch, M. G. O'Mullane & H. P. Summers; «Excitation of Ar 15+ and Fe 23+ for Diagnostic Application to Fusion and Astrophysical Plasmas»; Journal of Physics B: Atomic, Molecular and Optical Physics **35**, p. 3729 (2002)http://stacks.iop.org/0953-4075/35/i=17/a=309. 66, 71

[241] J. Suleiman, H. G. Berry, R. W. Dunford, R. D. Deslattes & P. Indelicato; «Observation of Doubly Excited States in Lithiumlike Calcium»; Phys. Rev. A **49**, p. 156–160 (1994)http://link.aps.org/doi/10.1103/PhysRevA.49.156. 69, 72

[242] E. Träbert, I. A. Armour, S. Bashkin, N. A. Jelley, R. O'Brien & J. D. Silver; «The X-Ray Spectra of H-Like, He-Like and Li-Like Silicon Ions after Foil Excitation»; Journal of Physics B: Atomic, Molecular and Optical Physics **12**,

p. 1665–1675 (1979)http://iopscience.iop.org/article/10.1088/0022-3700/12/10/013. 68, 72

[243] D. B. Thorn, G. V. Brown, J. H. T. Clementson, H. Chen, M. Chen, P. Beiersdorfer, K. R. Boyce, C. A. Kilbourne, F. S. Porter & R. L. Kelley; «High-resolution spectroscopy of K-shell praseodymium with a high-energy microcalorimeter»; Can. J. Phys. **86**, p. 241–244 (2008)https://www.nrcresearchpress.com/doi/pdf/10.1139/p07-134. 69, 72

[244] R. E. Marrs, S. R. Elliott & D. A. Knapp; «Production and trapping of hydrogenlike and bare uranium ions in an electron beam ion trap»; Physical review letters **72**, p. 4082 (1994)https://journals.aps.org/prl/abstract/10.1103/PhysRevLett.72.4082. 62

[245] R. E. Marrs; «Production of U92+ with an electron beam ion trap»; Review of scientific instruments **67**, p. 941–944 (1996)https://aip.scitation.org/doi/abs/10.1063/1.1146646. 62

[246] P. Beiersdorfer, S. R. Elliott, A. Osterheld, T. Stöhlker, J. Autrey, G. V. Brown, A. J. Smith & K. Widmann; «Search for 1s2s 3 S 1–1s2p 3 P 2 decay in U 9 0+»; Physical Review A **53**, p. 4000 (1996)https://journals.aps.org/pra/abstract/10.1103/PhysRevA.53.4000. 62

[247] C. Brandau, C. Kozhuharov, Z. Harman, A. Müller, S. Schippers, Y. S. Kozhedub, D. Bernhardt, S. Böhm, J. Jacobi, E. W. Schmidt *et al.*; «Isotope Shift in the Dielectronic Recombination of Three-Electron Nd 57+ A»; Physical review letters **100**, p. 073 201 (2008)https://journals.aps.org/prl/abstract/10.1103/PhysRevLett.100.073201. 62

[248] W. R. Johnson, S. Blundell & J. Sapirstein; «Many-body perturbation-theory calculations of energy levels along the lithium isoelectronic sequence»; Physical Review A **37**, p. 2764 (1988)https://journals.aps.org/pra/abstract/10.1103/PhysRevA.37.2764. 62

[249] J. F. Seely; «QED contributions to the 2p-2s transitions in highly charged Li-like ions»; Phys. Rev. A **39**, p. 3682–3685 (1989)https://journals.aps.org/pra/abstract/10.1103/PhysRevA.39.3682. 58, 62, 63, 64

[250] S. A. Blundell, W. R. Johnson & J. Sapirstein; «Improved many-body perturbation theory calculations of the n= 2 states of lithiumlike uranium»; Physical Review A **41**, p. 1698 (1990)https://journals.aps.org/pra/abstract/10.1103/PhysRevA.41.1698. 58, 64

[251] K. G. Dyall, I. P. Grant, C. T. Johnson, F. A. Parpia & E. P. Plummer; «GRASP: A general-purpose relativistic atomic structure program»; Computer Physics Communications **55**, p. 425–456 (1989)https://www.sciencedirect.com/science/article/pii/0010465589901367. 12, 15, 62

[252] Y. Kim, D. H. Baik, P. Indelicato & J. P. Desclaux; «Resonance transition energies of Li-, Na-, and Cu-like ions»; Physical Review A Atomic Molecular &

Optical Physics **44**, p. 148 (1991)https://journals.aps.org/pra/abstract/10.1103/PhysRevA.44.148. 58, 62, 64

[253] A. Ynnerman, J. James, I. Lindgren, H. Persson & S. Salomonson; «Many-body calculation of the 2p1/2,3/2-2s1/2 transition energies in Li-like 238U»; Phys. Rev. A **50**, p. 4671–4678 (1994)https://journals.aps.org/pra/abstract/10.1103/PhysRevA.50.4671. 58, 62

[254] M. H. Chen, K. T. Cheng, W. R. Johnson & J. Sapirstein; «Relativistic Configuration-Interaction Calculations for the n=2 States of Lithiumlike Ions»; Phys. Rev. A **52**, p. 266–273 (1995)http://link.aps.org/doi/10.1103/PhysRevA.52.266. 58, 62, 64

[255] W. R. Johnson, Z. W. Liu & J. Sapirstein; «Transition Rates for Lithium-Like Ions, Sodium-Like Ions, and Neutral Alkali-Metal Atoms»; At. Data, Nucl. Data Tab. **64**, p. 279–300 (1996)http://www.sciencedirect.com/science/article/pii/S0092640X96900248. 58, 62, 64

[256] U. I. Safronova & A. S. Shlyaptseva; «Inner-shell excitation energy and autoionization rates for Li-, Be-, B-like ions with Z = 6–54»; Physica Scripta **54**, p. 254 (1996)http://stacks.iop.org/1402-4896/54/i=3/a=005. 58, 62, 64, 66, 71, 73, 75, 77

[257] V. A. Yerokhin, A. N. Artemyev, V. M. Shabaev, M. M. Sysak, O. M. Zherebtsov, Soff & G.; «Two-Photon Exchange Corrections to the $2mathitp_{1/2}-2mathits$ Transition Energy in Li-Like High- $mathitZ$ Ions»; Phys. Rev. Lett. **85**, p. 4699 (2000)https://journals.aps.org/prl/abstract/10.1103/PhysRevLett.85.4699. 58, 62

[258] M. F. Gu; «Energies of 1s22lq ($1 \leq q \leq 8$) states for $Z \leq 60$ with a combined configuration interaction and many-body perturbation theory approach»; Atomic Data and Nuclear Data Tables **89**, p. 267 – 293 (2005)ISSN 0092-640X. http://www.sciencedirect.com/science/article/pii/S0092640X05000124. 58, 62, 64

[259] L. A. Vainshtein & U. I. Safronova; «Wavelengths and Transition Probabilities of Satellites to Resonance Lines of H- and He-Like Ions»; At. Data, Nucl. Data Tab. **21**, p. 49–68 (1978)http://www.sciencedirect.com/science/article/B6WBB-4DBJ1BP-4R/2/0d1af82df1b9a0cab467983280479be0. 66, 70, 71, 72

[260] S. Shuqiang, P. Feng & J. Gang; «Properties of the K_α and K_β x-ray transitions in CuXX through CuXXVIII»; J. Phys. B: At. Mol. Opt. Phys. **39**, p. 2087 (2006)http://stacks.iop.org/0953-4075/39/i=8/a=023. 66, 71

[261] H. Feng, Y. Jiamin, J. Gang, W. Chuangke & Z. Xuefeng; «Wavelengths, Oscillator Strengths and Radiative Transition Rates for K_α Lines in Titanium X-Ray Spectra»; Physica Scripta **2011**, p. 014 006 (2011)http://stacks.iop.org/1402-4896/2011/i=T144/a=014006. 66, 71

[262] Z. Li, J. Gang, H. Lianghuan & D. Banglin; «Relativistic Configuration Interaction Calculations on K_α X-Ray Satellites of Krypton»; Physica Scripta **83**, p. 025 302 (2011)http://stacks.iop.org/1402-4896/83/i=2/a=025302. 71

[263] F. F. Goryaev, L. A. Vainshtein & A. M. Urnov; «Atomic Data for Doubly-Excited States 2lnl of He-Like Ions and 1s2lnl of Li-Like Ions with $Z = 6\breve{}36$ and $N = 2, 3$»; Atomic Data and Nuclear Data Tables **113**, p. 117–257 (2017)http://www.sciencedirect.com/science/article/pii/S0092640X16300092. 66, 71, 72, 73, 75

[264] M. H. Chen; «Dielectronic satellite spectra for He-like ions»; Atomic Data & Nuclear Data Tables **34**, p. 301–356 (1986)https://www.sciencedirect.com/science/article/pii/0092640X86900069. 66, 70, 71, 72, 73, 75

[265] J. P. Santos, A. M. Costa, M. C. Martins, F. Parente & P. Indelicato; «Modeling Praseodymium K X-Ray Lines in an Electron Beam Ion Trap»; Eur. Phys. J. D **66**, p. 1–7 (2012)http://dx.doi.org/10.1140/epjd/e2012-30049-9. 66, 71, 73, 75

[266] M. H. Chen, B. Crasemann & H. Mark; «Relativistic Auger and x-ray emission rates of the 1 s 2 s 2 p configuration of Li-like ions»; Physical Review A **24**, p. 1852 (1981)https://journals.aps.org/pra/abstract/10.1103/PhysRevA.24.1852. 66, 71, 72, 73, 75, 77

[267] J. P. Marques, M. C. Martins, A. M. Costa, P. Indelicato, F. Parente & J. P. Santos; «Theoretical determination of K X-ray transition energy and probability values for highly charged (He-through B-like) Nd, Sm, Gd, Dy, Er, and Yb ions»; Radiation Physics and Chemistry **154**, p. 17–20 (2019)https://www.sciencedirect.com/science/article/pii/S0969806X17310459. 44, 72

[268] C. P. Bhalla & T. W. Tunnell; «Theoretical lifetimes, transition energies, fluorescence yields, and nonradiative branching ratios for highly excited states of lithium-like argon»; Journal of Quantitative Spectroscopy and Radiative Transfer **32**, p. 141–158 (1984)https://www.sciencedirect.com/science/article/pii/0022407384900785. 66, 71, 73, 75, 77

[269] E. V. Aglitskii, V. A. Boiko, S. M. Zakharov, S. A. Pikuz & A. Y. Faenov; «Observation in laser plasmas and identification of dielectron satellites of spectral lines of hydrogen- and helium-like ions of elements in the Na–V range»; Soviet Journal of Quantum Electronics **4**, p. 500 (1974)http://stacks.iop.org/0049-1748/4/i=4/a=R16. 67, 68, 72, 74

[270] V. Decaux, P. Beiersdorfer, S. M. Kahn & V. L. Jacobs; «High-Resolution Measurement of the Kα Spectrum of Fe XXV-XVIII: New Spectral Diagnostics of Nonequilibrium Astrophysical Plasmas»; The Astrophysical Journal **482**, p. 1076 (1997)http://stacks.iop.org/0004-637X/482/i=2/a=1076. 67, 68, 69, 72, 74, 76, 79

[271] H. D. Dohmann, D. Liesen & H. Pfeng; «High resolution spectroscopy of prompt and metastable decaying levels in highly ionized argon, especially of the metastable 3 P 2-state of Ar 16+ and the 4 P 5/2-state of Ar 15+»; Zeitschrift für Physik A Hadrons and Nuclei **285**, p. 171–176 (1978)http://dx.doi.org/10.1007/BF01408743. 74, 78, 79

[272] P. Beiersdorfer, M. Bitter, D. Hey & K. J. Reed; «Identification of the 1 s 2 s 2 p 4 P 5/2- 1 s 2 2 s 2 S 1/2 magnetic quadrupole inner-shell satellite line in the Ar 1 6+ K-shell x-ray spectrum»; Phys. Rev. A **66**, p. 032 504 (2002)https://link.aps.org/doi/10.1103/PhysRevA.66.032504. 67, 68, 69, 72, 74, 76, 78, 79

[273] TFR Group, M. Cornille, J. Dubau & M. Loulergue; «Charge-dependent wavelength shifts and line intensities in the dielectronic satellite spectrum of heliumlike ions»; Phys. Rev. A **32**, p. 3000–3004 (1985)https://link.aps.org/doi/10.1103/PhysRevA.32.3000. 67, 68, 69, 72, 74

[274] J. E. Rice, M. A. Graf, J. L. Terry, E. S. Marmar, K. Giesing & F. Bombarda; «X-ray observations of helium-like scandium from the Alcator C-Mod tokamak»; J. Phys. B: At. Mol. Opt. Phys. **28**, p. 893–905 (1995)http://iopscience.iop.org/article/10.1088/0953-4075/28/5/021. 67, 68, 69, 74

[275] I. M. George & A. C. Fabian; «X-ray reflection from cold matter in active galactic nuclei and X-ray binaries»; Monthly Notices of the Royal Astronomical Society **249**, p. 352–367 (1991)https://academic.oup.com/mnras/article/249/2/352/1029310. 70

[276] P. Beiersdorfer, D. Knapp, R. E. Marrs, S. R. Elliott & M. H. Chen; «Structure and Lamb shift of 2 s 1/2-2 p 3/2 levels in lithiumlike U 8 9+ through neonlike U 8 2+»; Physical review letters **71**, p. 3939 (1993)https://journals.aps.org/prl/abstract/10.1103/PhysRevLett.71.3939. 62, 65, 70

[277] K. Widmann, P. Beiersdorfer, V. Decaux, S. R. Elliott, D. Knapp, A. Osterheld, M. Bitter & A. Smith; «Studies of He-like krypton for use in determining electron and ion temperatures in very-high-temperature plasmas»; Review of scientific instruments **66**, p. 761–763 (1995). 70

[278] U. I. Safronova & M. S. Safronova; «Relativistic Many-Body Calculations of E1, E2, M1, and M2 Transitions Rates for the 1 S 2 L' 2 L' ' - 1 S 2 2 L Lines in Li-Like Ions»; Molecular Physics **102**, p. 1331–1344 (2004)https://doi.org/10.1080/00268970410001728591. 71

[279] S. A. Blundell; «Calculations of the Screened Self-Energy and Vacuum Polarization in Li-Like, Na-Like and Cu-Like Ions»; Phys. Rev. A **47**, p. 1790–1803 (1993)http://journals.aps.org/pra/abstract/10.1103/PhysRevA.47.1790. 50

[280] K. T. Cheng, M. H. Chen & J. Sapirstein; «Quantum Electrodynamic Corrections in High-Z Li-Like and Be-Like Ions»; Phys. Rev. A **62**, p. 054 501 (2000)http://journals.aps.org/pra/abstract/10.1103/PhysRevA.62.054501. 62, 64

[281] Y. S. Kozhedub, A. V. Volotka, A. N. Artemyev, D. A. Glazov, G. Plunien, V. M. Shabaev, I. I. Tupitsyn & T. Stöhlker; «Relativistic Recoil, Electron-Correlation, and QED Effects on the 2pj-2s Transition Energies in Li-Like Ions»; Phys. Rev. A **81**, p. 042 513 (2010)http://link.aps.org/doi/10.1103/PhysRevA.81.042513. 47, 50, 58, 62, 64

[282] P. J. Mohr; «Numerical Evaluation of the 1s1/2 State Radiative Level Shift.»; Annals of Physics **88**, p. 52–87 (1974)https://doi.org/10.1016/0003-4916(74)90399-6. 4, 22, 51

[283] P. J. Mohr; «Self-energy correction to one-electron energy levels in a strong Coulomb field»; Phys. Rev. A **46**, p. 4421–4424 (1992)https://link.aps.org/doi/10.1103/PhysRevA.46.4421. 51

[284] P. J. Mohr & Y. K. Kim; «Self-energy of excited states in a strong Coulomb field»; Phys. Rev. A **45**, p. 2727–2735 (1992)http://link.aps.org/doi/10.1103/PhysRevA.45.2727. 51

[285] P. Indelicato & P. J. Mohr; «Coordinate space approach to the one-electron self-energy»; Phys. Rev. A **46**, p. 172–185 (1992)https://link.aps.org/doi/10.1103/PhysRevA.46.172. 51

[286] E. O. Le Bigot, P. Indelicato & P. J. Mohr; «QED self-energy contribution to highly-excited atomic states»; Phys. Rev. A **64**, p. 052 508 (14) (2001)https://link.aps.org/doi/10.1103/PhysRevA.64.052508. 51

[287] V. A. Yerokhin; «Two-loop self-energy in the Lamb shift of the ground and excited states of hydrogenlike ions»; Physical Review A **97**, p. 052 509 (2018)https://journals.aps.org/pra/pdf/10.1103/PhysRevA.97.052509. 26, 53, 57

[288] V. Yerokhin, P. Indelicato & V. Shabaev; «Two-loop self-energy correction in high-Z hydrogenlike ions»; Physical review letters **91**, p. 073 001 (2003)https://journals.aps.org/prl/pdf/10.1103/PhysRevLett.91.073001. 4, 26, 53

[289] V. A. Yerokhin, P. Indelicato & V. M. Shabaev; «Evaluation of the two-loop self-energy correction to the ground state energy of H-like ions to all orders in Z *alpha*»; The European Physical Journal D-Atomic, Molecular, Optical and Plasma Physics **25**, p. 203–238 (2003)https://link.springer.com/article/10.1140/epjd/e2003-00270-x. 26, 53

[290] V. A. Yerokhin, P. Indelicato & V. M. Shabaev; «Two-loop QED corrections in few-electron ions»; Canadian Journal of Physics **85**, p. 521–529 (2007)https://www.nrcresearchpress.com/doi/pdf/10.1139/p07-022. 26, 53

[291] V. A. Yerokhin, P. Indelicato & V. M. Shabaev; «Two-loop QED corrections with closed fermion loops»; Physical Review A **77**, p. 062 510 (2008)https://journals.aps.org/pra/pdf/10.1103/PhysRevA.77.062510. 26, 27, 53

[292] V. A. Yerokhin; «Two-loop self-energy for the ground state of medium-Z hydrogenlike ions»; Physical Review A **80**, p. 040 501 (2009)https://journals.aps.org/pra/pdf/10.1103/PhysRevA.80.040501. 26, 53

[293] V. A. Yerokhin; «The two-loop self-energy: diagrams in the coordinate-momentum representation»; The European Physical Journal D **58**, p. 57–68 (2010)https://link.springer.com/article/10.1140/epjd/e2003-00270-x. 26, 53

[294] O. Gorceix, P. Indelicato & J. P. Desclaux; «MCDF studies of two electron ions I: Electron-electron interaction»; J. Phys. B: At. Mol. Opt. Phys. **20**, p. 639–650 (1987)http://dx.doi.org/10.1088/0022-3700/20/4/006. 56

[295] G. Plunien & G. Soff; «Erratum: Nuclear-polarization contribution to the Lamb shift in actinide nuclei»; Phys. Rev. A **53**, p. 4614–4615 (1996)https://link.aps.org/doi/10.1103/PhysRevA.53.4614.2. 4, 53, 64

[296] A. V. Nefiodov, L. N. Labzowsky, G. Plunien & G. Soff; «Nuclear polarization effects in spectra of multicharged ions»; Physics Letters A **222**, p. 227–232 (1996)https://www.sciencedirect.com/science/article/pii/0375960196006500. 53

[297] V. A. Yerokhin, A. N. Artemyev, V. M. Shabaev, G. Plunien & G. Soff; «Screened self-energy correction to the 2p 3/2-2s transition energy in Li-like ions»; Optics and spectroscopy **99**, p. 12–17 (2005)https://link.springer.com/article/10.1134/1.1999887. 47, 50

[298] V. A. Yerokhin & A. Surzhykov; «Energy Levels of Core-Excited 1 s 2 l 2 l' States in Lithium-Like Ions: Argon to Uranium»; Journal of Physical and Chemical Reference Data **47**, p. 023 105 (2018)https://aip.scitation.org/doi/abs/10.1063/1.5034574. 66, 67, 68, 69, 70, 71, 72, 73, 75, 76, 77, 79

[299] F. Bombarda, F. Bely-Dubau, P. Faucher, M. Cornille, J. Dubau, M. Loulergue, T. Group *et al.*; «Dielectronic satellite spectrum of heliumlike argon: A contribution to the physics of highly charged ions and plasma impurity transport»; Physical Review A **32**, p. 2374 (1985)https://journals.aps.org/pra/abstract/10.1103/PhysRevA.32.2374. 65, 68

[300] C. Biedermann, R. Radtke, G. Fussmann & F. I. Allen; «Extreme ultraviolet spectroscopy of highly charged argon ions at the Berlin EBIT»; dans «Journal of Physics: Conference Series», , tome 72p. 012004 (IOP Publishing) (2007). https://iopscience.iop.org/article/10.1088/1742-6596/72/1/012004/meta. 59, 60

[301] S. Martin, A. Denis, M. C. Buchet-Poulizac, J. P. Buchet & J. Désesquelles; «2s-2p transitions in heliumlike and lithiumlike krypton»; Physical Review A **42**, p. 6570 (1990)https://journals.aps.org/pra/abstract/10.1103/PhysRevA.42.6570. 60, 61

[302] R. Büttner, U. Staude, M. Nicolai, J. Braukhoff, K.-H. Schartner, F. Folkmann & P. H. Mokler; «Measurement of the 2s2S12- 2p2P32 wavelength in Li-like nickel»; Nuclear Instruments and Methods in Physics Research Section B: Beam Interactions with Materials and Atoms **98**, p. 41–44 (1995)https://www.sciencedirect.com/science/article/pii/0168583X95000283. 61, 65

[303] Y. Nakano, Y. Takano, T. Ikeda, Y. Kanai, S. Suda, T. Azuma, H. Bräuning, A. Bräuning-Demian, D. Dauvergne, T. Stöhlker *et al.*; «Resonant coherent excitation of the lithiumlike uranium ion: A scheme for heavy-ion spectroscopy»; Physical Review A **87**, p. 060 501 (2013)https://journals.aps.org/pra/abstract/10.1103/PhysRevA.87.060501. 62

[304] I. P. & M. P. J.; «Self-energy corrections for muonic atoms(unpublished)»; . 84, 93

[305] K.-N. Huang; «Calculation of the vacuum-polarization potential»; Phys. Rev. A **14**, p. 1311 (1976)https://journals.aps.org/pra/pdf/10.1103/PhysRevA.14.1311.

[306] T. Kinoshita & M. Nio; «Sixth-order vacuum-polarization contribution to the Lamb shift of muonic hydrogen»; Phys. Rev. Lett. **82**, p. 3240 (1999)https://journals.aps.org/prl/abstract/10.1103/PhysRevLett.82.3240.

[307] T. Beier, P. J. Mohr, H. Persson & G. Soff; «Influence of nuclear size on QED corrections in hydrogenlike heavy ions»; Phys. Rev. A **58**, p. 954–963 (1998)https://link.aps.org/doi/10.1103/PhysRevA.58.954. 84

[308] P. J. Mohr, G. Plunien & G. Soff; «QED Corrections in Heavy Atoms»; Physics Reports **293**, p. 227–372 (1998)https://www.sciencedirect.com/science/article/pii/S037015739700046X. 24, 84

[309] J. B. Bellicard & K. J. Van Oostrum; «Elastic Electron Scattering from lead-208 at 175 and 250 MeV»; Physical Review Letters **19**, p. 242 (1967)https://journals.aps.org/prl/abstract/10.1103/PhysRevLett.19.242. 90

[310] G. J. C. Van Niftrik & R. Engfer; «Elastic electron scattering from lead and bismuth at 53 MeV»; Physics Letters **22**, p. 490–492 (1966)https://www.sciencedirect.com/science/article/pii/003191636691239X. 90

[311] H. L. Acker, G. Backenstoss, C. Daum, J. C. Sens & S. A. De Wit; «Measurements and analysis of muonic X-ray spectra in the spherical nuclei Au, Pb and Bi and the deformed nuclei W and U»; Physics Letters **14**, p. 317–320 (1965)https://www.sciencedirect.com/science/article/pii/0031916365902210. 90

[312] H. L. Anderson, R. J. McKee, C. K. Hargrove & E. P. Hincks; «Fine Structure and Isotope Shift in Muonic Lead»; Physical Review Letters **16**, p. 434 (1966)https://journals.aps.org/prl/abstract/10.1103/PhysRevLett.16.434. 90

[313] H. L. Anderson, C. K. Hargrove, E. P. Hincks, J. D. McAndrew, R. J. McKee, R. D. Barton & D. Kessler; «Precise measurement of the muonic x rays in the lead isotopes»; Physical Review **187**, p. 1565 (1969)https://journals.aps.org/pr/abstract/10.1103/PhysRev.187.1565. 90

[314] H. Euteneuer, J. Friedrich & N. Voegler; «The charge-distribution differences of 209Bi, 208, 207, 206, 204Pb and 205, 203Tl investigated by elastic electron scattering and muonic X-ray data»; Nuclear Physics A **298**, p. 452–476 (1978)https://www.sciencedirect.com/science/article/pii/0375947478901434. 90

[315] D. Kessler, H. Mes, A. C. Thompson, H. L. Anderson, M. S. Dixit, C. K. Hargrove & R. J. McKee; «Muonic x rays in lead isotopes»; Physical Review C **11**, p. 1719 (1975)https://journals.aps.org/prc/abstract/10.1103/PhysRevC.11.1719. 90

[316] T. J. Wasowicz; «Electronic and nuclear properties from the analysis of the isotope shifts in the spectral lines of lead»; The European Physical Journal D **53**, p. 263–272 (2009)https://link.springer.com/article/10.1140/epjd/e2009-00133-6. 90

[317] G. Fricke, C. Bernhardt, K. Heilig, L. A. Schaller, L. Schellenberg, E. B. Shera & C. W. Dejager; «Nuclear ground state charge radii from electromagnetic interactions»; Atomic Data and Nuclear Data Tables **60**, p. 177–285 (1995)https://www.sciencedirect.com/science/article/pii/S0092640X85710078. 90

BIAN GUOJIE **20er september 2019**

Sujet : Effets électrodynamiques et nucléaires quantiques dans les ions de type lithium et les atomes muoniques

Résumé : Nous avons effectué des calculs Dirac-Fock multi-configuration des énergies de transitions de structure fine $1s^2\,2p\,^2P_J \rightarrow 1s^2\,2s\,^2S_{1/2}, J = 1/2, 3/2$, les transitions à partir d'états excités en couche internes $1s\,2s\,2p\,^2P_J \rightarrow 1s^2\,2s\,^2S_{1/2}, J = 1/2, 3/2$ et $1s\,2s\,2p\,^4P_J \rightarrow 1s^2\,2s\,^2S_{1/2}, J = 1/2, 3/2, 5/2$, et les transitions Auger à partir de ces mêmes états $1s\,2s\,2p\,^4P_J \rightarrow 1s^2\,^1S_0, J = 1/2, 3/2$ dans la séquence isoélectronique du lithium, pour des ions de numéro atomique $10 \leq Z \leq 96$. Des corrections électrodynamiques quantiques avec modèle d'opérateur efficace et des corrections de corrélation électronique sont incluses dans les fonctions d'onde de Dirac avec une taille nucléaire finie. Des corrections de polarisation de Breit et de polarisation du vide de tous les ordres sont également incluses dans le calcul, avec une fonction d'onde d'ensemble actif entièrement optimisée. Des comparaisons approfondies entre les résultats théoriques existants et l'expérience sont effectuées. Nous évaluons également les paramètres nucléaires qui minimisent l'écart pondéré entre la théorie et l'expérience dans les modèles muoniques ^{208}Pb avec des modèles Fermi à deux paramètres et Gauss à trois paramètres. Nous avons obtenu r = 5.5057 fm dans le modèle de Fermi et r = 5.5031 dans le modèle de Gauss par ajustement polynomial. Nous analysons également les contributions individuelles de ^{226}Ra et ^{248}Cm muoniques en utilisant la même prescription de corrections exactes de QED pour les expériences à venir.

Mots clés : Méthode MCDF, QED, Énergie de transition, Atomes muoniques, Rayons nucléaires

Subject : Quantum Electrodynamic and nuclear effects in Li-like ions and muonic atoms

Abstract: We have performed multi-configuration Dirac-Fock calculations of the transition energies in the transitions of $1s^2\,2p\,^2P_J \rightarrow 1s^2\,2s\,^2S_{1/2}, J = 1/2, 3/2$, core-excited transitions of $1s\,2s\,2p\,^2P_J \rightarrow 1s^2\,2s\,^2S_{1/2}, J = 1/2, 3/2$ and $1s\,2s\,2p\,^4P_J \rightarrow 1s^2\,2s\,^2S_{1/2}, J = 1/2, 3/2, 5/2$, and Auger transition energies of $1s\,2s\,2p\,^2P_J \rightarrow 1s^2\,^1S_0$ and $1s\,2s\,2p\,^4P_J \rightarrow 1s^2\,^1S_0, J = 1/2, 3/2$ in the lithium isoelectronic sequence for low- to high-Z ions (Z=10-96). Quantum-electrodynamic corrections with effective operator model and electronic correlation corrections are included in Dirac wave functions with finite nuclear size. All-order Breit and vacuum polarization corrections are also included in the calculation, with a fully optimized active set wavefunction. Extensive comparisons between existing theorical results and experiment are performed. We also evaluate nuclear parameters that minimize the weighted theory-experiment discrepancy in muonic ^{208}Pb with two-parameter Fermi and three-parameter Gauss models. We obtain r=5.5057 fm in the Fermi model and r=5.5031 in Gauss model by polynomial-fitting. We also analyze the individual contributions of muonic ^{226}Ra and ^{248}Cm using the same prescription of exact QED correction for the upcoming experiments.

Keywords : MCDF method, QED, Transition energy, Muonic atoms, Nuclear radii